
THE UNIVERSITY *of* EDINBURGH

# Numerical and experimental studies on the mechanical behaviour of the distal femur following total knee arthroplasty

Noel Conlisk


Doctor of Philosophy

The University *of* Edinburgh

2013

# *Declaration*

This is to certify that this thesis titled, "Numerical and experimental studies on the mechanical behaviour of the distal femur following total knee arthroplasty" and the work contained within has been composed by me. Where I have consulted the published work of others, this is always clearly attributed. Where I have quoted from the work of others the source is always given, with the exception of such quotations, this thesis is entirely my own work. No part of this thesis has been submitted for any other degree or professional qualification.

Noel Conlisk

July 2013

"*A journey of a thousand miles begins*

*with a single step*" – Lao Tzu

# *Abstract*

*by*

Noel Conlisk BEng (Hons)

The history of total knee arthroplasty stretches back over 70 years. Many studies have shown that TKA is, in general, a successful operation for the relief of joint pain, with patient satisfaction rates of 90-95% and implant survival rates at 10-15 years of greater than 90%. However, a number of studies have also shown the potential for failures or complications arising post-implantation leading to revision surgery.

This thesis presents finite element (FE) models of the distal femur following primary and revision total knee arthroplasty. Pre-arthroplasty models are also developed for comparison. Particular attention is given to how femoral component design and method of fixation impacts the mechanical environment of the distal femur and stability of the prosthesis. FE analyses with fully bonded interfaces indicate that femoral components are subject to areas of low stress (stress shielding) immediately under the anterior flange and chamfer regardless of internal implant features. However, internal implant features were found to play a role in the pattern and magnitude of stress concentrations. Both stresses and motions were observed to increase with increasing flexion angle, indicating the importance of testing at multiple angles.

The initial models of the distal femur were extended to incorporate the effects of ageing and endosteal thinning of the femoral cortex, through novel application of pre-existing FE modelling techniques, specifically the ability to assign variable material properties corresponding to the nodal temperatures output from a heat transfer analysis. The findings from this study indicate that older patients with osteoporosis may be at increased risk of periprosthetic fracture compared to younger healthy patients. The use of a revision femoral component with a cemented stem as a means to mitigate this fracture risk was also investigated.

FE analyses using frictional interfaces were employed to determine the influence of femoral component design on micromotion at the interface. These models showed

that all primary implants were subject to similar magnitudes of relative motion at the interface, however, the distinct internal implant features led to very different regional variations. Furthermore, certain internal implant features (i.e. femoral box) were found to be highly sensitive to errors in surgical bone cuts. This aspect of the thesis also concluded that the addition of a stem served to significantly reduce motions at the interface in comparison to primary stemless implants. Long stemmed prostheses were found to result in the smallest levels of interface motion.

This study also detailed the design and creation of an *in vitro* test setup for the purposes of determining the influence of stem length and fixation on the stability of revision prostheses. Experimental results using this test rig showed that a cemented short stem provides as much initial stability as the uncemented long stem, and is easier to fit surgically. Corresponding FE models incorporating a virtual representation of the test rig and *in vitro* loading conditions revealed that the relative motion at the multi-planar bone-prosthesis interface cannot be adequately described using a single reference point. However, *in vitro* setups may be used to predict a general measure of implant stability and to provide a source of calibration for FE.

The distal femur models were further modified to investigate how the presence of condylar defects as classified by AORI defect classification system (Engh 2006) and weak osseous support due to osteoporosis may adversely affect the survival of the prosthesis. These investigations revealed that fixation of the femoral component, the presence of a large condylar defect and the level of osseous support all had an impact on stress in the implant, it is concluded that a non-modular approach should be adopted in older patient groups with severe osteoporosis to mitigate the risk of component junction failure and distal femoral fracture.

# *Dedication*

***For 刘维佳***

# *Acknowledgements*

First and foremost, I would like to thank my supervisors Dr. Pankaj and Mr. Colin Howie, for sharing their wealth of clinical and engineering knowledge over the years. Our early discussions greatly inspired the direction of this project, and while I'm not quite sure we got to "42", it has been my sincerest privilege to have participated in this research. I would like to gratefully acknowledge the financial support received for this work from the Lothian University Hospitals NHS Trust Brown and Ireland Estates Fund and The University of Edinburgh. Thanks also go to Stryker UK for providing implants and surgical instrumentation during the experimental portion of this work. A great deal of this research would not have been possible without the tireless efforts of individuals such as David Stewart, Matthew Richardson and the whole of the Engineering IT team (past and present). My sincerest thanks for keeping CLX functional as long as possible and for always responding in a timely manner to help resolve technical issues encountered.

I would like to gratefully acknowledge my examiners Dr. Andrew Philips (Imperial College) and Mr. James Patton (NHS and The University of Edinburgh) for their insight and comments during the viva, which have helped to greatly add to the quality of this thesis.

I am indebted to several other PhD students for their input and advice on problems encountered over the years, and for selflessly sharing their knowledge, time and skills to help me in the pursuit of my research. Thanks to both Dr. Finn Donaldson and Mr. Alisdair Macleod for always providing a second opinion, thus ensuring a deeper meaning behind results was sought. Dr. John Morrissey, for our talks on all things technological, they provided a welcome distraction during the hard times. A special mention must go to Dr. Nick Brown, for both his prize winning "office vegetable garden" and for the founding of the annual A.G.B. indoor office golf tournament. Thanks also to the following individuals without whom the working environment in A.G.B 3.13 would simply not have been the same: Dr Shiqing Li, Dr. Yin Wang, Dr. Xiaoqin Li, Dr. Chong Zhou, Dr. Vijayabaskar Narayanamurthy, Dr. Nick Brown, Mr. Subhash Thakur and Mr. Feng-Chen An. Thank you for your friendship and for all the laughs.

To all at EUTKD, I am proud to have shared part of my Taekwondo journey with such friendly and highly skilled individuals. The lessons learned from our world class coaching team (Nikos Jakubiak, Kam Dogra and Leslie Jakubiak) extend far beyond the walls of the Dojang and will stay with me for years to come.

To my brothers; Kevin, Paul and Keith, life would not have been the same without all of you. Special thanks go to Kevin for the words of encouragement which started me down this path. To my parents; Ann and Patrick, who over the years, gave up so much so that each of us could pursue our own dreams in life. I thank you both for the continuous love and support throughout my education and life. I sincerely hope to one day repay you both in some small way for all that you have given me and done for me. Finally, most of all I would like to thank 维佳. None of this would have been possible without your constant love and unwavering support!

# *Publication History*

The following section details the dissemination of key findings, based on work carried out while in candidature for the PhD, through publication in peer-reviewed journals and conference contributions at a national and international level.

## Journal Publications (Peer – Reviewed)

N.Conlisk, H. Gray, P. Pankaj and C.R. Howie. "The influence of stem length and fixation on initial femoral component stability in revision total knee replacement", *Bone Joint Res November 2012 1:281-288.*

N. Conlisk, P. Pankaj and C.R. Howie. "Influence of age related changes on the mechanical environment of the distal femur following total knee arthroplasty: A finite element study" *Computer Methods in Biomechanics and Biomedical Engineering* – under review

## Conference Contributions (Oral talks, Posters and Proceedings)

Conlisk, N., Pankaj, P., Howie, C. R., "Evaluation of Femoral Component Micromotion after Total Knee Arthroplasty: An Experimental Study", 18th Congress of the European Society of Biomechanics, oral contribution (Lisbon, Portugal, 2012).

Conlisk, N., Pankaj, P., Howie, C. R., "The Mechanical Environment In The Distal Femur: Influence Of Boundary Conditions On FE Models", 10th International Symposium of Computer Methods in Biomechanics and Biomedical Engineering, oral contribution, paper 115Ortho1, (Berlin, Germany, 2012).

Conlisk, N., Pankaj, P., Howie, C. R., "Evaluation Of Femoral Component Micromotion After Total Knee Arthroplasty: An Experimental Study", 10th International Symposium of Computer Methods in Biomechanics and Biomedical Engineering, poster, paper 115P, (Berlin, Germany, 2012).

Conlisk, N., Pankaj, P., Howie, C. R., "implant-bone micromotion after total knee arthroplasty", 23rd Congress of the International Society of Biomechanics, poster, (Brussels, Belgium, 2011).

Conlisk, N., Pankaj, P., Howie, C. R., "Reduction in distal femoral bone stresses post total knee arthroplasty", 23rd Congress of the International Society of Biomechanics, poster, (Brussels, Belgium, 2011).

Conlisk, N., Pankaj, P., Howie, C. R., "Micromotion of Uncemented Femoral Components after Primary and Revision Total Knee Arthroplasty", 57th Annual meeting of the Orthopaedic Research Society, poster, (Long Beach California, USA, 2011).

Conlisk, N., Pankaj, P., Howie, C. R., "Stress Shielding in the Distal Femur after Total Knee Arthroplasty", 57th Annual meeting of the Orthopaedic Research Society, poster, (Long Beach California, USA, 2011).

Conlisk, N., Pankaj, P., Howie, C. R., "The distal femur: Stress/strain environment and implant stability after TKA", British Orthopaedic Research Society, poster, (Cardiff, UK, 2010).

Conlisk, N., Pankaj, P., Howie, C. R., "Effect of femoral component design and fixation on the mechanical environment of the distal femur", 17th Congress of the European Society of Biomechanics, oral contribution, paper 340, (Edinburgh, UK, 2010).

Conlisk, N., Pankaj, P., Howie, C. R., "Stability of uncemented implants after total knee arthroplasty", 17th Congress of the European Society of Biomechanics, poster, (Edinburgh, UK, 2010).

Conlisk, N., Pankaj, P., Howie, C. R., "Mechanics and Stability after TKA", Proceedings of 9th International Symposium of Computer Methods in Biomechanics and Biomedical Engineering, oral contribution, paper 96Ortho2, (Valencia, Spain, 2010).

# *Table of Contents*

# *Table of Figures*

# *Table of Tables*

# I

# Introduction

## I.1 Total Knee Arthroplasty: History and overview

The knee joint is one of the largest and most complex joints in the human body. It is capable of withstanding loads many times that of body weight on a daily basis depending on the activities undertaken.

Due to traumatic injury or through diseases such as osteoarthritis the function of this joint can become severely impaired. This can lead to pain, reduced mobility and can greatly impact on the overall quality of life. This is particularly difficult for individuals in certain eastern cultures where bending or kneeling forms a much larger part of daily life (e.g. as part of religious rituals) than in western cultures. In the case of irreparable damage to the articular surfaces of the knee a common treatment method employed by surgeons is total knee arthroplasty (TKA). In short, this involves the replacement of damaged or diseased tissue with prosthesis in an attempt to ease pain and restore "normal" function to the joint.

The number of TKA operations performed each year continues to increase across the world, with Scotland seeing 6884 knee replacements (Figure 1.1) in 2009, 8.20% of which were revision procedures (NHS Scotland 2010). The history of total knee arthroplasty stretches back over 70 years. Initially the underlying mechanisms of the knee joint were not well understood and as a result this led to poor outcomes and survival rates for early implant designs, as evident by the comments of one author in an early review of the procedure:

*"Patients need to be aware that if the operation fails they may end up with a stiff knee or even no knee at all"(Anonymous 1976).*

In the 1970s, spurred on by the advent of the low-friction hip arthroplasty (Charnley 1972) and its apparent success, surgeons and engineers once again began to investigate ways to improve the functionality and outcomes of total knee replacement. This led to the development of a range of more sophisticated components with much less constraint than the early hinge type prostheses. The current generation of prostheses leverage advances in materials and manufacturing, coupled with a greater understanding of the underlying mechanisms, to provide more durable components for restoring near physiological function to the affected joint.

Studies have shown that TKA is, in general, a successful operation with patient satisfaction rates of 90-95% and implant survival rates at 10-15 years of greater than 90% (Scuderi et al. 1989, D'Lima et al. 2001b). However, a number of studies have also shown the potential for failures or complications arising post-implantation leading to a greater need for revision surgery (Frosch et al. 2004).

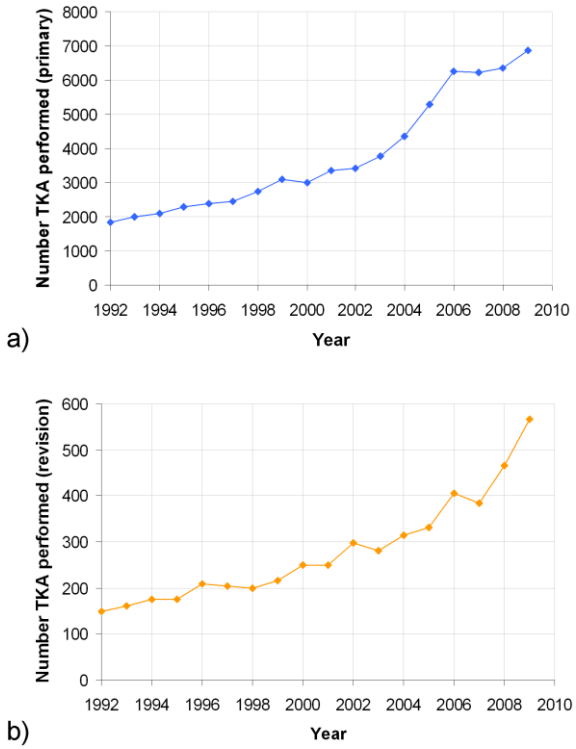


**Figure 1.1:** a) Number of knee surgeries in Scotland from 1992-2008 b) Number of revision knee surgeries 1992-2008, reproduced from (NHS Scotland 2009, NHS Scotland 2010).

Global trends as evident from information provided by several national arthroplasty databases indicate that currently as many as 9% of all TKA operations performed will require revision (Table 1.1), with increasing risk proportional to time since operation (AOA 2011).

**Table 1.1:** Joint Replacement Registry information.

| Database | Revision rate (%) |
|---|---|
| Australian Orthopaedic Association (AOA) | 8.3 |
| Canadian Joint Replacement Registry (CJRR) | 6.3 |
| Norwegian Arthroplasty Register (NAR) | 8.9 |
| Scottish Arthroplasty Project (SAP; NHS Scotland) | 8.2 |
| National Joint Registry for England and Whales (NJR) | 6.2 |

The most commonly attributed cause reported for revision is aseptic loosening and/or osteolysis (CJRR 2009, NAR 2010, NHS Scotland 2010, AOA 2011, NJR 2011) followed by infection (NJR 2011).Though revision of the tibial component is far more widely investigated e.g. (Hashemi and Shirazi-Adl 2000, Completo et al. 2008a, Chong et al. 2010, Bhimji and Meneghini 2012, Cawley et al. 2012, D'Lima et al. 2012, O'Brien et al. 2012), it has been reported by some (AOA 2011) that there is less than 3% difference between number of revised tibial and femoral components. This data indicates the importance of correctly understanding the underlying mechanisms which influence long term outcomes of femoral components.

Due to advances in medicine and health care the population of the world as a whole is currently ageing (W.H.O. 2012), in short people are living longer and leading more

active lifestyles well into old age. This combination of a physically active population and drop in the average age of patients undergoing total knee arthroplasty (NAR 2010) has led to much higher demands being placed on the prosthesis in terms of physical performance, which may adversely affect its long term survival. It must also be recognised that as more and more people in an ageing population undergo TKA, there will be a corresponding increase in the rate of revision surgeries performed (Carr and Goswami 2009).

## I.2 Thesis motivation

In response to the increasing number of individuals undergoing both primary and revision TKA, for an array of different conditions and diseases, numerous manufacturers offer a wide variety of implant designs aimed at an even wider array of clinical applications. However, very few studies have been conducted on the effectiveness of key internal design features and how they may impact on component fixation and longevity. As such, the main focus of this project is to determine the effect TKA has on the mechanical environment of the femur post-operatively and the efficacy of different implants and fixation methods on the overall stability and longevity of the prosthesis. Of particular interest is:

1. The role of internal implant features in stress shielding and implant micromotion.
2. The role of fixation and stems (both cemented and uncemented) in femoral component stability.
3. The influence of age and osteoporosis on the mechanical environment in the femur.
4. How prosthesis modularity may affect clinical outcomes for patients with/without osteoporosis.
5. How incorporation of condylar defects may affect the response of the prosthesis under loading.

This study aims to answer these questions through a combination of finite element (FE) modelling and *in vitro* experimentation. The merits and issues of each approach will be presented and their application and clinical relevance considered.

## I.3 Structure of thesis

The following outlines the structure of this thesis and gives a brief overview of the contents of each chapter.

In Chapter II, a brief background to the structure and function of the human knee joint is presented. This chapter also details key characteristics of bone and the pattern of loading found at the knee joint, followed by common conditions affecting the knee joint and details of current treatment methods employed by orthopaedic surgeons such as TKA.

Chapter III presents a brief introduction to the topic of FE and outlines the core steps required to create FE models and ensure solution accuracy.

In Chapter IV, stresses and strains in the distal femur under near physiological loading are investigated using three dimensional FE models of pre- and post-total knee arthroplasty scenarios. In this chapter particular focus is given to the influence internal implant features exert on the mechanical environment in the femur.

Chapter V details the novel application of pre-existing FE modelling techniques, for the purpose of assigning inhomogeneous properties through the thickness of the cortex, and incorporating the effects of age related changes and endosteal thinning of the femur to the previously generated models introduced in Chapter IV.

In Chapter VI, FE models of the distal femur incorporating elderly patient properties and endosteal thinning are used to explore the influence of stem length on periprosthetic stress.

Chapter VII presents FE models of the distal femur in the setting of primary and revision TKA. These models incorporate frictional interfaces for the purpose of

investigating the influence of various implant types on motion at the bone-prosthesis interface under near physiological loading conditions. Issues of implant fit are also considered.

Chapter VIII details the development and implementation of a custom *in vitro* test rig which permitted the measurement of relative motion between bone and implant in all six degrees of freedom at a range of flexion angles.

In Chapter IX, FE models based on the previous lab setup are developed with the purpose of providing additional information to compliment the *in vitro* study. Of particular interest is the quantification of elastic deformations and how they may affect the trends observed *in vitro*.

Chapter X details the investigation of stresses at the interface between the stem and implant in the presence of condylar defects of varying severity treated with augments. Factors leading to a potential increase in the risk of junction failure are discussed in this chapter.

In Chapter XI, the key findings are summarised and the main conclusions drawn from this body of research are presented. The scope for possible improvements and future development is also considered.

## I.4 Original contribution to knowledge

This thesis contributes to the current body of knowledge in a number of key areas:

1. Detailed three dimensional models of the distal femur both pre- and post-total knee arthroplasty are developed to determine what influence femoral component internal geometry exerts on the mechanical environment in the distal femur. Information on the pattern and magnitude of stress shielding caused by various implant types can also be obtained from these models.
2. A novel approach for the incorporation of age and endosteal thinning of the cortex has been presented. This method has the potential to become a powerful tool, due to its ability to model a wide range of patient scenarios on a single geometry.
3. An *in vitro* laboratory setup capable of measuring relative motion between femoral component and bone at the knee joint in all six degrees of freedom for multiple implant types is developed. This test rig provides valuable insight into the loosening behaviour of the various implants tested, and provides a basis for a more informed decision making process when determining a suitable level of implant fixation at the time of operation (e.g. cemented/uncemented and stemmed/stemless).
4. Three dimensional models of the distal femur are developed based on the *in vitro* laboratory setup. These models implement a virtual representation of the micromotion rig and allow the extraction of 'true' levels of motion at each surface of the bone-implant interface under *in vitro* loading conditions.
5. Models of the distal femur following treatment for condylar defects of increasing severity (F2 and F3) based on the Engh classification system (Engh 2006) are also developed; these models provide insight into the role of osseous support on stress in the junctions of modular components.

The above items collectively contribute to the current body of knowledge on the fixation and long term stability of total knee arthroplasty.

# II

# Background

## II.1 Introduction

This Chapter first discusses the human knee joint, its anatomy and function. This is followed by an overview of the loads which act on the knee joint under the various patterns of gait common to daily life. The final portion of this Chapter focuses on the possible ways in which the knee joint can deteriorate, and the manner in which implanted joints can fail.

### II.1.1 Anatomical reference system

In the field of biomechanics, terms used to define position, direction and movement are typically expressed relative to the anatomical position. This anatomical referencing system (Figure 2.1) provides a framework to facilitate a common understanding between experts from fields such as biomechanics, medicine and engineering when discussing matters relating to the positioning of medical devices within the body or when simply discussing the relative motion of one or more body segments. In keeping with this common framework, this thesis will make extensive use of anatomical directions and terminology, both during the description of models or experimental setups and when conveying the key findings.

Referring to Figure 2.1, the planes serve the purpose of segmenting the entire body into different regions:

- The frontal plane, alternatively referred to as the coronal plane, divides the body into anterior (front) and posterior (back) sections.

- The transverse plane divides the body into superior (upper) and inferior (lower) regions.
- The sagittal plane splits the body into left and right segments.

Other relevant anatomical directional terminologies are:

- Medial: towards the longitudinal axis in the frontal plane.
- Lateral: away from the longitudinal axis in the frontal plane.

Some further positions are referenced with respect to the particular body segment which they are describing such as:

- Proximal: A location close to the trunk (torso).
- Distal: A location away from the trunk (torso).

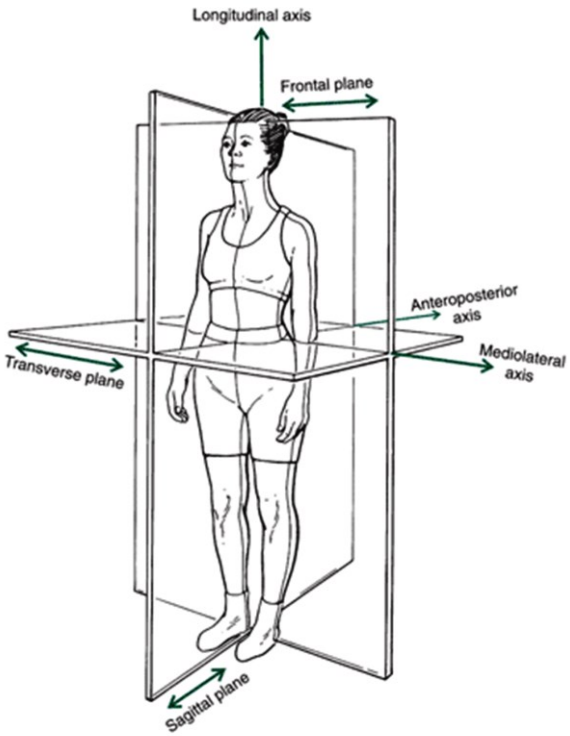


**Figure 2.1:** Illustration of a person in the anatomical reference position with main body planes identified. From Hamill and Knutzen (2008).

## II.2 The human knee joint

The knee joint is one of the largest joints in the human body. Its relative size is matched only by its underlying complexity. Structurally, the knee is composed of the distal femur (thigh bone), the proximal tibia (shin bone), the patella (knee cap) and the fibula, as illustrated in Figure 2.2. Attached to these bones are a number of muscles, ligaments and soft tissue. Stability of the skeletal structure during stationary and ambulatory tasks is achieved through a complex arrangement of fibrous structures (muscles and ligaments). These structures are found in all the regions of the human body where two or more bones meet to form a joint. The composition and function of each of these structures is explained in more detail in the following subsections.

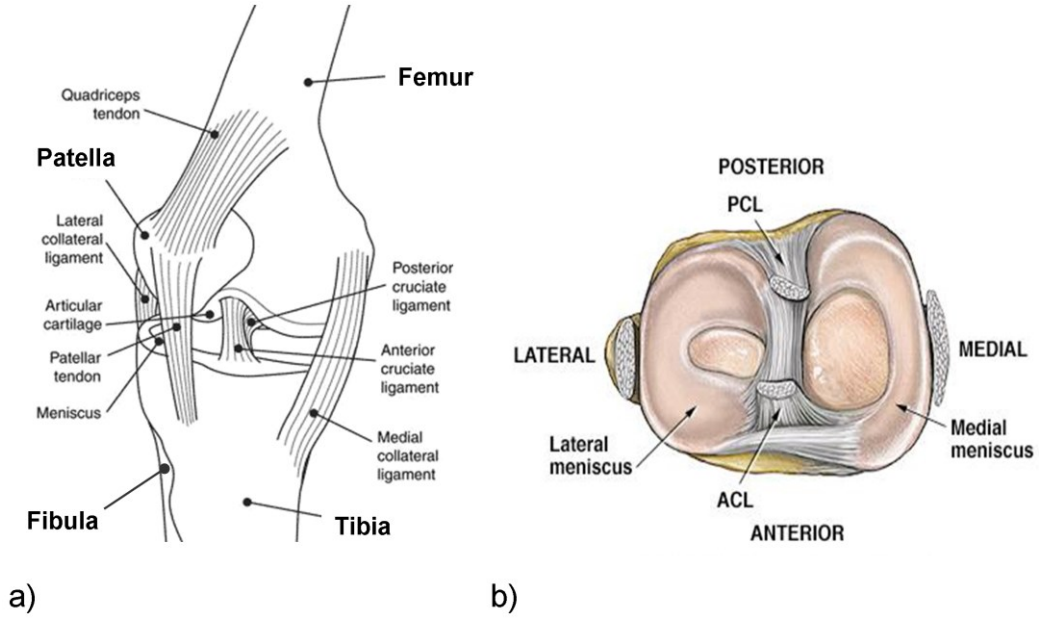


**Figure 2.2:** Illustration showing a) lateral view of the human knee joint with bony landmarks identified and b) a cross-sectional view of the ligaments in the transverse plane. Lateral view of the knee and transverse images of ligamentous structures of the knee, Retrieved on 28/05/2009, 2009, from (http://www.niams.nih.gov/health_info/Sports_Injuries/default.asp#ra_13) and (http://www.arthroscopy.com/sp05001.htm) respectively.

### II.2.1 Ligaments of the knee joint

Ligaments are tough yet flexible chord like structures that span the joint space between the bones. Their primary function is to add stability to the joints and restrain certain components of motion during articulation of the joints. Referring to Figure 2.2, the four main ligaments associated with stability of the knee are, the anterior cruciate ligament (ACL), the posterior cruciate ligament (PCL) and the medial and lateral collateral ligaments (MCL and LCL).

The ACL originates on the medial side of the lateral femoral condyle and passes anteriorly and down to attach to the anterior intercondylar area of the tibial plateau. The function of the ACL is to restrain forward sliding of the tibia on the femur during flexion. The PCL is the stronger of the cruciate ligaments and prevents backward motion of the tibia or forward displacement of the femur. This ligament is attached to the posterior intercondylar area of the tibia and the lateral side of the medial femoral condyle.

The MCL ligament runs from the medial epicondyle of the femur to the medial condyle of the tibial shaft. The LCL ligament runs from the lateral femoral epicondyle to the fibular head. Both the MCL and LCL are primarily responsible for preventing medial and lateral rotations of the joint when the knee is in the fully extended position. The collateral ligaments also serve to prevent side to side movements with the aid of the meniscal cartilage (Hamill and Knutzen 2008).

In addition to the role of the aforementioned ligaments in the stability of the knee, the knee joint itself is enclosed by a tough but flexible membrane referred to as the joint capsule or capsular ligament, which further assists in stabilising the knee joint and protecting it from injury while also allowing freedom of movement (Waugh and Grant 2010).

### II.2.2 Muscles of the lower limb

Muscles, on the other hand, are the primary movers of our limbs. All the motions necessary for daily life are achieved through a complex coordination of muscle contraction and relaxation acting about the various bodily segments of the skeleton. In the case of the lower limb, muscles act in different combinations about the pelvis, femur, and tibia to produce the desired pattern of gait (e.g. walking or chair rise).

Our skeleton is composed of 206 bones and over three times as many muscles. In the lower limb region some of these muscles span the entire length of the femur from pelvis to tibia (e.g. Gracilis), and are involved in the articulation of the femur at both the hip and knee joints. These muscles, though not directly connected to the femur, still exert an influence on its motion. For example, at the hip joint Gracilis is responsible for adduction of the thigh, whereas at the knee joint it aids in flexion of the leg (Warfel 1993). If the leg is in a fixed position then Gracilis is responsible for flexing the pelvis at the hip (Wheeless 1996b). Similarly, the Biceps femoris muscle is responsible for extension of the pelvis at the hip and flexion of the tibia at the knee.

Muscles are commonly grouped or classified according to their role in motion, e.g. *flexors* and *extensors*, however, as shown in the previous example some muscles can act as both a flexor and an extensor depending on which joint is being investigated. Figure 2.3 illustrates some of the major muscles of the lower limb, Table 2.1 then provides a brief overview of their role in motion at the knee joint.

It can be seen from Table 2.1 that the role of straightening the knee following flexion, relies on the rectus femoris, vastus lateralis, vastus medialis and the vastus intermedius. Collectively these muscles are known as the *quadriceps*. Extension of the knee joint is opposed by several muscles, however, the strongest of these are known as the hamstrings and consist of the semimembranosus, semitendinosus and biceps femoris. It can also be seen from Table 2.1 that many muscles work together and assist in performing the same function. However, that there are instances where opposing muscle also work together. This simultaneous contraction and relaxation of

the different muscle groups, or agonistic/antagonistic relationship, allows for better control of limb speed and orientation during more challenging movements. The most recognisable example of this control mechanism in action is the simultaneous activation of the quadriceps and relaxation of the hamstrings muscle groups to allow the lower limb to be straightened into full extension from a flexed position.

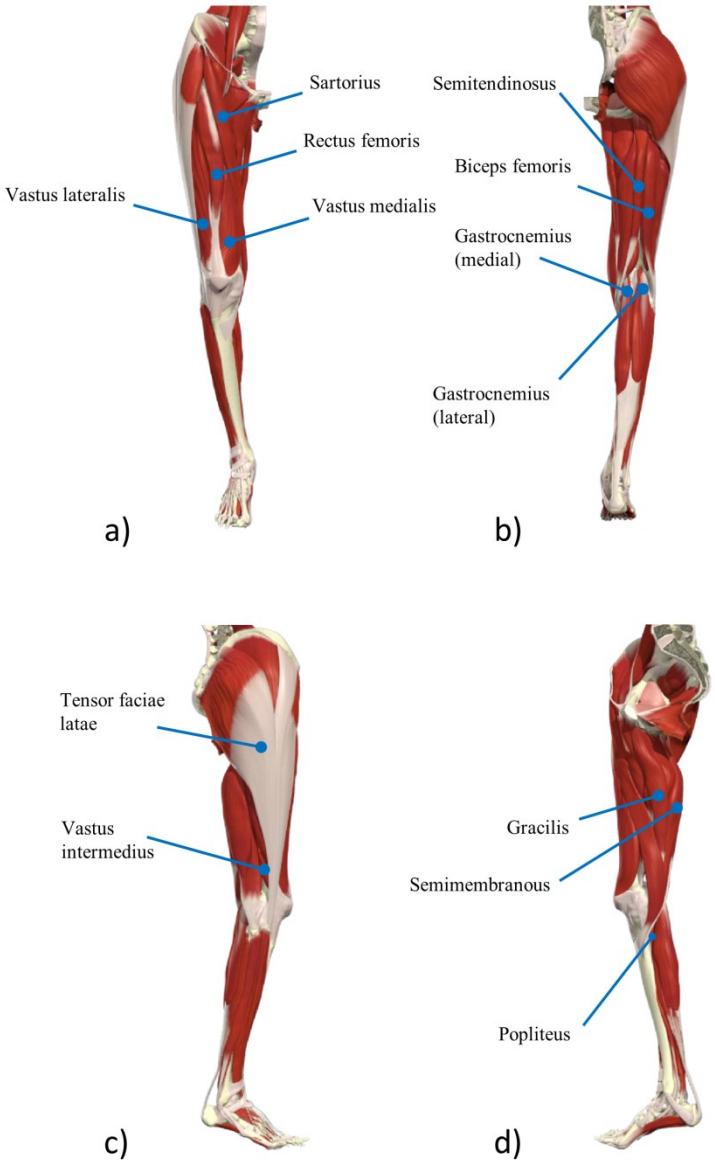


**Figure 2.3:** Illustration of the lower limb in a) the anterior, b) posterior, c) lateral, and d) medial directions, with a number of key muscles identified corresponding to those discussed in Table 2.1, illustration of the lower limb adapted from primal pictures (Primal Pictures 2007).

**Table 2.1:** Example of origin/insertion data for some of the key muscles in the lower limb, with information on the muscles role in motion at the knee joint.

| Muscle | Origin | Insertion | Action |
|---|---|---|---|
| Biceps femoris | Ischial tuberosity | Lateral condyle of tibia, head of fibula | Flexion |
| Gastrocnemius | Medial, lateral condyles of the femur | Calcaneus | Assists in flexion |
| Gracilis | Inferior rami of pubis | Medial surface of tibia | Assists in flexion |
| Popliteus | Laterial condyle of femur | Proximal tibia | Assists in flexion |
| Rectus femoris | Anterior inferior iliac spine | Tibia via patella | Extension |
| Sartorius | Anterior inferior iliac spine | Medial surface of tibia | Assists in flexion |
| Semimembranous | Ischial tuberosity | Medial condyle of tibia | Flexion |
| Semitendinosus | Ischial tuberosity | Medial surface of tibia | Flexion |
| Vastus intermedius | Anterior lateral femur | Tibia via patella | Extension |
| Vastus lateralis | Intertrochanteric line, linea aspera | Tibia via patella | Extension |
| Vastus medialis | Linea aspera, intertrochanteric line | Tibia via patella | Extension |
| Tensor fasciae latae | Anterior iliac crest | Iliotibial tract | Stabilises knee laterally |

Apart from their role in movement and stabilisation of the joints, muscles also provide a number of other essential functions, such as generation of body heat, protection of organs and regulation of internal pressure (Hamill and Knutzen 2008).

### II.2.3 Cartilage structure and function

Due to the magnitude of load experienced by the knee on a daily basis (in excess of eight times body weight, as discussed later), direct bone on bone contact would result in high interface friction and rapid wear of the articulating surfaces, leading to severe joint pain during motion.

Articular or *hyaline* cartilage is a special type of soft tissue that lines the contacting surfaces of the bones in the knee joint (distal surface of the femur, the proximal surface of the tibia and the posterior surface of the patella), as shown in Figure 2.2. This cartilage is formed by several generations of cells known as *chondrocytes*, which create a dense extracellular matrix principally composed of water (60-80%), collagen fibres (Figure 2.4) and proteoglycan gel (Mow et al. 1992, Hamill and Knutzen 2008, Fox et al. 2009). Unlike other structures of the knee joint (e.g. bone or muscles), the articular cartilage is avascular in nature and contains no nerve endings. The presence of collagen gives the cartilage its stiffness and strength, while the highly hydrated proteoglycan gel aids in its viscoelastic response to instantaneous shock loading (Fox et al. 2009).

Stress distribution in the cartilage is principally determined by the alignment of the joint and by cartilage thickness. The articular cartilage serves an important function in the knee joint by increasing the contact area over which loads are distributed. It has been suggested that the presence of cartilage on the contacting surfaces of joints can help to reduce contact stresses by as much as 50% (Soderberg 1986). In a young person's knee the articular cartilage can be up to 7mm thick. However, with ageing, the cartilage becomes thinner and loses its elasticity (Waugh and Grant 2010). Loss of cartilage thickness combined with a more stiff matrix may seriously impact on the

ability of the cartilage to protect the load bearing surfaces of the joint, leading to increased wear on the joint due to load being distributed over a smaller area.

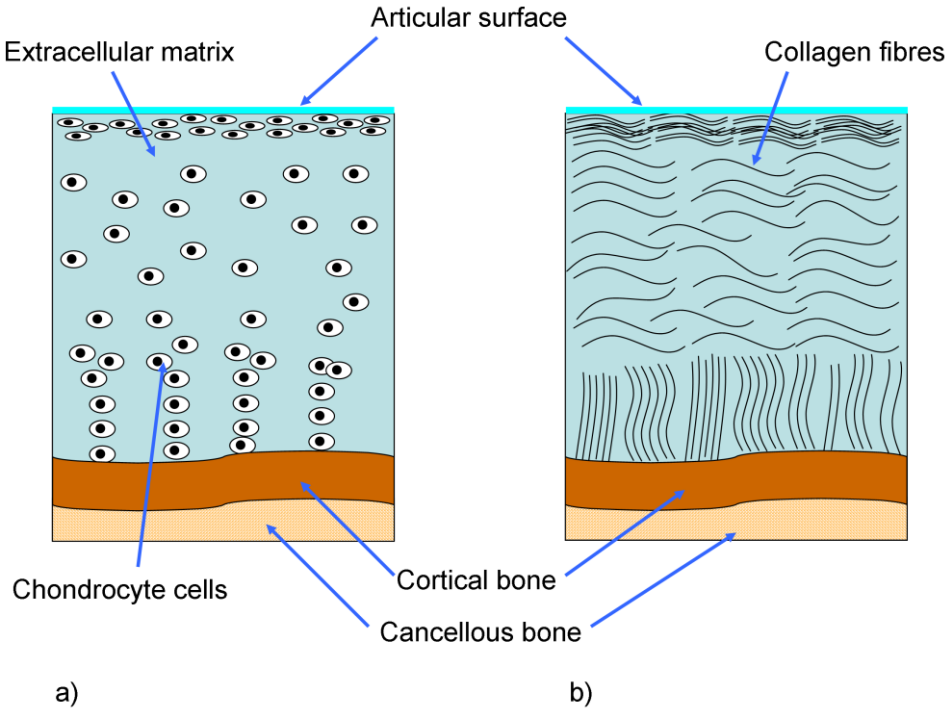


**Figure 2.4:** Cross-sectional illustration of the composition of healthy hyaline joint cartilage. a) Represents the extracellular matrix and b) shows the arrangement of collagen fibres within the cartilage (Author illustration).

Another important function of the articular cartilage is to assist the synovium[1] by aiding in the lubrication of the joint lining. In this role, the cartilage helps to clear away debris by washing out the joint space, and aids in maintaining an almost frictionless interface between the articulating bony structures, thereby allowing the various joint structures to effortlessly glide over one and other. The coefficient of friction for this type of joint is reportedly in the range of 0.01-0.04 (Hamill and Knutzen 2008).

In addition to the articular cartilage, another type of cartilage exists in the knee joint, the fibrocartilage. This tough form of cartilage is found at the transition of hyaline

[1] The synovium is a thin layer of cells between the joint capsule and the joint space and is responsible for the production and filtering of synovial fluid.

cartilage and other connective tissue and is crescent shaped in appearance. As with the articular cartilage, the composition of the fibrocartilage is a complex extracellular matrix composed primarily of water (72%), collagen (22%) and interposed with cells known as fibrochondrocytes (Fox et al. 2012).

In the knee joint, two fibrocartilage discs exist, these discs more commonly referred to as the menisci, attach to the tibia, one each to the medial and the lateral tibial condyle (Figure 2.2b). Each meniscus serves to deepen the articulating surface of the tibia and helps to improve conformity of the distal femoral condyles during articulation. Due to the shape of the menisci, these structures also help to restrain side to side translational motions of the joint (Hamill and Knutzen 2008, Waugh and Grant 2010). Fibrocartilage structures are found throughout the body where tensile strength and the ability to withstand significant pressure are necessary.

### II.2.4 Articulation of the knee joint

According to Komdeur et al.(2002), the human knee joint is considered to behave as a *"bicondylar modified hinge joint"* with six degrees of freedom, characterized by three translational and three rotational components of motion (Figure 2.5). The translational components are described clinically in the anatomical reference system as medial/lateral, anterior/posterior and superior/inferior motion. The three rotational components in the same system are described as flexion/extension, internal/external rotation and abduction/adduction.The terms used to describe the degrees of freedom at the knee joint have the following meanings:

**Anterior/Posterior:** this motion describes front to back displacement of the tibia relative to the femur in the sagittal plane.

**Medial/Lateral:** this motion describes the side to side displacement of the tibial relative to the femur in the frontal plane.

**Superior/Inferior:** this motion describes the displacement of the femur or tibial along its own axis.

**Flexion/Extension:** in general, flexion is a motion which results in a decrease of the relative joint angle between two adjacent bones. In the case of the knee, this describes the decreasing joint angle between the distal portion of the femur and the proximal portion of the tibia. Extension, on the other hand, can be thought of as the opposite to flexion and describes a relative increase in joint angle between bones until they have returned to the anatomical position commonly known as 'full extension'. This motion is one of the characteristic motions of the knee joint and plays a major role in permitting a wide range of daily activities to be performed such as ascending/descending stairs, kneeling, sitting down or rising from a chair. However, two other key rotational components of motion are required to fully allow the wide range of motions required for daily life.

**Internal/External rotation:** this is the rotation of the tibia about its own axis.

**Abduction/Adduction:** this describes the rotation of the tibia away from/towards the midline of the body in the frontal plane.

The characteristic motions of the knee joint necessary to carry out everyday motions and movements are achieved through the coordinated movements of two separate articulating surfaces; the patella-femoral joint and the tibio-femoral joint.

The patella-femoral joint consists of the articulation of the patella, more commonly referred to as the 'knee cap', on the anterior surface of the distal femur. The patella is most active from approximately 20° to 90° of knee flexion. During this range of motion, the patella glides over the front surface of the femur and is drawn downward into the trochlear groove where it is held in place by the lateral condyle. At higher flexion angles, for example during a deep knee bend, the patella moves laterally over the condyle until around 135° is reached. At this point, contact is made with the odd facet of the patella (Hamill and Knutzen 2008). The patella is attached to the femur through the quadriceps tendon proximally and to the tibia through the patellar ligament distally. The patella serves to increase the distance between the quadriceps tendon and the centre of rotation of the knee joint, thereby increasing the lever arm

of the quadriceps. At higher flexion angles the patella-femoral joint reaction force can be many times that of body weight (BW), as is discussed later in section II.3.3.

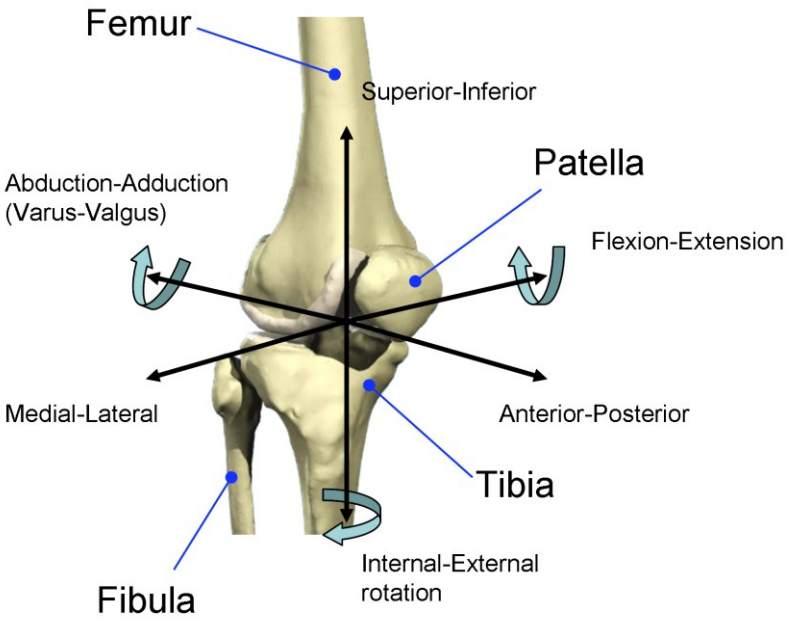


**Figure 2.5** Illustration of knee joint, showing all the major bony structures, the individual degrees of freedom and corresponding directional terminology. Image of knee adapted from primal pictures (Primal Pictures 2007).

The tibio-femoral joint consists of the proximal tibia and distal femur, its articulation results in the characteristic flexion/extension motion of the knee, while also allowing small amounts of internal/external rotation. The articulation of the tibio-femoral joint consists of two components of motion that occur almost simultaneously. For example in the task of rising from a chair, the first motion involved is sliding of the femur in the posterior direction on the posterior aspect of the condyles, as the femur begins to erect the condyles roll forward bringing the distal femur into contact with the menisci (Hamill and Knutzen 2008), and the final phase in this movement cycle is medial rotation of the medial femoral condyle on the tibial surface thus locking the knee in a rigid position capable of supporting full body weight. This small rotation of the femur on the tibia allows the femur to achieve full extension without causing undue fatigue of the surrounding muscles. This function is commonly referred to as the screw home mechanism (Komdeur et al. 2002). The rotation of the femur on the tibia

(or in the case of a fixed femur external rotation of the tibia) is an important step in the extension process as without this rotation the femur cannot fully extend due to the asymmetrical nature of the femoral condyles (i.e. the medial condyle is slightly larger than the lateral).

## II.3 Physiological loading of the knee joint

In the following subsections, issues associated with alignment of the lower limb, components of the gait cycle, and the typical forces the knee joint is under will be discussed.

### II.3.1 Alignment of the lower limb

In the field of biomechanics alignment of the lower limb is traditionally expressed in terms of its mechanical axis. The mechanical axis is described in the frontal plane by a line drawn from the centre of the femoral head to intercondylar notch and from the centre of the proximal tibia to the centre of the ankle (Scuderi and Tria 2006), as shown in Figure 2.6. In the sagittal plane, this line is placed just behind the femoral head and in front of the knee joint, and is almost perpendicular to the ground. In the frontal plane, this line is approximately 3° from the true vertical axis of the body due to the distance separating the hips being larger than the distance of separation at the ankles.

An important measure of alignment can be gained by comparing the mechanical axis to the weight bearing axis, where the weight bearing axis is represented by a line drawn from the center of the femoral head to the center of the ankle (Figure 2.7a). In healthy joints with ideal alignment, the mechanical axis and the weight bearing axis of the lower limb overlap (Wheeless 1996a). However, in situations where malalignment of the limbs occur due to geometrical irregularities or through deformities as a result of disease, these two axes may not necessarily be aligned, as shown in Figure 2.7b.

Malalignment is traditionally categorised based on whether the affected limb has moved towards *"varus"* (Figure 2.7c) or away from *"valgus"* the midline of the body (Figure 2.7d). The degree of malalignment can have serious implications for joint longevity, according to Burstein (1994), load distribution across the condyles may be drastically altered depending on the extent of malalignment. Recent work by Halder et al. (2012) quantified the relationship between varus malalignment and increased medial compartmental stress as a linear relationship, where a change of 1° varus from the neutral alignment caused a 5% increase in medial compartmental loading. Alteration of the loads acting across the condyles which lead to an increase in local contact forces in some regions may be a contributing factor to accelerated wear of the articular cartilage, and ultimately failure of the joint itself.

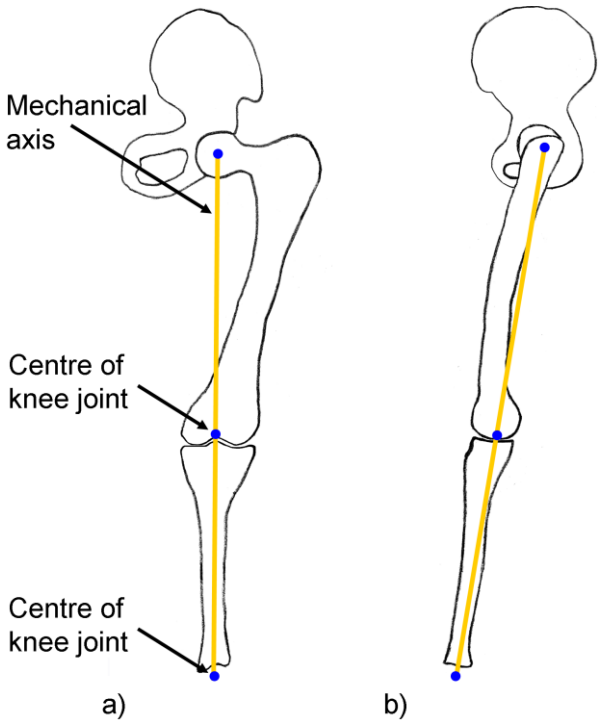


**Figure 2.6:** Anatomical illustration of the lower limb indicating the mechanical axis in a) the frontal and b) the sagittal plane. (Author illustration).

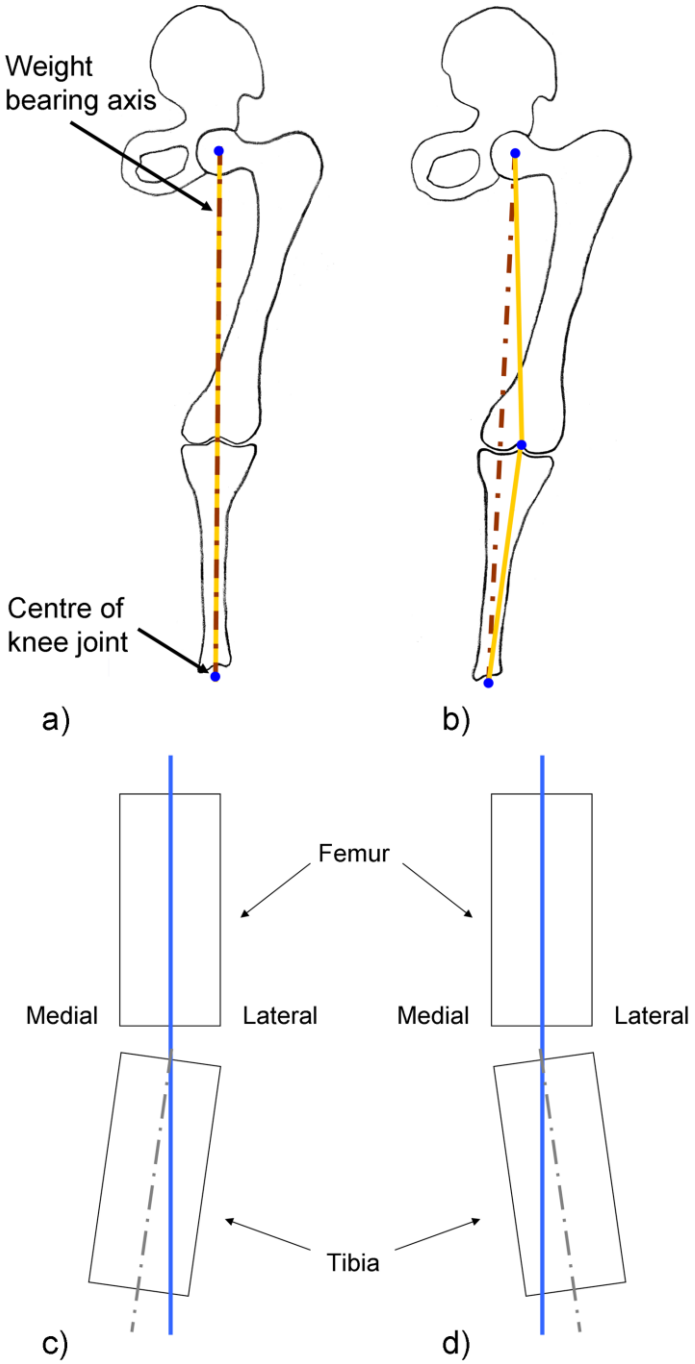


**Figure 2.7:** Anatomical sketches showing a) how the mechanical (yellow) and weight bearing (dashed brown) axes in a healthy lower limb with normal alignment overlap and b) how malalignment of the lower limb results in a difference between mechanical axis and weight bearing axis. Parts c) and d) present schematic drawings of the two types of malalignment, where c) represents varus, and d) valgus malalignment of the lower limb, normal tibio-femoral alignment is indicated by the solid blue line. (Author illustration).

In replacement knee surgery, surgeons attempt to correct deformities to the joint line and the mechanical axis through correct placement of the prosthesis, and thereby restore the patient's normal pattern of gait. To ensure proper placement of the prosthesis is achieved, specialist guides are used to align the implants in the frontal, sagittal and horizontal planes. The recommended generic guidelines for alignment of a femoral component according to Scuderi and Tria (2006) are as follows:

- Implant should be placed with a valgus angle of 4°-6°.
- Implant should be centred on the end of the femoral shaft with respect to the anteroposterior plane.
- Component should avoid being too flexed or extended and should include 3°-4° of external rotation.

In an effort to restore a more natural alignment to the lower limb following TKA, some surgeons opt for implant placement on the basis of the kinematic alignment, rather than the mechanical axis. In contrast to the method for defining the mechanical axis, e.g. alignment in two planes based on x-rays, the kinematic method attempts to align the implant in three-dimensional space using detailed measurements of a patient's joint from MRI reconstructions, from which custom guides are created to align the implant to the patient's weight bearing axis. Though the kinematic alignment technique provides a better patient specific placement, recent research suggests comparable outcomes for both techniques (Nogler et al. 2012).

### II.3.2 Components of a gait cycle

Gait is the term used to describe the manner in which a person achieves motion through the coordinated movement of their limbs. The most common and widely investigated form of gait in humans is level walking. A typical walking cycle lasts approximately 1 second and is measured from heel strike to heel strike of the same

foot. This gait cycle is essentially composed of two phases; the stance phase and the swing phase. In level walking, the stance phase of gait accounts for 60% of the cycle time, the remaining 40% is dedicated to the swing phase as shown in Figure 2.8.

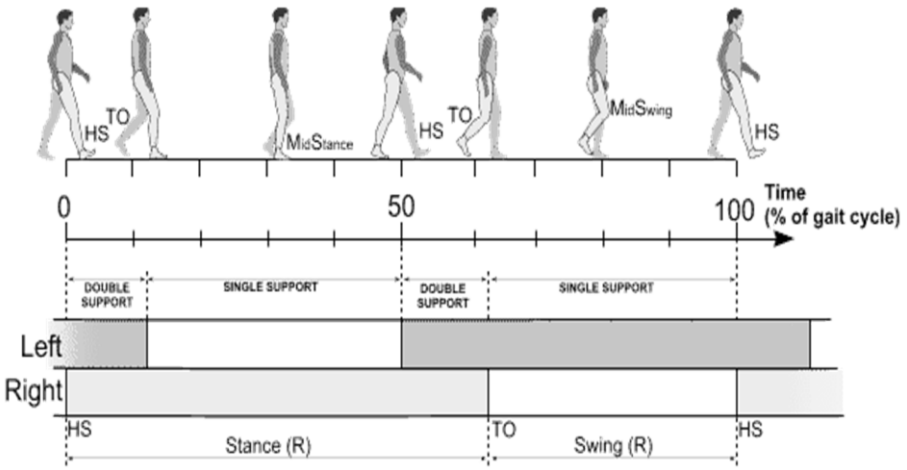


**Figure 2.8:** Illustration of the major components of a normal walking gait cycle indicating heel strike (HS) and toe off (TO) for the right lower limb. Illustration adapted from. (http://www.gla.ac.uk/ibls/US/fab/tutorial/anatomy/hfgait.html), retrieved 19/10/2011, 2011.

- The stance phase of gait is the period during which the lower limb is in contact with the ground.
- The swing phase of gait is the period when the lower limb is no longer in contact with the ground following toe off, as such the force in the limb during swing phase is significantly lower than during stance phase.

Referring to Figure 2.8, it can be seen that the stance phase of gait consists of a number of subdivisions, dependent on the manner of limb contact with ground. Initially at heel strike both legs are in contact with the ground simultaneously, this period is known as *double support*, from heel strike the foot then progresses to foot flat and *single support* at the instance of contralateral toe off. The final 10% of stance phase then reverts to double support in preparation for toe off of the load bearing foot at the instance of heel strike of the contralateral foot.

Daily activities are often categorised based on the required range of motion necessary to carry out a specific task, for a normal walking cycle the required range of motion at the knee joint is approximately 0°- 70° (Taunton et al. 1985). However, certain activities, e.g. squatting, require a significantly larger range of motion. Activities which require flexion of the knee joint greater than 120° are collectively referred to as "high flexion" activities (Murphy et al. 2009), in comparison to normal walking and a few other daily activities which are considered to be "low flexion" activities. Details of the range of knee joint motion required for a number of common daily activities is presented in Table 2.2.

**Table 2.2:** Typical values of knee flexion required for common daily activities (Taunton et al. 1985, Zhou et al. 2012).

| Activity | Knee flexion angle (°) |
|---|---|
| Walking | 0-70 |
| Ascending stairs | 0-83 |
| Descending stairs | 0-90 |
| Squatting | 0-150 |
| Kneeling | 0-140 |
| Kneeling for prayer | 0-165 |
| Running | 0-80 |
| Rising from a chair | 0-93 |

Most studies from literature tend to focus on tasks such as walking, stair climbing and rising from a chair, due to the prevalence of these particular activities in western lifestyles. However, for many cultures, in particular those of Middle Eastern and Asian origin for example, much more demanding high flexion activities, such as regularly kneeling to pray, constitute a major part of daily life (Acker et al. 2011).

Such high flexion activities require a much larger range of motion than that of stair climbing and normal walking (Table 2.2).

In a review of post-operative range of motion, Chiu et al. (2002) reported upper functional limits of between 95° and 115° flexion, for a number of early TKA designs. While adequate for the majority of low flexion activities, this is significantly lower than that required to carry out squatting or kneeling motions. This limited range of motion and the average drop in patient age at time of implantation has led to the increasing demand for greater knee flexibility after TKA, as a result, a number of high flexion implant designs have been developed (e.g. Triathlon™ CR, Stryker UK and Sigma™ CR150, DePuy UK). However, a number of post-operative studies have shown that the functional range of motion rarely exceeds 141° (Huang et al. 2005, Acker et al. 2011), this range of motion while an improvement on that reported previously by Chiu et al. still prohibits a wide range of activities that constituent a core part of daily life for many cultures (Acker et al. 2011, Zhou et al. 2012).

### II.3.3 Forces acting on the knee under different daily activities

Introduction of new implant designs is only possible after adequate testing and investigation to ensure the characteristic features of the new design do not adversely influence its fixation or longevity. This process usually involves pre-clinical testing in the form of mechanical simulators (Knight et al. 2007), FE simulations (Barink et al. 2005) and/or cadaveric testing (Wackerhagen et al. 1992). The determination of forces acting on the knee joint is essential to this pre-clinical phase. Knowledge of such forces allows for realistic patterns and magnitudes of loading to be applied *in vitro* in knee wear simulators or mechanical testing rigs and *in silico* in the numerical analysis of anatomical structures. The complex anatomical arrangement at the knee joint significantly increases the difficulty of accurately quantifying the forces which act upon it under various daily activities. The principle components of loading which the knee joint experiences are as follows:

- The axial force: due to the shape of the femur, this force is divided between the medial (Fm) and lateral (Fl) condyles usually in a 60-40% relationship, subject to varus/valgus alignment of the lower limbs (Burstein 1994, Shi 2007).
- The patella-femoral force: this is the resultant force acting on the anterior articulating surface of the femur due to the patella.
- Anteroposterior shear force: this force occurs due to front to back movement of the femur on the tibial plateau, which is resisted by the cruciate ligaments.
- Internal/external moment: The rotation of the femur on the tibial plateau.

Early investigations in the field of biomechanics employed the use of mathematical models to determine the forces acting on the knee joint (Morrison 1969), later work improved the accuracy of these techniques through the inclusion of ground reaction forces using force plate technology (Morrison 1970). However, there exists a large variability in reported loading between different analytical studies employing similar techniques (Morrison 1970, Kuster et al. 1997, Taylor et al. 2004). Part of this variability may be due to oversimplification of the degrees of freedom at the knee joint or to slight differences in behaviour considered for the surrounding soft tissue of the knee joint.

Instrumented implants first pioneered in the hip (Carlson et al. 1974, Bergmann et al. 1988) arose out of the need for accurate quantification of *in vivo* loads at the articulating interfaces. In 1988, Bergmann et al. (1988) introduced a fully instrumented hip prosthesis capable of being "safely implanted" into a human patient, for the purpose of recording the individual components of force acting on the femoral head. This prosthesis design built upon the novel inductive telemetric power and sensing techniques proposed by Carlson et al. (1974) almost a decade earlier, albeit for the purposes of cartilage contact pressure prediction.

One of the first instrumented knees was trialled in 1996, though this trial necessitated cables to supply power to the device from an external source and to feedback results to a computer (Kaufman et al. 1996) thereby limiting its potential application to *in vitro* measurements. The first *in vivo* experiments conducted for the determination of forces acting on the knee joint appears to have been carried out by Taylor et al. (1998). In this study, a single patient suffering from a malignant bone tumour was treated with an instrumented distal femoral replacement (DFR). This device replaced the entire lower portion of the femur and was connected to the tibia through a hinged femoral prosthesis. Strain measurements were taken at a level 232mm above the hinge and subsequently used to estimate components of force acting on the knee joint itself. The forces estimated for level walking ( 220-250% BW) by Taylor et al. (1998) were found to be much smaller than those suggested by analytical studies (Morrison 1970, Kuster et al. 1997, Taylor et al. 2004).

More recently, Morris and colleagues detailed the development and manufacturing of a fully instrumented TKA prostheses (e-knee) for the purpose of measuring the true value of force *in vivo* at the knee joint (Morris et al. 2001). Results from the successful application of the aforementioned device have been widely publicised (D'Lima et al. 2005, D'Lima et al. 2006, Zhao et al. 2007, D'Lima et al. 2008, Mündermann et al. 2008) and formed the corner stone of "The Grand Knee Challenge[2]" (Fregly et al. 2012).

Studies conducted with the e-knee implant, however, have been largely limited to reporting of the compressive force at the tibio-femoral joint only, and most trials were conducted with a relatively small sample size ($n = 2$). Employing a similar device to the e-knee, Heinlein et al. (2009) described the forces and moments along all three principle tibial tray axes for level walking and stair climbing. A follow on study by Kutzner et al. (2010) expanded on the work by Heinlein et al. to include a greater number of patients ($n = 5$) and a wider range of daily activities (level

[2] Now in its fourth incarnation, this has become a yearly event where researchers from around the globe try to predict the *in vivo* joint reaction forces based on an array of information from gait analysis data to instrumented implant data.

walking, ascending/descending stairs, double leg stance, single leg stance, sitting down, standing up and knee bend). A sample of the wide range of loading reported in the literature is presented in terms of tibio-femoral force (TF), patella-femoral force (PF), anterior-posterior shear force (AP) and internal-external moment (IE) in Table 2.3.

It is clear from Table 2.3 that a large variation in the reported values of loading exists. This variation is found to increase dramatically in patterns of gait which are less well investigated (e.g. squatting). Instrumented implants suggest much lower values of force for both TF and AP components in comparison to analytical and gait analysis studies. Many studies (both FE and *in vitro*) base loading conditions at the femur on the guidelines laid out by the International Standards Organisation (ISO 2004, ISO 2009). However, it is apparent from the literature that significantly larger magnitudes of force can be experienced by the knee joint under daily activities. Additionally, the limited range of flexion imposed on the implant in the ISO standards is not representative of the range experienced during daily activities other than walking (Table 2.2). A common limitation of the both the ISO standard and the instrumented knee implants is the lack of consideration of the patella-femoral force which has been seen to be significant in flexion (Table 2.3).

**Table 2.3:** Example of commonly reported values for peak knee joint loading from literature for different activities.

| Level walking | | | |
|---|---|---|---|
| Force | Range | Study | Method |
| TF (BW) | 2.5 – 4.0 | (Morrison 1970, Taylor et al. 1998) | Gait analysis and analytical model; Instrumented DFR. |
| PF (BW) | 0.7 – 1.8 | (Morrison 1970, Kuster et al. 1997) | Gait analysis and analytical model; Inverse dynamics model. |
| AP (BW) | 0.29 – 0.6 | (Taylor et al. 2004, Heinlein et al. 2009) | Gait analysis and inverse dynamics model; Instrumented TKA. |
| IE (BWmm) | 7.0 – 10.0 | (Taylor et al. 1998, Heinlein et al. 2009) | Instrumented DFR; Instrumented TKA. |
| Stairs up/down | | | |
| TF (BW) | 2.8 – 5.0 | (Taylor and Walker 2001, Taylor et al. 2004) | Instrumented DFR; Gait analysis and inverse dynamics model. |
| PF (BW) | 2.1 – 5.6 | (Nisell 1985) | Biomechanical model of the knee |
| AP (BW) | 0.26 – 1.3 | (Taylor et al. 2004, D'Lima et al. 2007) | Gait analysis and inverse dynamics model; Instrumented TKA. |
| IE (BWmm) | 6.2 – 8.0 | (Taylor et al. 1998, Heinlein et al. 2009) | Instrumented DFR; Instrumented TKA. |
| Squatting | | | |
| TF (BW) | 2.3 – 7.6 | (Dahlkvist et al. 1982, Thambyah 2008) | Motion analysis and analytical model; 3D motion analysis. |
| PF (BW) | 7.6 – 8.0 | (Reilly and Martens 1972, Nisell 1985) | Mathematical model of the knee; Biomechanical model of the knee |
| AP (BW) | 0.15 – 0.16 | (Taylor et al. 2004, D'Lima et al. 2007) | Gait analysis and inverse dynamics model; Instrumented TKA. |

## II.4 Bone: composition and mechanical properties

In the human body, the function of bone is diverse. It acts as the load bearing structure, protects vital organs from direct trauma, houses the factories from which our red blood cells are manufactured, and in combination with the skeletal muscles, it allows us to move.

At the macroscopic level, bone is primarily composed of two distinct tissues types; the compact outer layer or *cortical* bone and the spongy inner layer or *cancellous/trabecular* bone. This mixture of bony tissues permits the bone to behave in a manner similar to composite materials, allowing for relatively good strength and flexibility to be achieved while keeping overall weight and size to a minimum.

Cortical bone accounts for approximately 80% of the body's bone mass. At the macroscopic level, cortical bone has the appearance of a stiff and inert solid structure, while at the microscopic level, it is in reality a dynamic and highly vascularised complex living structure riddled with canals and passageways that serve as conduits for nerves, blood vessels and lymphatic vessels (Figure 2.9a). This type of bone is formed by a series of parallel "tubes" called osteons. Individual osteons (Figure 2.9b) are characterised by a central canal surrounded by expanding rings which resemble the cross-section of a tree trunk. Each osteon is composed of multiple lamellar layers interspersed with lacuna (small gaps containing osteocytes).

At the external surface, the cortical bone is encased in a vascular membrane known as the periosteum, internally in the metaphysis (Figure 2.9c), the bone transitions from the compact osteonal form to a less densely packed spongy structure known as cancellous bone. In this type of bone there are no haversian canals and no osteons are present. Instead, a series of thin bony bars (trabeculae) form a honeycomb or lattice structure. Red bone marrow fills in the spaces between adjoining trabeculae. Cancellous bone can have a relatively wide array of densities depending on the arrangement of its irregular microarchitecture. A study by Hodgskinson and Currey (1992) suggested a density range of 0.04-0.6 g/cm$^3$, in contrast to cortical bone, which is a much more densely packed material with maximal density estimated at 1.8

g/cm$^3$ (Terrier 1999). Cancellous bone is always surrounded by cortical bone, though the relative quantity and thickness of the cortex varies from region to region and bone to bone in the skeletal system (Cowin 2001).

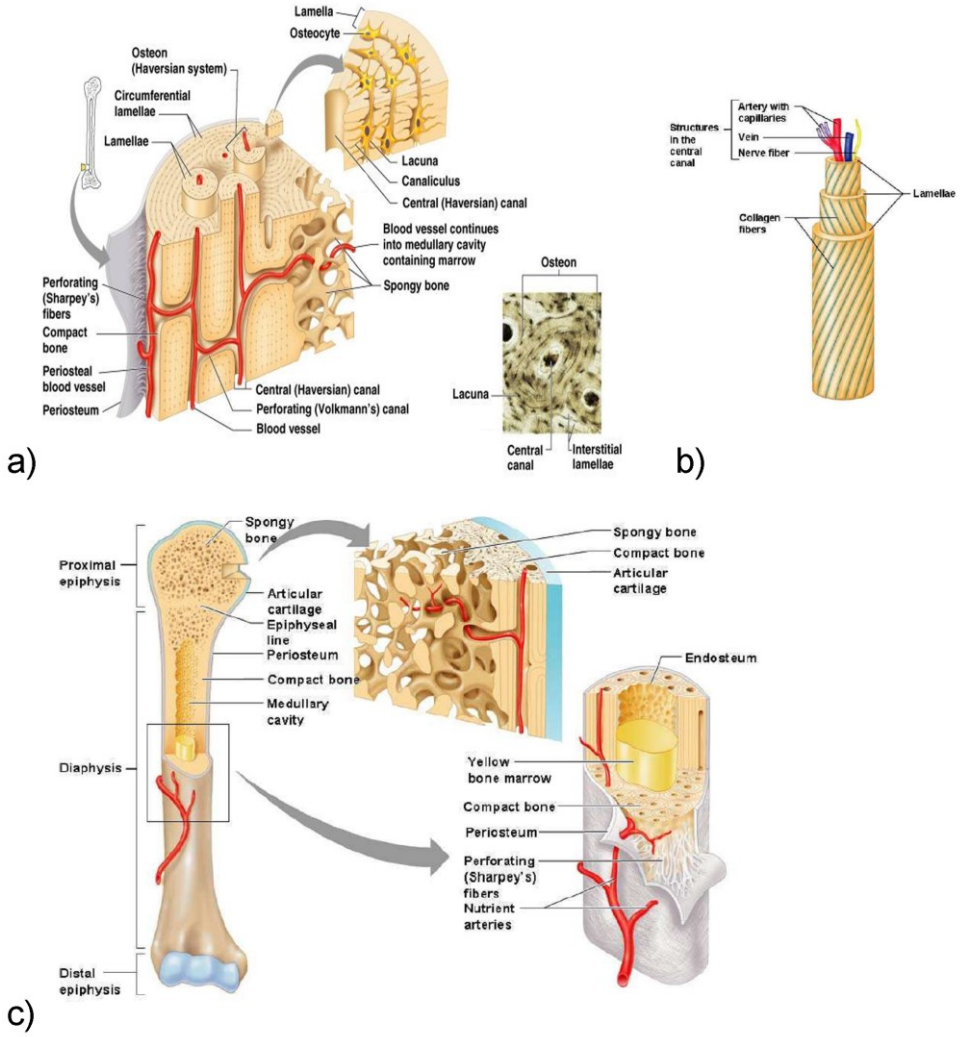


**Figure 2.9:** Illustration of a) the micro architecture of cortical bone, b) an individual osteon, and c) whole long bone structure and cancellous bone segment. Images from Marieb and Hoehn (2007).

Bone, due to its complex microstructure, exhibits anisotropic and inhomogeneous properties, and also viscoelastic behaviour when loaded at a high rate (Currey 2002). This behaviour occurs in part as a result of the intricate arrangement of osteons and trabeculae at the microscopic level, and due to the presence of water, marrow and other fluid in the interstitial regions of the bone. At lower rates of loading

(approximately 1Hz or less), as experienced during everyday activities such as walking, the viscoelastic response of bone can largely be neglected.

Extensive studies have been conducted on both human and mammalian bone tissues to evaluate their mechanical properties (Reilly and Burstein 1974, Runkle and Pugh 1975, Townsend et al. 1975a, Townsend et al. 1975b, Ashman and Rho 1988, Rice et al. 1988, Kuhn et al. 1989, Mente and Lewis 1989, Ryan and Williams 1989, Choi et al. 1990, Jensen et al. 1990, Rho et al. 1993, Terrier 1999, Zysset et al. 1999, Currey 2002). Results from a number of past investigations into both cancellous and cortical bone material properties are presented in Table 2.4.

It is apparent from Table 2.4 that quantification of bone material properties is no simple task, with numerous studies in the literature reporting very different values for both cortical and cancellous bone. It has been suggested that the wide variability in reported properties of bone can be attributed to a number of factors, such as differences in specimen orientation (e.g. longitudinal or transverse) (Reilly and Burstein 1974, Goldstein et al. 1993), specimen preparation (wet or dry) (Turner 1999), experimental protocol adopted (e.g. tensile test or ultrasound) (Townsend et al. 1975b, Turner 1999), bone type (cortical or cancellous) (Kuhn et al. 1989, Turner 1999)and species variation (human or animal) (Ryan and Williams 1989). Additionally, factors such as variation with age (Bousson et al. 2000, Bousson et al. 2001) or healthy vs. pathological (Wackerhagen et al. 1992) samples may all influence the apparent values of stiffness, strength and toughness obtained.

A recent review by Helgason et al. (2008), which discussed the mathematical relationships commonly employed to determine mechanical properties of bone from its apparent density, lends support to this conclusion. In their study, the authors showed that a certain amount of the variability in stiffness could be attributed to the previously mentioned factors (e.g. loading protocol, specimen preparation and testing methodology), indicating that greater standardisation of experimental procedures may be required in order to minimise the observed inter-study variations. However, it is important to note that after normalisation for the aforementioned factors a large

variability in stiffness still existed which cannot be fully explained by inter-study variations alone.

**Table 2.4:** Summary of commonly reported values for Young's modulus of cancellous and cortical bone structures, extract from Table 5.1 (Currey 2002).

| Study | Region | Type | Method | Young's modulus (GPa) |
|---|---|---|---|---|
| (Runkle and Pugh 1975) | Human distal femur | Cancellous | Buckling | 8.7 (dry) |
| (Townsend et al. 1975b) | Human proximal femur | Cancellous | Buckling | 14.1 (dry) |
| (Choi et al. 1990) | Human tibia | Cortical | 3-point bending | 4.4 (wet) |
| (Kuhn et al. 1989) | Human illium | Cortical | 3-point bending | 4.8 (wet) |
| (Mente and Lewis 1989) | Human femur | Cancellous | Cantilever and FE | 6.2 (wet) |
| (Jensen et al. 1990) | Human vertebra | Cancellous | Structural analysis | 3.8 |
| (Turner 1999) | Human femur | Cancellous | Ultrasound | 17.5 (wet) |
| | | Cortical | Nano-indentation | 20.0 (dry) |
| (Zysset et al. 1999) | Human femur | Cancellous | Nano-indentation | 11.4 (wet) |

The lack of consensus in reported mechanical properties of bone in the literature has been a long running issue in the field of biomechanics, particularly when trying to quantify the difference between cancellous and cortical bone structures. To quote Professor Currey:

"*The results are a real dog's breakfast, with different workers suggesting very different values…..*" - (Currey 2002).

In the same text Professor Currey went on to state:

*"....consensus is that the Young's modulus for the material of cancellous bone is lower than that of neighbouring compact bone.*"

On comparing individual trabeculae to cortical bone specimens of similar size and volume, at the microscopic scale both materials have been found to exhibit similar magnitudes of stiffness. At the macroscopic level, however, these two tissue types display vastly different behaviour. The arrangement of the microarchitecture and highly porous nature of cancellous bone as a whole greatly influences its macroscopic properties, resulting in a much lower macro-level or apparent stiffness than that of the densely packed neighbouring cortical bone (van Rietbergen et al. 1995). The apparent macro-level stiffness for cancellous bone has been reported to be in the range of 0.1 – 8.0 GPa (Goldstein 1987, Choi et al. 1990, Hodgskinson and Currey 1992, Hodgskinson et al. 1997), whereas for the compact cortical bone it is significantly higher at 11-20 GPa (Reilly and Burstein 1974, Katsamanis and Raftopoulos 1990, Rho et al. 1993).

Though less dramatic, the microstructure of cortical bone too plays a significant role in its macroscopic properties. A study by Reilly and Burstein (1974) reported that the Young's modulus of cortical bone varied with orientation; in this study the authors reported values of approximately 17 GPa in the longitudinal direction and 11 GPa in the transverse direction. Work by Cowin and Hegedus (1976) also support the notion that there is a preferential direction of loading in cortical bone. Donaldson et al. (2011) showed that not only is cortical bone orthotropic, but also its directional nature becomes increasingly pronounced with age. Similarly, it is widely believed that individual trabeculae form in the optimum load carrying configuration, by alignment of the bony bars with the principal stress directions resulting from routine loading (Goldstein 1987). The alignment of cortical osteons and cancellous trabeculae to an optimum or preferential direction is possible through a process known as remodelling. The bone in human bodies continually adapts to the loads placed upon it (Wolff 1892), and is capable of repairing itself if damaged (e.g. callus formation after fracture). The quality of bone deteriorates with time, and so to maintain structural integrity, damaged or defective bone must therefore be renewed

on a regular basis. The cells responsible for maintaining homeostasis of the bone tissue are the osteoblasts (bone forming cells) and osteoclasts (bone destroying cells). In young healthy bone, the rate of resorption of old bone and deposition of new bone is in equilibrium. The process of bone renewal is continuous throughout life, however, it has been shown that cancellous tissues are renewed on a much more regular basis than cortical bone tissues (Cowin 2001). The constant resorption and deposition of bone further contributes to its inhomogeneity.

Moreover, biological changes brought about by ageing can influence the body's natural remodelling process. These changes can affect the normal state of equilibrium between resorption and deposition resulting in the formation of lower density bone tissue. Age related variations to the bone geometry and porosity at the microscopic (Bousson et al. 2001, Cooper et al. 2007) and macroscopic levels (Russo et al. 2006) can have considerable impact on its mechanical properties.

## II.5 Conditions affecting knee joint function

There are a number of reasons why a human knee joint might fail. Classification of failure is usually dependent upon which regions of the knee are affected and what impact this has on the functionality of the joint.

The leading degenerative disease of the knee joint and one of the main reasons for TKA according to current medical statistics (NHS Scotland 2010) is arthritis. This condition is characterised by inflammation of the joint and surrounding tissue and by painful joints during motion. The three most common forms of arthritis are osteoarthritis, rheumatoid arthritis and trauma induced arthritis.

Worldwide approximately 15% of the entire population is believed to suffer from osteoarthritis (Poole et al. 2002). In the UK alone, an estimated 8 million individuals a year seek treatment for this condition (Arthritis Research UK 2011). Osteoarthritis (OA) affects the entire knee joint, e.g. the bone, synovium and the joint capsule (Callaghan et al. 2002). One mechanism by which OA degrades the function of the

knee joint is through changes to the structure of the articular cartilage. It has been seen that the development of OA corresponds with a loss or reduction in specific components (e.g. proteoglycans) which make up part of the extracellular matrix (Poole et al. 2002), this in conjunction with fibrillation of the cartilage leads to the eventual exposure of the underlying bone. The bone on bone articulation which follows the formation of fissures in the articular cartilage may also lead to the development of bone spurs on the exposed surfaces, joint articulation in the presence of bone spurs can result in further damage to the lining and induce severe pain in the affect joint (Figure 2.10).

The second most common form of arthritis known as rheumatoid arthritis (RA) is characterised by a chronic inflammatory response across several joints. Its exact cause is unknown, but it is believed to be caused by a systemic disease which can affect the whole body and organs simultaneously (Panayi 2003). This form of arthritis is characterised by inflammation of the joint lining due to the presence of white blood cells. Secretions from these blood cells cause the inflammation and swelling associated with RA, leading to the debilitating joint pain suffered by patients. It is estimated that RA affects 1-2% of the global population (Callaghan et al. 2002). If appropriate medical intervention is not sought in time, RA will eventually lead to permanent joint damage.

One final form of arthritis commonly encountered is trauma induced arthritis. This is a form of arthritis which occurs in the joint as a direct result of a repeated or severe injury to the affected area. In principle, the initial response is similar to that of inflammatory arthritis, though unlike RA this is not due to the presence of a virus or systemic infection.

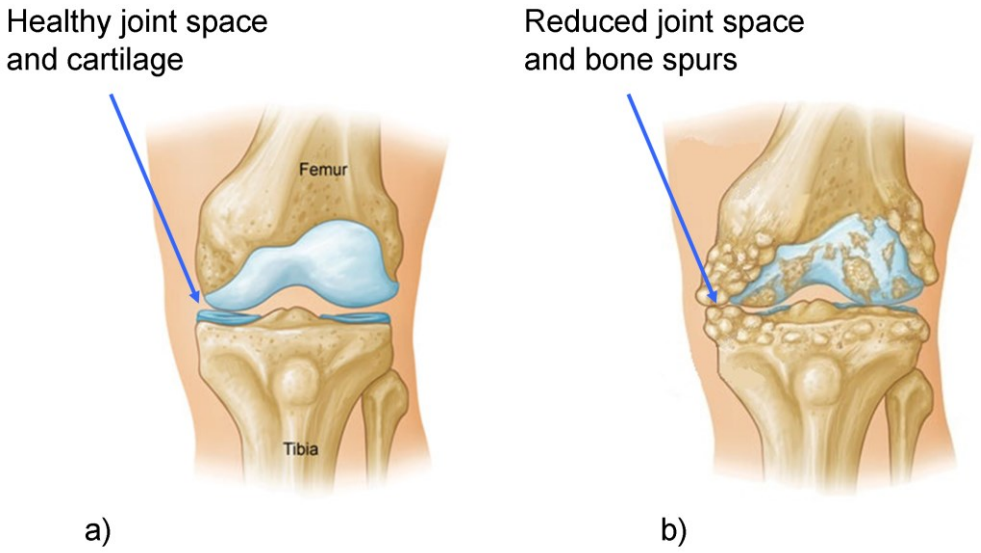


**Figure 2.10:** Illustration of a) a healthy knee joint with intact cartilage and normal joint spacing and b) an osteoarthritic knee joint with damaged articular cartilage reduced joint spacing and bony spur formations. Images adopted and modified from (AAOS 2010b).

Other conditions affect the structure and composition of the bone. As we age, the mineral content in our bones decreases, our bones become more brittle, less dense and as a result suffer a reduction in their stiffness (Bousson et al. 2001, Russo et al. 2006, Cooper et al. 2007). These changes occur in both men and women, though elderly women in particular can suffer a far more accelerated bone loss due to the hormonal changes brought about by menopause (NIH 2012). Osteoporosis is a condition in which the rate of new bone formation is slower than the rate of bone resorption. This affects the normal state of equilibrium, leading to bone mineral loss and thinning of the cortical bone structure (Figure 2.11). Some studies have suggested that these changes can lead to a reduction in cortical thickness by as much as 40% (Russo et al. 2006). Though adequate mineralisation of the bone occurs in the presence of osteoporosis, the formed bone is fragile, and on a microscopic level may have an abnormal appearance (Waugh and Grant 2010). Disorders such as osteoporosis, which have a dramatic impact upon a patient's bone mass, can lead to a significantly increased risk of fracture. In addition, other less common conditions such as Paget's disease and osteomalacia also influence the structural integrity of the

bones, which can affect normal joint function and lead to an increased likelihood of fracture.

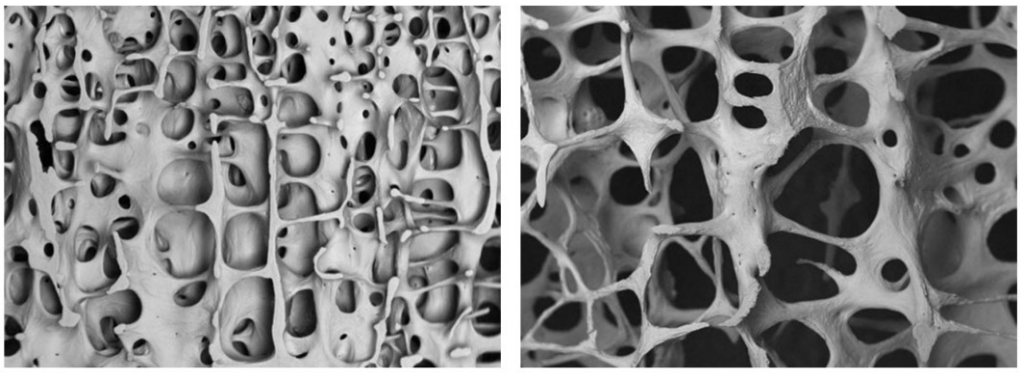


**Figure 2.11:** Scanning electron micrograph of microarchitecture of a) healthy and b) osteoporotic cancellous bone from the fourth lumbar vertebra of a healthy 30 year old male and an 89 year old female with osteoporosis (x20 magnification), taken from (Boyde 2012).

In elderly individuals with extensive osteoporosis, fractures may occur as a result of low energy impacts or due to an awkward fall. In younger patients, fracture of otherwise healthy bone usually occurs as a result of a direct trauma due to high intensity interactions such as during contact sports or as a result of an accident (Figure 2.12).

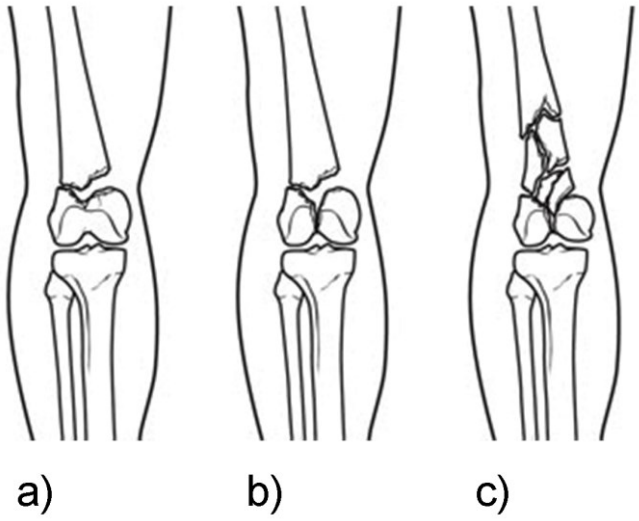


**Figure 2.12:** Illustration of a) a transverse fracture propagating across the distal femur, b) an intra-articular fracture that extends both across the distal femur and down into the knee joint and c) a comminuted fracture that extends into both the knee joint and the shaft, taken from (AAOS 2010a).

## II.6 Total Knee arthroplasty

As discussed in the previous section, through disease or traumatic injury knee joints can become painful, leading to a reduced mobility and impacting on the patients quality of life. If degradation of the knee joint progresses to such a stage that pain can no longer be managed through medical treatment (e.g. painkillers or steroid injections) and motion becomes severely impaired, then surgical intervention may be necessary.

Total knee arthroplasty (TKA) is the name given to a surgical procedure which involves replacing damaged or diseased portions of bone tissue with man-made prosthetic components. Depending on a range of factors such as the extent to which the biological structures of the knee are damaged or how far the disease has progressed, the surgeon can opt for either a partial or complete replacement of the articulating surfaces in the knee joint (Figure 2.13).

### II.6.1 Types of knee arthroplasty prosthesis

There are currently several different types of primary knee replacement prosthesis available, which can be divided into two broad categories based on the amount of bone to be removed.

Total knee arthroplasty has been performed in one form or another for over 70 years, and in general, is considered to be a successful operation (Scuderi et al. 1989, D'Lima et al. 2001b). However, there has been a gradual shift in recent years towards the use of more conservative minimally invasive techniques such as patella-femoral replacement (PFR) and unicompartmental knee replacement (UKR) (Figure 2.13a and 2.13b). One of the key goals in any type of joint replacement surgery is to minimise the amount of bone removed and restore near normal function to the affected area. Unicompartmental techniques offer the distinct advantage of preserving the healthy portions of the knee joint (including both cruciate ligaments),

provided the impairment is isolated to one of the joint compartments[3] (Figure 2.14b) (AAOS 2010b). Due to the more conservative nature of these minimally invasive procedures, UKR and PFR often result in improved recovery times, lower initial costs and a more natural range of motion post op. However, these potential benefits may be offset by the comparatively shorter life spans observed in comparison to conventional knee replacement implants and the added costs associated with extra revisions (Koskinen et al. 2008).

In contrast, as the name suggests, total knee replacement (Figure 2.13c) involves a much more aggressive approach to treatment where the articulating surfaces of all the bones in the knee joint are replaced with prosthesis.

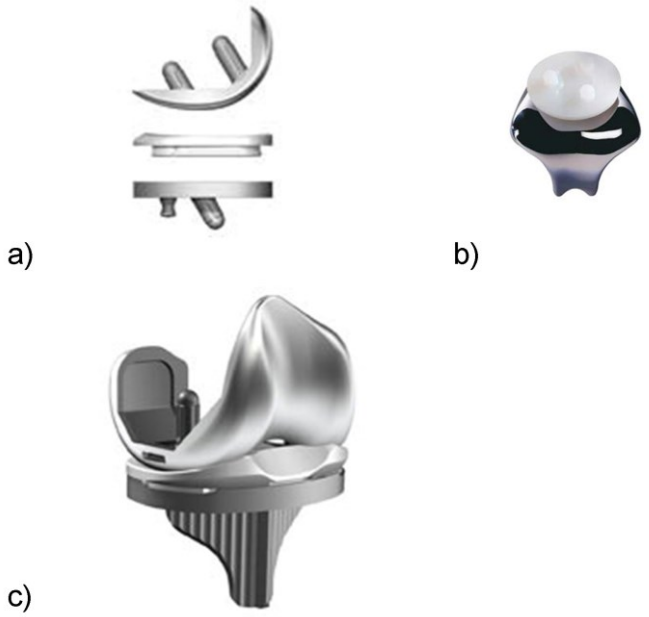


**Figure 2.13:** Images of a) a unicompartmental implant showing femoral component, tibial tray and polyethylene insert (Triathlon™ Partial Knee Resurfacing PKR, Stryker, UK), b) a patella-femoral implant showing articular surface component and patella resurfacing component (Avon Patello-Femoral™ Joint Replacement System PFJ, Stryker, UK) and c) a cruciate retaining total knee prosthesis showing femoral component, tibial tray and polyethylene insert (Triathlon™ Total Knee Replacement System, Stryker, UK).

[3] The knee joint is generally divided into three different regions or 'compartments', these compartments consist of the articulating surfaces of: the medial condyle, the lateral condyle and trochlear groove.

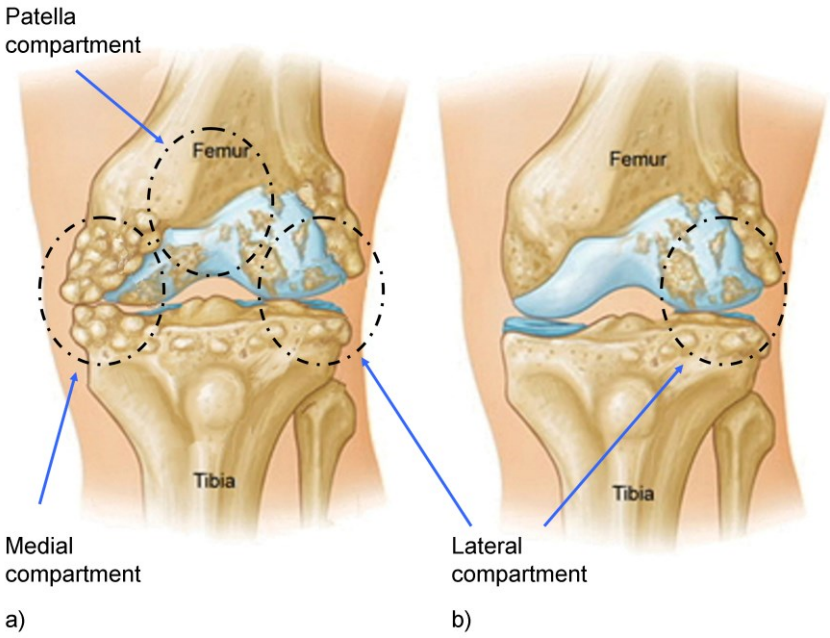


**Figure 2.14:** Illustration of the left knee joint with a) osteoarthritis in all three compartments and b) osteoarthritis isolated to just the lateral compartment. In this case the first knee would be considered a suitable candidate for TKA whereas the second knee could be treated with UKR. Illustration adapted from (AAOS 2010b).

### II.6.1.1 Components of primary total knee arthroplasty (TKA)

Though differences in size and internal geometry of prosthesis exist between manufacturers, in general all TKA prosthesis consist of three major components (Figure 2.15); the femoral component, the tibial tray and the tibial bearing component. The femoral component attaches to the distal end of the femur, the tibial tray inserts into the proximal tibia and the tibial bearing component sits between these two components. Depending on bearing type used, this may be fully anchored in the tibial tray using a snap fit (fixed bearing) or may allow a small amount of rotational motion to occur about the proximal/distal axis of the tibia (mobile bearing). An optional fourth component used to resurface the underside of the patella is sometimes employed.

Material selection in TKA is of great importance. The femoral components are usually manufactured from a cobalt chromium alloy (CoCr), and tibial trays from titanium (Ti), though the use of ceramic materials is gaining some support. The tibial bearing component and patellar resurfacing component on the other hand are constructed from an ultra-high-molecular-weight polyethylene (UHMWPE) material. The materials are specifically chosen for their biocompatibility characteristics and their ability to resist wear. The highly polished finish on both the contacting surface of the femoral and the tibial bearing component create an almost frictionless environment for joint articulation ($\mu$ in the range of 0.03 – 0.10) (Fisher and Dowson 1991).

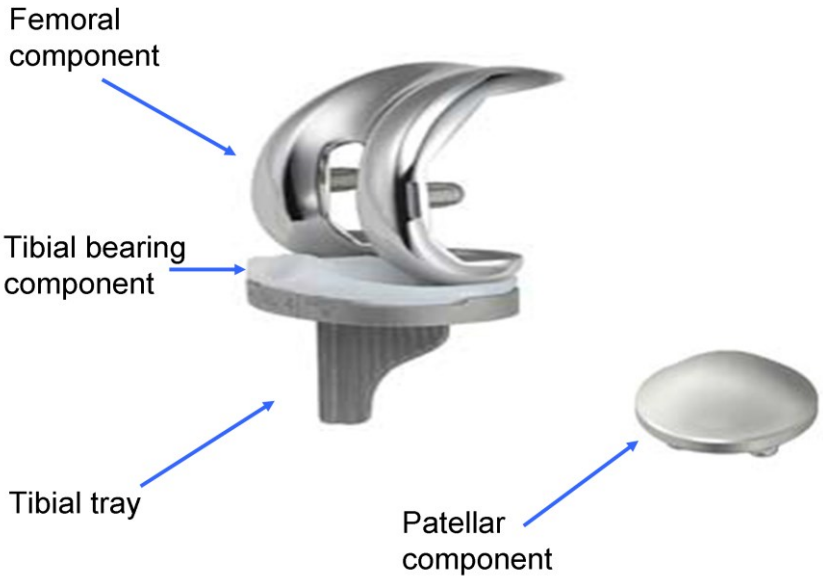


**Figure 2.15:** Image of the different components of a standard total knee replacement, (Stryker Orthopaedics 2008b).

### II.6.1.2 Role of ligament constraint in primary TKA

As discussed earlier in this chapter, the ligaments surrounding the knee joint play a vital role in its stability. In the category of primary knee arthroplasty, implant type can be further categorised on the basis of preservation or removal of the cruciate ligaments. At the time of operation if the ligamentous structures are intact and

healthy, surgeons may employ a cruciate retaining implant (CR), this implant type preserves the PCL (Figure 2.16a) and relies on this ligament in combination with the collateral ligaments and surrounding soft tissue to maintain joint stability. On the other hand if the ligaments are deemed to be diseased or otherwise unable to carry out their function then, both ACL and PCL may be removed and replaced with a more constrained prosthesis. This more constrained prosthesis known as a posterior stabilising implant (PS) recreates part of the functionality of the cruciate ligaments through a post-cam mechanism (Figure 2.16b) designed to restrain excessive forward translation of the femur on the tibial bearing component. In almost all cases, implantation of replacement knee prostheses results in the removal of the anterior cruciate ligament.

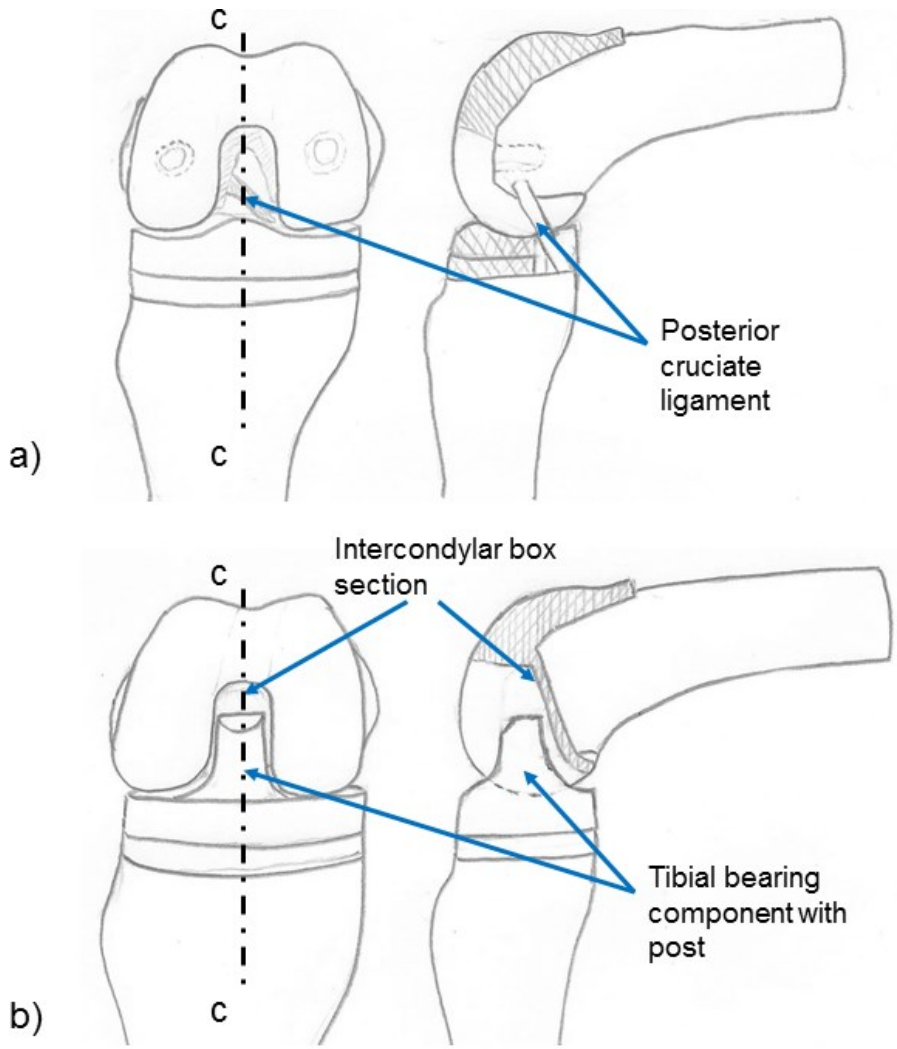


**Figure 2.16:** Shows frontal and sectional elevations through the plane c-c of a) a CR implanted femur, and b) a PS implanted femur, in a flexed position. The sectional view details the differences in mechanism of restraint for each implant type, e.g. PCL for CR implant and post-cam mechanism for PS implant (Author illustration).

### II.6.2 Fixation in TKA

Ensuring proper fixation of the prosthesis to the bone at the time of operation is essential to long term implant survival and satisfactory patient outcomes. Attachment of the prosthesis to the bone is carried out using one of two potential methods (Cemented or Press-fit). The first method employs the use of bone cement or *polymethylmethacrylate* (PMMA) at the prosthesis bone interfaces to bond the

implant to the bone structures. In the second method (Press-fit), no cement is used during fixation. Instead, the implant is designed to attach to the femur through an interference fit with the distal surfaces of the femur, additionally the internal surfaces of the implant are coated with a special porous structure which encourages ingrowth of bone into the implant, creating a biological interlock between prosthesis and bone at the microscopic level. Fixation by ingrowth of bone into the prosthesis is known as osseointegration (Figure 2.17).

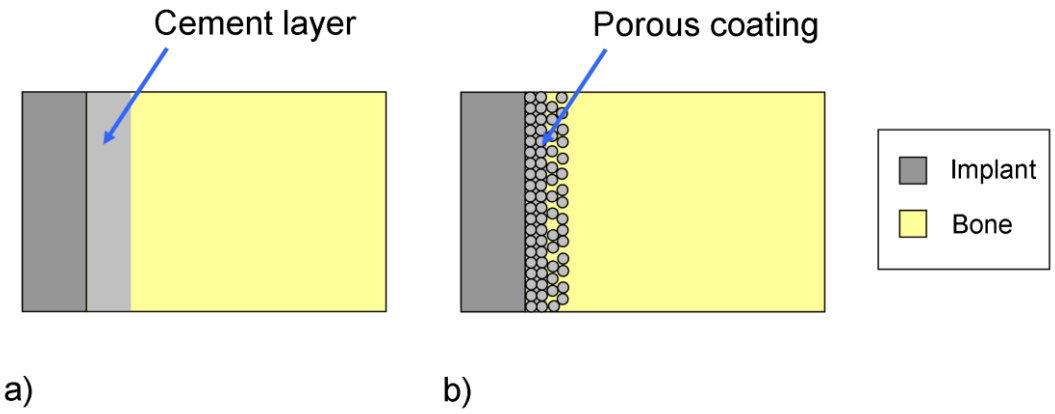


**Figure 2.17:** Illustration of a) a cemented knee replacement and b) a porous coated osseointegrated implant. (Author illustration)

The role of fixation (cemented vs. uncemented) in TKA remains a widely debated issue (Laskin 2001), with the majority of the orthopaedic community being firmly divided on the topic. A number of studies highlight the benefit of uncemented fixation (Rand 1991, Nilsson et al. 2006), while equally numerous are the reports suggesting that cemented fixation remains the gold standard for implantation (Duffy et al. 1998, Park and Kim 2011). Based on the current body of knowledge, neither technique appears to have a clear advantage over the other (Toksvig-Larsen et al. 1998, Park and Kim 2011). The debate on fixation is further complicated in revision TKA by the presence of bone loss and the possibility of large contained or uncontained defects.

### II.6.3 Reasons for failure of TKA

Compared to other joints in the human body, the knee has a far more complex structure and geometry, resulting in more complex biomechanics thus making the same level of success in implantation more difficult to achieve, according to an anonymous report in the Lancet (Anonymous 1976). In spite of this, knee replacement operations in general have been successful, with high patient satisfaction rates and good long term implant outcomes at 10-15 years post op (Scuderi et al. 1989, Font-Rodriguez et al. 1997, D'Lima et al. 2001a). However, complications do occur (Frosch et al. 2004), these complications if severe can often necessitate further operation and replacement of the prosthesis (Figure 2.18). As increasing numbers of patients undergo TKA annually, it is recognised that there will be a corresponding increase in revision TKA. Some of the main factors which lead to this increasing need for revision TKA are discussed in the following subsections.

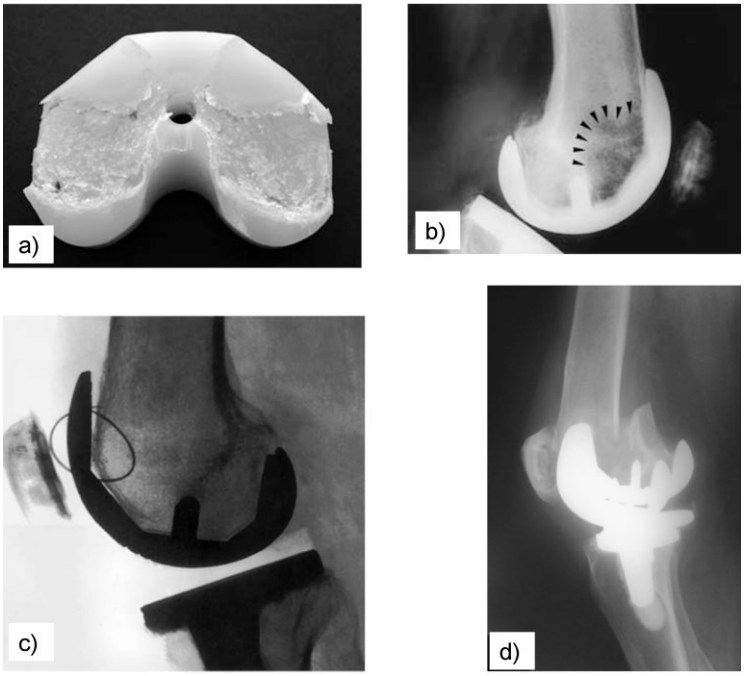


**Figure 2.18:** Images highlighting the main modes of failure for primary TKA implants; a) shows a worn polyethylene insert which failed through pitting and delamination (Naudie et al. 2007), b) shows a loss of bone mineral density under the anterior flange of the femoral component due to stress shielding (van Loon et al. 2001), c) shows a fluoroscopic image of a femoral component subject to aseptic loosening at the anterior surface (Fehring and McAvoy 1996) and d) shows a lateral x-ray of a periprosthetic femoral fracture (Rayan et al. 2008).

### II.6.3.1 Prosthesis wear

Though TKA components are manufactured from materials optimised to resist abrasive wear, the articulation of a well fixed prosthesis during daily activities still results in the generation of microscopic wear particles, range in size from 0.1-100µm (Abu-Amer et al. 2007, Kuiper 2007). In an *in vitro* study, Spinelli et al. (2010) estimated that metal on polyethylene articulation generated particle debris ranging from 3.8mm$^3$ to 15mm$^3$ depending on number of cycles. However, an *in vivo* study by Gill et al. (2006) places this figure much higher at 100mm$^3$ a year.

Wear particle generation can be significantly influenced by the shape of the articulating surfaces, the joint contact loads and implant kinematics (Fregly et al. 2003, Bei et al. 2004, McEwen et al. 2005). Furthermore, the thickness of the insert and its material properties (Petty et al. 1999) also have a role to play in component wear. Other notable factors which are known to greatly increase local particle wear generation are mechanical alignment and fixation of the prosthesis (Naudie et al. 2007), as well as the degree of conformity between femoral component and tibial bearing component (Kuster and Stachowiak 2002) through the full range of motion. Any irregularity in contacting surfaces may lead to point or edge loading and could potentially result in yielding and failure of the UHMWPE insert due to high localized contact stresses.

Polyethylene wear is closely linked to aseptic loosening of the implant. It is suggested that the size and shape of wear particles generated may influence the response from the cells to these particles (Abu-Amer et al. 2007, Scuderi 2011). If the debris generated through the articulation of the femoral component on the bearing surface of the tibia reaches a threshold size, it can elicit a serious reaction from the body's immune system (Abu-Amer et al. 2007), this inflammatory response is referred to clinically as osteolysis. Cells called macrophages try to break down the particles from the UHWPE tibial insert but die in the process (Abu-Amer et al. 2007). Repetition of this process causes the release of enzymes and chemicals that lead to resorption of the bone surrounding the prosthesis (Jacobs et al. 2001), and eventual loosening of the implants. Outside of this threshold range, if the wear

particles are sufficiently small, the body may be able to clear them with other debris from the joint tissues, if they are too large, however, they may contribute to abrasive wear of the insert (Scuderi 2011).

### II.6.3.2 Aseptic loosening

Aseptic loosening in the context of total knee arthroplasty is deemed as any loosening of one or more of the prosthetic components without underlying infection. Based on available joint registry database information, aseptic loosening of the implant is one of the predominant causes of revision globally (CJRR 2009, NAR 2010, AOA 2011, NJR 2011, Sundberg et al. 2011). Loss of fixation through aseptic loosening can lead to pain, malalignment of the prosthesis and eventual failure.

Aseptic loosening can have many different causes (Abu-Amer et al. 2007); it can occur as a result of inadequate initial fixation or develop due to (mechanical or biological) loss of fixation over many months and years. The three main causes of aseptic loosening are particle induced osteolysis due to excessive wear of the articular surfaces (Abu-Amer et al. 2007), bone loss due to periprosthetic stress shielding and fibrous tissue formation instead of bone ingrowth as a result of relative motion at the bone prosthesis interface (Bahraminasab et al. 2012).

In the knee joint, aseptic loosening of the femoral component may be brought about by one or all of these underlying causes. The manner in which loosening occurs and the degree to which the prosthesis has loosened will determine the complexity of treatment required, e.g. if replacement components merely need to be cemented or if augments are required to rebuild lost bone.

### II.6.3.3 Micromotion

Micromotion is the term used to describe the relative interfacial motion which can occur at the prosthesis-bone, prosthesis-cement and cement-bone interfaces. Aseptic loosening of the prosthesis and micromotion are closely linked. Relative motion can occur at the interface as a result of aseptic loosening or particle induced osteolysis.

However, relative interfacial motions of a poorly fixed implant may also be a driving factor of aseptic loosening. In both uncemented and cemented fixation, another contributing factor to micromotion is long term bone loss due to the stress shielding effect of the implant. Continuous micromotion of the prosthesis irrespective of the root cause (loosening or bone loss) may further disrupt any remaining fixation by the process of fatigue failure of the surrounding bone and/or cement structures. If yielding of the surrounding tissues occurs, this can result in the prosthesis undergoing an irreversible displacement resulting in malalignment; this process is known as permanent migration of the prosthesis. As discussed previously, any change in the alignment of the prosthesis can have a serious influence on the distribution of joint contact forces, joint function, pain, prosthesis wear and ultimately failure.

Through examination of canine models (Pilliar et al. 1986, Bragdon et al. 1996), it has been suggested that there is a threshold range of motions above which osseointegration may be prevented ($40-150\mu m$). On the other hand, lower levels of motion at the bone implant interface ($<40\mu m$) may be beneficial in promoting bone ingrowth into the prosthesis and thereby increasing component stability (Vandamme et al. 2007, Suárez et al. 2012).

Early indications of loosening and implant failure are observed clinically by tracking changes in the position and orientation of the implant over time through examination of x-rays or through more specialist techniques such as radio stereo photogrammetric analysis (RSA). Micromotion of the prosthesis is closely linked to both aseptic loosening and prosthesis wear. Indeed in a paper by Nilsson et al. (1996), it was suggested that particle induced osteolysis as a result of wear particles breaching the interface rather than slow migration may be a more significant factor in causing long term aseptic loosening of the implant. The authors of this particular paper believed that “ingress of wear particles into the interface” as a result of small but repetitive interfacial motions was likely to be a driving factor in particle induced osteolysis.

#### II.6.3.4 Stress shielding

Based on the observed phenomenon commonly known as Wolff's law, bone is said to adapt to the stresses placed upon it by optimizing bone so that material is removed from relatively unstressed regions and deposited in regions where it is need (Wolff 1892), thus maintaining a strong but lightweight structure. This process is known to occur continuously throughout life. The implantation of any prosthesis into the bone, however, disrupts the natural homeostasis of the resorption/formation process by dramatically altering the distribution of stress in the surrounding regions. It is suggested that this is due to the mismatch in stiffness between the implant and the bone, leading to a reduction in stress in areas immediately under the implant (Tissakht et al. 1996, van Lenthe et al. 1997, van Loon et al. 2001, Barink et al. 2003, Bougherara et al. 2010, Chong et al. 2011) relative to an intact healthy knee. As a consequence the natural adaptation process begins to remove bone which is deemed unnecessary. Frequently at the time of revision surgery, it has been found that areas immediately under the primary implants, particularly behind the anterior flange and posterior condyles of the femur develop significant periprosthetic osteoporosis (Petersen et al. 1995, Spittlehouse et al. 1999, Soininvaara et al. 2004, Saari et al. 2006). Long term bone loss adjacent to the bone-implant interface can cause instability, increasing the risk of component loosening and migration (Mintzer et al. 1990, Petersen et al. 1995, van Lenthe et al. 1997, Soininvaara et al. 2004). The lack of good quality bone for the purpose of fixation ultimately makes revision TKA operations much more complex and requires the use of larger prosthesis to rebuild lost bone.

It is also recognised that loss of bone from critical areas under the implant in combination with implant induced stress concentrations may increase the risk of periprosthetic femoral fracture (Saari et al. 2006, Rayan et al. 2008, Meek et al. 2011).

### II.6.3.5 Fracture

A rare but potentially devastating failure mode of primary TKA is periprosthetic fracture. This mode of failure can arise due to a number of different factors such as, a direct trauma to the replaced joint resulting from a low velocity fall or car accident (Rayan et al. 2008), loss of supporting bone (Soininvaara et al. 2004, Saari et al. 2006) due to stress shielding, osteolysis and osteoporosis, increase in localized stress concentrations due to loosening (Meek et al. 2011).

Fracture of the distal femur may also occur as a direct or indirect result of surgical technique. At the time of implantation a slight mismatch in fit between the internal geometry of the implant and the prepared surfaces of the femur during impaction may result in fracture, particularly in PS implants with intercondylar box (Lombardi Jr et al. 1995). In addition, if a femoral component is slightly undersized, it may lead to the creation of a stress riser as a result of notching of the anterior femoral cortex and may pose an increased risk of fracture (Aaron and Scott 1987). Other known risk factors include patient age, gender and prior history of surgery (Ritter et al. 1988, Rayan et al. 2008, Julin et al. 2010, Meek et al. 2011).

The current incidence of periprosthetic fracture worldwide following primary TKA is believed to be in the range of 0.6 – 3.0% (Merkel and Johnson 1986, Ritter et al. 1988, Inglis and Walker 1991, Healy et al. 1993, Rayan et al. 2008, Meek et al. 2011). However, this failure mode has the potential to become a more serious clinical issue as the population ages and a greater proportion of younger more active patients undergo TKA.

Fractures are traditionally treated through intramedullary nailing or external plating. In the case of the distal femur, however, their treatment can be further complicated by the design of implant used, e.g. the presence of an intercondylar box may negate the use of intramedullary fixation and may make fixation of a plate to the distal condyles difficult, particularly in the case of bicondylar femoral fracture surrounding the box.

## II.7 Revision TKA

Revision knee surgery is often a more complicated procedure than primary TKA. Surgeons may have to deal with a wide range of factors due to the manner in which the original prosthesis failed, such as aseptic loosening due to severe bone loss or possibly even dislocation of the implant as a result of periprosthetic fracture. All these potential complications significantly increase the complexity of the procedure and make restoration of the joint line more challenging. Furthermore, the presence of such complications may necessitate the removal of a greater proportion of bone in order to find a suitable base for fixation of the prosthesis. As a consequence, revision implantation rarely achieves the same measure of success and longevity as seen in primary implantation (Goldberg et al. 1988).

In general, due to the loss of supporting bone structures over time (through stress shielding or disease) and potential degradation of surrounding soft tissue, revision prostheses tend to require stems to anchor the device to the bone (Figure 2.19a and 2.19b) and a greater level of joint constraint distally to prevent instability. This added constraint is usually provided by means of a central post mechanism similar in function to the PS implant mentioned earlier. However, if the functionality of the ligaments is severely impaired, it may be necessary to employ a highly constrained hinge type of prosthesis (Figure 2.19c). As the level of prosthesis constraint increases the functional range of motion invariably decreases, potentially impacting on patient's quality of life.

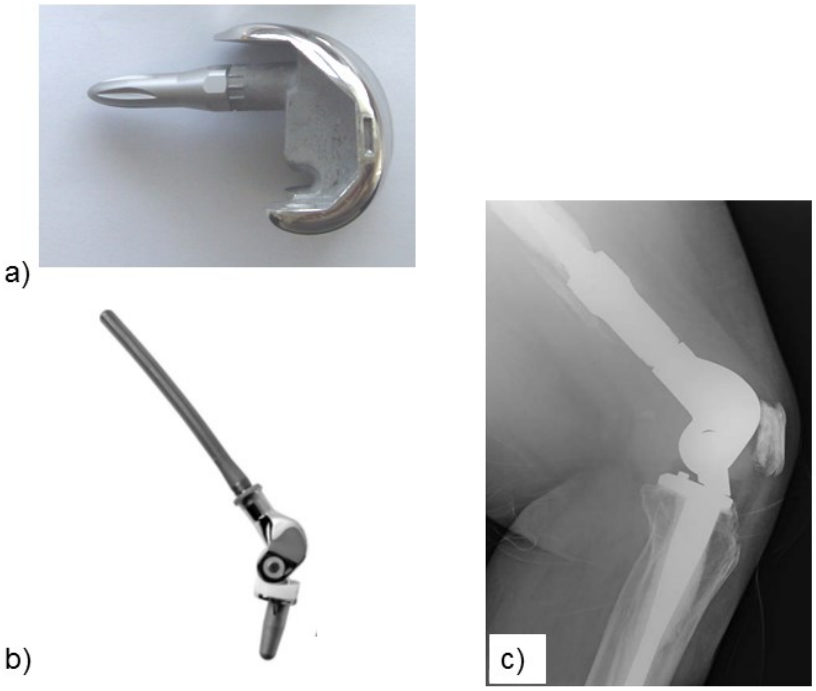


**Figure 2.19:** Image of a) a revision femoral component with modular short stem, b) distal femoral hinge type prosthesis (Orthopaedic Salvage System, Biomet Inc., Warsaw, IN) and c) lateral x-ray of an implanted distal femoral replacement (Berend and Lombardi 2009).

### II.7.1 Dealing with bone loss

Good metaphyseal fit is essential for component stability and longevity. The quality of metaphyseal fit obtained, however, is largely dependent on the quality of underlying bone and the technical skill of the surgeon. As discussed previously, poor quality bone stock is frequently encountered at the time of revision (Jensen et al. 2010), due to stress-shielding or other biological processes such as osteoporosis. Changes to the quality of bone stock through mechanobiological means leads to a more challenging surgery, requiring the use of larger more complex prosthesis and more aggressive removal of damaged or diseased bone until bone of a sufficient quality for fixation is encountered.

Engh (2006) described a classification system which categorised the bones of the knee joint based on severity of bone defect present at the time of operation. Under this classification system defective femoral and tibial bone is placed in one of three

main categories and an appropriate level of treatment is suggested for each. The three main classifications from a femoral perspective are as follows:

- The first type known as an F1 defect consists of minor damage to the cancellous bone structure of the distal femur (Figure 2.20a).
- The second type of defect (F2) is further subdivided into two categories depending on the severity of the defect encountered F2A/F2B as shown in Figure 2.20b and Figure 2.20c respectively. The F2A defect is usually confined to a single condyle, whereas the F2B defect affects both condyles.
- The final defect type (F3) represents an extreme loss of bone and is characterised by the loss of one or more collateral ligament attachment sites and a deficient metaphyseal segment, usually due to severe osteolysis or supracondylar fracture.

To return normal function to the knee it is essential that the joint line be restored, which means any bone lost through disease or surgical resection must be replaced. According to the guidelines laid out under the Engh defect classification system (Engh 2006) for contained defects such as category F1 and F2A, a simple cement fill or if necessary bone graft techniques can be used to restore lost bone in order to create a stable platform on to which they can attach the prosthesis. In the case of a more severe F2B defect, it may be necessary to remove a greater portion of bone to find tissue of adequate quality for fixation. To preserve bone stock, the surgeon may instead opt to repair the damaged distal portion of the femur with morselised bone graft, provided the cortical rim is intact, if not, metal augments may be used to build the back surface of the implant up to the level of remaining healthy bone in order to obtain good metaphyseal fit and restore the patients joint line/function. The use of stemmed femoral components has been reported to be able to provide initial mechanical stability and protect the graft (van Loon et al. 2000, Scuderi and Tria 2006, Whittaker et al. 2008, Scuderi 2011) until fully incorporated into the host bone. Stemmed femoral components can either be of fixed length or modular in design.

Modular components are often preferred on the basis that they provide a greater level of intraoperative flexibility by allowing the surgeon to adapt the configuration of the implant to the needs of the specific patient. For example, the natural bow in the shaft of the femur may be more pronounced in some individuals compared to others, if traditional fixed implants were to be used, this may result in a malaligned implant distally; in effect, the long stem would pull the prosthesis out of alignment. Furthermore, a modular stem in combination with an offset adapter may be used to create a more favourable alignment of the implant distally while fitting the stem more centrally into the canal (Fehring 2005, Brilhault and Ries 2012).

Treatment of F3 defects due to extensive bone loss and damage to the metaphyseal segment requires the use of large structural grafts and depending on severity, may necessitate replacement of the entire distal/metaphyseal segment with a femoral replacement or highly constrained hinge type prosthesis (Harrison et al. 2006, Berend and Lombardi 2009).

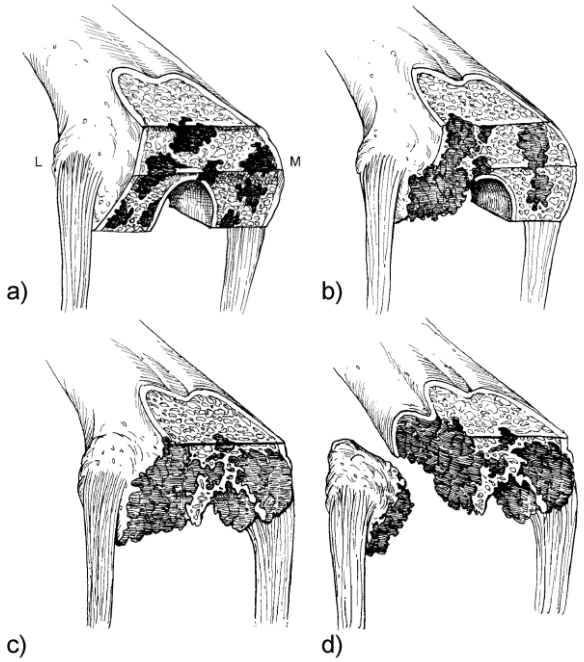


**Figure 2.20:** Illustration of femoral defected in order of increasing severity, a) F1, b) F2A, c) F2B and d) F3. Image adapted from (Scuderi and Tria 2006).

### II.7.2 Failure modes in revision TKA

Revision TKA prostheses are susceptible to all the same failure modes as primary prostheses. The complexity of the implants used in revision implantation also increases their susceptibility to additional modes of failure. The addition of long stemmed prostheses in particular has been found to dramatically increase the level of stress shielding observed in the femur (van Lenthe et al. 2002). This more pronounced bone loss may occur in revision TKA due to the stiff stem carrying a larger proportion of load away from the condyles and plateau to the shaft of the bone.

Aseptic loosening may also occur after revision TKA, as with primary implantation. This can be as a result of osteolysis or the pronounced bone loss due to the presence of the stem. Loosening of the femoral component distally could lead to greater bone loss through an "ice-cream cone" effect (van Loon et al. 1999) and may have serious implications for failure of modular components (Chu et al. 2000, Lim et al. 2001, Issack et al. 2007, Nikolopoulos et al. 2012), as is discussed in more detail in Chapter X. Proximal loosening of the stem, in conjunction with the high Young's modulus of the stem and its design may lead to an increased risk of end of stem pain (Barrack et al. 1999, Brown et al. 2002, Barrack et al. 2004) as a result of highly localised contact stresses between the stem tip and femoral shaft (i.e. due to rubbing of the stem against the internal cortex of the femoral mid-shaft).

Revision of a component due to infection is also further complicated by the presence of a well fixed stemmed femoral component, as such an operation may necessitate the removal of a large portion of cement and potentially healthy bone surrounding the stem to allow the infection to be treated, thus providing less healthy bone for attachment of the replacement prosthesis.

Furthermore, as with primary TKA, revision TKA is susceptible to periprosthetic fracture. Depending on severity of fracture, the patient may require a further re-revision of the prosthesis or replacement of the entire distal femur with a distal femoral replacement (DFR) (Kim et al. 2006). A number of potential failure modes of revision TKA components are shown in Figure 2.21.

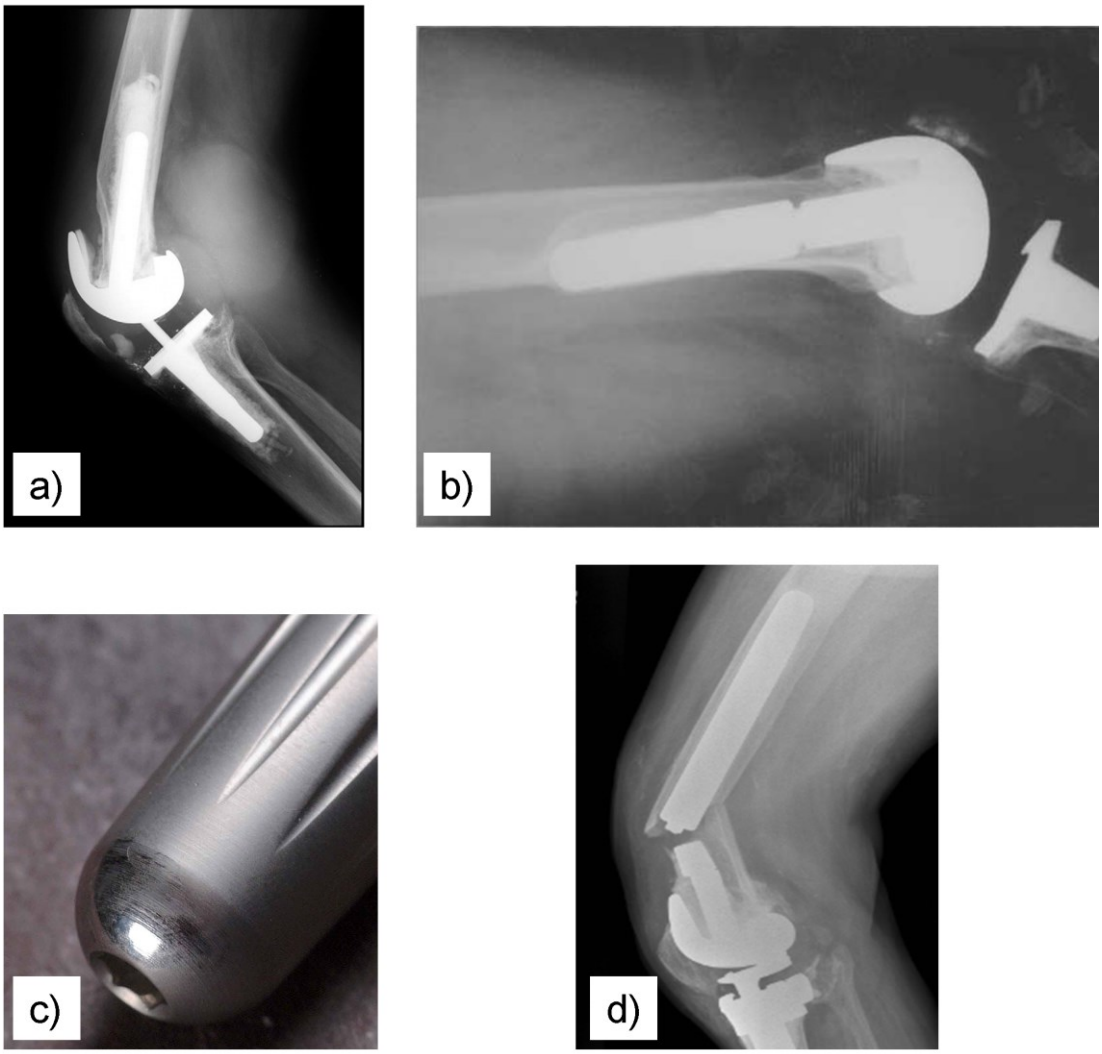


**Figure 2.21:** Images highlighting some of the potential modes of failure for revision TKA implants; a) shows severe osteolysis and loosening around both the femoral and tibial components of a revision knee system (Mabry et al. 2007), b) shows a loss of bone mineral density under the anterior flange of the femoral component due to stress shielding and erosion of the posterior femoral cortex due to migration of the stem tip (Fehring et al. 2003), c) shows the polished end of a diaphyseal engaging stem due to repeated frictional interaction with the surrounding cortex (Howie 2010) and d) shows a lateral x-ray of a periprosthetic femoral fracture of both the bone and prosthesis at the level of the stem junction (Howie 2010).

## II.8 Summary

The structure and function of the knee joint is complex. This complexity and the relatively high magnitude of loading it must withstand on a daily basis predispose it to injury and degenerative disease.

Total knee arthroplasty has been found to be a largely viable surgical procedure for easing patient pain and restoring motion to affected joints through the use of man-made prosthesis. Though TKA is reported to have high patient satisfaction rates (around 90%), this still leaves a large proportion for which the surgery is not completely successful or the relief from pain is only temporary.

Based on currently available clinical information, leading causes of premature implant failure relate to loss of fixation and/or loss of supporting bone directly under the implant. Though revision of the tibial component is far more widely investigated (Hashemi and Shirazi-Adl 2000, Completo et al. 2008a, Chong et al. 2010, Bhimji and Meneghini 2012, Cawley et al. 2012, D'Lima et al. 2012, O'Brien et al. 2012), it has been reported by some (AOA 2011) that there is less than 3% difference between number of revised tibial and femoral components. This data indicates the importance of correctly understanding the underlying mechanisms which influence long term outcomes of femoral components.

The mechanisms of revision failure are more complex and have been seen to be influenced by component design and implant modularity (Chu et al. 2000, Lim et al. 2001, Issack et al. 2007, Nikolopoulos et al. 2012). A better understanding of the stresses in the knee joint as a result of daily life both pre- and post-TKA, and how implant design/fixation influences interfacial motions are essential to promoting longevity of the prosthesis and better quality of life for the patient.

# III

# An Introduction to Finite Element Analysis

## III.1 Introduction

The remainder of the thesis relies on the extensive application of *the finite element method* (FEM) through the use of a commercially available finite element package (Abaqus, Dassault Systemes, Simulia. Providence, RI, USA). In this chapter a brief introduction to the finite element method and an overview of its application to the field of orthopaedic biomechanics is given. Details of the hardware used and methodologies applied to solve the more complex models presented in subsequent chapters are also outlined.

FEM was pioneered in the early 1950s in an attempt to better understand the vibration response of new aircraft wing designs under loading (Turner et al. 1956). From its early application in the field of aeronautical engineering, FEM has since permeated almost all other engineering disciplines and numerous textbooks on the subject are now available (Zienkiewicz and Taylor 2000a, Zienkiewicz and Taylor 2000b, Zienkiewicz and Taylor 2000c, Liu and Quek 2003).

The finite element method is recognised as a powerful tool to aid in the solving of complex problems which may be difficult to examine in a purely analytical manner (Zienkiewicz and Taylor 2000a). In the field of biomechanics FEM has been used to model everything from endovascular interactions between the circulatory system and stent grafts (Callanan et al. 2011) to studying the mechanical response of a razor blade to skin and hair during shaving (Cowley and Neale 1998). In the area of

orthopaedic biomechanics in particular it has found numerous applications on both microscopic and macroscopic scales. Microscopically it has been used to investigate the mechanical properties of individual trabeculae (Verhulp et al. 2008) and the effects of increased porosity (Donaldson et al. 2011) on mechanical properties of bone. At the macroscopic level it has frequently been employed to investigate implant wear and contact stresses in the prosthesis e.g. (Bei et al. 2004), fracture (Keyak et al. 2001, Bessho et al. 2009, Hambli et al. 2012), fracture treatments (Cheung et al. 2004), the characteristics of prosthesis-bone interactions (Abdul-Kadir et al. 2008, Andreaus and Colloca 2009, Chong et al. 2010) and assess pre-clinical performance of new implant designs (Harrysson et al. 2007).

## III.2 Fundamental concepts of FEM

In simple terms the finite element method is based on subdividing the complex geometry of the object being analysed into small regions or "elements": these elements are usually formed by simple regular geometric shapes such as tetrahedral or bricks (for three-dimensional analyses), and can be thought of as small building blocks of material, the behaviour of which can be more easily described mathematically. The overall behaviour of the complex structure is then recreated based on the behaviour of each of these interconnected elements. Meshing or "discretisation" of a problem is the term used to describe the subdivision of a structure's geometry into these elements. An example of this for a simple three-dimensional object is shown in Figure 3.1.

The element type used in this example is a tetrahedral element; this element type is primarily used in stress/displacement analyses. However, a wide variety of different element types exists in most commercial FE packages to suite an array of different applications (e.g. stress analysis, heat transfer analysis and acoustic analysis).

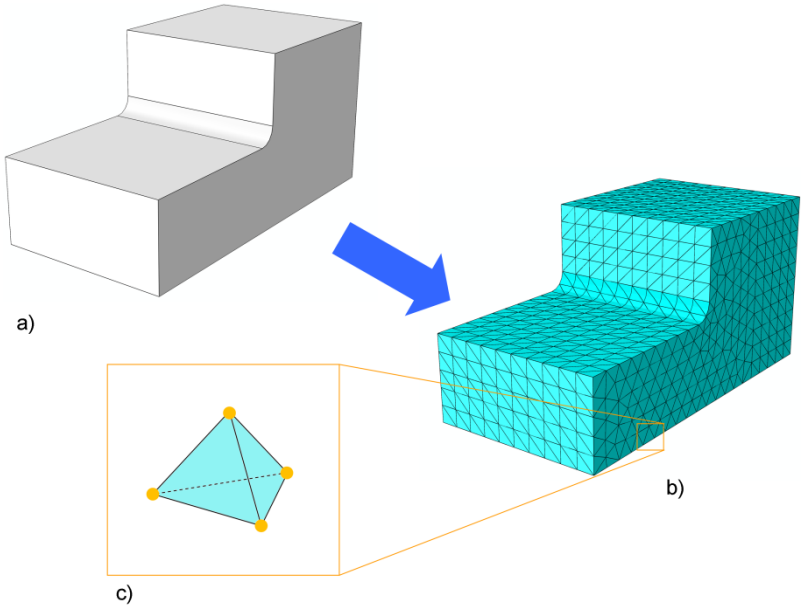


**Figure 3.1:** shows a) original geometry of a three-dimensional object, b) an example tetrahedral mesh of the three-dimensional object created in Abaqus/CAE (Simulia, USA) and c) a close up illustration of a single element from the mesh.

Element types are usually classified based on which family they belong to (e.g. continuum, beam, truss, shell, and spring elements). The particular elements of interest in the current study fall into the continuum family of elements, of which tetrahedral elements are a part. As shown in Figure 3.1c, each element is composed of a number of nodes (orange dots) joint by vertices. Nodes are the key points where equilibrium is enforced. Each node can have one or more degrees of freedom (DOF). The degrees of freedom in a model are the fundamental variables calculated during an FE analysis and are directly related to the number of nodes in that model and the element type. In the case of a stress analysis, using three-dimensional continuum elements, the DOF are the translations which occur in the x, y, and z directions at each node, for all the elements in the structure. In a heat transfer analysis, as discussed in Chapter V, the DOF at each node is temperature.

In terms of the analysis procedure, key variables such as displacements and temperature are calculated at the nodes. All other values within the element (e.g.

stresses and strains) are determined through use of interpolation functions, which make the values obtained at any generic point, fully dependent on the nodal values of that element. These interpolation functions are also often referred to as *shape functions*. Elements whose interpolations functions can be used to represent both displacement and its geometry are known as *isoparametric* elements.

The order of the interpolation function used in an element is usually depends on the type of element and the number of nodes it has. For example in Abaqus, tetrahedral elements which only contain nodes at their corners (Figure 3.2a) use a linear interpolation function and as such are referred to as linear or *first-order* element. Elements containing nodes both on the corners and midway along the vertices (Figure 3.2b) use a quadratic interpolation function; as a result these elements are usually referred to as quadratic or *second-order* elements.

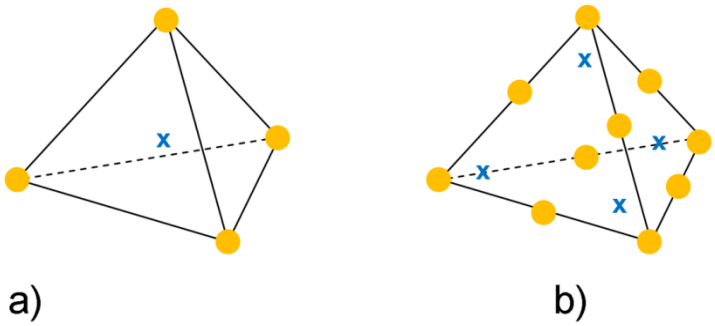


**Figure 3.2:** Illustration of a) a four node and b) a ten node tetrahedral element, where orange dots represent the nodes and the blue x represents the approximate location of the integration points within each element (Author illustration).

As previously stated key variables are evaluated at the nodes. The values of stress and strain, however, are evaluated within the element at select points, called *integration points* or *Gauss points* (Figure 3.2).

As stated earlier, each element can be considered a simple building block of material used to recreate the complex geometry of the system being analysed. To conduct any FE analysis it is therefore necessary for the material properties of each of these elements to be defined. For a simple isotropic elastic material, one needs only specify two parameters, namely Young's modulus and Poisson's ratio, however, if material non-linearity is considered or anisotropy included, then much more parameters are required.

The boundary conditions or the manner in which the system is restrained must also be considered. This may represent a plane of symmetry where only part of a structure is modelled, or may be representative of where an object is attached securely to another structure. In either case these conditions often require that the displacement of certain nodes in one or more DOF be set to zero. As well as restraining nodes against motion, boundary conditions may also be used as a means of applying a predefined displacement, to one or more nodes, in a specific direction.

Another key factor is the manner in which load acts on the system. Loading can be static or dynamic, and may be uniformly distributed over the faces of multiple elements in the mesh or applied as concentrated forces at the nodes.

Consideration of realistic geometry, material properties, boundary conditions and loading are essential in order to obtain accurate results from any FE analysis.

The purpose of this section was to briefly introduce some of the key concepts and principles of FEM, several books have been written on this topic and provide a more in-depth and technical explanation of all the points covered here (Zienkiewicz and Taylor 2000a, Liu and Quek 2003). In the next section, a simple example problem is introduced and the practical aspects of applying the finite element method in the solution of three-dimensional problems are discussed.

## III.3 Example problem

To analyse any problem with FE requires definition of the system geometry, all externally applied loads acting on the system, the material properties of each component in the system and the manner in which the system is restrained. This section provides a brief overview on the practical aspects of creating an FE mesh, for a simple example, once the above mentioned parameters are known. This example details the creation of an FE mesh from the simple three-dimensional CAD geometry introduced in Figure 3.1. The steps required to ensure simulation accuracy using different mesh densities and element types are also explored.

Referring to Figure 3.3, the first step in this process is importing the CAD geometry into the FE package (Figure 3.3a). This is traditionally done by first converting the native CAD file into one of the standard interchange formats such as .iges or .step. The model is then meshed with the desired element type (based on model application). In this case four node tetrahedral elements were employed. For problems with a simple geometry, such as shown in Figure 3.3a, it is often possible to create the geometry directly in most current FE packages. The details relating to the nature of the load acting on the system, the manner in which the system is restrained and its material properties are then used to setup the FE model (Figure 3.3b).

It is considered best practice to run a convergence study on an FE model prior to any investigation being conducted. This entails varying the mesh density (i.e. element size) until the parameter of interest reaches a preselected criterion for convergence. In theory the greater the number of elements, the more closely the approximated solution will match that of the theoretical solution. However, there usually exists a trade off in terms of solution accuracy and simulation runtime. Typically a change of 2-5% in the parameter of interest between successive increments of the mesh size is deemed an acceptable indication of convergence. An example of the results obtained for such a convergence study on the current model is presented in Figure 3.3c. This graph shows how the peak von Mises stress varies with increasing refinement of the mesh.

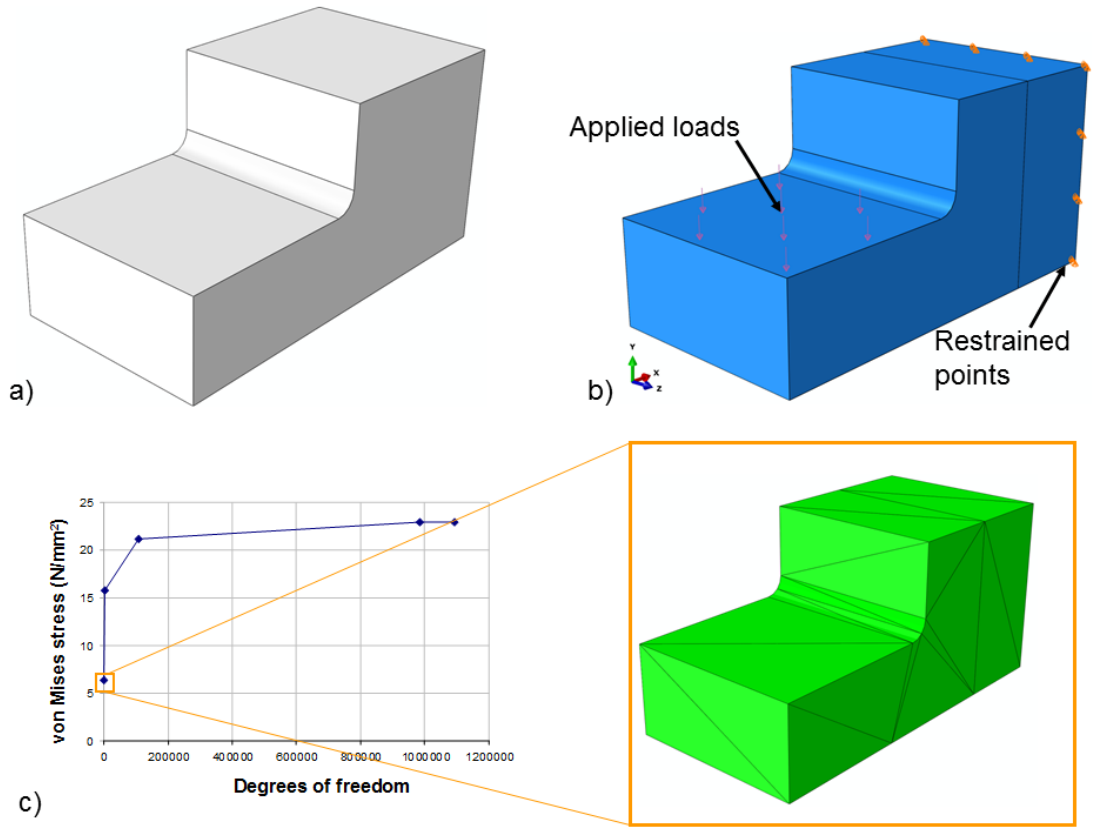


**Figure 3.3:** a) A simple three-dimensional geometric part, b) loading and boundary conditions applied to the part in Abaqus, and c) example of graph showing the variation of peak von Mises stress with increasing mesh density (zoomed in region indicating original base line mesh consisting of 45 elements). A Young's modulus E = 16700 N/mm$^2$ and Poisson's ratio v = 0.3, and a uniformly distributed pressure load of 1MPa was applied to the top surface of the part as indicated.

It is important to note that for many simple problems reasonably accurate solutions can be obtained with a relatively small number of elements.

Tetrahedral elements are frequently employed in FE stress analyses of biological structures due to their ability to more closely approximate the complex organic shapes found in the body. Referring to Figure 3.2a, the standard tetrahedral element available in most FE packages consists of four nodes. This is a constant stress element and is in general considered to be a poor stress predictor (Payen and Bathe 2011). Some of the limitations of this element can be overcome through significant

refinement of the mesh. However, this can result in a large increase in computational cost particularly in large complex assemblies.

A common alternative to increasing the number of elements is to increase its order. *Second-order* tetrahedral elements (Figure 3.2b) are much more accurate stress predictors and overcome many of the problems associated with the linear four node version (Lo and Ling 2000, Payen and Bathe 2011). The addition of mid-side nodes and the use of quadratic interpolation functions also offer improvements in element accuracy due the ability to model deform/curved surfaces (e.g. mid-side nodes do not necessarily have to be in one plane). Due to increased element accuracy fewer quadratic elements (10 node tetrahedra) are required than their linear (4 node) counterpart in order to obtain a similar solution accuracy for the same geometry. A comparison of CPU runtime required to solve the example problem and the DOF of each model analysed, using both ten node and four node meshes optimised based on a 5% convergence criteria, is shown in Figure 3.4.

The runtime for a mesh constructed of ten node tetrahedral elements in this example is three orders of magnitude less than that of the four node elements, to achieve approximately the same peak value of stress. In this particular example, the convergence study indicates that the mesh employing ten node tetrahedral elements is best. Interestingly this is not necessarily the case with more complex geometries, as evident by the results of a study on the proximal femur by Ramos and Simões (2006). In their study the authors found that for the same level of refinement (approximately 144,000 elements) no significant difference was observed between the results of femurs meshed with first and second-order tetrahedral element. In such cases the added degrees of freedom associated with ten node tetrahedral elements may actually result in a significant increase in computational runtime.

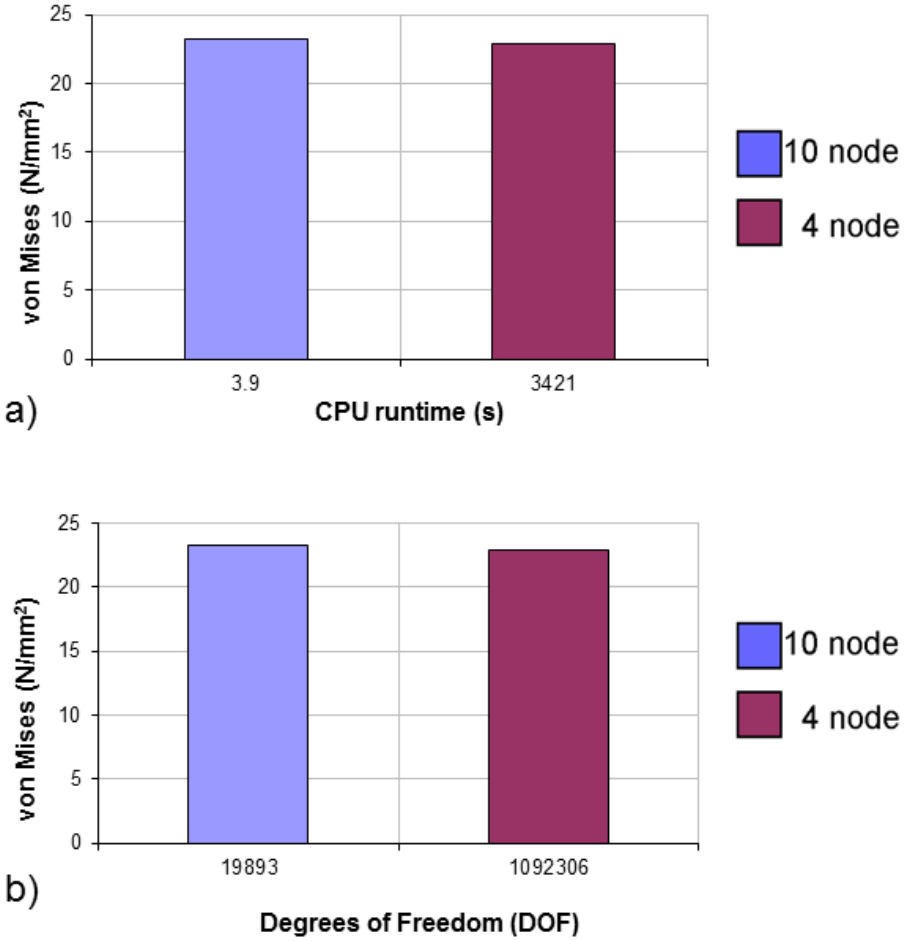


**Figure 3.4:** a) comparison of CPU runtime and b) DOF required to solve a simple three-dimensional problem using both four node (linear) and the ten node (quadratic) tetrahedral meshes,

Similarly, the inclusion of complexities such as frictional contact, as discussed in Chapter VII, can increase CPU runtime dramatically, from approximately 2.5 hours with linear elements to $\geq$ 48 hours with quadratic elements for a frictional model of the femur post-TKA. This highlights the necessity to conduct a convergence study prior to the main investigation to ensure the appropriate element type and density is selected, so as to optimise the balance between solution accuracy and efficiency of the analysis.

## III.4 Model parameters and hardware requirements

In the field of biomechanics determination of any one of the number of parameters required to analyse a problem with FE can often be very challenging. Figure 3.5 highlights potential sources for some of the key parameter.

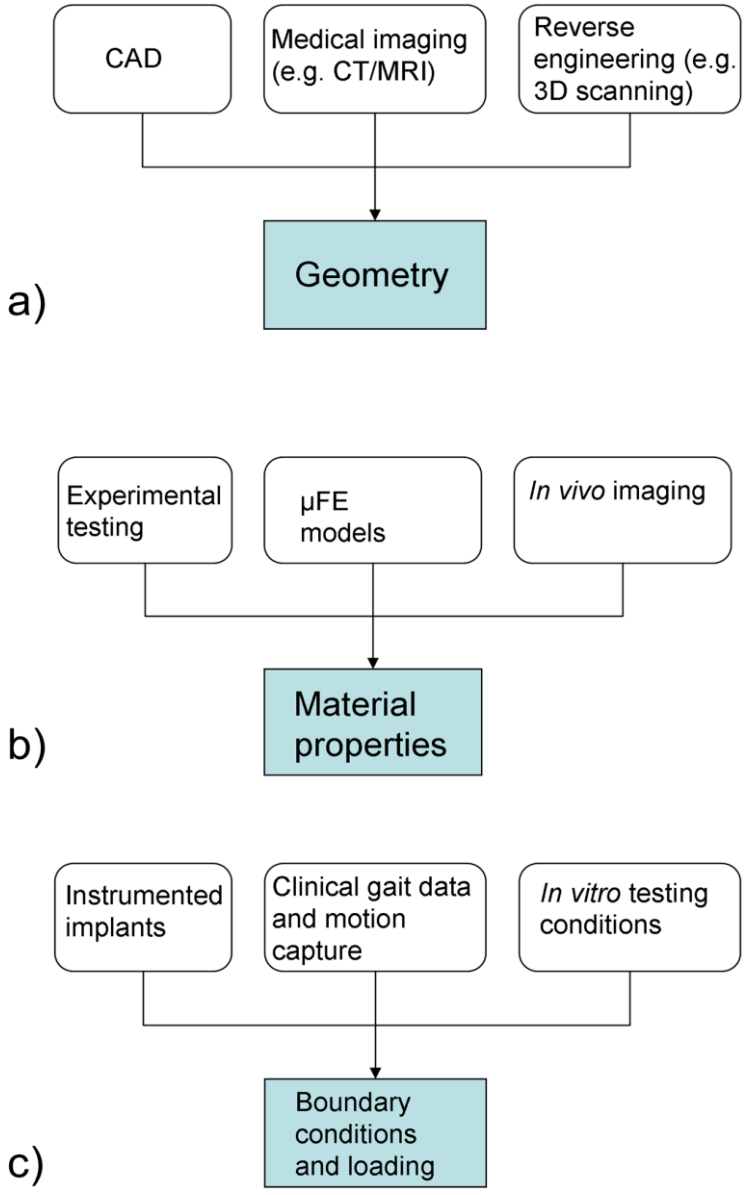


**Figure 3.5:** Flowcharts showing potential sources for a) system geometry, b) material properties and c) system loading and boundary conditions.

Thus far the example models presented here are small enough to be solved on a modern laptop (Intel first generation i5 dual core processor with 8GB of ram), however, the more realistic models required to answer clinical questions in the field of biomechanics often require millions of elements and to solve them in a reasonable time frame would be above the operational limit of most normal computers. Model complexity and runtime also significantly increase once aspects such as frictional interfaces are considered.

The majority of the models presented in the following chapters often exceeded the operational constraints of a normal personal computer and therefore relied heavily on high performance parallel computing to obtain a solution within a reasonable time frame. High performance computing in its most basic form consists of a collection of computing resources or "cluster" networked for the purposes of provide a more powerful tool for resource intensive tasks, this method leverages the computing resources and memory of each machine to provide a tool which collectively can offer superior computing power and speed when compared to the individual capabilities of each machine. The majority of the models investigated in this thesis were solved in this manner. The use of a high performance computing cluster allowed access to multiple CPUs and RAM in excess of 40GB for individual model applications. The specific cluster used for these studies (EDDIE) is operated and maintained by The Edinburgh Compute and Data Facility (ECDF)[4]. This cluster consists of a number of nodes, each node in turn contains eight or more processors giving an overall total of 2980 processors altogether.

To run FE jobs on a computing cluster requires the creation of some additional files, a brief overview of the workflow is given in Figure 3.6.

The FE model is first created using Abaqus, as previously described in the example. Once the FE model is prepared Abaqus/CAE is then used to generate a job input file (.inp extension). This job file in combination with a job submission script file is then uploaded to the computing cluster and submitted for analysis. The job submission

[4] (https://www.wiki.ed.ac.uk/display/ecdfwiki/Eddie+and+the+ECDF).

script contains details of memory requirements, time allowance, number of CPUs to request and program used to analyse the job file. An example script is shown in Figure 3.7 with key commands highlighted.

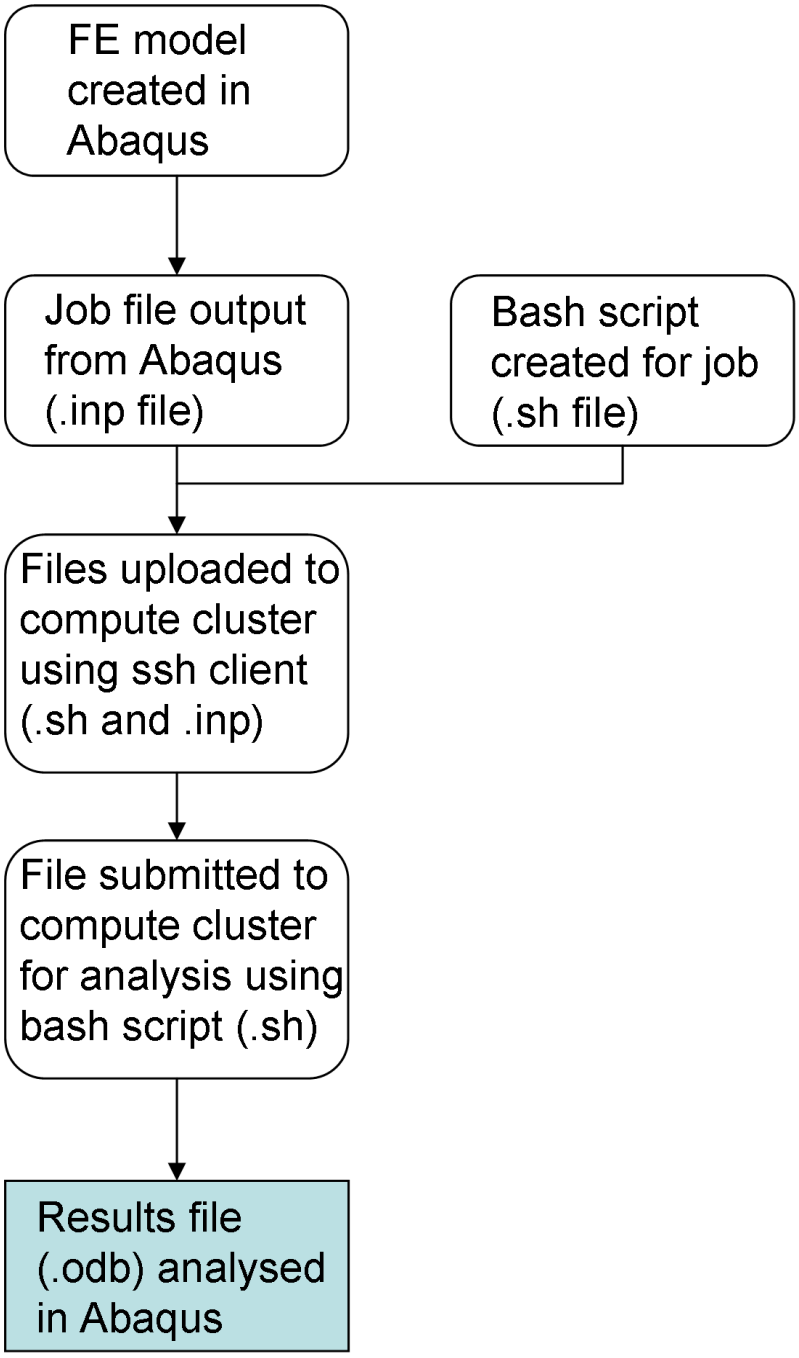


**Figure 3.6:** Workflow for conducting an FE analysis using a high performance computing cluster.

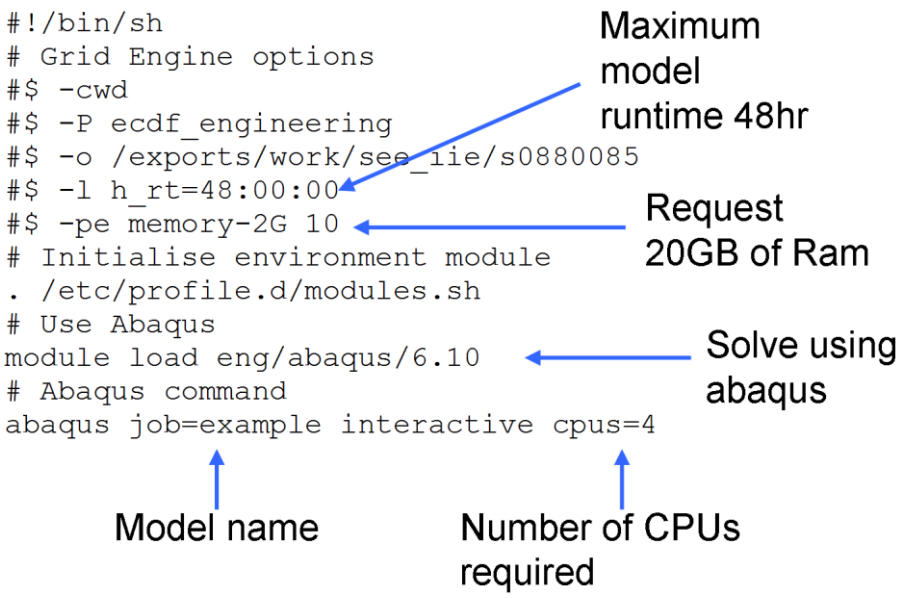


**Figure 3.7:** Example of a bash job script used to solve FE models over a computing cluster.

## III.5 Discussion

This chapter outlined the basic procedure for conducting a FE analysis of a simple part and briefly showed how to ensure solution accuracy. Though the complexity of the models increases in the subsequent chapters, the core methodology outline here remains the same.

The widespread use of FE in recent years for the purpose of investigating complex clinical scenarios has been aided by advances in both computational power and medical imaging technologies. As a consequence it is now possible to generate highly detailed patient specific models in a relatively short period of time. However, proper care must be taken in the setup and analysis of any FE model to ensure meaningful results are obtained. In conclusion the use of highly detailed and realistic FE models allow access to a whole range of information that for ethical or physiological reasons cannot be easily obtained from a lab or clinical research investigation.

In the following chapters, the techniques and methodology discussed here will be applied to obtain clinically relevant information regarding implant stability and fracture risk for a wide range of implant configurations and patient scenarios.

# IV

# Post – TKA Mechanical Environment in the Distal Femur

## IV.1 Introduction

In this Chapter, the modelling and FE methodology described in the previous chapter is employed to model the distal femur following primary total knee arthroplasty (TKA).

The quality of bone at the time of surgery is important in terms of achieving good initial fixation and stability of the prosthesis. Indeed bone quality is one of the key factors which can influence component longevity. In the setting of revision TKA, the quality of the underlying bone is perhaps even more important. Increasingly surgeons are finding that areas immediately under primary implants, in particular behind the anterior flange and posterior condyles of the femur have suffered large amounts of bone loss (Petersen et al. 1995, Spittlehouse et al. 1999, Soininvaara et al. 2004, Saari et al. 2006). As discussed in Chapter II, this loss of bone may occur as a result of particle induced osteolysis or prosthesis induced stress shielding, the latter being of particular interest in this study due to the direct relationship between prosthesis design and bone loss.

Bone loss under the implant and stress concentrations around the implant can greatly influence the pattern of periprosthetic femoral fracture (Saari et al. 2006). The prostheses used in TKA need to be able to survive longer and deal with the correspondingly greater physical demands as the average patient age at the time of

surgery decreases. Furthermore, should the need for revision arise, it is desirable that the quality of the underlying bone remains adequate for fixation. Several studies documented the application of FE for the purpose of investigating both the natural knee joint and the knee following TKA. The majority of these studies tend to focus on wear of the tibial bearing component (Bei et al. 2004, Shi 2007) or loosening of the tibial tray (Hashemi and Shirazi-Adl 2000, Chong et al. 2010). In contrast relatively fewer studies have focused on the distal femur (Tissakht et al. 1996, van Lenthe et al. 1997, van Lenthe et al. 2002, Barink et al. 2003, Moran 2005, Completo et al. 2007, Shi 2007, Shi et al. 2007, Completo et al. 2009, Bougherara et al. 2010).

The effect of modelling the bone-implant interface as bonded, frictional or smooth has been considered by a few studies (Tissakht et al. 1996, van Lenthe et al. 1997, van Lenthe et al. 2002, Barink et al. 2003, Completo et al. 2009). Some studies considered either a single implant (Tissakht et al. 1996, van Lenthe et al. 1997, Barink et al. 2003, Bougherara et al. 2010) or a single load case (Tissakht et al. 1996, Completo et al. 2007, Completo et al. 2009). Studies sometimes use CT based properties to assign inhomogeneous material properties to bone (van Lenthe et al. 1997, van Lenthe et al. 2002, Barink et al. 2003), in which the variation of elastic modulus is estimated from the variation of apparent bone density from the CT scan of the specific femur being modelled. While post TKA stress shielding was found to occur in these studies (van Lenthe et al. 1997, van Lenthe et al. 2002, Barink et al. 2003), the pattern of changes in the mechanical environment and the mechanism through which this occurs is not generally considered.

This study details the creation and application of FE models to examine the post TKA mechanical environment in the distal femur after implantation with two different types of implants: a cruciate retaining (CR) implant with two distal femoral pegs and a posterior stabilising (PS) implant with intercondylar box, as shown in Figure 4.1. It must be noted that as both implants are from the same product line (Triathlon®, Stryker, UK), both share the same external articular surface geometry and very similar internal implant geometry, with the exception of minor alterations due to the presence of the femoral pegs or box.


**Figure 4.1:** Image of a) a CR implant highlighting the femoral pegs, and b) a PS implant highlighting intercondylar box section.

The specific focus of this study was to examine the influence of internal features (i.e. pegs or box) for a range of functional flexion angles simulating close to physiological loading conditions.

## IV.2 Methods

In this study finite element (FE) models were created to examine the influence of internal implant geometry on the mechanical environment in the distal femur after TKA. As previously stated in Chapter III, a clear definition of the system geometry, material properties, boundary conditions and loading are required to correctly simulate a problem of biomechanics using FE.

### IV.2.1 Geometry of the femur

In this instance femoral geometry was based on a CAD model reconstruction of a synthetic bone analogue commonly employed in *in vitro* investigations as an alternative to cadaveric testing. Known as the "third generation composite femur" and originally created from CT scans of a synthetic bone lab specimen (Cheung et al. 2004) by Papini and colleagues (Ryerson University, Ontario, Canada), this model is freely available in the public domain through the BEL repository

(https://www.biomedtown.org/biomed_town/LHDL/Reception/datarepository/repositories/BelRepWikiPages/3rdGenerationCompositeFemurASolidModel) and represents an accurate three-dimensional reconstruction of a large left composite femur (Product 3406, Sawbones, Pacific Research Laboratories, Vashon, USA). This femur model consists of three solid volumes, representing both the stiff outer cortical structure of the femur and the spongy internal regions of cancellous bone in the distal and proximal metaphysis (Figure 4.2). The model also incorporates a hollow region between the boundaries of the distal and proximal cancellous bone structures representative of the medullary canal as is found in the physical specimen on which it is based. This particular CAD geometry was selected to avoid patient specific issues and to allow for potential comparisons with any *in vitro* tests conducted with the composite femurs.

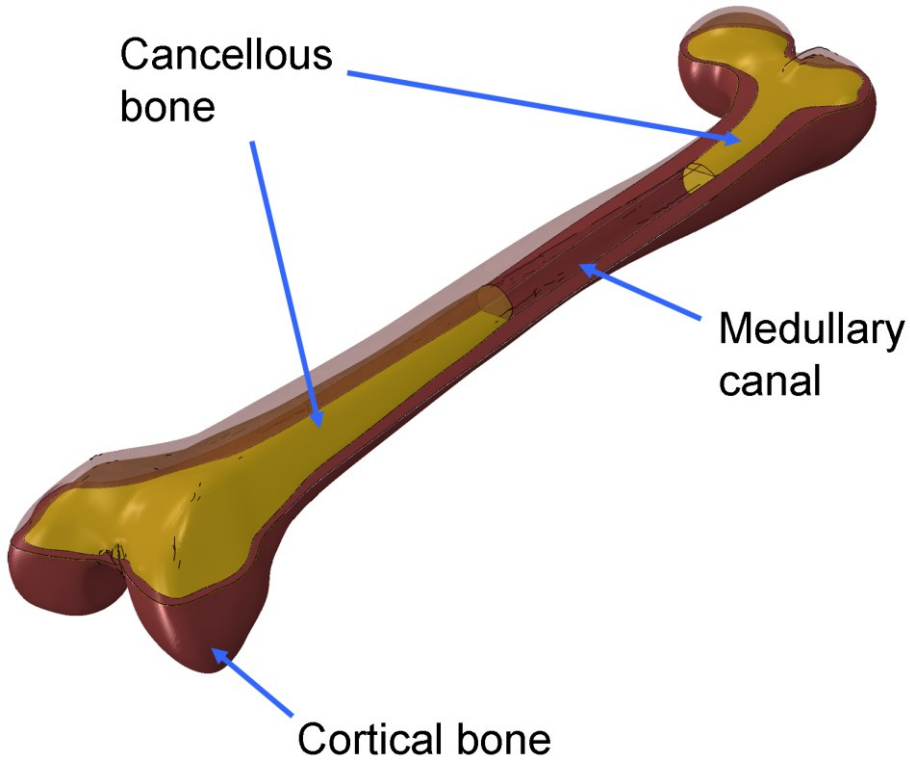


**Figure 4.2:** Rendered CAD model of third generation composite femur, transparent anterior surface reveals the medullary canal and cancellous bone regions.

### IV.2.2 Femoral component geometry

The base femoral component geometry employed in this study was created using computer aided design software (Autodesk Inventor 2010, Autodesk inc. San Rafael, California, U.S.). The overall shape and dimensions were derived from visual inspection and detailed measurements of a cruciate retaining implant (size 4 right, Triathlon® series, Stryker, UK).

The geometry of the composite femur and lab specimens upon which it is based are all modelled on the left side of the appendicular skeleton. Due to the asymmetrical nature of the femoral component and to ensure compatibility of the model with the femur, all major features and dimensions were transformed about a central axis in the CAD package to convert the prosthesis from a right knee to a left knee. It became apparent, however, that the geometry approximated from this implant when loaded into the same virtual environment as the chosen femur was not a suitable match. To be compatible with the composite femur required that the implant be scaled up to the next size in the implant range (size 5). One complication of this process is that not all implant features scale linearly between sizes, with the Triathlon® series providing for a wide array of sizes based on anthropometric data (Stryker Orthopaedics 2008a). To overcome this issue key leading dimensions were approximated based on in theatre surgical templates used for sizing implants to patient X-rays. The procedure to produce the base CAD model geometry is outlined in Figure 4.3.

One of the key aims of this study was to determine the influence of internal implant features on the mechanical environment in the femur post implantation. In this instance commonly employed internal features such as distal femoral pegs and an intercondylar box were considered. Though minor details of an implant's external/internal geometry may vary between manufacturers, these internal features (pegs or box) are used extensively by the medical device industry (e.g. Stryker: Triathlon® series; DePuy: P.F.C. Sigma series; Smith & Nephew: Genesis series). To permit a controlled and adequate comparison between implant types, both geometries were derived from the initial femoral component presented in Figure 4.3d. This was considered to be a far assumption since both CR and PS implants in

the Triathlon® series (Stryker, UK) share the same internal geometry and external articulating surface, in other words the only difference between the two implant types being the presence of femoral pegs or intercondylar box (Figure 4.1).

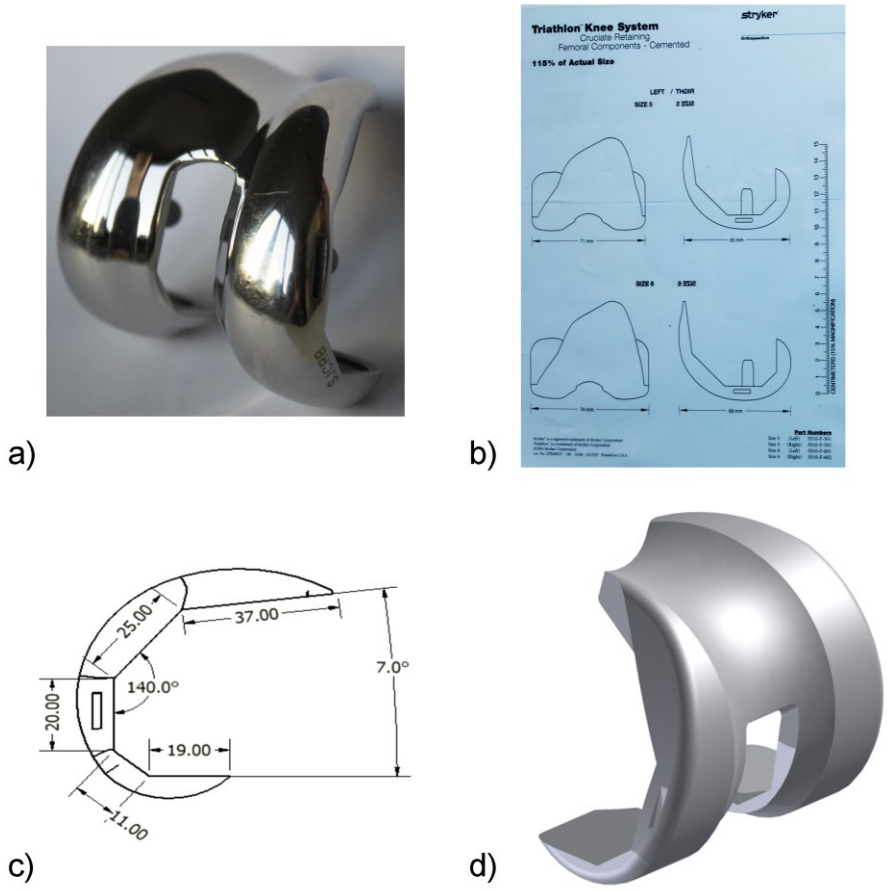


**Figure 4.3:** a) Image of a size 4 right Triathlon® CR implant (Stryker, UK), b) image of surgical templates used to approximate size 5 left dimensions, c) two-dimensional sketch of implant cross-sectional profile and d) final rendered CAD model of implant created from the 2D profile using a series of sweeps and extrude commands in Autodesk Inventor (Autodesk, USA).

The CAD reconstructions of each implant can be seen in Figure 4.4, it should be noted that for ease of modelling some simplifications were made to the implant geometry, e.g. cement recess removed. These simplifications were carried out to ensure maximum contact at the bone-implant interface in the absence of cement. It is believed that due to the comparative nature of this study and the fact that both reconstructions were derived from the same initial geometry (Figure 4.3d), these simplifications will only have a minor impact on the results of this study.

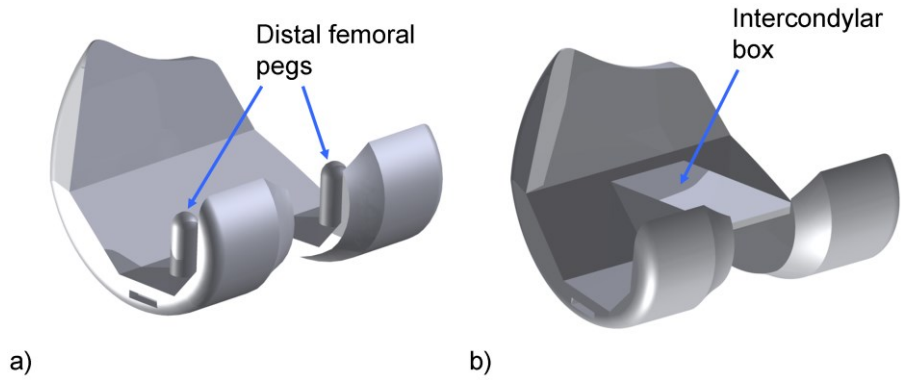


**Figure 4.4:** Rendered CAD model of a) a cruciate retaining (CR) implant with two distal femoral pegs and b) posterior stabilising (PS) implant with intercondylar box section.

### IV.2.3 Virtual implantation and creation of FE models

The full composite femur model was imported into Autodesk Inventor (Autodesk), once in the CAD environment a series of virtual "surgical cuts" were performed in accordance with the relevant implant's recommended surgical protocol (Figure 4.5). It can be seen from Figure 4.5b and 4.5c that the cuts performed during virtual surgery expose the underlying cancellous bone (light green). It can also be seen that the characteristic profile of both femurs are the same, though the cuts to receive a PS implant necessitate removal of a larger proportion of bone material to accommodate the intercondylar box section of the PS implant. Each femur model (intact and implanted) was then transferred into Abaqus for model assembly and mesh generation.

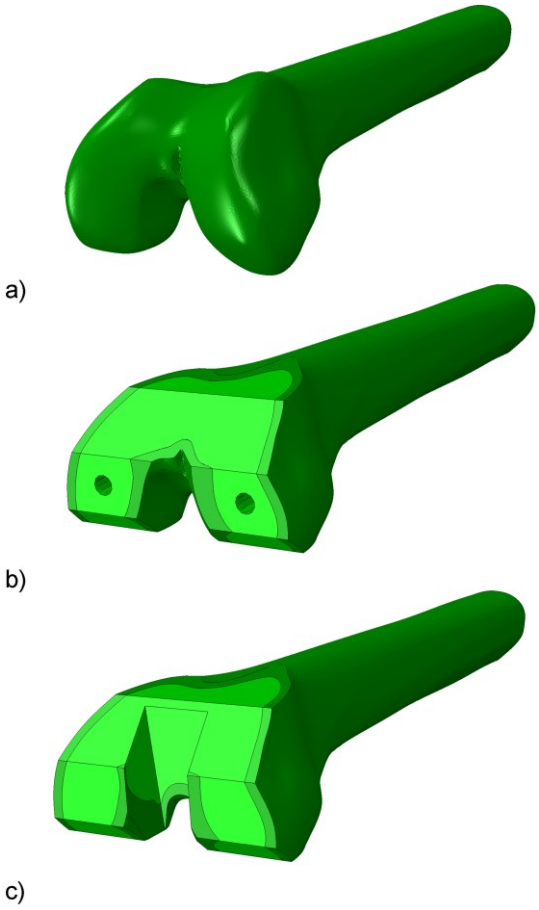


**Figure 4.5:** Rendered CAD models showing a) an intact distal femur, b) a distal femur prepared according to the CR implantation protocol, and c) a distal femur prepared according to the PS implantation protocol. Light green indicates cancellous bone regions and dark green cortical bone regions.

In this study second-order tetrahedral elements consisting of ten nodes and four integration points were employed. It is important to note that while the four node tetrahedral elements are known to provide poor stress predictions, the ten node elements used in this study have been shown to be much more accurate (Lo and Ling 2000, Payen and Bathe 2011). The FE meshes generated for the intact and implanted femurs are presented in Figure 4.6. It should be noted that these meshes were considerably finer than that used in previous studies (Tissakht et al. 1996, van Lenthe et al. 1997, Barink et al. 2003) and typically consisted of 290,000 elements with a characteristic edge length of 2mm (based on convergence studies).

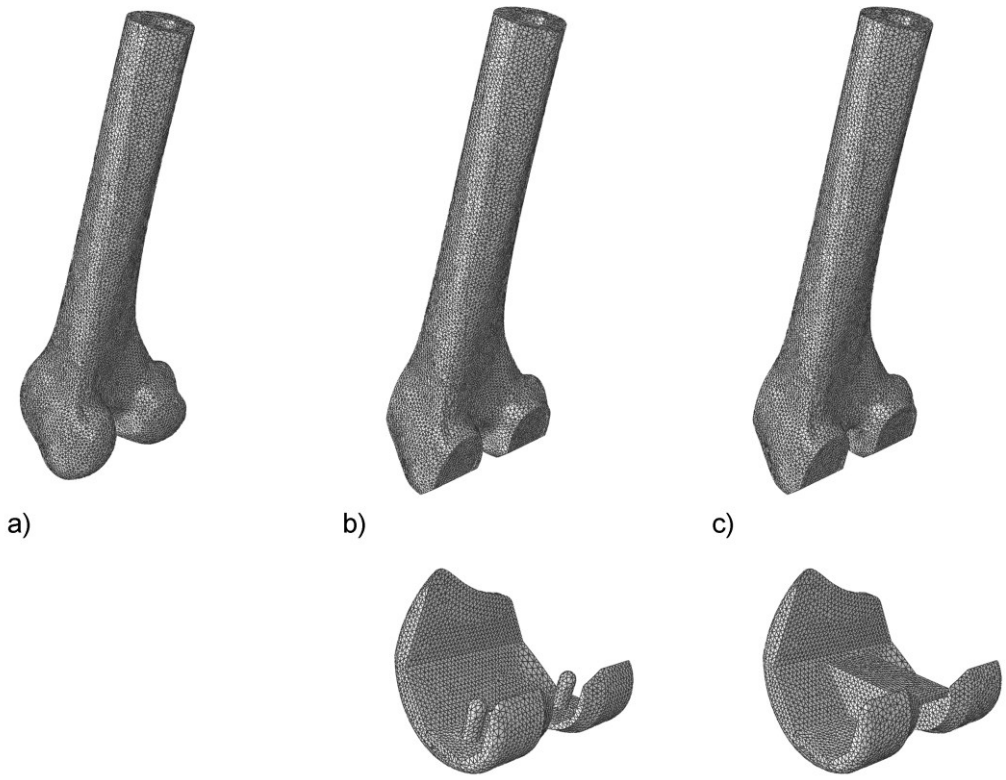


**Figure 4.6:** a) Mesh view of an intact distal femur, and b) an exploded mesh view of a CR implanted femur and c) an exploded mesh view of a PS implanted femur.

### IV.2.4 Material properties

All materials were assumed to be linear elastic and isotropic. Elastic constants used for bone and implant structures are presented in Table 4.1. In the field of biomechanics correct definition of material behaviour is critical to obtain realistic clinically relevant results. Some previous studies have used inhomogeneous material properties based on CT scans (van Lenthe et al. 1997, van Lenthe et al. 2002, Barink et al. 2003). To avoid the associated specificity of scan based data homogeneous properties were used for cortical and cancellous bone regions, as has been done in many previous studies (Completo et al. 2007, Completo et al. 2009).

**Table 4.1:** Material properties applied to bone and implant structures.

| Region | Poisson's ratio | Young's modulus ($N/mm^2$) |
|---|---|---|
| Cancellous bone | 0.3 | 155 |
| Cortical bone | 0.3 | 16700 |
| Femoral component (Co-Cr) | 0.3 | 210000 |

As discussed in Chapter II, the behaviour of bone as a structure is quite complex, the simplification of its material properties without careful consideration of the effects may introduce large errors (Au et al. 2010). It is known that bone is anisotropic (Donaldson et al. 2011). This feature is likely to affect the mechanical environment with changes in loading direction, however, due to an absence of reported data, on the femoral condyles in particular, bone was considered isotropic as in almost all previous studies. However, it should also be noted that for investigations where the comparative behaviour, rather than an exact magnitude is required, the assumption of isotropy may be adequate.

In the current study values for cancellous and cortical bone structures were taken from available sawbones product information (Sawbones 2008). These properties as recommended by the manufacturer are within the range of reported values from current literature (Reilly and Burstein 1974, Goldstein 1987, Choi et al. 1990, Katsamanis and Raftopoulos 1990, Hodgskinson and Currey 1992, Rho et al. 1993, Hodgskinson et al. 1997).

### IV.2.5 Boundary conditions

The choice of boundary conditions can greatly affect some of the output parameters being considered in any FE analysis. *In vivo* the femur is supported by a complex biological system of muscles, ligaments and fibrous cartilage. Previous studies have

shown that the stress distribution in the femur or pelvis can be altered significantly by inclusion of boundary conditions that incorporate muscles and ligaments (Phillips et al. 2007, Speirs et al. 2007, Phillips 2009). However, it has also been observed that the mechanical environment close to the point of load application is minimally influenced by boundary conditions at some distance (Phillips et al. 2007, Conlisk et al. 2012). As the region of interest in this particular study was confined to the distal portion of the femur where it meets the tibia to form the knee, each femur model was truncated at the mid-diaphysis and all its translations/rotations fixed. Based on initial investigations, an optimum distance of 242mm from the distal most point on the condyles was selected. This manner of fixation is consistent with numerous previous FE (Tissakht et al. 1996, van Lenthe et al. 1997, van Lenthe et al. 2002, Barink et al. 2003, Completo et al. 2009, Bougherara et al. 2010) and experimental investigations (Moran 2005, Completo et al. 2007, Bougherara et al. 2010). In addition by reducing the overall geometrical size of the model by half a higher resolution mesh could then be applied without significant increase in computational run time.

### IV.2.6 Loading

As discussed in Chapter II, there exists a large variability in the reported loading at the knee joint for the same activity. To minimise the potential for errors, the present study considered forces acting on the knee as reported by *in vivo* telemetric implant studies (Taylor et al. 1998, Bergmann 2008). To enable the generation of a single consistent set of forces acting on the knee joint, both data sets were normalised in terms of their respective patients body weight (BW) and then applied to the FE models for an assumed average body weight of 775N. In this study, three functional flexion angles during the stance phase of gait for a normal walking cycle were investigated. Each flexion angle was modelled as a static load step. Referring to Figure 4.7a, the loads acting on the femur in this instance comprised of six separate components: the patella-femoral force (PF); the medial and lateral components of the joint normal force (Fm and Fl); the medial and lateral components of the joint shear force (APm and APl); and the internal/external moment (IE).The exact magnitudes

applied for each component of force are indicated in Table 4.2. All forces were applied as distributed pressure loads over realistic contact areas (Goudakos et al. 2010), with a 60-40% (medial/lateral) load distribution acting across the condyles assumed for the axial components of force (Burstein 1994, Shi 2007).

In Figure 4.7b it can be seen that each of the six components of force were applied over three distinct contact areas at each flexion angle; PF, Fm and Fl acting normally and APm/APl acting tangentially on the patella-femoral and tibio-femoral contact surfaces assuming correct alignment of the implant. Computationally the IE moment was included by altering the values of APm and APl applied to the femur, which was necessary to avoid unrealistic peak stresses occurring as a result of applying high forces to individual nodes to create the moment. The basic procedure is illustrated in Figure 4.8. This procedure was applied to incorporate the IE moment into the AP shear force for each of the three flexion angles investigated.

**Table 4.2:** Forces used in the FE analyses.

| | 0° | 22° | 48° |
|---|---|---|---|
| Fm (N) | 436 | 1159 | 1160 |
| Fl (N) | 291 | 772 | 773 |
| APm (N) | -57 | 130 | -3 |
| APl (N) | -57 | 130 | -3 |
| PF (N) | 45 | 327 | 567 |
| IE (Nmm) | -829 | 3292 | -7029 |

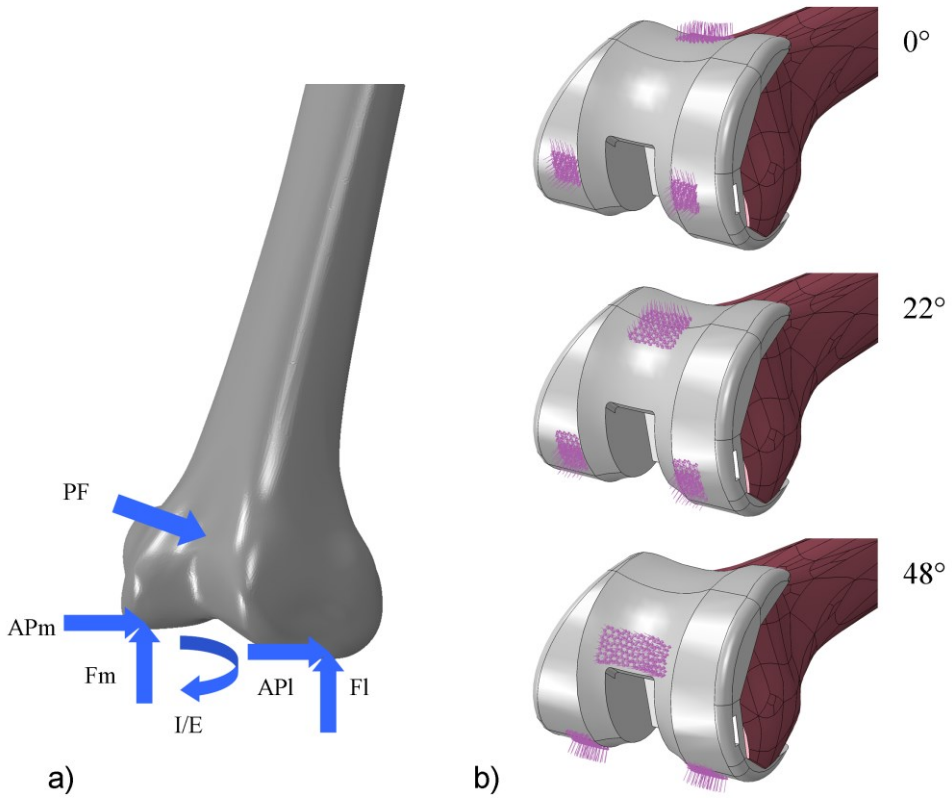


**Figure 4.7:** Images of distal femur model showing a) the arrangement of forces and b) the location these are applied to for each flexion angle investigated.

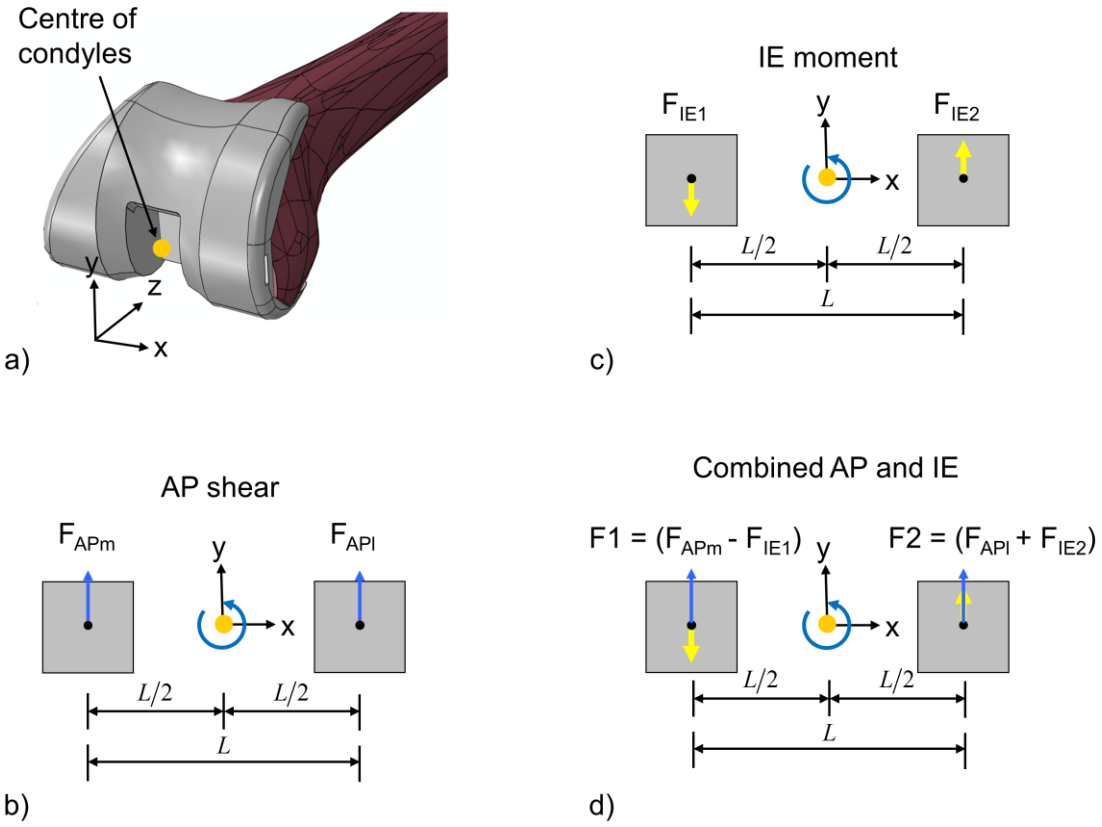


**Figure 4.8:** a) shows a rendered view of the femur with centre of the condyles highlighted by the orange dot, b) shows a simple schematic of the tibio-femoral joint contact regions viewed in the x-y plane (approximately 100mm$^2$ and indicated by grey box) and two point loads representing the medial (APm) and lateral (APl) shear forces acting at the centre of the joint contact areas (represented by the black dots), c) shows the same schematic, but with the shear forces replaced by two point loads, one of which is acting in the opposite direction, in the x-y plane, these two point loads act at a known distance away from the centre of the condyles (*L/2*) so as to create the desired IE moment about the z-axis. Finally d) shows the combination of both AP and IE loads. It is important to note that the sum of the force in the y-direction (∑Fy) is not altered through this process. The combined forces represented by F1 and F2 are then applied as a uniformly distributed surface traction load over the joint contact area to avoid unrealistic peak stresses.

### IV.2.7 Interface properties

In this study all bone-implant interfaces were tied modelling full osseointegration of the implant into the bone.

## IV.3 Results

Previous studies (Tissakht et al. 1996, Behrens et al. 2009) have shown that strain energy density (SED) is a good indicator of potential regions of bone remodelling. To examine the change in strain energy density a number of representative sagittal sections were taken in the condylar region as shown in Figure 4.9. The planes a-a and b-b represent sections through the medial and lateral condyles respectively. The resulting pattern of SED for the intact and implanted femur models at the three flexion angles considered is shown in Figure 4.10. The cancellous bone regions, of both implanted femurs, show considerably reduced levels of SED in comparison to the intact case. The lateral section experiences significantly lower SED in comparison to the medial section, which is apparently due to higher loads being applied to the medial femoral condyle in physiological loading. It is also interesting to note that at higher flexion angles, in the stance phase of gait, the regions of high strain energy density increase for both the intact and implanted cases, however this increase is far more significant and obvious for the intact case. The commonly examined load case of 0° flexion only shows small localised regions of high SED for the intact case.

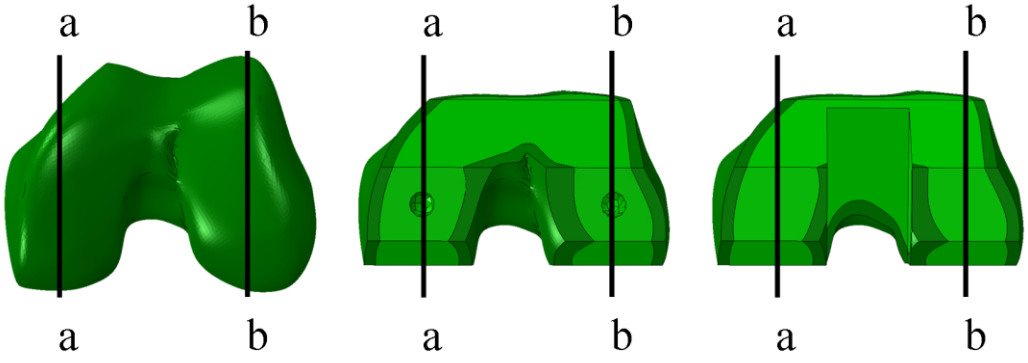


**Figure 4.9:** Showing the sectional views through the medial (a-a) and lateral (b-b) condyles of each femur model investigated.

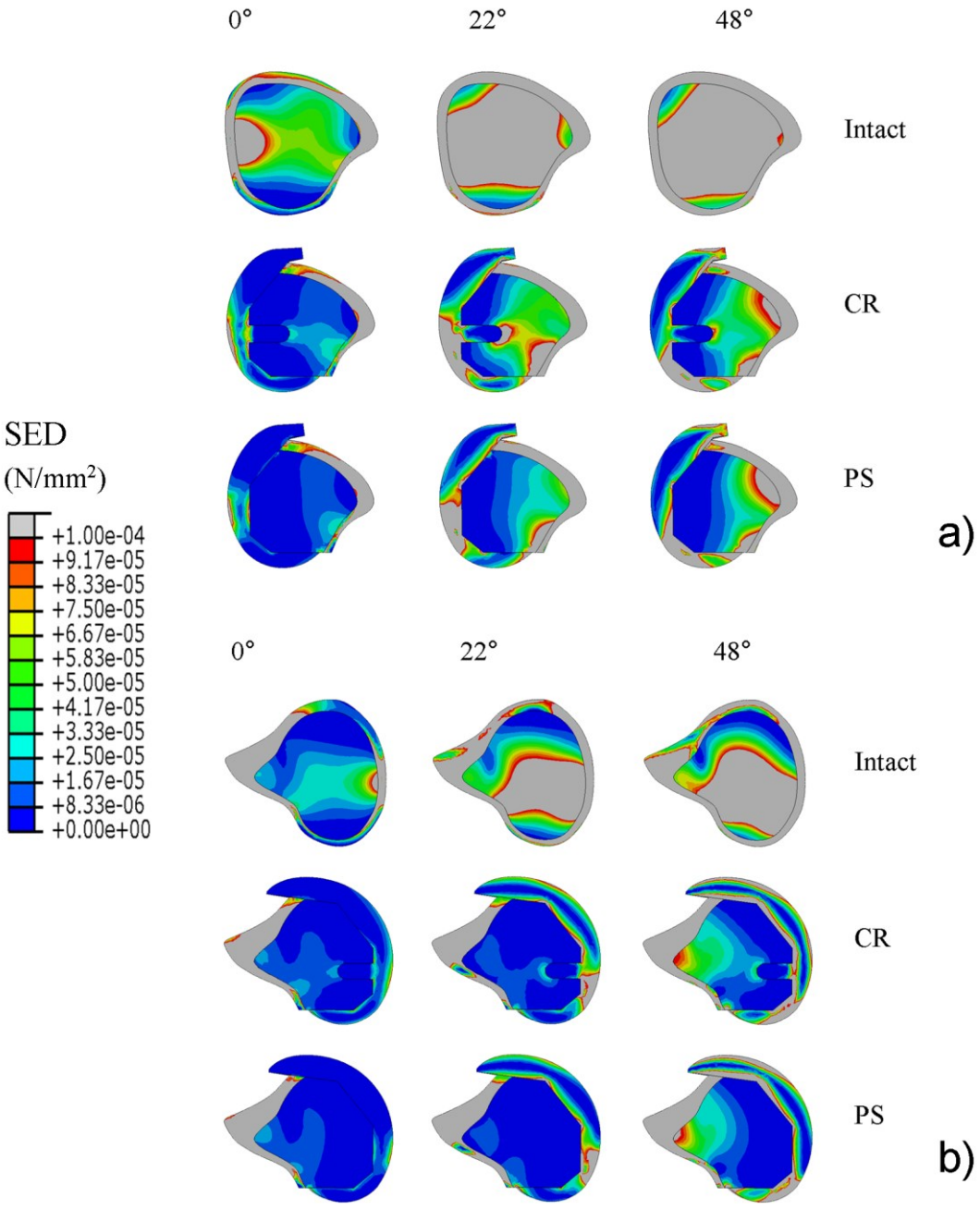


**Figure 4.10:** Contour plots showing the pattern of SED in a) the medial (a-a) and b) the lateral (b-b) condyles for each of the three flexion angles investigated.

To investigate the overall impact of the implants on the changes in the mechanical environment in the femur post total knee arthroplasty each model was divided into four volumes corresponding to the four regions of interest (ROI), shown in Figure

4.11a. Regions of interest were chosen to be in line with the Gruen zones used in previous clinical DEXA imaging studies (Soininvaara et al. 2004). The average strain energy density for each region calculated across the volume of elements falling within that region of interest was evaluated for the three flexion angles considered and is shown in Figure 4.11b-e. It is clear from the figure that both implanted femurs experience much lower levels of SED in ROI 1-3 (immediately under the implant). The level of reduction of SED in these regions varied from 70-90% in comparison to the intact case. ROI 4, however, shows a marked increase in SED.

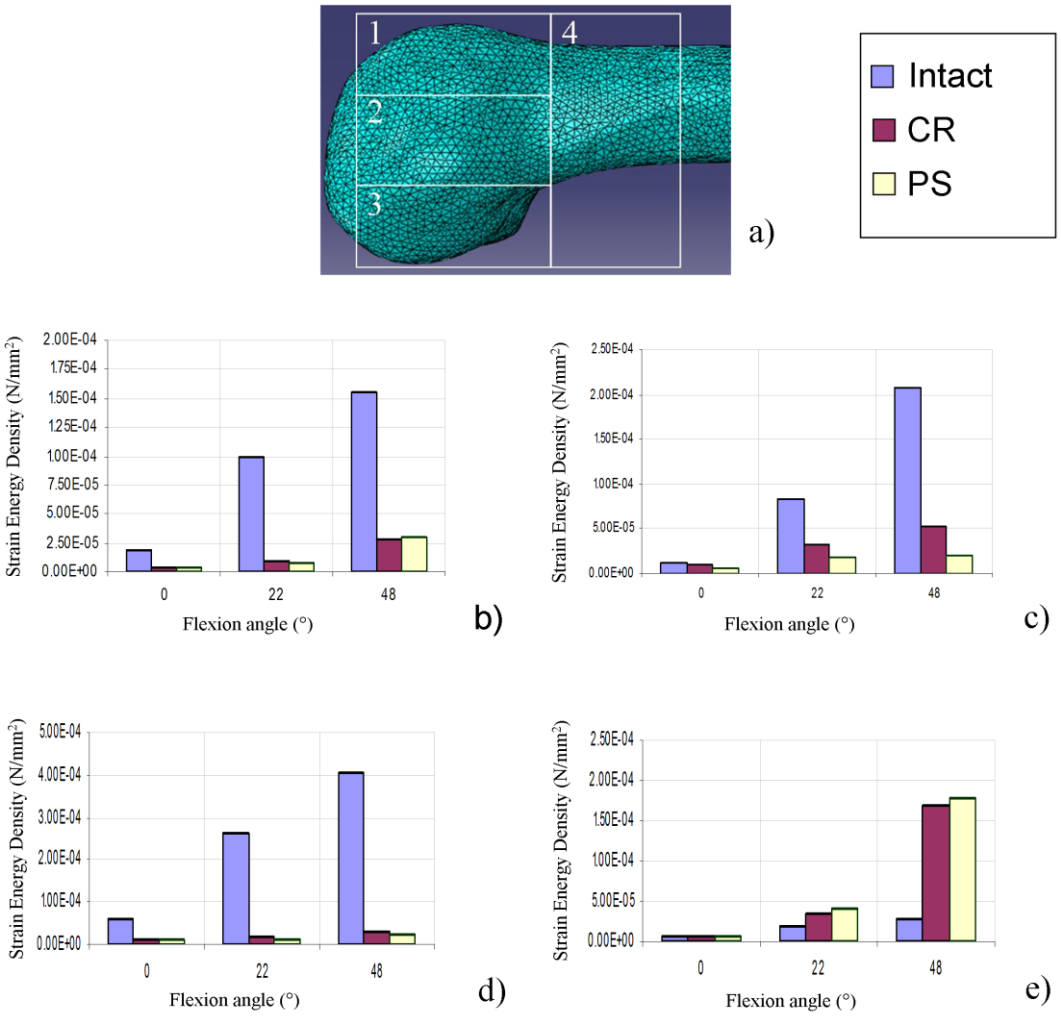


**Figure 4.11:** a) Periprosthetic regions of interest in the distal femur corresponding to Gruen zones used in DEXA imaging and the average value of strain energy density (SED) in b) ROI 1, c) ROI 2, d) ROI 3 and e) ROI 4 found in all distal femur models.

On consideration of changes to the mechanical environment due to internal implant features, it is found that the CR implant induces high localised stress concentrations at the tip of the femoral pegs (which can also be seen in SED plots shown in Figure 4.10). The PS implant on the other hand shows stress concentrations at the corners of the femoral box cut (Figure 4.12). The magnitude of these concentrations was found to increase at higher functional flexion angles.

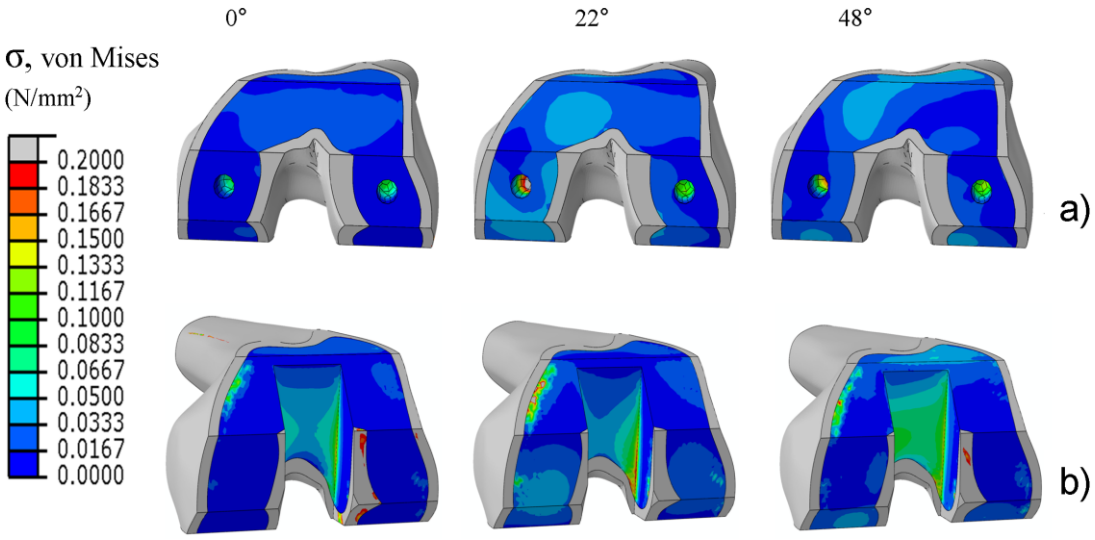


**Figure 4.12:** Stress concentrations in the distal femoral cancellous bone structure due to internal implant features for a) CR and b) PS implanted femurs.

Low SED values in regions close to the implant as shown in Figure 4.10 and Figure 4.11 were also found to correspond to reduced stresses in these regions post implantation. To gain a better understanding of the load transfer mechanism, stresses in a transverse section (c-c) just above the implant were evaluated. The variation of von Mises stresses under the two implants for the three flexion angles is shown in Figure 4.13. At 0° flexion all three distal femur models are subject to a similar magnitude and distribution of stress. However, as flexion angle increases, it can be seen that the magnitude of stress on the anterior and posterior aspects of the cortex of both implanted femurs increases significantly in comparison to the intact femur model, indicating that the implants are directly transferring loads to the cortical bone region proximal to the implant.

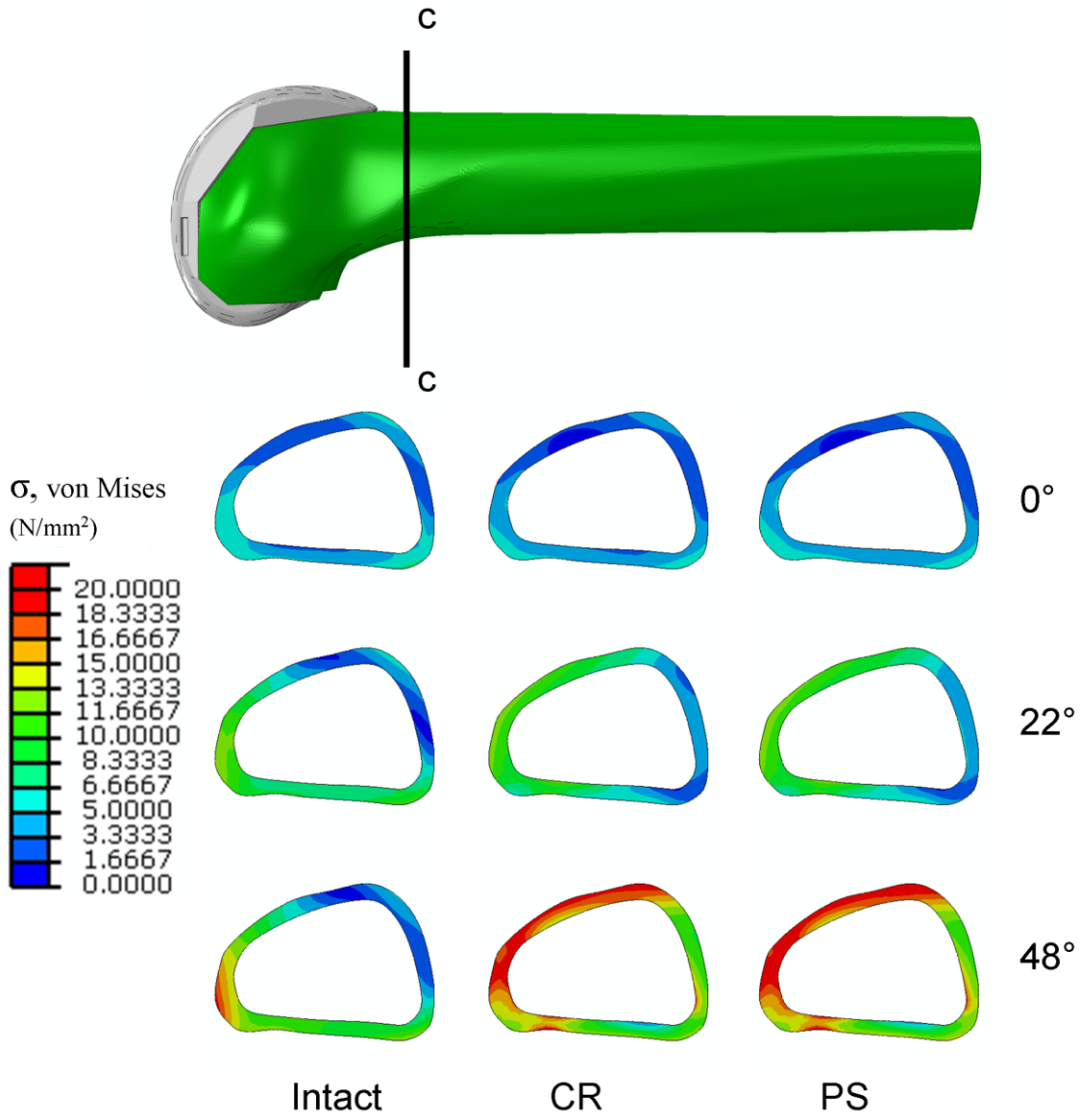


**Figure 4.13:** Location of transverse section c-c and resulting contour plots showing the pattern of von Mises stress in the cortical bone of the Intact, CR implanted and PS implanted femurs at 0°, 22º and 48º flexion.

## IV.4 Discussion

In this study three FE models of the distal femur representing both pre and post primary TKA scenarios were investigated. The specific focus of this study was to develop a better understanding of the mechanisms which contribute to stress

shielding and clinically observed bone loss under implants and to determine what influence if any that internal implant features (i.e. pegs or box) exert on the femur post implantation.

The present study shows that the pattern of SED changes significantly with changes in loading directions and magnitude. In particular it is found that loading corresponding to 0° flexion induces relatively small changes in SED post implantation, this finding is contrary to that proposed by some previous studies (Bougherara et al. 2010, Bougherara et al. 2011) which cited 0° as a critical case for stress shielding. It is likely that the lack of a patella femoral force in the aforementioned studies may have influenced recorded values in flexion where redistribution of the PF force on the articular surface is found to cause significant shielding of the anterior region. The current study indicates that predictions often made on the basis of a single load case representing full extension may not be sufficient. The highlighted differences between the results of the current study and that reported in literature (e.g. Bougherara et al. 2011) reinforce the importance of applying realistic 'physiological' loading patterns to the femur.

The values of mean SED show that there is a reduction in the three distal regions (ROI 1-3) and a slight increase in the more proximal region (ROI 4). The reductions are similar to those found in previous clinical studies that examined changes in post-operative bone mineral density (BMD) using Dual-Energy X-ray Absorptiometry (DEXA) imaging which is now a widely accepted clinical method for tracking BMD changes in long bones over extended periods of time (Petersen et al. 1995, Spittlehouse et al. 1999, Soininvaara et al. 2004, Saari et al. 2006). In the current study, the maximum change was found to occur in the central metaphyseal region (ROI 2), followed by the anterior metaphyseal region (ROI 1) and then the posterior metaphyseal region (ROI 3). This sequence is consistent with the clinical investigations of Soininvaara et al. (2004), who found a decrease in BMD of around 25%, 17% and 12% in ROI 2, 1 and 3 respectively one year after implantation. In this study we found the average SED to increase in the diaphyseal region (ROI 4), which is similar to some of the previous computational studies (van Lenthe et al.

1997, van Lenthe et al. 2002) which have reported values in this region. However many clinical studies appear to suggest a small decrease in BMD in this region as well (Soininvaara et al. 2004, Saari et al. 2006). The reasons for this are not apparent. Regional averages of SED or stresses show little difference between the two implants considered in this study, indicating that internal implant features have little influence on these average values, which is consistent with previous studies e.g. (van Lenthe et al. 2002). However, internal implant features do play an important role in the magnitude and location of localised stress concentrations in the bone. Stress concentrations were found to occur at the tip of the pegs for the CR implant and the corners of the box for the PS implant. These differences in localised stress concentrations become more important as secondary conditions such as osteoporosis become established, enhancing the fracture risk around the prosthesis (Meek et al. 2011). As the box in the PS implant spans almost the entire anterior-posterior region, stress concentrations accompanied with bone loss due to stress shielding in this implant in particular can lead to specific patterns of periprosthetic fracture, which can be difficult to treat (e.g. bicondylar femoral fracture). At present, the worldwide incidence of periprosthetic fracture post TKA is reported to be about 3% and is expected to continue increasing over time (Rayan et al. 2008, Meek et al. 2011).

One limitation of the present study is that the same loading conditions were applied for both the CR and PS implants. As discussed in Chapter II, Figure 2.16 the CR implant can expect contributions from the cruciate ligaments, whereas the PS implant would be subject to stresses due to the post-cam mechanism. Another consideration is that a number of ligaments and muscles cross the knee joint, each of these muscles and ligaments have a role to play in motion and stability of the knee joint. However, directly or indirectly these may also serve to alter the pattern of stress distribution observed in the distal femoral condyles (e.g. gastrocnemius). Incorporation of muscles and ligaments, however, is no trivial task and would necessitate information on origin/insertion points and material behaviour throughout the loading cycle. As such it was deemed outside the scope of the present study. One final limitation of the current study is that only the immediate post-operative situation is considered,

whereas in reality, the remodelling and resorption of bone from around the prosthesis is a dynamic process and may continue for a number of years post op (van Lenthe et al. 2002). However, it is believed that the potential regions of bone loss due to prosthesis induced stress shielding observed in the current study are a good predictor of possible sites or regions which may impact upon long term implant stability.

Often the mismatch in component stiffness and the bone it is replacing is cited as the reason for stress shielding (Petersen et al. 1995, Tissakht et al. 1996, van Lenthe et al. 1997, Soininvaara et al. 2004, Shi et al. 2007), while this make sense to a certain extent in the context of a hip replacement where the prosthesis is implanted in parallel with the bone and the stiff shaft transmits the majority of load. The arrangement at the knee after implantation is more representative of components in series e.g. the prosthesis is in series with the bone. Therefore it is not immediately obvious as to why shielding should occur merely as a result of component stiffness. A series of simple benchmark tests, as detailed in Appendix A, were conducted to explore this aspect further. Results from the study presented in Appendix A indicate that component stiffness is partly responsible for observed stress shielding, though the mechanism at work differs slightly from that observed in the hip. The benchmark study revealed that in the intact scenario stress bulbs extended outward from the joint contact locations. In the implanted scenarios, however, these stress bulbs are noticeably absent due to the stiff implant redistributing the joint contact force over a greater surface area. On inspection of the complex distal femur models, similar behaviour to the benchmark tests was observed. In Figure 4.14, it can be seen that the cancellous regions of the intact femur are subject to concentrated bulbs of stress extending outward from the region of loading on the cortex.

When the same locations in the implanted femurs are examined, it can be seen that the stress bulbs are noticeably absent. This indicates that implant stiffness plays a role in stress shielding by redistributing concentrated loads over a greater surface area eliminating these localised bulbs of stress. Shielding of the tibio-femoral force combined with shielding of the patella-femoral force lead to implanted femurs having significantly reduced stresses and strains distally particularly in flexion.

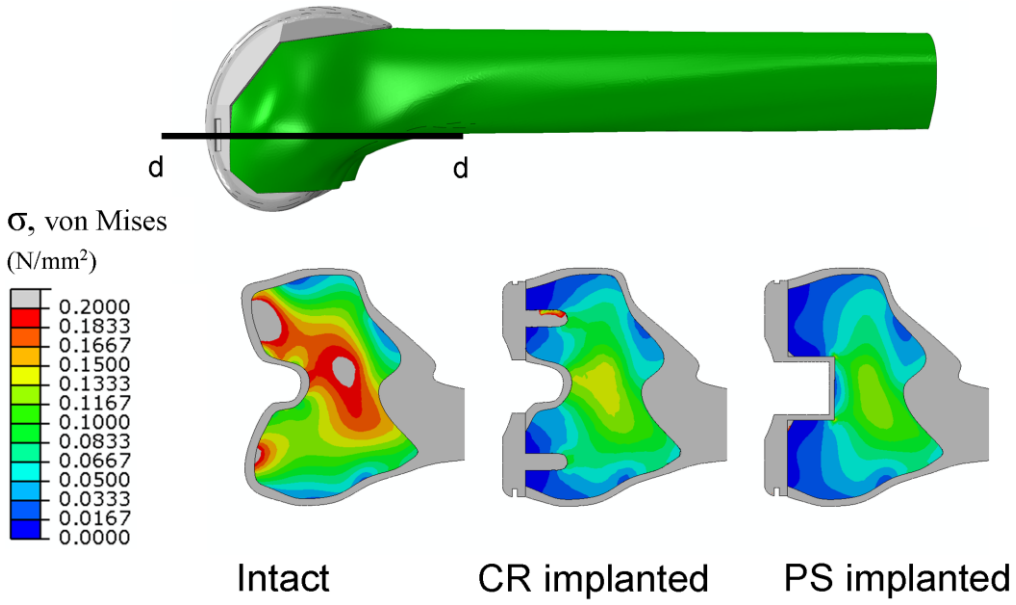


**Figure 4.14:** Sectional view of intact and implanted femur models highlighting the presence of stress bulbs extending outward from the region of load application in the intact femur and the lack of these stress bulbs at the same location in both implanted femurs.

This study also shows that the implants serve as a bridge (primarily spanning the anterior-posterior direction). The implants shield the distal periarticular region from stresses and strains, transferring the loads to the cortical bone immediately proximal to the implant. It is important to recognise that internal stresses need to be in equilibrium with externally applied forces and as a result stress shielding in some regions (or components) leads to an increase in stresses in other regions (Shi et al. 2007). This FE study considered fully osseointegrated cementless implants; however these conclusions will also apply to cemented implants which have been observed to behave in a similar manner to fully tied cementless models (Bougherara et al. 2010).

Though the overall level of shielding in the implants tested was found to be of a similar magnitude regardless of internal implant features, it is important to note that the pattern and magnitude of stress concentrations was found to be highly influenced by the internal features of the implant. Furthermore, the preparation of the femur to receive a PS implant requires the removal of a greater proportion of bone than that of the CR implant, resulting in an overall larger net loss of bone which when combined

with bone loss due to stress shielding may lead to compromised bone stock should revision of the femoral component become necessary and an increased risk of periprosthetic fracture.

This study considered geometry and material properties of an average patient; however, this is not very representative of the wide array of patient type that can undergo TKA. As such the next chapter will focus on expanding the clinical relevance of the present models of the distal femur through incorporation of the effects of ageing and osteoporosis.

# V

# Incorporation of Age Related Changes to the Femur

## V.1 Introduction

The majority of literature tends to focus primarily on cases modelling that of an average patient. However, it has been well documented that as we age our bones undergo mechanical and structural changes (Bousson et al. 2001, Russo et al. 2006, Cooper et al. 2007). As a result, implants designed to suite an average and otherwise healthy patient may induce a very different response in an elderly or pathological patient.

A study by Bousson et al. (2001) employed microradiographs and image analysis techniques to investigate the influence of age and gender on the porosity of three sub-regions (endosteal, mid-cortical and periosteal) from the anterior cortex of the femoral mid-shaft in 163 people. The authors found that pore size and number increased with increasing age in younger patients (<60 years). Furthermore, it was observed that pore size and number were proportionally similar in each of the three sub-regions in male specimens, whereas female specimens exhibited significant cortical thinning in the endosteal sub-region in particular. A more recent study of 688 women and 561 men by Russo et al. (2006) indicated that cortical thickness in female specimens of 80 years or greater is approximately 50% of that measured in younger female samples. The authors suggest that changes to cortical thickness and porosity are usually compensated for through apposition of bone on the periosteal surface, however, this process is found to be less effective in elderly women

suffering from severe cortical thinning. Age related variations to the bone geometry and porosity at the microscopic (Bousson et al. 2001, Cooper et al. 2007) and macroscopic levels (Russo et al. 2006) can have considerable impact on its mechanical properties and may have serious implications for fracture risk.

Few studies in the literature directly compare the influence of healthy and osteoporotic bone on the femur (van Rietbergen et al. 2003, Verhulp et al. 2008, Zdero et al. 2010), fewer still have investigated the influence of bone properties following joint arthroplasty on the mechanical environment in the femur e.g. (Brown et al. 2007).

In general, the majority of past studies have tended to focus on the associated fracture risk due to osteoporosis at the femoral head, often under normal walking (van Rietbergen et al. 2003) or sideways fall conditions (Verhulp et al. 2008). The aim of this study was to determine how incorporation of the effects of ageing on bone material properties and changes to cortical bone geometry influence the observed mechanics post implantation. As in Chapter IV, this study employed three core FE models; an intact femur, a CR implanted femur and a PS implanted femur.

## V.2 Method

In the present study all geometry, material properties, boundary conditions and loading remained the same as defined previously in Chapter IV, with one exception. In this study, cortical bone material properties were altered based on whether healthy patients or pathological patient scenarios were being considered. In these groups models were further divided to account for geometrical differences between young and osteoporotic patients in the distal femoral cortex. This gave a total of four cortical bone material variations applied to each of the femurs being investigated. It is important to note that all other aspects of the FE meshes and model setup as applied in Chapter IV were used in the current study.

A study by Davis et al. (2011) highlighted the usefulness of temperature dependent material properties as an effective means of defining regional inhomogeneous properties over complex structures. In the present study, the facility to perform heat transfer analysis in FE packages was leveraged to define a gradient varying from the endosteal surface to the periosteal surface of the femoral cortex. The gradient was achieved by means of a sequentially coupled thermal-stress analysis, this involved firstly solving an uncoupled heat transfer analysis and subsequently conducting a stress analysis, which incorporated nodal temperatures.

In the first stage thermal boundary conditions were applied to both the endosteal and periosteal surfaces of the cortical bone structure (Figure 5.1a). At the endosteal surface temperature ($\theta_1$) was set to 0 and at the periosteal surface ($\theta_2$) to 1. An arbitrary value of $k = 1$ was assigned as the thermal conductivity of cortical bone. The cortical structure was then meshed with ten node tetrahedral heat transfer elements (DC3D10), solving this nominal 'heat transfer' analysis resulted in a gradient of temperature throughout the cortex as shown in Figure 5.1b. It is important to note that all implanted models referenced the nodal values of temperature derived from the heat transfer analysis conducted on the intact femur. This was necessary so as to preserve material distribution relative to the intact femoral cortex, particularly in cortical regions where new surfaces were generated through removal of bone during the implantation process.

The calculated nodal temperatures from the heat transfer simulation were read into the stress analysis as a predefined field variable and applied to the cortical bone part only. Element shape functions were used to obtain temperature at integration points from the nodal point values, resulting in up to four possible values of temperature per element (for 10 node elements with four integration points).

In the stress analysis material properties of the cortical bone structure were then assigned based on a predefined relationship between Young's modulus and temperature using built in features of the commercial FE package (Abaqus 6.10). In this manner the variation of mechanical properties from endosteum to periosteum

(i.e. inhomogeneous properties in one direction through the thickness) could be incorporated into the previously defined models from Chapter IV in an efficient manner without the need for complex user subroutines.

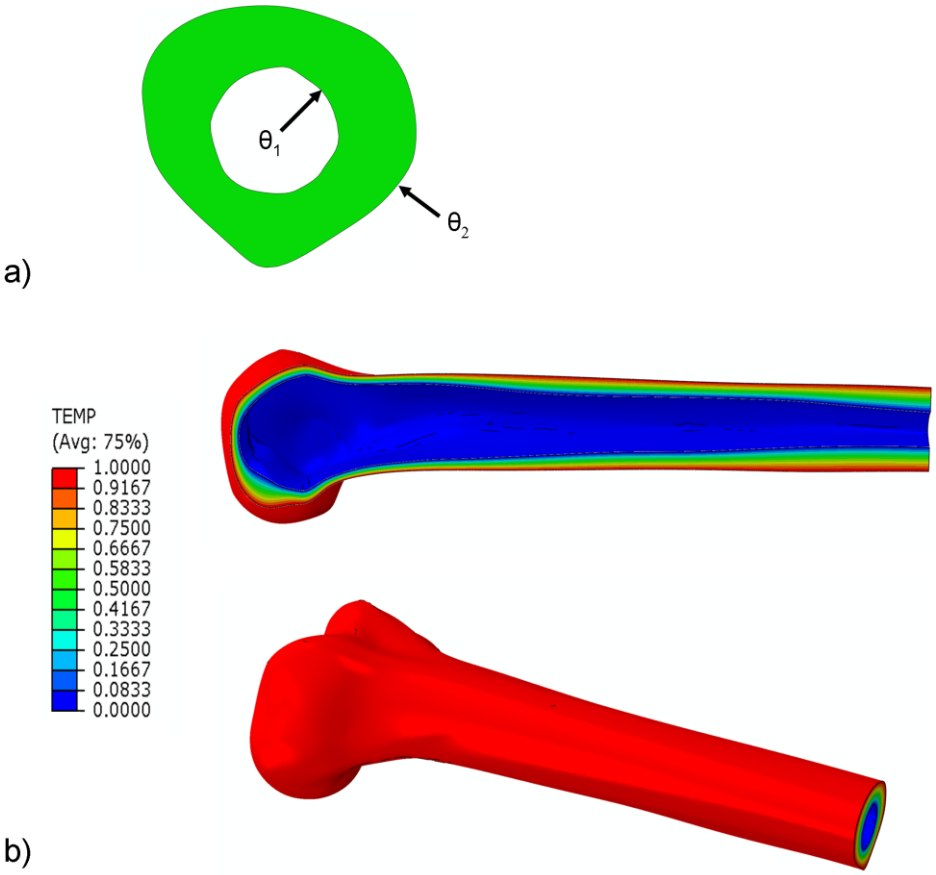


**Figure 5.1:** Showing a) applied thermal boundary conditions across transverse femoral section and b) sagittal section view and 3D isometric view of resulting temperature gradient through the cortex for a CR implanted femur.

It is important to note that the 'thermal' properties as applied to the bone in this initial phase of the analysis were merely used as an artifice for assigning variable material properties at normalised positions through the thickness of the cortex, in this instance Young's modulus, and as such are not representative of the actual thermal properties of bone which may be required to determine the influence of thermal strains on the femur. To avoid ambiguity from this point forward the gradient of nodal temperatures resulting from the heat transfer analysis used to assign material

properties at normalised positions through the thickness will simply be referred to as normalised cortical distance.

### V.2.1 Healthy and osteoporotic modelling of the femur

As stated earlier, models were categorised based on whether they represented changes to the mechanical properties only (young to old) or changes to both the mechanical and geometrical properties of the femur (healthy to pathological). The aim of the healthy model group was to investigate the influence of age on mechanical environment in the femur pre and post TKA. Appropriate values for both young and old bone material properties were derived from literature (Donaldson et al. 2012) and are presented in Table 5.1.

**Table 5.1:** Cortical bone properties (Young's moduli and Poisson's ratio) for young and older patients.

| | Endosteum ($N/mm^2$) | Periosteum ($N/mm^2$) | Poisson's ratio |
|---|---|---|---|
| Young | 16700 | 22000 | 0.3 |
| Old | 7000 | 16700 | 0.3 |

Two linear relationships were then defined between Young's modulus ($E$) and normalised cortical distance in order to characterise the inhomogeneity of bone properties for both young and older patient scenarios, as shown in Figure 5.2 (YH and OH). In the stress analysis, the value of $E$ assigned at the integration points of each element was then determined through linear interpolation between the endosteal and periosteal values presented in Table 5.1 for the corresponding normalised cortical distance at each integration point. In this manner each element could potentially be assigned up to four individual values of Young's modulus (i.e. one at

each integration point), resulting in a gradient of $E$ across the element rather than a single value for each element.

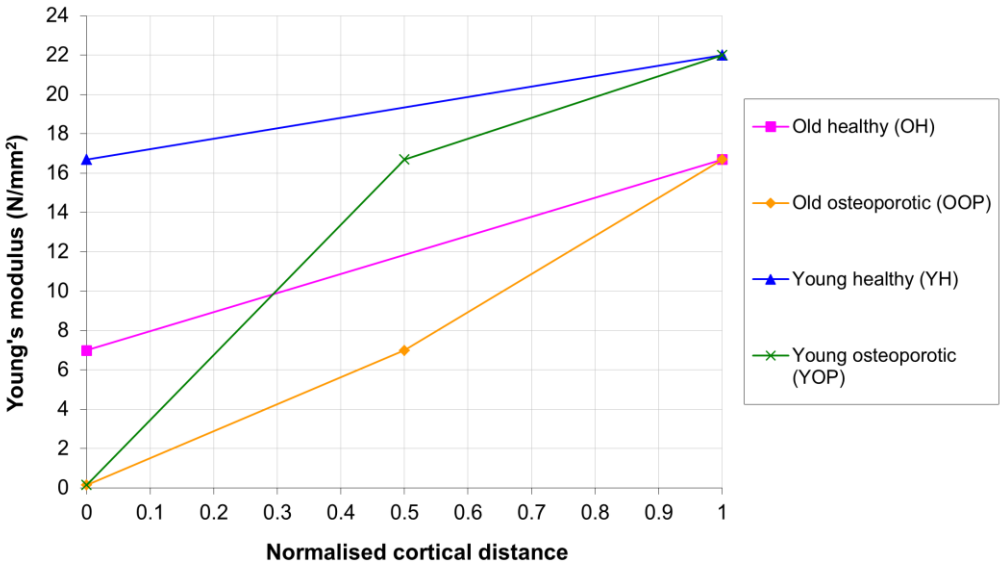


**Figure 5.2:** Variation of Young's modulus for young healthy (YH), old healthy (OH), young osteoporotic (YOP) and old osteoporotic (OOP) bone.

This method was then extended to incorporate the effects of osteoporosis as characterised by endosteal thinning of the cortex. To achieve this, a bi-linear relationship was implemented as shown in Figure 5.2 (YOP and OOP). In this relationship the initial portion of the normalised cortical distance-Young's modulus graph is set to the value of cancellous bone ( $E_{cancellous} = 155MPa$ ) and the original Young's modulus of the endosteal surface was offset to a normalised cortical distance of $0.5$, modelling an approximate 50% reduction in cortical thickness simulating the effects of endosteal trabecularisation. The equivalent reduction in thickness represented by this process is within the range reported (Bousson et al. 2001) for older female patients. Female rather than male values for cortical thinning were considered in the current study, as the rate of cortical thinning is known to be more severe in female patients compared with male patients. Moreover, endosteal

thinning of the cortex is usually counteracted through apposition on the periosteal surface in male patients

Application of inhomogeneous properties and endosteal thinning methodologies to the previously defined FE models of the distal femur pre- and post-implantation resulted in a total of 12 different models (i.e. four different material conditions for each of the three models investigated).

## V.3 Results

In this first set of results, the distribution of Young's modulus, for all patient scenarios, was examined to verify that the linear and bi-linear relationships presented previously had been applied correctly to the models of the distal femur. Figure 5.3 shows a colour coded contour plot of Young's modulus through an arbitrary transverse section of the distal femur. It can be seen from the contour plots that a greater proportion of the YH model is in the orange to red band of stiffness in comparison to the YOP model, additionally in the YOP model it can be seen that the endosteal surface is close to the value of cancellous bone (blue) and only increases in stiffness at approximately the halfway through the thickness of the cortex, thus verifying that endosteal thinning has been incorporated. Similar observations can be made about the OH and OOP models.

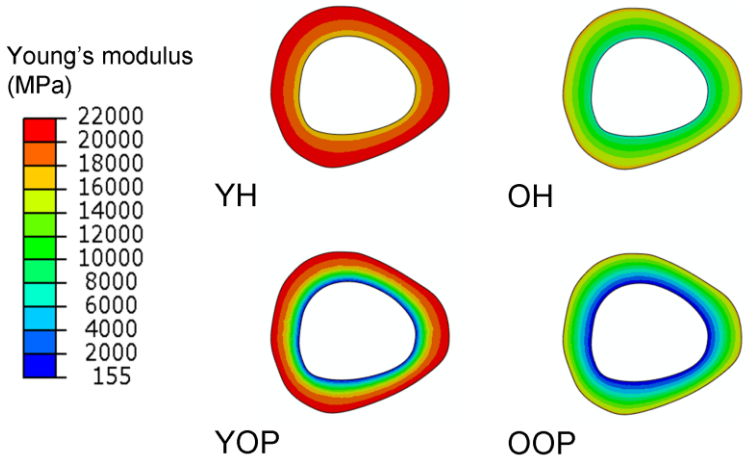


**Figure 5.3:** Transverse section of the distal femur showing the resulting distribution of Young's modulus for young healthy (YH), old healthy (OH), young osteoporotic (YOP) and old osteoporotic (OOP) bone.

To determine the effect of variations in bone quality and shape, transverse sections were again taken at a location c-c in the region just above the implant (as previously identified in Chapter IV Figure 4.11) for all patient models investigated and are presented in Figure 5.4 and Figure 5.5. The resulting contour plots (for 48° flexion) compare the variation of equivalent strain (Figure 5.4), calculated using

$$\varepsilon_{Equivalent} = \sqrt{\frac{(\varepsilon_{11}-\varepsilon_{22})^2+(\varepsilon_{22}-\varepsilon_{33})^2+(\varepsilon_{33}-\varepsilon_{11})^2+6(\varepsilon_{12}^2+\varepsilon_{23}^2+\varepsilon_{13}^2)}{2}} \qquad (5.1)$$

and von Mises stress (Figure 5.5) in young healthy patients (YH), old healthy patients (OH), young osteoporotic patients (YOP) and old osteoporotic patients (OOP).

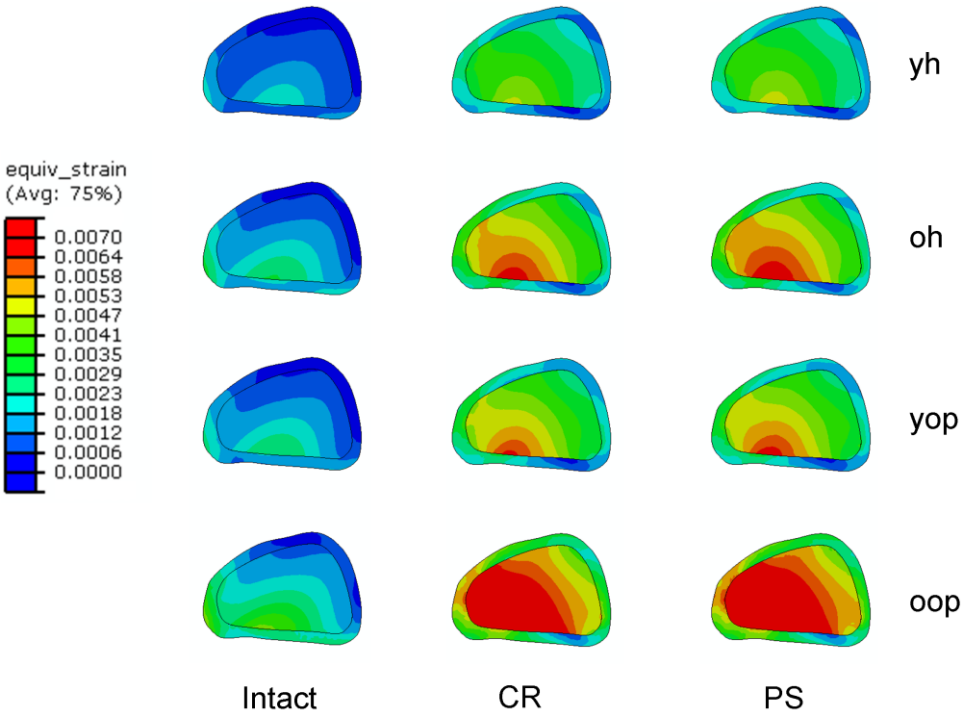


**Figure 5.4:** Contour plots of the equivalent strain in the transverse section c-c for all cases at 48° flexion.

It is found that models which incorporate older patient bone material properties but maintain their original shape (OH) lead to slightly higher cancellous and cortical

bone strains in regions directly above the implant in comparison to the young healthy case. Femurs which maintained younger patient material properties but incorporated the effects of endosteal thinning (YOP) also influenced the pattern of strain, though to a lesser extent than that of ageing. The most significant increase in periprosthetic femoral bone strain (both cancellous and cortical), however, was noted to occur in femur models which incorporated both older patient material properties and endosteal thinning of the cortical structure (OOP). Referring to Figure 5.5 similar trends were observed with respected to the pattern of von Mises stress for the same models. The contour plots of von Mises stresses also serve to verify the material distribution of the models, e.g. it can be seen that for YH and OH models the high stresses are carried by the majority of the cortex, whereas in the YOP and OOP cases high stress regions are confined to the remaining stiff outer portion of the cortical structure.

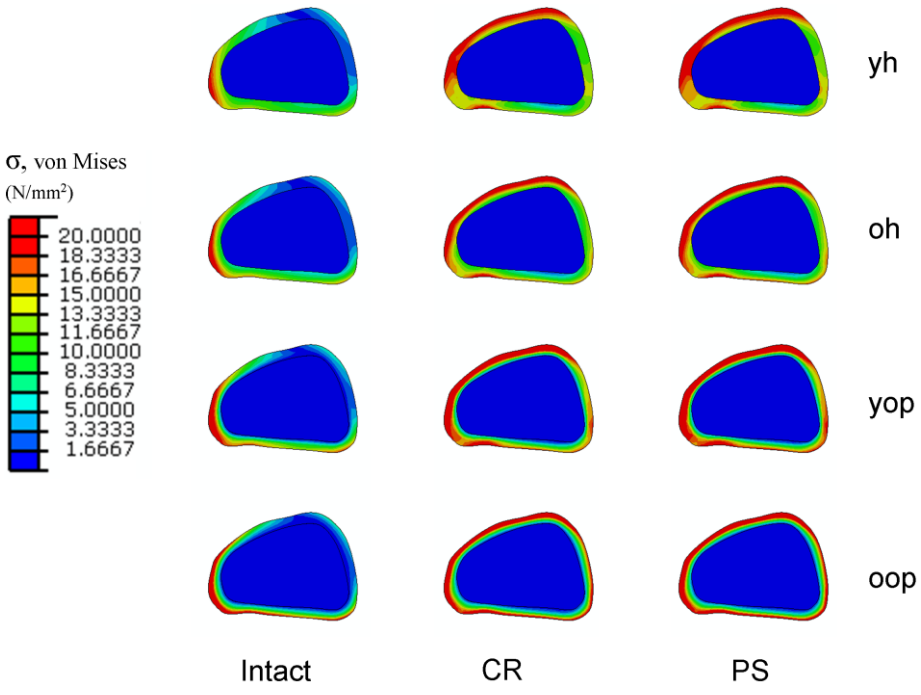


**Figure 5.5:** Contour plots of the von Mises stress in the transverse section c-c for all cases at 48° flexion.

To quantify the changes in periprosthetic region for all scenarios investigated, four points of interest were defined on the transverse section c-c (Figure 5.6) and the

resulting value of von Mises stress and equivalent strain were evaluated at each point for the three flexion angles investigated (Figure 5.7- 5.9).

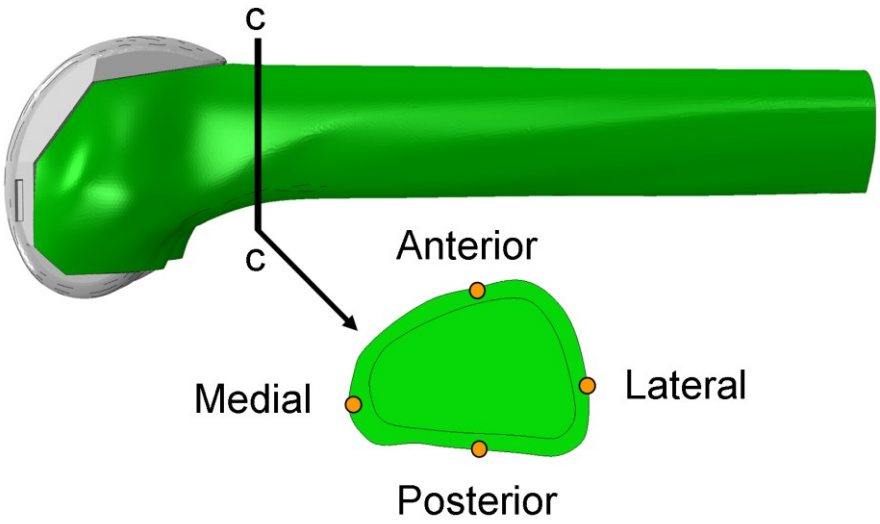


**Figure 5.6:** Section view of cortical bone along c-c indicating the four points of interest in the periprosthetic region.

It can be seen from Figures 5.7-5.9, that there is a clear trend with respect to increasing levels of stress in the periprosthetic region due to both ageing and endosteal thinning of the cortex. In general, ageing alone contributed to an increase in stress of 16% for both pre and post TKA cases (averaged over all four points of interest for the three flexion angles), thinning of the cortex in younger patients caused an increase of 26% and the combined effect of endosteal thinning and elderly properties contributed to an overall average increase in stress of 61%.

The stress shielding effect discussed earlier is also evident at 0° flexion (Figure 5.8), where it can be seen that the anterior cortex of the implanted femurs carry approximately 25% less stress than the intact femur. The equivalent strains at the four points of interest followed similar trends with the greatest increase in strains resulting from a combination of endosteal thinning and elderly bone material properties. At 0° flexion, a slight decrease in strain of the implanted relative to intact femur may indicate the presence of strain shielding in this region (Completo et al. 2008b).

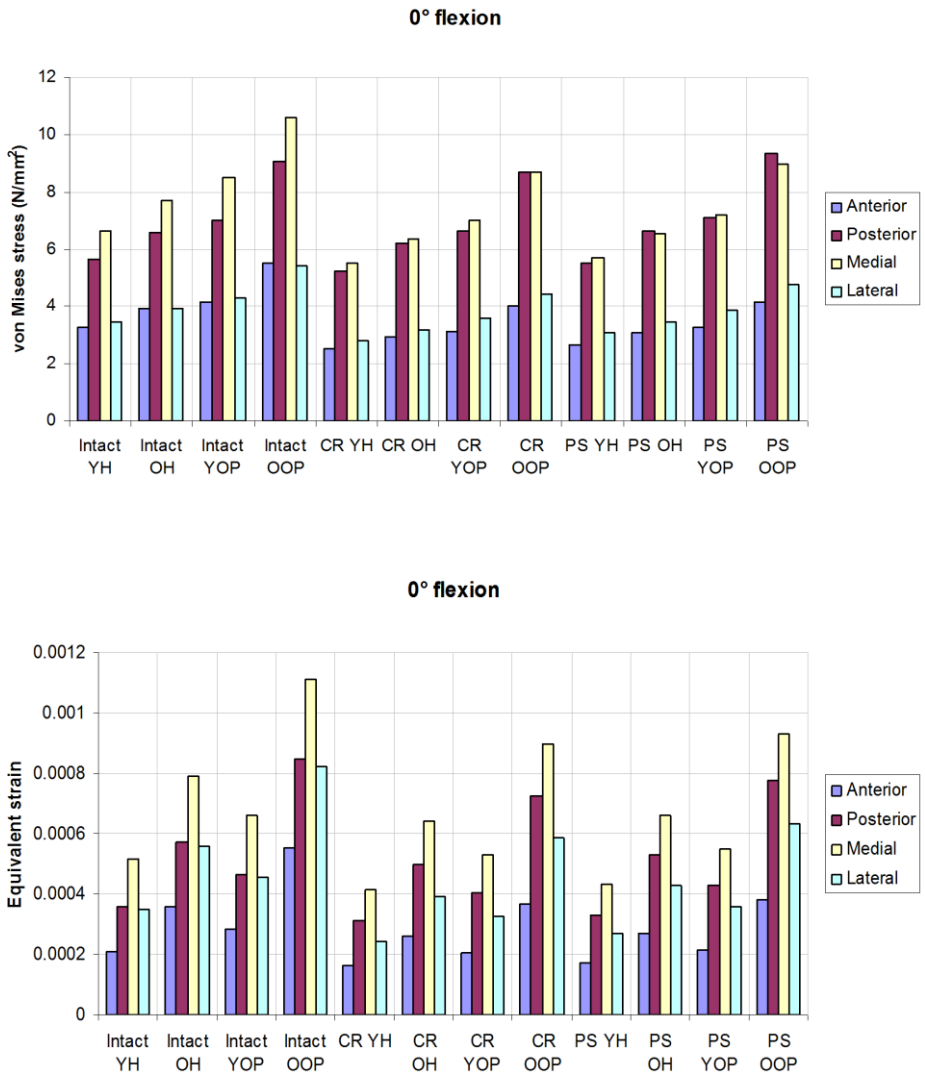


**Figure 5.7:** von Mises stress (Top) and equivalent strain (Bottom) at each of the points of interest for all the cases investigated at 0° flexion.

From the graph of equivalent strain at the four points of interest, it can be seen that the YOP case experiences a lower level of strain than the OH case, in contrast to the behaviour observed in the corresponding plot of stress. It is important to note that as the effective cross section of the YOP case is reduced due to the incorporation of endosteal thinning, the stress in that region will increase under the same loading. However, as the original material properties are maintained the femur remains

significantly stiffer than the OH model, and therefore results in a lower value of strain in the periprosthetic region of interest.

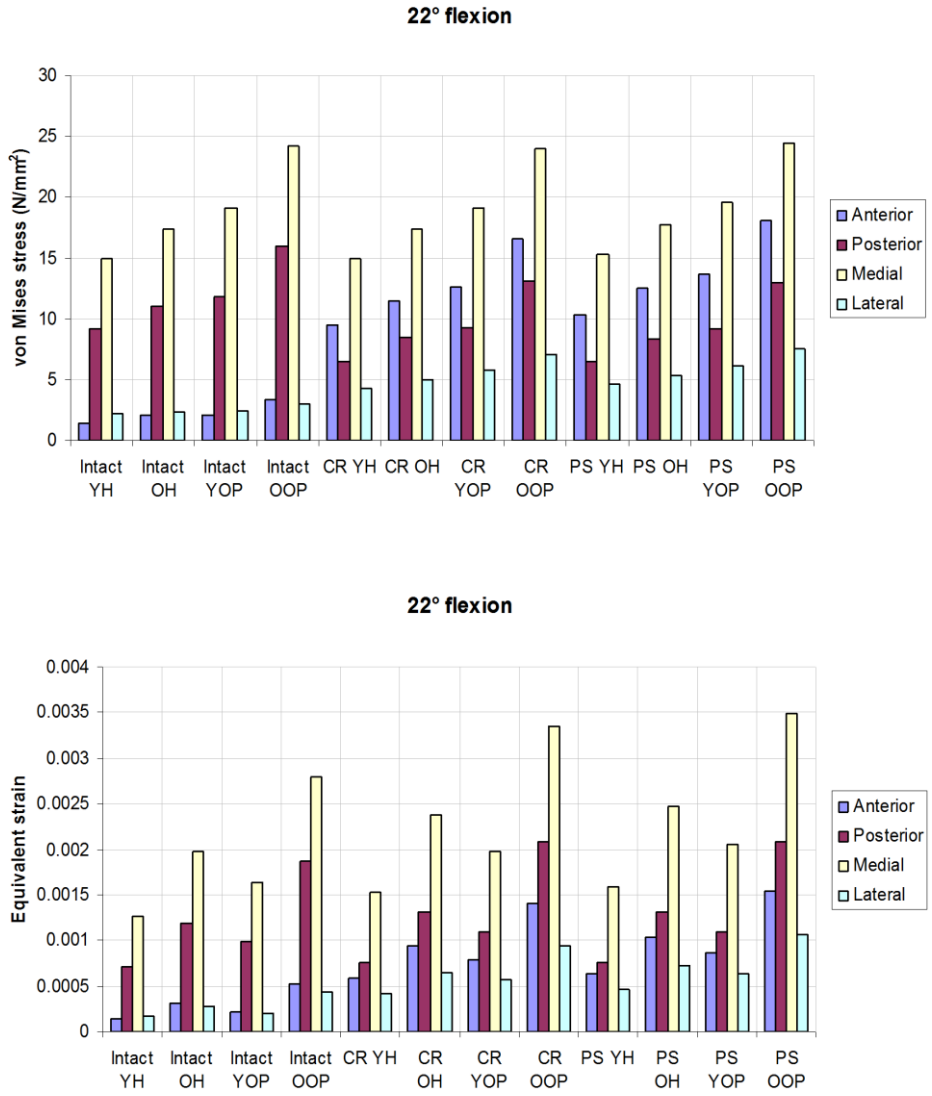


**Figure 5.8:** von Mises stress (Top) and equivalent strain (Bottom) at each of the points of interest for all the cases investigated at 22° flexion.

As in Chapter IV, it was observed that the magnitude of both stress and strain increased with flexion for all cases investigated, this again highlights the importance of considering the changes in magnitude and direction of loading at the knee joint when examining the mechanical environment in the femur.

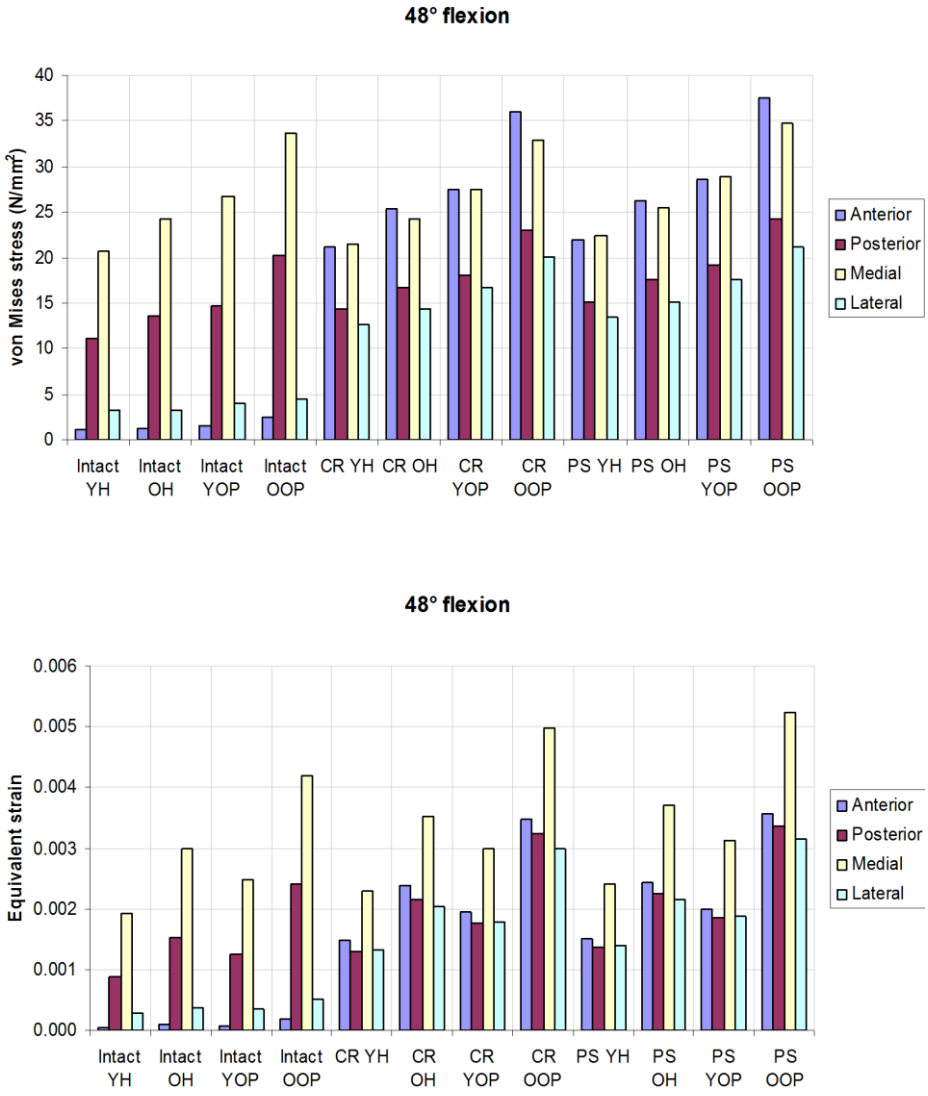


**Figure 5.9:** von Mises stress (Top) and equivalent strain (Bottom) at each of the points of interest for all the cases investigated at 48° flexion.

To determine the influence of ageing and of endosteal thinning associated with osteoporosis on the magnitude of stress concentrations due to internal implant features (i.e. pegs and box), the percentage increase in stress (von Mises) of each implanted model relative to its respective young healthy model was plotted as shown in Figure 5.10. This figure highlights the percentage change in stress which occurs for both the CR and PS implanted femurs for the three flexion angles investigated at two points of interest (one medial and one lateral). For the CR implant these points were close to the femoral pegs and for the PS implant close to the femoral box at the

same depth in the frontal plane as the femoral pegs. It can be seen that changes to the material properties of the cortical bone structure only (OH) lead to an average increase in cancellous bone stress of about 35%, changes due to mild thinning (YOP) on the other hand lead to an increase of 25%. However, it can be observed that the combination of older patient material properties and more pronounced thinning of the cortex (OOP) results in the largest increase in implant related stress concentrations (80% increase relative to the young healthy patient model).

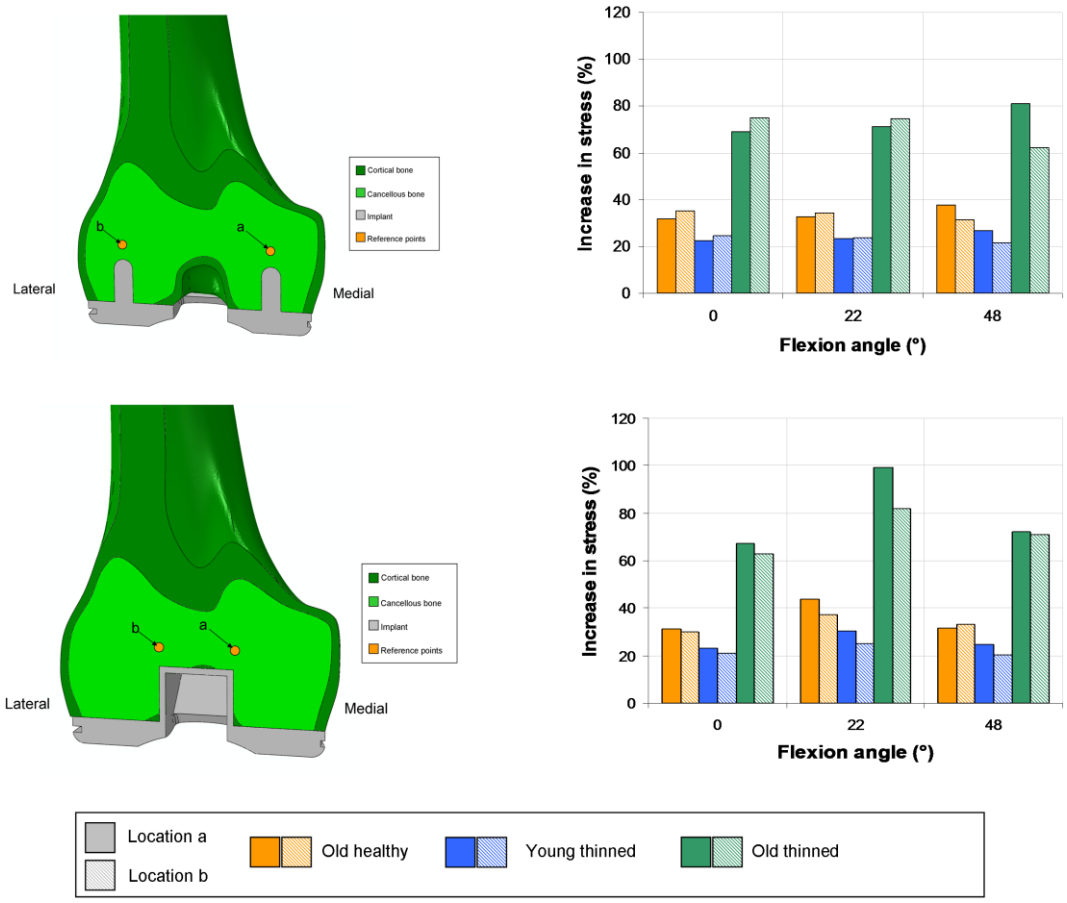


**Figure 5.10:** Percentage increase in stress at the two reference points indicated for the CR implanted cases (Top) and PS implanted cases (Bottom).

## V.4 Discussion

Building on the models presented in Chapter IV, this study aimed to quantify the influence of age related changes and osteoporosis on the mechanical environment

pre- and post-implantation, this was achieved through the novel application of pre-existing FE modelling techniques, specifically the ability to assign variable material properties corresponding to the nodal temperatures output from a heat transfer analysis. The two particular applications considered in this study were; to create an inhomogeneous distribution of Young's modulus through the thickness of the cortical structure of a healthy femur, and to incorporate the effects of endosteal thinning through modification of the normalised cortical distance – Young's modulus relationship for both young and older patient scenarios.

Au et al. (2010) compared varying degrees of homogeneity in an orthotropic model of the distal femur and proximal tibia in an attempt to characterise its influence on the resulting stresses and strains. The authors showed that a single value of stiffness may lead to large errors in predicted SED and nodal displacements of up to 170% for patient specific models when compared to the same model with stiffness values assigned based on the patients CT scan (over 500 values of stiffness). However, the authors also showed that this error decreased significantly when inhomogeneity of the sample was increased slightly (e.g. 50 values of stiffness). In the present study, the use of inhomogeneous properties through the thickness, from endosteum to the periosteum, was employed to more accurately represent the *in vivo* material distribution through the distal femoral cortex and to minimise the potential error associated with the representation of bone through a single homogeneous value of stiffness.

In the present study, it was found that both age related changes and endosteal thinning, as modelled by the modification of the normalised cortical distance – modulus relationship, resulted in an increase in stress. Age related changes alone were found to produce an average increase in cortical bone stress of 15%, endosteal thinning or trabecularisation of the endosteal surface on the other hand was observed to result in a marked increase in periprosthetic stress of 26%. It must be noted, however, that the most significant increase in stress and strain was observed in models representative of older patients with osteoporosis (60%), e.g. models which incorporated both elderly patient material properties and severe thinning of the

cortex, indicating that this group in particular may be at a greater risk of periprosthetic femoral fracture under the same loading conditions. Qualitative support can be found for this statement in a number of recent clinical and retrieval studies which cite weak osseous support as a large contributing factor to distal femoral fracture in elderly patients following knee arthroplasty (Lim et al. 2001, Issack et al. 2007, Nikolopoulos et al. 2012). Similar trends were also observed with respect to the effects of age and osteoporosis on localised stress concentrations in cancellous bone regions, where the greatest increase in stress occurred as a result of both elderly material properties and thinning of the cortex (Figure 5.10).

In a study by van Rietbergen et al. (2003), both healthy and osteoporotic μFE models of the proximal femur were developed for the purpose of examining how changes at the tissue level influence the resultant strains in the femur during a normal walking cycle. The authors found that it was necessary to reduce the applied joint reaction load to 59% of its original value to produce strains similar to that of the healthy femur model over the same regions of interest. A more recent study by Verhulp et al. (2008) expanded on the work of van Rietbergen to examine the effects of a sideways fall on the same healthy and osteoporotic femur models. The authors concluded that similar to the physiological load investigation a reduction of 61% was required to produce equivalent strains in both models. However, in both studies the osteoporotic group with reduced loading still maintained a higher standard deviation in values of strain than the corresponding healthy group, indicating that the effects of osteoporosis may be driven by more than just alteration of the joint reaction alone. Though it is possible that a portion of the bone loss which occurs in patients with osteoporosis may be attributed to the suggested reduction of remodelling in the femur in response to the lower loads (van Rietbergen et al. 2003).

In the context of the present study, the work by van Rietbergen and Verhulp does lend support the conclusion that geometrical changes due to osteoporosis lead to an increase in femoral stresses and strains. Furthermore, the range in terms of the percentage increase in stress observed (e.g. Figure 5.10) going from a healthy patient

to an older patient with osteoporosis is found to be consistent with previously reported tissue level behaviour (van Rietbergen et al. 2003).

A study by Anderson (2010) investigated the effects of age related differences in joint torques and strain of the proximal femur during gait. It was concluded by the author that age did not significantly influence the likelihood of femoral fracture. However, as with the studies conducted by van Rietbergen and Verhulp, changes to the material properties of the femur at the macroscopic level, between young and old scenarios were not considered. This combined with reduced loading applied in elderly models could account for the less dramatic differences observed between young and old patient scenarios in the study by Anderson.

In a combined numerical and experimental study, Zdero et al. (2010) investigated how varying the thickness of the cortex impacted upon the response of the femur under mechanical testing conditions. The study concluded that only large amounts of bone loss in the cortical region would lead to a dramatic change in stiffness, and that the normal effects of ageing would have less impact on its mechanical properties. In the present study, however, it was observed that age related changes alone can have an effect on periprosthetic stress in the cortex of both the intact and implanted femurs, leading to an average increase of 15%. This finding in particular, may have serious implications with respect to periprosthetic fracture risk following TKA in elderly patients, where the cortical bone structure may be further compromised by implant induced stress shielding (van Lenthe et al. 1997, Spittlehouse et al. 1999, van Lenthe et al. 2002, Soininvaara et al. 2004).

In the present study, cancellous and cortical bone stresses and strains were found to increase with age and thinning of the cortex. It is important to note that in situations where material properties degrade over time it is likely that both cancellous and cortical bone regions may be simultaneously affected e.g. (Milovanovic et al. 2012). If changes to the cancellous bone structure were also considered this may result in an even greater proportion of load being carried across the thinned cortex increasing the potential risk of fracture even further. It is therefore suggested that the models

presented here may be slightly conservative. It should also be noted that while the method presented here is sufficient for modelling endosteal thinning of the cortical bone structure, it currently does not extend to geometrical changes of the external surface (apposition), as may be observed in male patients (to combat the internal bone loss). However, due to the much lower rate of apposition observed in female patients this limitation will have had a negligible impact on the findings of the current study.

Due to the difference in slope between young and old bone material properties the effective thickness of both models was not the same, though this may correspond to the physiological scenario where young bone suffers a lower rate of thinning than old bone. For a fair comparison, the inclusion of a controlled transition zone between cancellous and cortical regions would be desirable to maintain a comparable cortical thickness in both young and old osteoporotic bone models. Initial tests of this controlled transition zone, however, showed that this resulted in discontinuities in the mesh due to interlocking tetrahedral elements potentially having a mixture of both cortical and cancellous bone properties.

Another consideration is that the same magnitude of loading was considered for young and older patient scenarios, while this assumption permitted the direct comparison of the influence of age and thinning, it may not be fully reflective of the *in vivo* situation where elderly patients may be more protective of their joints, particularly in the post-operative period following joint replacement and as a consequence, may avoid full weight bearing on the operated limb for much longer than their younger counterparts.

In conclusion, the present study has shown that changes to both properties and geometry in the intact and implanted femurs can significantly influence the pattern and magnitude of stress in the distal femur. The results underscore the importance of considering both material and geometrical change when quantifying the influence of age and osteoporosis on the femur. Moreover, the method presented here allows for the incorporation of such changes independent of patient specific CT data.

Often an average case or limited number of patient specific cases is represented during testing and validation of new implant designs. However, this does not adequately account for the wide range of patients who may undergo TKA with the same prosthesis, and as such may not represent all possible clinical scenarios. In the current study, a novel method for modelling inhomogeneity and geometrical changes to the femur has been proposed, and has been shown to be a powerful tool to allow rapid consideration of multiple clinical scenarios using the same model geometry. Furthermore, by comparing multiple clinical scenarios using the same core model and geometry limits the influence of potential patient specific parameters from obscuring important trends.

In the next chapter, the method developed here for modelling elderly patients with severe osteoporosis will be applied to investigate the clinically relevant question of optimum stem length in the context of revision total knee arthroplasty, and what role it may play in the mitigation of periprosthetic fracture.

# VI

# Investigation of Optimum Stem Length

## VI.1 Introduction

It has been suggested in Chapter V that older patients with osteoporosis may be at a greater risk of femoral fracture as a result of higher periprosthetic stresses due to both age related changes to the material properties and thinning of the cortical bone structure.

As discussed in Chapter II, stemmed femoral prosthesis are primarily used in revision of a failed TKA to aid in stability in the presence of bone loss and to protect bone grafts prior to integration with the host bone through load sharing at the interface. It must be noted, however, that the initial stability afforded by the use of certain large diaphyseal stem configurations may lead to an increase in bone loss over time as a result of greater levels of stress shielding (van Lenthe et al. 2002, Completo et al. 2008b), thus compromising the long term survival of the prosthesis. Studies on cemented non-diaphyseal engaging stems report a slightly more favorable outcome in terms of the level of reported stress shielding (van Lenthe et al. 2002, Completo et al. 2008b). Careful consideration of the impact stemmed prosthesis can have on the mechanical environment of the surrounding bone is essential to a successful patient outcome when treatment requires stemmed prosthesis.

By understanding the potential limitations and shortcomings of stems and their impact on the host environment, surgeons and engineers can better leverage these devices to generate better clinical outcomes. Indeed a good example of this can be

found in a recent *in vitro* study by Completo et al. (2012), in which the authors suggested the use of a long press fit stem as a means of reducing strain and therefore fracture risk at the notch edge following notching of the anterior femoral cortex during TKA, thus turning a normal disadvantage of stemmed prosthesis into a clear advantage for a particular clinically encountered scenario.

The present study investigated the application of femoral prostheses with cemented non-diaphyseal engaging stems of varying length to determine if there was an optimum stem length which could reduce the level of stress in the region immediately above the implant in an effort to mitigate some of the fracture risk associated with ageing and osteoporosis of the distal femur without compromising the long term survival of the implant.

## VI.2 Methods

This study employed identical loading and boundary conditions as in the previous two studies, however, the geometry and therefore the FE mesh changed slightly from the previous studies to incorporate a total stabilising (TS) implant (Stryker, UK). As this implant is based on the same product line as the primary implants used in the previous studies, it shares the majority of its core geometry and internal features with the PS implant. One key difference between the TS implant and the previously employed PS implant is the addition of a femoral boss to provide an attachment site for a modular stem (Figure 6.1). This feature was aligned at six degrees in the frontal plane and its outer diameter was 16mm, matching that of the outer diameter of the collar at the threaded end of the stems.

In this study, three different stem lengths were considered; a short stem (Ø12x50mm), a medium stem (Ø 12x75mm), and a long stem (Ø 12x100mm). In the Triathlon® product line stem diameters range in size from 9mm to 21mm (Stryker Orthopaedics 2011), in the present study a non-canal filling 12mm stem diameter was chosen as this represents a common size employed by surgeons for cementing.

The three model configurations investigated in this study are presented in Figure 6.2, with implant, stem, cement and bone structures identified.

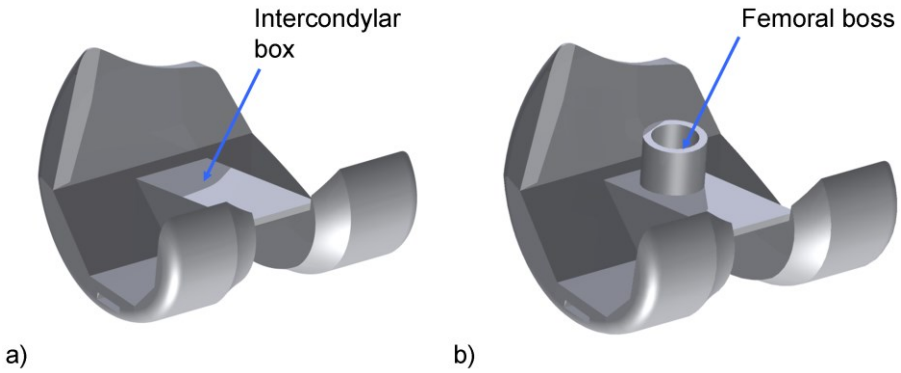


**Figure 6.1:** Rendered CAD model of a) PS implant and b) TS implant showing boss for attachment of femoral stem.

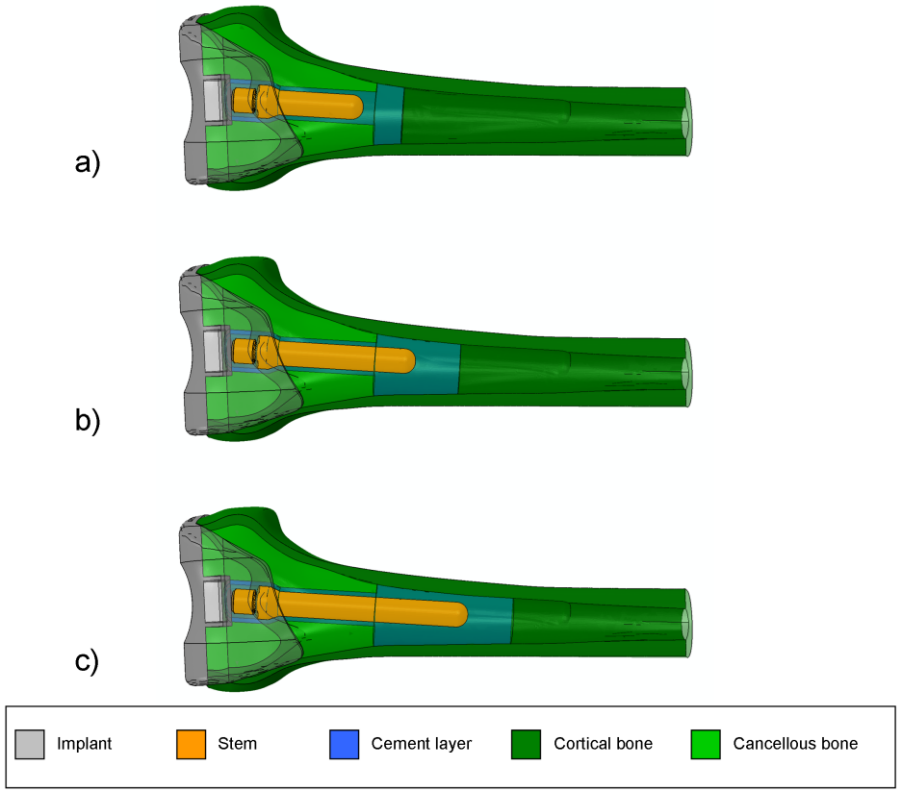


**Figure 6.2:** Semi-transparent rendering of a) a femur implanted with 50mm stem, b) a femur implanted with 75mm stem, and c) a femur implanted with 100mm stem, with bone and prosthesis regions indicated through the colour coded legend at the bottom.

### VI.2.1 Material properties

As in Chapter IV, the femoral component and cancellous bone regions were assumed to behave in a linear elastic, isotropic manner. The value of Young's modulus and Poisson's ratio applied to these structures being presented in Table 4.1. The values for Young's modulus applied to femoral stem and cement regions in the present study are presented in Table 6.1. The cortical bone structure, on the other hand, was modelling as inhomogeneous with endosteal thinning of the cortex using the methodology introduced in Chapter V for the OOP scenario.

Table 6.1: Material properties for FE model with cemented stems.

| Model | Young's modulus E ($N/mm^2$) | Poisson's ratio (v) |
|---|---|---|
| Cement | 2280 | 0.3 |
| Femoral stem (ti-6al-4v) | 110000 | 0.3 |

### VI.2.2 Interface conditions

All interfaces were assumed to be fully bonded, where the implant-stem assembly was fully tied to the internal surface of the cement and the external surface of the cement layer tied to the surrounding bone, e.g. no relative motion was allowed between the structures modelling full osseointegration of the implant.

### VI.2.3 Cement layer

To remain consistent with the previously generated models of the distal femur used in Chapters IV and V, the cement layer was only modelled explicitly from the back surface of the implant box along the stem to a distance of 20mm past the stem tip, representing where the cement is retained by the cement restrictor in the clinical setting (Faraj and Rajasekar 2006). The cement layer then extended outward to the endosteal surface of the cortical bone modelling permeation of the cement through

the cancellous structure to the cortex, as is achieved in vivo through pressurisation of the cement into the bone. One complication of the previously described temperature dependent approach to modelling endosteal thinning of the distal femoral cortex (OOP) was that this method effectively offset the material and geometrical representations of the cortical bone, meaning structures previously in direct contact with the cortex were now contacting with a transitional region of cancellous and cortical bone (Figure 6.3a). Practically, this means that the cement is not directly in contact with the cortex and therefore load transfer at the stem-cement-cortex interface would be significantly reduced. To overcome this issue the model was partitioned at the start and end points of where the cement layer made contact with the cortical bone geometry (Figure 6.3b). To ensure optimum load transfer the properties in the partitioned region were then set to vary from cement to cortical bone modelling the permeation of the cement into the trabecularised cortex.

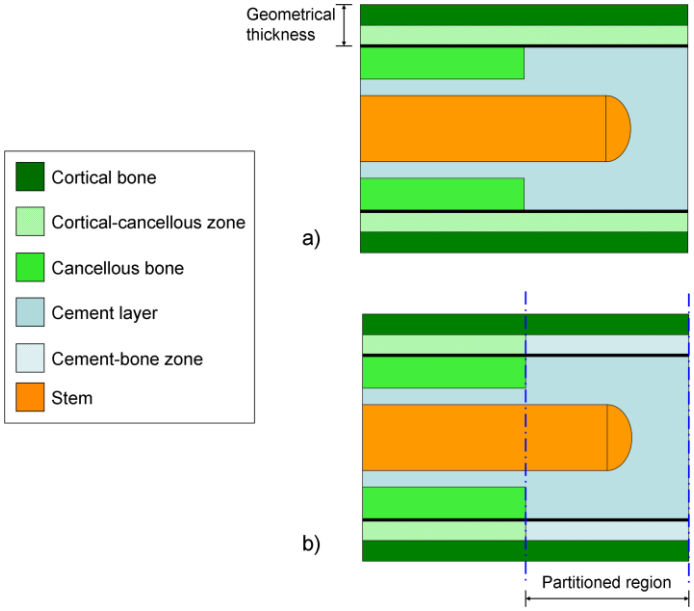


**Figure 6.3:** a) Schematic of material distributions after temperature dependent endosteal thinning of the cortex, where the hatched green region represents a transitional zone between cancellous and cortical bone regions, and b) schematic of partitioned model with cement-cortical transitional zone highlighted by the hatched blue region.

## VI.3 Results

To characterise the influence of stemmed femoral prosthesis on the periprosthetic mechanical environment, the values of von Mises stress and equivalent strain were recorded at the same four cortical points of interest defined in Chapter V at the location of the transverse section c-c, as shown in Figure 6.4. It can be seen for all stemmed femoral components that the largest values of strains occur on the medial cortex and the largest reported values of stress act on the anterior femoral cortex.

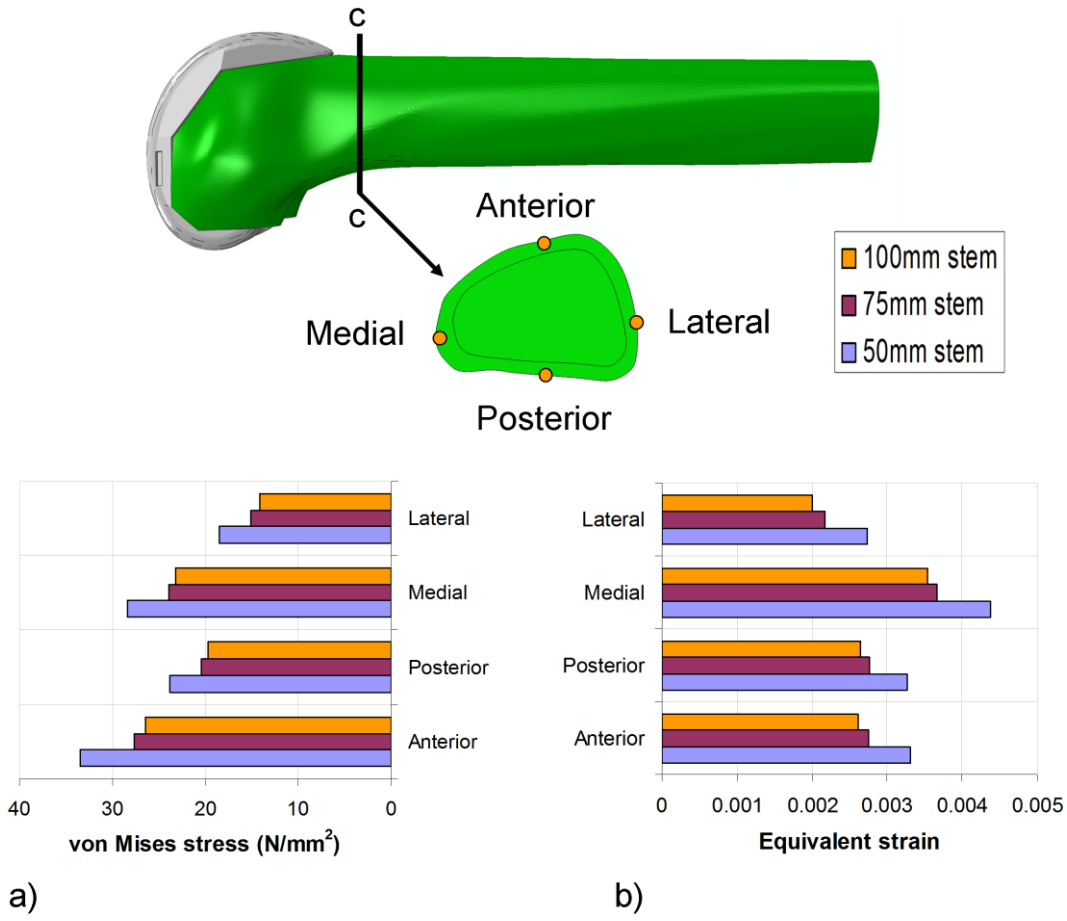


**Figure 6.4:** a) von Mises stress and b) equivalent strain at each of the points of interest for varying stem length at 48° flexion.

The short stem (50mm) is observed to have a response closest to that of the stemless PS implanted femur (OOP) and leads to the highest levels of periprosthetic stress of all the revision stemmed implants investigated.

If we compare the values of stress and strain from all stemmed prostheses to that of the OOP model from Chapter V, the percentage reduction in stress and strain due to stem length can be determined (Table 6.2). The table shows that on average the 50mm stem resulted in an overall decrease of approximately 11% in periprosthetic stress and 10% in periprosthetic strain, the 75mm stem lead to a 26% reduction in both stress and strain, whereas the 100mm stem resulted in a 29% reduction in stress and strain.

Table 6.2: Reduction in periprosthetic stress and strain relative to OOP model of distal femurs implanted with stems of varying length.

| Model | Stem length (mm) | % decrease in von Mises stress | % decrease in equivalent strain |
|---|---|---|---|
| OOP | N/A | 0.00 | 0.00 |
| TS short | 50 | 10.89 | 10.01 |
| TS medium | 75 | 25.65 | 25.53 |
| TS long | 100 | 28.72 | 29.30 |

A number of transverse sections through the femur (Figure 6.5a) were taken to better understand the impact of cemented stems on its mechanical environment, and to examine how alterations to the stresses and strains distally may affect other regions of the femur (e.g. the region surrounding the end of the stem). The section c-c is the same as previously described in Figure 6.4 and Chapter IV Figure 4.11. This section represents a location just above the implant. Section d-d is taken at the location near the end of the 50mm stem, section e-e at a location near the end of the 75mm stem and finally section f-f at a location near the end of the 100mm stem. It should be noted that to ensure consistency of results, all transverse sections were examined for each case.

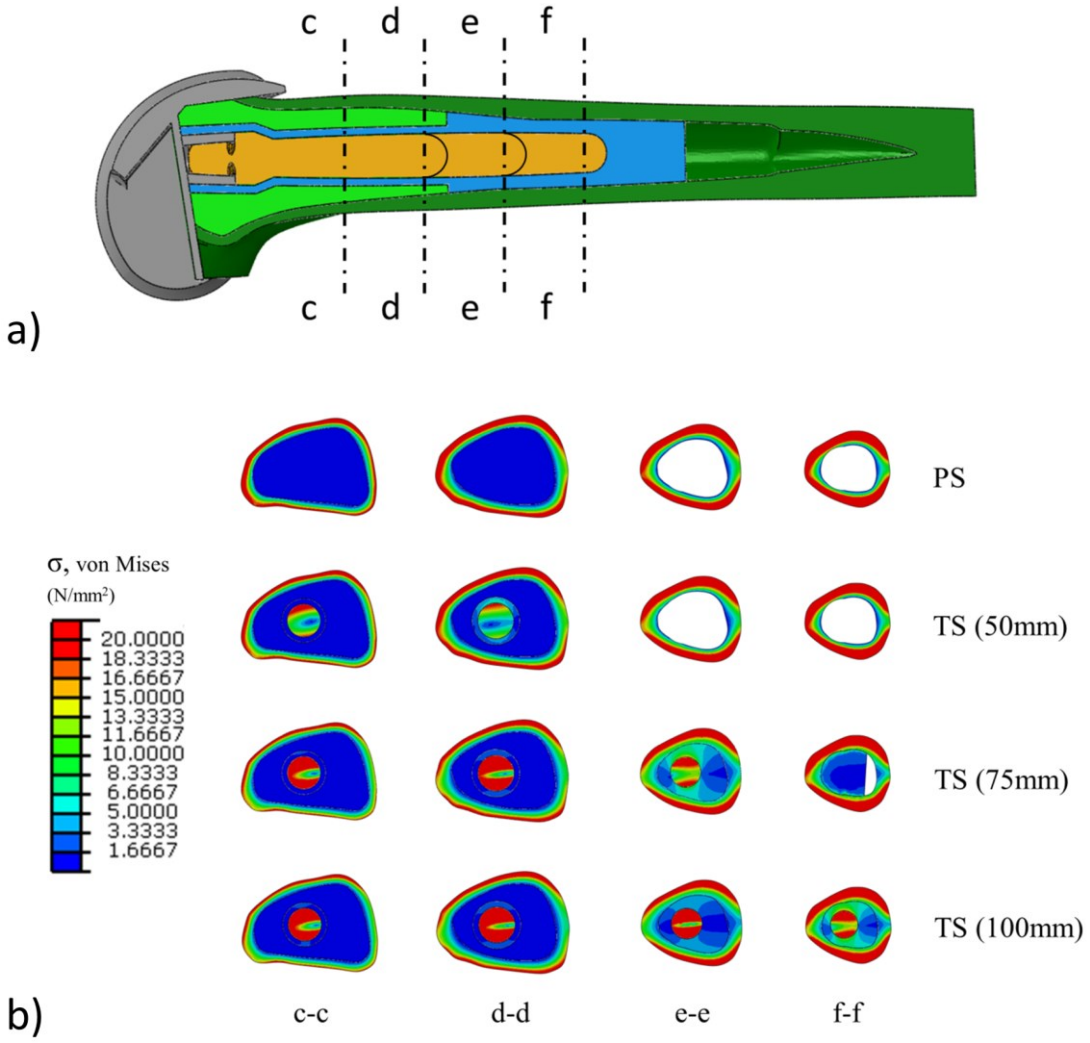
a)
c
d
e
f
c
d
e
f
σ, von Mises
(N/mm²)
20.0000
18.3333
16.6667
15.0000
13.3333
11.6667
10.0000
8.3333
6.6667
5.0000
3.3333
1.6667
PS
TS (50mm)
TS (75mm)
TS (100mm)
b)
c-c
d-d
e-e
f-f

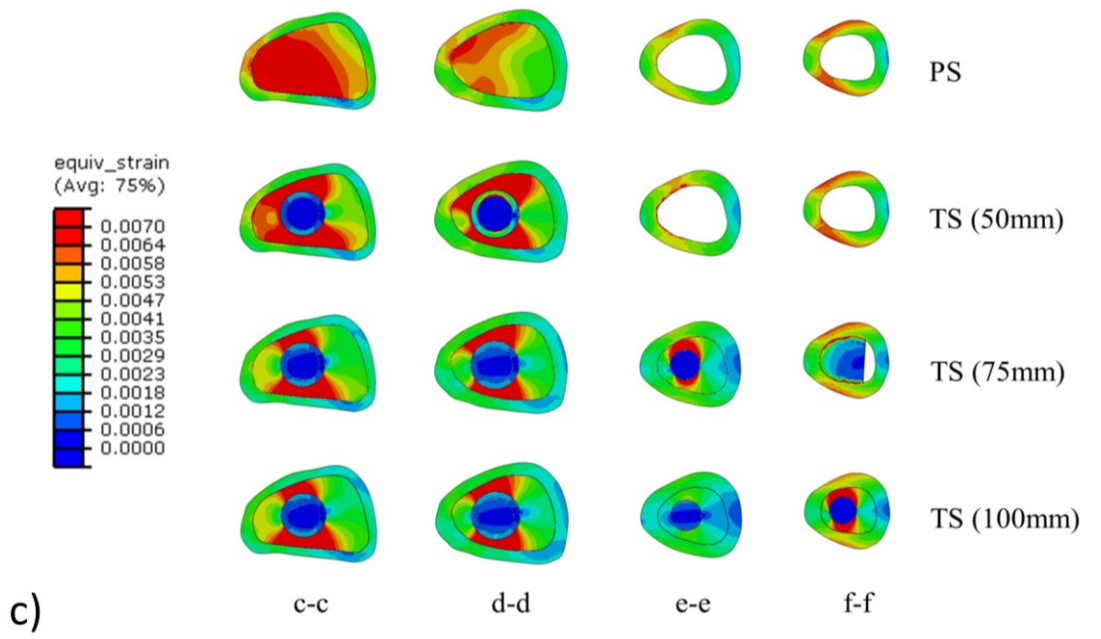


**Figure 6.5:** Showing a) the location of each of the transverse sections through the femur, b) the resulting plots of von Mises stress, and c) equivalent strain at the transverse sections for all cases investigated.

It can be seen from Figure 6.5b that the majority of the stress (von Mises) is transmitted through the stem-cement construct leading to a reduction in stress distally for femurs implanted with stemmed prostheses (section c-c). As the end of each stem is approached; section d-d for the TS implant with 50mm stem, section e-e for the TS implant with 75mm stem, and section f-f for the TS implant with 100mm stem, it can be seen that the stress in the cement increases indicating increased load transfer at the stem-cement and cement-bone interfaces, leading to a slight increase in cortical regions above the end of the stem.

Similarly in Figure 6.5c, it can be observed from the plots of equivalent strain that the added stiffness of the stems serve to reduce the level of strain in the distal femur.

## VI.4 Discussion

This study investigated the use of femoral components with a cemented non-diaphyseal engaging short stem in an at risk patient group (older patients with osteoporosis), as a means to reduce stress in the periprosthetic region just above the implant and thus mitigate some of the associated fracture risk. Secondary to this aim was to determine if there was an optimum stem length of the three investigated which could balance the desired reduction in stress without significantly compromising the long term stability of the implant.

As stated in Chapter IV, on the topic of stress shielding, it is important to recognise that internal stresses need to be in equilibrium with externally applied forces and as a result a reduction in stress or strain in some regions (or components) leads to an increase in stresses in other regions (Shi et al. 2007). In the context of the current study the observed reduction distally leads to an increase in stress proximally in the cement and stem structures. However, it should be noted that as the load transfer is distributed along the shaft for the length of the stem-cement construct the overall result is that implanted femurs with longer stems (i.e. 75mm and 100mm stems) are subject to slightly lower stresses and strains proximally than the stemless or short stemmed cases. Furthermore as the cortex is significantly thicker in the region of the mid-shaft, it may be less susceptible to fracture than the much thinner and less stiff cortical bone structure found immediately adjacent to the implant in the distal region of the femur.

Stems are widely accepted as being necessary to ensure successful outcomes during revision TKA, particularly in instances of severe bone loss, where bone grafts are required to replace damaged or diseased host bone. In this capacity stems serve to transmit the load to healthy bone structures above the implant and away from the bone graft, thereby allowing the bone graft to fully incorporate into the host structure without risk of damage and overloading in the initial post-operative period (Engh et al. 1997). Stemmed prosthesis have also found use in the treatment of ligament laxity through aiding in the stability of more constrained implant types (Kwon et al. 2012). It has been suggested previously that the addition of a stem may also serve to

decrease the likelihood of periprosthetic femoral fracture following notching of the anterior femoral cortex during surgery (Lesh et al. 2000, Completo et al. 2012).
In the present study, the novel application of stems as a preventative measure against periprosthetic fracture in older patients with osteoporosis was investigated. It was found that the addition of a cemented stem to the distal femur causes a reduction in periprosthetic stress. The short cemented stem (50mm) causes a reduction of approximately 11% while longer stems (75mm and 100mm) are seen to result in reductions of 26-29% when compared with a stemless PS implanted femur (OOP). The reduction resulting from both the medium and long stems brings the periprosthetic stress close to that experienced by the older patient with healthy bone (OH model from Chapter V). The reduction in strain is observed to follow a similar trend with respect to stem length. Moreover, the reduction in strain which occurs as a result of the medium stem is found to be of a similar magnitude to that found previously in a study which employed stemmed femoral prosthesis to reduce fracture risk at the notch edge after notching of the anterior femoral cortex during implantation (Completo et al. 2012). These findings suggest that a small diameter medium length cemented stem could have beneficial applications in reducing periprosthetic stress and therefore fracture risk in elderly patients with osteoporosis.

However, it must also be noted that several clinical reports suggest a higher incidence of fracture in stemmed vs. stemless prosthesis. Meek et al. (2011), reported a fracture risk of 0.6% for primary and 1.7% for revision knee arthroplasty at 5 years, these values increased to 1.3% and 2.2% respectively at 10 years. The authors identified female patients over 70 years of age to be most at risk of fracture following knee replacement. A study by Singh et al. (2013) spanning a 19 year period reported similar periprosthetic fracture rates following primary (1.1%) and revision (2.5%) knee arthroplasty. However, very different conclusions were drawn with respect to at risk patient groups, contrary to the findings of Meek et al., Singh and colleagues suggest a U shaped relationship between age and fracture risk, with the greatest risk being patients aged less than 60 years and greater than 80 years old. This somewhat contradictory evidence for periprosthetic femoral fracture following primary and

revision TKA indicate that the exact mechanisms at work are quite complex, and that this area may warrant closer examination.

On the other hand, it is important to recognise that the implantation of a revision femoral prosthesis in the setting of primary TKA is not the same as implantation of the same prosthesis during revision surgery. Both scenarios will have very different initial conditions, particularly with respect to bone quality for fixation of the prosthesis. It must therefore be considered that the clinical observances that revision stemmed prostheses have a higher fracture rate than primary stemless implants, may not be directly applicable to the present study, as a wide array of factors may influence the outcome in revision surgery, such as age, gender, bone quality and overall health.

Based on the findings of the present study, it can be seen that the stem length is an important parameter for the reduction of periprosthetic stress in older osteoporotic patients. Of the three stems investigated, the use of a 75mm cemented stem is recommended, as this stem affords a reduction in stress almost comparable to the 100mm stem (e.g. less than 4% difference between the two) while also preserving a greater level of bone stock (e.g. less bone removed during implantation of smaller stems). It is also known that shorter stems in general are easier to fit at the time of operation and are less influenced by the curvature of the femur.

The selection of a smaller stem has also been suggested on the grounds of preserving bone density in the femur post-implantation. In a study by van Lenthe and colleagues (van Lenthe et al. 2002) on bone remodelling around revision prosthesis, the authors investigated the influence of two stemmed femoral components (thick and thin) relative to a primary implant with intercondylar box. The findings of their study suggested that a femoral component with a thin stem performed in a similar manner to the primary stemless implant, and had a much more favourable rate of bone loss than a femoral component with a thick stem.

In this study only a single diameter of stem was considered, with stem length varied using three common sizes. However, van Lenthe et al. (2002) showed that stem

diameter was also an important property when investigating bone remodelling around stemmed prosthesis (e.g. larger diameter led to greater bone loss distally). It should be noted that most manufacturers provide a range of different stem diameters, sizes, lengths and end designs. As such it must be recognised that alterations to parameters other than stem length may also significantly influence the load sharing at the bone-prosthesis interface. It is therefore recommended that further studies be conducted to assess the importance of other stem parameters.

Another consideration is that only cemented stems were investigated. Cementing in all cases was modelled on pressurizing to the cortex to achieve optimum load transfer for the stem-cement-bone construct. These models assumed full contact of the cement layer with the cortex and as such may not be fully representative of that found *in vivo*. If full contact was not achieved between the cement and cortical bone regions then this could severely reduce the load sharing capacity of the construct (van Lenthe et al. 2002) and limit its effectiveness for preventing periprosthetic fracture. Furthermore, reduction in load share between the cortex and non-diaphyseal engaging stems may lead to bone loss and eventual loosening due to overloading of the surrounding cancellous bone (Taylor and Tanner 1997).

In conclusion, in the present study stems have been shown to be beneficial in reducing periprosthetic stress in the region immediately above the implant and may therefore aid in reducing the risk of fracture in older patients with osteoporosis following TKA. As such, it is recommended that surgeons should consider selection of an implant with a medium cemented stem for use in particularly at risk patient groups (older patients with severe osteoporosis), rather than a standard stemless primary implant, to reduce the likelihood of distal femoral fracture due to poor quality bone stock. However, it should be noted that this recommendation is made on the basis that the patient's metaphyseal and condylar regions remain largely intact. If, on the other hand, large defects exist in the distal femur at the time of surgery, the addition of a modular stem may not be appropriate, as is further explored in Chapter X.

In the preceding chapters the main focus of the FE models was on the pattern of stress observed for different implant configurations and different patient scenarios. As such the bone-implant interface was assumed to be fully tied, modeling full osseointegration of the implant. In the next chapter, the bone-implant interface will be examined in more detail, and the influence of component geometry on relative motion at the interface will be explored.

# VII

# Influence of Internal Implant Features and Fit on Motion

## VII.1 Introduction

In the previous chapter, consideration was given to how internal implant features influenced the pattern of stress in the femur post-implantation. These models, assumed full osseointegration had occurred between implant and bone. As such, these models are unable to adequately describe the relative motions which may occur at the interface. However, as aseptic loosening and osteolysis (CJRR 2009, NAR 2010, NHS Scotland 2010, AOA 2011, NJR 2011), followed by infection (NJR 2011), are the most commonly reported reasons for revision TKA. It is desirable to incorporate this aspect into the model to characterise the more complex interactions of the implant with the bone.

Revision of the tibial component is far more widely investigated (Hashemi and Shirazi-Adl 2000, Completo et al. 2008a, Chong et al. 2010, Bhimji and Meneghini 2012, Cawley et al. 2012, D'Lima et al. 2012, O'Brien et al. 2012) due to the perception that tibial component loosening leads to a higher percentage of revisions (Gao et al. 2009). It has been shown, however, that there is less than a 3% difference between the number of revised tibial and femoral components as a result of aseptic loosening (AOA 2011). Though it is possible that a small percentage of femoral component revisions may occur in parallel to revision of a loose tibial component (to ensure conformity), with increasing clinical evidence lending support to this practise

(Mackay and Siddique 2003), it is unlikely that this factor alone would account for the majority of femoral components revised due to aseptic loosening. The reported trends with respect to loosening and the increasing number of revision TKAs performed each year suggests that aseptic loosening of the femoral component has the potential to become a more serious clinical issue.

In a canine model, Pilliar et al. (1986) reported that motions in excess of 150µm were disruptive to osseointegration at the prosthesis bone interface and led to the formation of fibrous tissue. A later study again using a canine model placed this figure much lower at 40µm (Bragdon et al. 1996). On the other hand lower levels of motion at the bone implant interface (< 40µm) may be beneficial in promoting bone ingrowth into the prosthesis and increase stability through a strong bond between prosthesis and bone (Vandamme et al. 2007, Suárez et al. 2012). Early indications of loosening and implant failure are observed clinically by tracking changes in the position and orientation of the implant over time through examination of X-rays or through more specialist techniques such as radio stereo photogrammetric analysis (RSA). RSA commonly uses radiopaque tantalum markers attached directly to the implant or placed in the surrounding bone at the time of implantation (Selvik 1989) to determine motion of orthopaedic implants. This non-invasive technique is considered to be the standard clinical method for the evaluation of implant motions in-vivo (Kärrholm 1989, Selvik 1989, Nilsson et al. 1991, Nilsson and Kärrholm 1996) and offers an accuracy of approximately ten times that in comparison to conventional X-ray systems (Nilsson et al. 1991). However, there are some limitations to this system. It is only possible to determine changes in position of the prosthesis using RSA when the values of inducible motions or permanent migrations exceed 100µm (Ryd 1986, Selvik 1989, Nilsson et al. 1995, Allen 2011). In a paper by Nilsson and Kärrholm (1996) it was suggested that particle induced osteolysis as a result of wear particles breaching the interface rather than slow migration may be a more significant factor in causing long term aseptic loosening of the implant. The study suggested that “ingress of wear particles into the interface” as a result of small but repetitive interfacial motions was likely to be a driving factor in particle induced

osteolysis. The inability of RSA to capture the relatively small interfacial motions which may occur (<40µm) limits the application of this technique to detect early signs of loosening and to determine small variations in motion due to different fixation techniques and implant designs. Another factor to consider is that this method relies on tracking the relative change in position of special markers in the body, thereby limiting the application of this method to a select few predefined patients.

Whether an implant is cemented or uncemented and whether it employs the use of a stem or is stemless may influence the relative micromotions between bone and implant. However, the influence of the internal implant features and geometry itself has received only limited attention (van Lenthe et al. 2002, Shi 2007, Bollars et al. 2011, Kluess et al. 2012). In a recent study by Bollars et al. (2011), the influence of anteroposterior slope on force to loosening was investigated using an *in vitro* setup. Bollars and colleagues found that as the AP slope increased the force to loosening in flexion decreased, highlighting that the internal geometry of the femoral component may play a role in aseptic loosening. In a finite element study of bone remodelling following knee replacement, Shi (2007) found that placement and size of distal femoral pegs had a significant influence on preservation or loss of bone stock. In an earlier study by van Lenthe et al. (2002), it was concluded that the primary and revision femoral component geometries lead to a similar net bone loss, though large regional variations were observed due to differences in prosthesis geometry.

Kluess et al. (2012) studied the effect of a wedge fit for a single implant geometry and found that the wedge angle significantly altered the stresses in the transitional regions between distal surface and anterior/posterior chamfers. The authors indicated that an implant with a poor fit may lead to high implant stress in these regions and may compromise the long term survival of ceramic implants.

Many other factors in addition to shape of the implant may influence the outcome, such as method of fixation, skill of surgeon during implantation, appropriate placement of guides and correct use of tools during the surgery. It has been shown

that oscillation of the saw blade during operation can lead to errors in femoral cuts (Plaskos et al. 2002, Bäthis et al. 2005, Yau and Chiu 2008), with displacement of the free end of the saw blade being related to blade thickness (Yau and Chiu 2008). Out of plane motion of the saw blade in combination with displacement of pinned cutting blocks during surgery has been found to result in surgical cut errors of the range of 0.8mm – 1.2mm (Otani et al. 1993, Plaskos et al. 2002, Bäthis et al. 2005), leading to a less than optimal positioning of the prosthesis and compromised long term survival of the implant. It has also been suggested that the addition of a stem to the femoral component serves to significantly increase component stability (van Loon et al. 2000, Completo et al. 2009) in comparison to a stemless implant.

Micromotion of the tibial bearing component and failure of the tibial tray have received considerable attention using *in vitro* and *in silico* techniques (Hashemi and Shirazi-Adl 2000, McLean 2007, Completo et al. 2008c, Chong et al. 2011). However, there is a lack of corresponding studies which deal with micromotion of the femoral component in current literature despite the similarly reported instances of loosening as discussed earlier. This is possibly due to a belief that the complex U-shaped design of the femoral component makes it less susceptible to motion than the flat plate like structure of the tibial tray.

In the present study the influence of internal implant features and implant fit is explored using three-dimensional FE models of the distal femur following primary and revision TKA scenarios. Two main goals were established for this study; the first was to determine the influence of internal implant features in preventing femoral component micromotion, and the second was to determine which of these internal implant features were more resistant to saw blade induced errors during preparation of the femur for implantation.

## VII.2 Methods

To fully characterise the component interactions that are not fully bonded (e.g. aseptic loosening of femoral components), the interfaces need to be frictional. Inclusion of frictional interfaces in FE models presents a number of challenges and requires the definition of an array of parameters to fully describe its behaviour.

### VII.2.1 Contact definition

In Abaqus there are several different contact models and algorithms to choose from, with each method having its own merits and application. In the current study, the Penalty method of contact was employed. This method represents the Abaqus implementation of the standard Coulomb friction model in which no relative motion occurs if the equivalent frictional stress ( $\tau_{eq}$ ):

$$\tau_{eq} \leq \mu p \tag{7.1}$$

where $\mu$ is the coefficient of friction and $p$ is the contact pressure.

In the Abaqus implementation of frictional contact, as in many other available FE packages, a degree of slip is permitted between contacting nodes before frictional behaviour is enforced. This elastic slip occurs even while the above inequality is satisfied so as to ease computational cost. In Abaqus the allowable elastic slip $y_i$ is calculated as the product of the elastic slip tolerance $F_f$ and the characteristic edge length $l_i$ as:

$$y_i = F_f l_i \tag{7.2}$$

The elastic slip tolerance can be specified by the user, otherwise the default value of $F_f = 0.005$ is applied. The characteristic edge length $l_i$ on the other hand is calculated automatically by Abaqus during the analysis and is usually based on the edge length of the smallest element on the contact surface of the mesh. Allowing Abaqus to automatically calculate elastic slip based on the characteristic element

edge length may pose problems for dissimilar meshes. A series of benchmark tests using simplified cubical domains, as detailed in Appendix B, were conducted to quantify the influence of these parameters on the relative motion at the interface.

A study by Kuiper and Huiskes (1996) showed that going from a coefficient of friction $\mu = 0.0$ to a coefficient of friction of $\mu = 0.15$ dramatically influenced the magnitude of interfacial motions, whereas changing from $\mu = 0.15$ to $\mu = 0.4$ only slightly affected the level of motion at the bone-implant interface. In a frictionless case the prosthesis relies solely on the normal force to resist motion, however, with frictional interactions the stability of the prosthesis is influenced by both the normal force and the shear force which develops at the interface. A later study by Viceconti et al. (2000) suggested that a coefficient of friction in the range of 0.2 – 0.5 best correlated with experimental studies.

In addition to these settings several other software specific parameters are required for contact analyses conducted in Abaqus, details of these parameters and the values used can be found in section B.4 of Appendix B.

### VII.2.2 Model setup

In the present study, FE models of the distal femur following implantation with a cruciate retaining (CR) implant, a posterior stabilising (PS) implant, a total stabilising implant with short stem (TSSS) and a total stabilising implant with long stem (TSLS) were created. The PS and CR models were modified from those presented in Chapter IV to employ frictional contact conditions at the prosthesis bone interface. The main focus of this study was to examine relative motions which can occur at the bone-implant interface. In the previous chapters, second-order tetrahedral elements (C3D10) were employed to accurately capture the stresses and strains in the femur for different patient and implantation scenarios. However, this element type is unsuitable for the modelling of frictional interfaces, due to issues with the way consistent nodal loads are calculated, as discussed in the Abaqus documentation (Dassault Systèmes 2010a):

*"Second-order tetrahedra are not suitable for the analysis of contact problems: a constant pressure on an element face produces zero equivalent loads at the corner nodes. In contact problems this makes the contact condition at the corners indeterminate, with failure of the solution likely because of excessive gap chatter."*

Some of the issues with this element type can be resolved by switching to a modified second-order element (C3D10M), e.g. the issue of excessive gap chatter. However, these elements are much more computationally expensive. In the present study, due to hardware limitations and the added computational cost associated with the simulation of friction in complex three-dimensional assemblies (≥ 48hrs for second-order elements vs. 2.5 hrs for linear elements per model), all models were re-meshed with linear tetrahedral elements (C3D4). Linear tetrahedral elements have been employed successfully in many previous studies (Abdul-Kadir et al. 2008, Completo et al. 2009, Chong et al. 2010) for the purposes of analysing contact. A study by Ramos and Simões (2006) highlighted that for stress and strain, once a sufficient number of elements are employed, there should be no significant difference between the results obtained using linear and quadratic elements. In their study, the number of linear elements used was approximately 144,000. Due to small model features (e.g. pegs); a significantly larger number of elements were employed in the current study as detailed in Table 7.1.

**Table 7.1:** Number of linear elements used.

| Model | Number of elements |
|---|---|
| CR | 330623 |
| PS | 293536 |
| TSS | 310359 |
| TSLS | 317641 |

### VII.2.3 Model geometry

As in Chapter IV, to model primary implantation of the distal femur the composite femur model was modified to accept both CR and PS implants. Further local

refinement of the mesh was carried out as required, such as around the peg holes in the CR implanted femur (Figure 7.1), to optimise interface contact and improve accuracy of recorded motions at key internal features during frictional simulations.

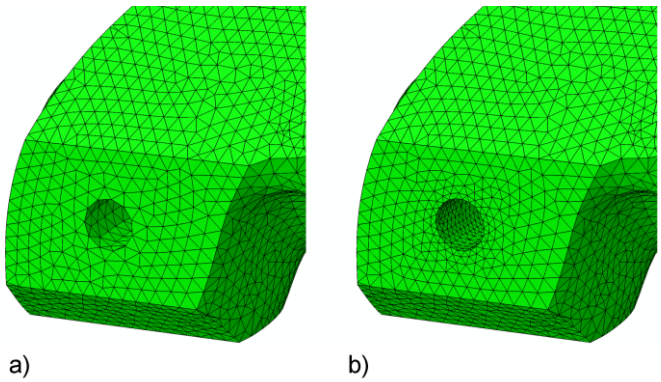


**Figure 7.1**: Example of local mesh refinement at a key region of interest, showing a) unrefined peg hole and b) refined peg hole.

To investigate the influence of revision implantation on interfacial motions, a TS implant with two different stem lengths and diameters was also considered. Unlike the stemmed models presented in Chapter IV, all models (both primary and revision) employed in the present study were modelled on uncemented implantation of the prosthesis. The implant geometries used in the current study are shown in Figure 7.2.

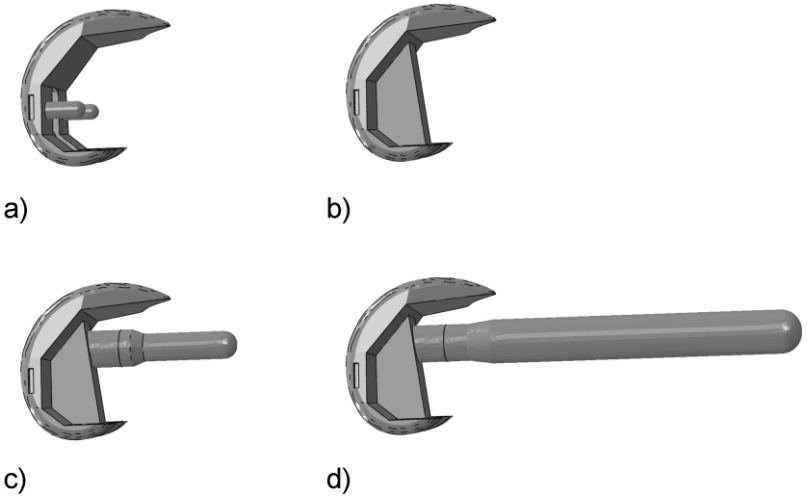


**Figure 7.2**: a) CR implant, b) PS implant, c) TS implant with Ø12x50mm stem and d) TS implant with Ø19x150mm stem.

### VII.2.4 Model interface conditions

In the present study, Coulomb friction was implemented at all bone-implant interfaces, with a frictional coefficient of $\mu = 0.3$ representing an average of the reported values in literature (Rancourt et al. 1990, Kuiper and Huiskes 1996, Viceconti et al. 2000, Abdul-Kadir et al. 2008). Based on the results from the studies conducted in Appendix B and to eliminate dependency of numerical parameters on mesh density, an allowable elastic slip of $y_i = 0.005$ or $5\mu m$ was specified directly for all model variations.

### VII.2.5 Model fit conditions

Based on initial two-dimensional investigations into femoral component loosening and considering the evidence in literature for errors due to saw blade oscillation, two different fit conditions were investigated. The first considered a perfect fit between the internal geometry of the implant and the femoral bone cuts and the second simulated a loose fit between bone and implant. In this case the loose fit models were characterised by excessive removal of material to a depth of 1mm from both the anterior and posterior surfaces of the femur, as shown in Figure 7.3. These two conditions of fit were then applied to all primary and revision implant scenarios described previously in Figure 7.2.

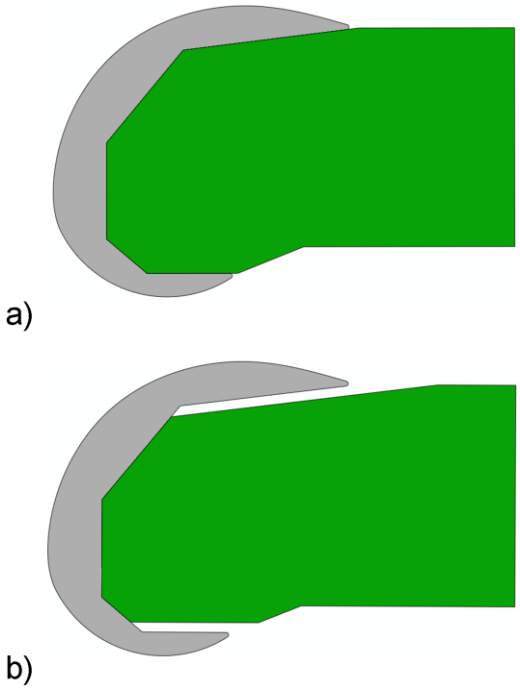


**Figure 7.3:** Two-dimensional illustration of the two interface conditions considered, where a) represents a perfect fit and b) a loose fit due to excessive removal of bone from the anterior and posterior surfaces.

### VII.2.6 Material properties, boundary conditions and loading

As in Chapter IV, all materials were assumed to behave in a linear elastic, isotropic manner. The value of Young's modulus and Poisson's ratio applied to all the structures in the present study was as presented in Chapter IV Table 4.1 and Chapter VI Table 7.1 respectively. Applied loading and boundary conditions remained unchanged from that presented in Chapter IV (Table 4.2 and Figure 4.6).

## VII.3 Results

In this first section, the influence of internal implant features (e.g. pegs or box) on implant stability following primary TKA with uncemented implants is investigated.

### VII.3.1 Cruciate retaining vs. posterior stabilising – normal fit

The relative motion of each implant to the bone is described using three built in parameters in Abaqus. The first (Copen) describes the relative separation of two surfaces in the normal direction, the second (Cslip 1) and third (Cslip 2) represent micromotions tangential to the contact surfaces in two orthogonal directions. The variation of these parameters with increasing flexion angle can be seen in Figure 7.4 – Figure 7.6. At lower flexion angles, all components of motion for both CR and PS implanted femurs are found to be well below $40\mu m$, and in some cases below $25\mu m$. At higher flexion angles, however, the difference in implants due to internal features becomes more noticeable. At 48° flexion the CR implanted femur experiences the majority of motion on the anterior chamfer, whereas for the PS implanted femur the largest area of motion is located on the distal aspect of the medial femoral condyle. Separation of the bone and implant surfaces as defined by Copen is found to be largest on the anterior surface in the CR implanted femur and on the medial aspect of the intercondylar box in the PS implanted femur.

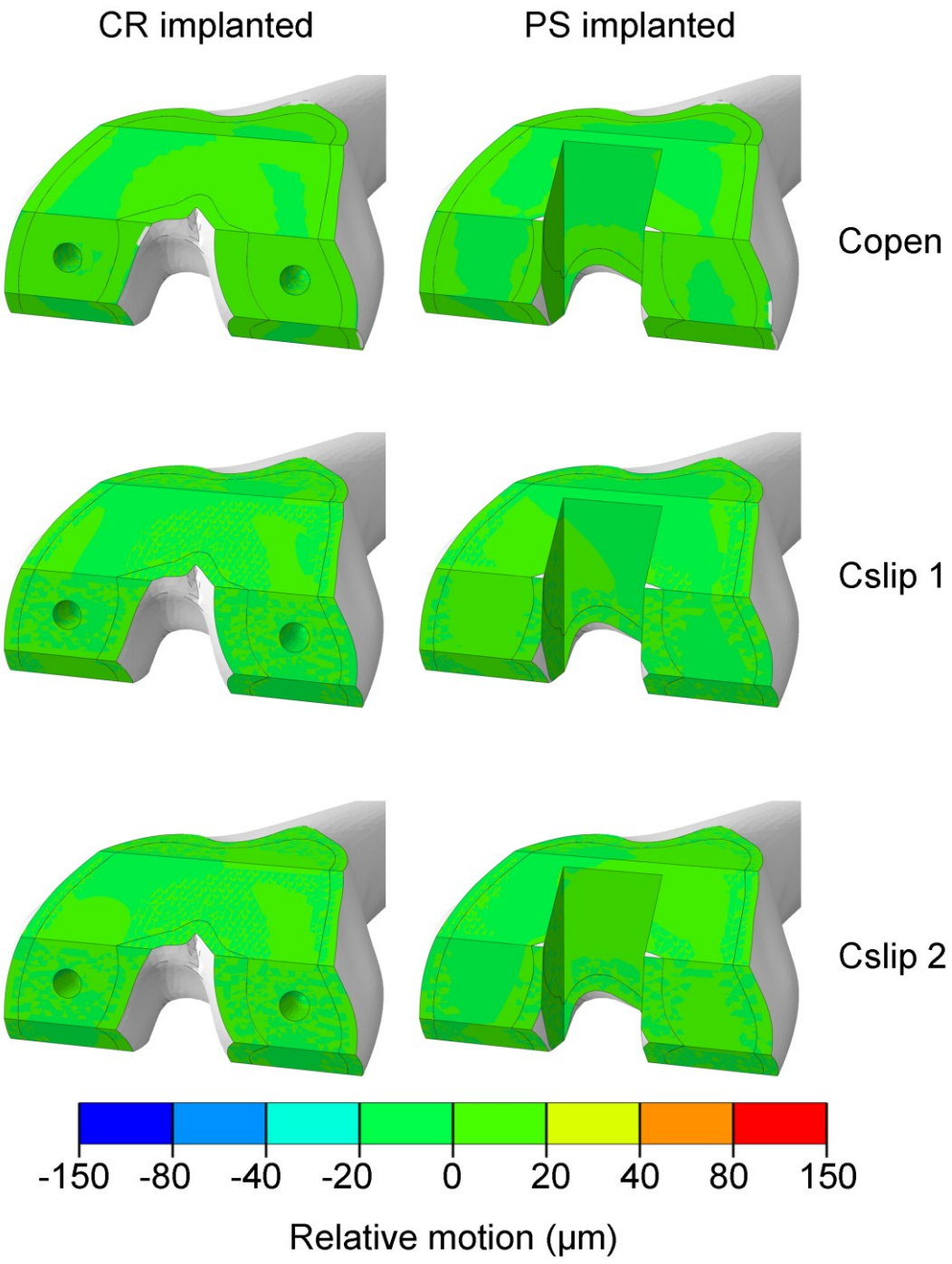


**Figure 7.4:** Femoral component relative motion expressed as contact separation and tangential motion in two orthogonal directions for a CR implanted femur (first column) and a PS implanted femur (second column) at 0° flexion.

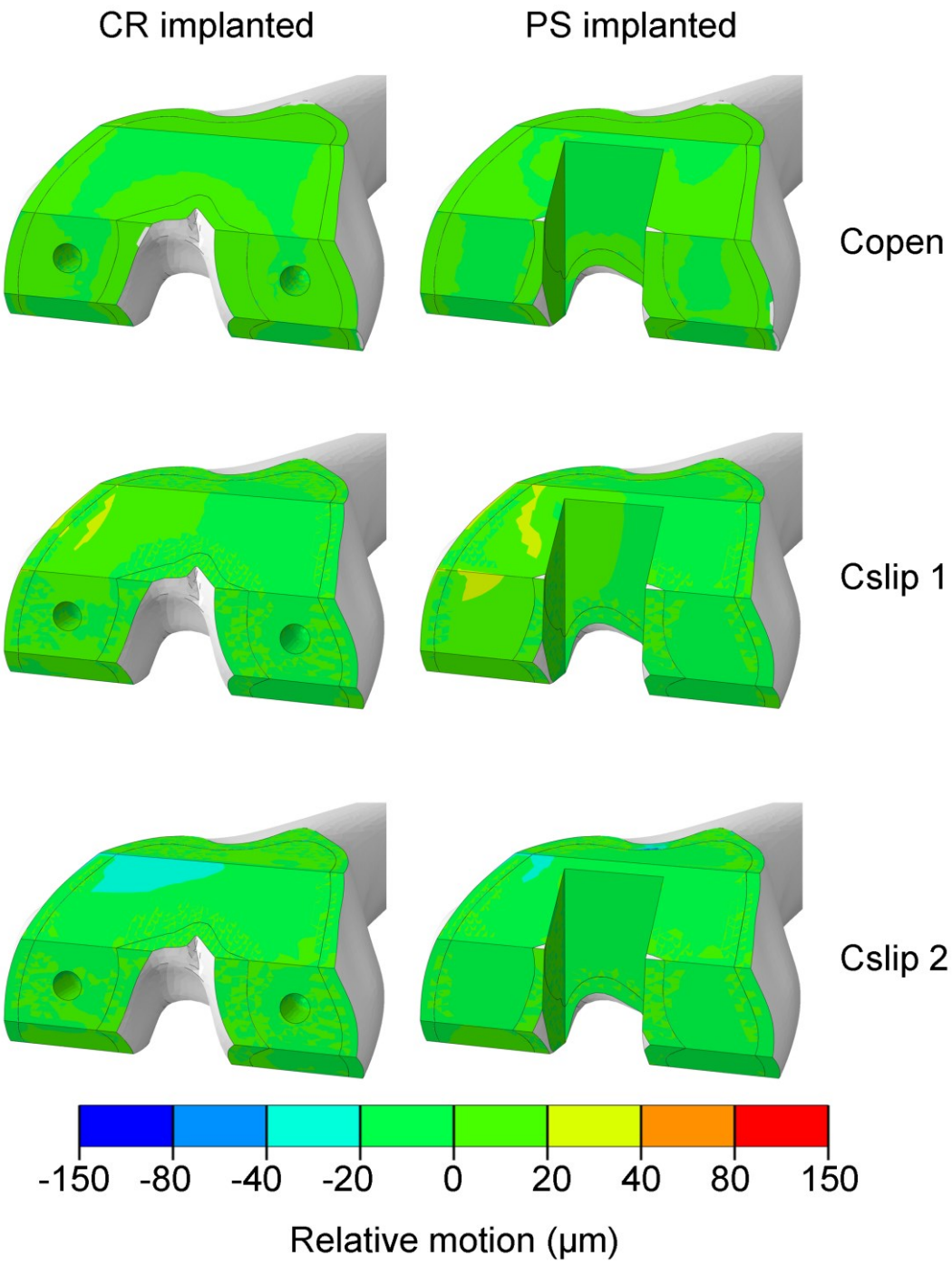


**Figure 7.5:** Femoral component relative motion expressed as contact separation and tangential motion in two orthogonal directions for a CR implanted femur (first column) and a PS implanted femur (second column) at 22° flexion.

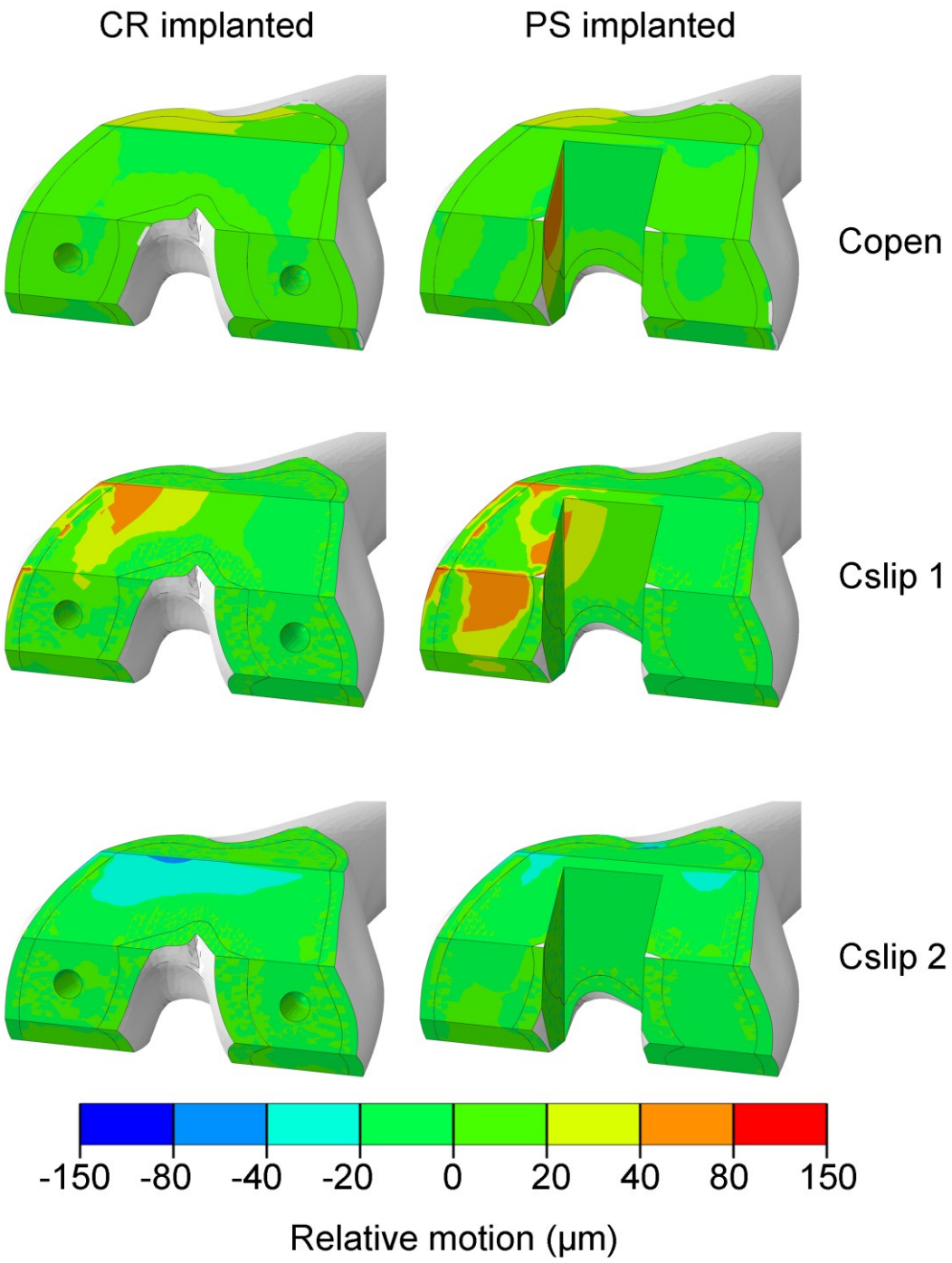


**Figure 7.6:** Femoral component relative motion expressed as contact separation and tangential motion in two orthogonal directions for a CR implanted femur (first column) and a PS implanted femur (second column) at 48° flexion.

In general, the majority of motions for both implant types are found to be well below the limit for osseointegration. However, small portions of the anterior chamfer in the

CR implanted femur and distal surface PS implanted femur are found to experience levels of motion within the fibrous tissue formation region, e.g. motions in the range of $40-70\mu m$, where $40\mu m$ represents the suggested lower boundary of the range ($40-150\mu m$), at both 22° and 48° flexion. Though peak values are of a similar magnitude at the lower flexion angles for both implant types, the internal implant features are found to result in distinct differences in surface areas that experience relative motions, with the PS implanted femur subject to a much larger area of motion which may present a greater risk to bone in growth. However, it must be noted that in the second tangential direction (Cslip 2), the surface area associated with motion for the CR implant is greater than that associated with the PS implant, though at a much lower level of motion.

### VII.3.2 Cruciate retaining vs. posterior stabilising – loose fit

This second section investigated the influence of defective surgical cuts due to saw blade motion. From the contour plots of interface relative motion, it can be seen that in general poor implant fit causes an increase in motion (Figure 7.7). By comparing the CR and PS implants at 48° flexion[5] under both normal and loose fit conditions, it can be seen that the loose fit condition has a more significant impact on the PS implanted femur than the CR implanted femur. In the CR implanted femur, there is a slight increase in the surface area associated with peak motions on the anterior chamfer in the first tangential direction (Cslip 1). In comparison, the PS implanted femur shows an increase in all three components of interfacial motion (Copen, Cslip 1 and Cslip 2), a large proportion of which is in the band for fibrous tissue formation $40-80\mu m$. Furthermore, a portion of the medial aspect of the intercondylar box and the anterior chamfer experience motions in excess of $80\mu m$ under loose fit conditions.

[5] Supplementary contour plots of interfacial motion for all remaining models investigated, at 0° and 22° flexion can be found in Appendix B section B.5.

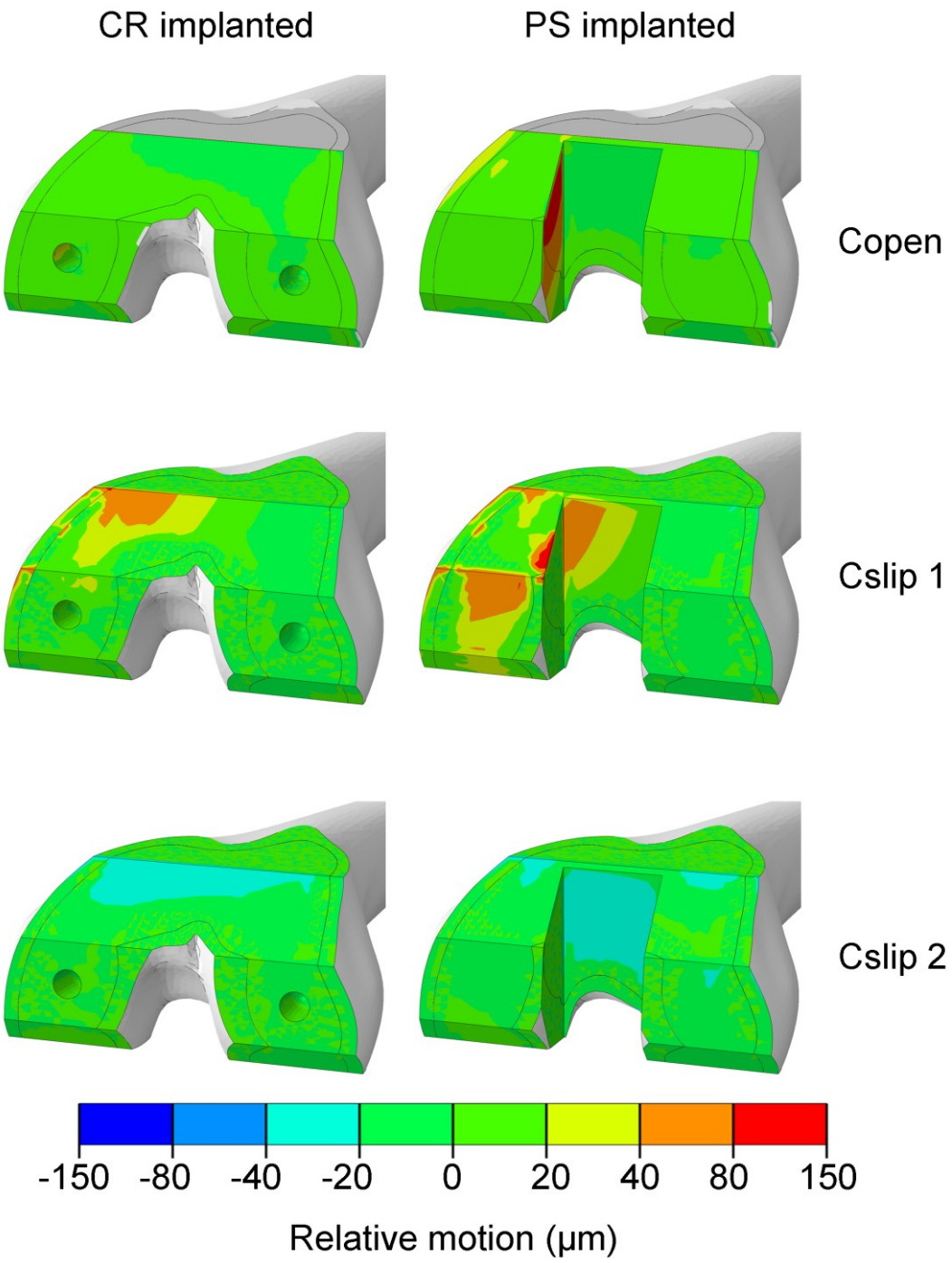


**Figure 7.7:** Femoral component relative motion expressed as contact separation and tangential motion in two orthogonal directions for CR implanted femur (first column) and a PS implanted femur (second column) at 48° flexion under loose fit conditions.

### VII.3.3 Effect of stemmed femoral prosthesis on motion

This section attempts to quantify the influence of femoral stems on motion at the bone implant interface. Following on from the findings in the primary implant studies which showed motions were maximal in flexion, contour plots for the different components of interface motion (Copen, Cslip 1 and Cslip 2) at 48° flexion were generated (Figure 7.8). The figure compares motion at the interface for both the TSSS (Ø12x50mm) and the TSLS (Ø19x150mm) implanted femurs.

It can be seen that the TSSS implanted femur exhibits a similar distribution of motion to the PS implanted femur, though it should be noted that the addition of a fully frictional short stem leads to a slight reduction of motion on both the distal surface of the femur and the distal aspect of the intercondylar box when compared with a stemless PS implanted femur. The addition of a long stemmed femoral component (TSLS), on the other hand, is found to result in peak motions below all other implants, typically less than $38\mu m$ in peak areas and less than $20\mu m$ over the majority of the distal surface. Though the magnitude of peak motions were found to vary between implants, interestingly the pattern and distribution of smaller ( $20-40\mu m$ ) motions for the PS, TSSS and TSLS was found to be very similar. This is likely due to the shared internal implant features of these three components.

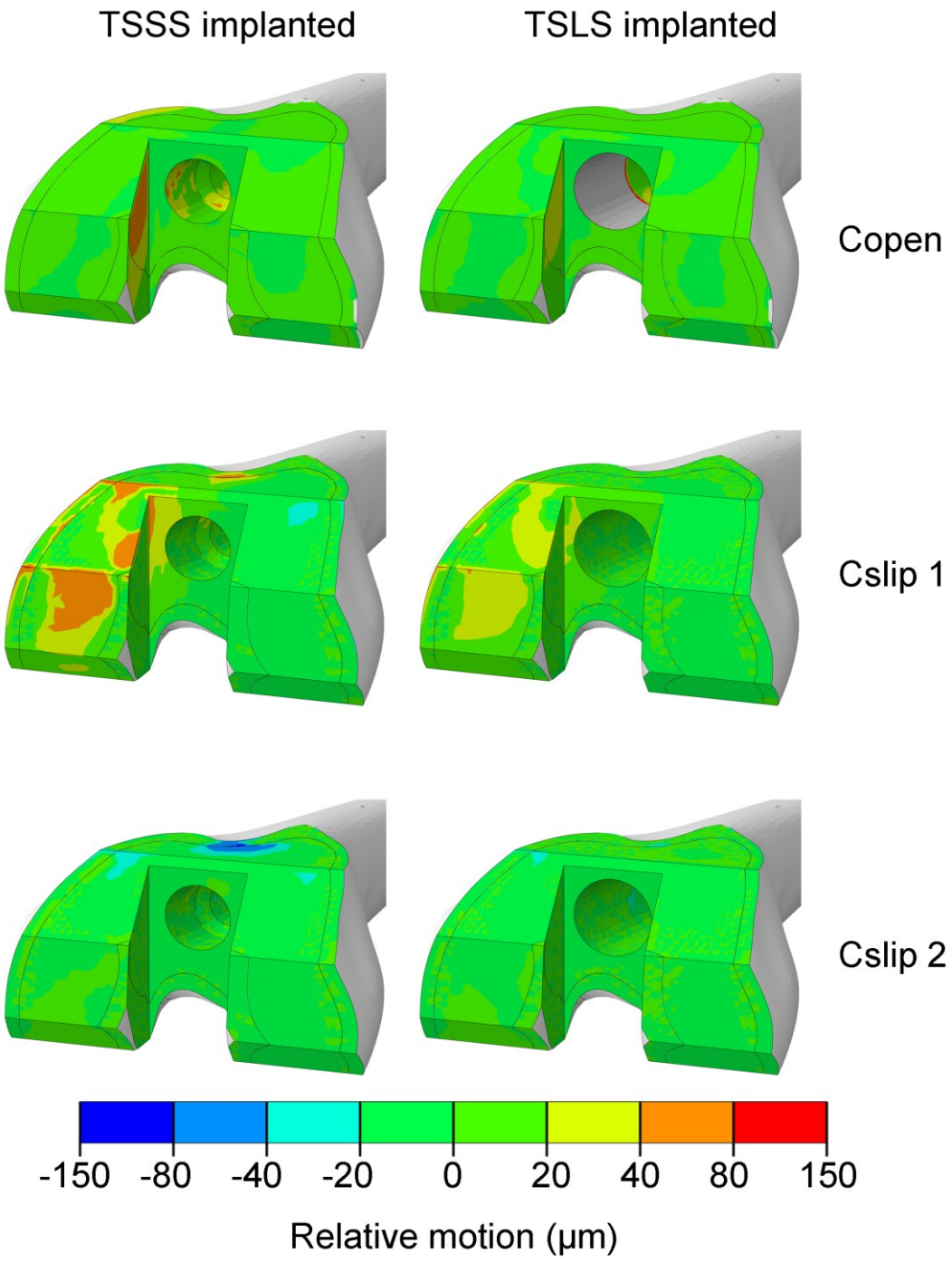


**Figure 7.8**: Femoral component relative motion expressed as contact separation and tangential motion in two orthogonal directions for a TS implanted femur with short stem (first column) and a TS implanted femur with long stem (second column) at 48° flexion.

### VII.3.4 Effect of loose fit on component motion for stemmed implants

In this last section, the role of distal femoral stems in the presence of loose fit conditions was investigated. Interestingly, the femur implanted with a short stemmed femoral component (TSSS) was found to exhibit increased motion in the upper limit of the fibrous tissue formation range, e.g. $> 80\mu m$ .This places the short stemmed implant's performance in the same category to that of the PS implant under similar fit conditions. However, it can be observed by comparing Figure 7.9 and Figure 7.7 that the stem, much like the femoral pegs in the CR implanted femur, serves to resist translational motion thereby reducing the level of relative motion in the direction of Cslip 2, this is particularly noticeable on the distal surface of the intercondylar box.

The TSLS implanted femur, on the other hand, showed the greatest reduction in motion under both normal and loose fit conditions. Under loose fit conditions, it was observed that the addition of a long stem lead to motions comparable to that of a PS implant under normal fit conditions (with minor regional variations). Typically, peak motions for the TSLS implanted femur on the anterior chamfer and distal femoral surface under loose fit conditions remained below $55\mu m$ . This significant reduction in motions compared to other implant types is likely due to the large diameter canal filling stem which aids alignment of the prosthesis and component stability in instances of bad fit. However, it is worth noting that if the prosthesis becomes reliant on the stem to maintain position in the absence of adequate bone support, this may increase the likelihood of prosthesis failure (explored further in Chapter IX).

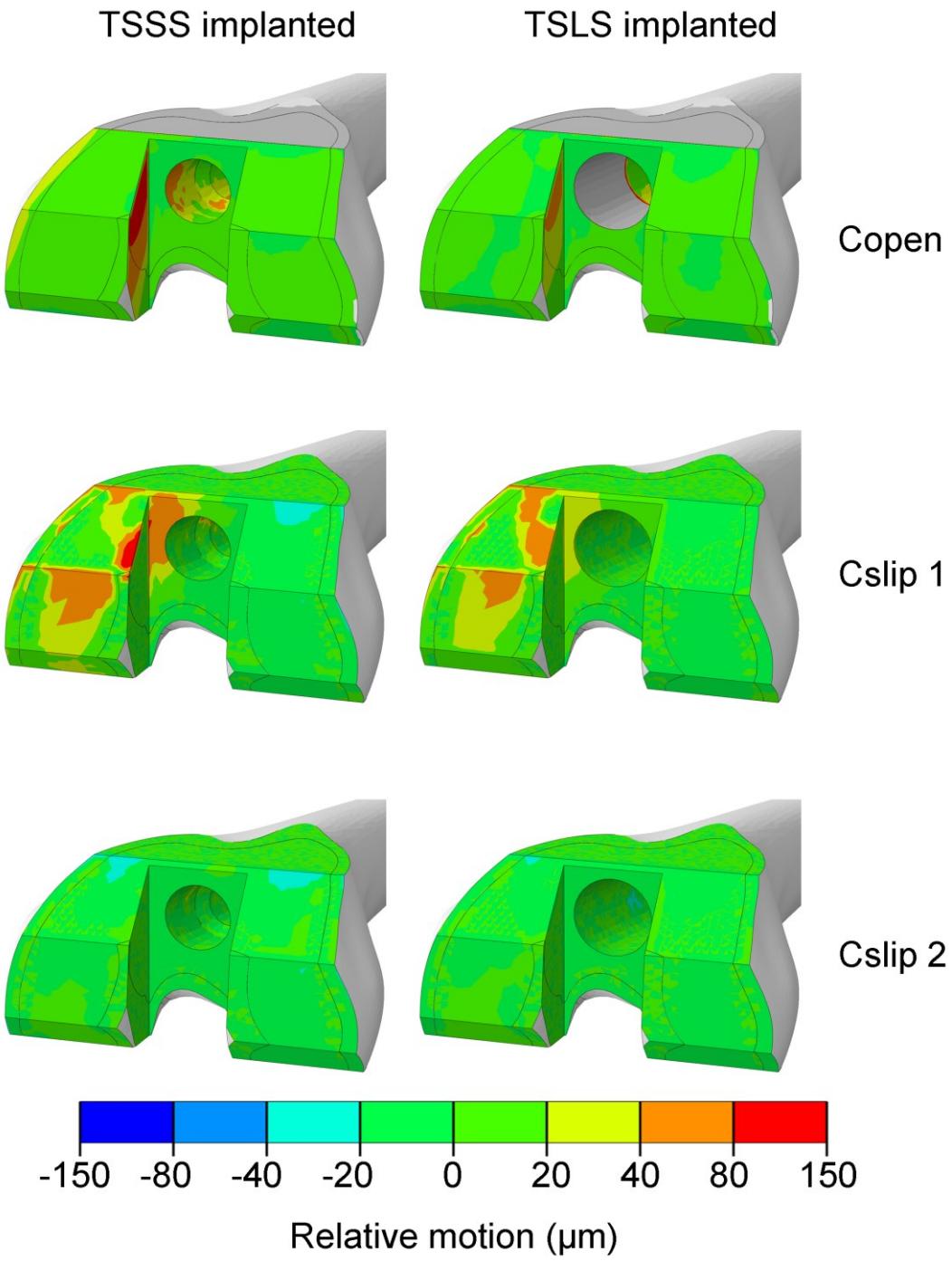


**Figure 7.9:** Femoral component relative motion expressed as contact separation and tangential motion in two orthogonal directions for a TS implanted femur with short stem (first column) and a TS implanted femur with long stem (second column) at 48° flexion for loose fit conditions.

## VII.4 Discussion

In this chapter, computational models of the femur following primary and revision TKA scenarios were employed to test the influence of internal implant features and implant fit on relative motions at the bone-implant interface.

As discussed in Chapter II, small amounts of relative motion (< $40\mu m$) at the prosthesis-bone interface can be beneficial in promoting bone in growth and fixation, however, motion of the order of 150µm or greater are seen to result in fibrous tissue formation and ultimately failure of the implant. The primary implants investigated in this study represent two common industry standards in terms of internal implant features (i.e. pegs or box). Both primary implants tested exhibited similar magnitudes of motion at all three flexion angles investigated, with average interface motions remaining well below the limit for fibrous tissue formation ( $40-150\mu m$ ) at 0° and 22°, although, at 48° flexion the interfacial motions were observed to approach the recommended limits for osseointegration. The location of peak motions were found to vary considerably between implants, i.e. in the CR implanted femur greatest levels of motion were seen to occur on the anterior chamfer, whereas in the PS implanted femur the largest reported motions occurred on the distal surface, this may have implications for implant design. It is important to note that the peak values of motion were found to be similar for both models, indicating that internal implant features do not significantly influence the magnitude of peak motions. However, the increased surface area of motion associated with the PS implant may indicate a slightly higher risk of loosening than in CR implanted femurs. Furthermore, loosening over a greater surface area may expose the underlying surface to wear debris from the joint.

Moreover, due to the presence of the femoral box section in the PS implant, the effects of loosening may not be readily apparent from standard two-plane radiographs (Nadaud et al. 2004), particularly when largely confined to a single condyle as reported in the present study, leading to an increased risk of osteolysis induced bone loss and eventual failure of the component if untreated.

In general relative micromotions at the interface were found to increase with flexion angle, which lends support to studies that have inferred loosening of implants in high flexion from increases in interfacial shear stresses (Zelle et al. 2011).

The influence of stemmed femoral components was also investigated in this study. It was observed that slight differences occur in the location of peak motions when comparing the PS implanted femur with the short stemmed TS implanted femur, however, in general the short stem was found to reduce the levels of motion at the interface (approximately 10%). On the other hand, the addition of a long stem was found to significantly reduce distal motions in comparison to the other two implant types, by approximately 30%. An recent FE study by Completo et al. (2009) reported similar reductions in motion (up to 41%) when comparing contact separation at the cement-bone graft interface for a prosthesis with press-fit stem, and no stem.

This study also investigated variations in fit through introduction of a loose fit at the bone-implant interface characterised by excessive removal of material due to saw blade motion. By comparing interface motions at 48° flexion for both normal and loose fit conditions it can be observed that the PS implant is more sensitive to changes in fit conditions. It is expected that this difference would again become more dramatic as flexion angle increases in more strenuous activities such as squatting and sitting down into a chair, e.g. activities where the defect gap becomes compressed. A clinical study by King and Scott (1985) observed the loosening behaviour of femoral components following total knee arthroplasty. In that study the authors suggested that loss of posterior support through poor cementing technique, surgical cut errors or bone loss leads to increased motion at the interface, particularly during higher flexion activities where the joint force would be transmitted directly to the distal surface causing the implant to shift into flexion. By comparing the relatively small change in interfacial motion for a TS implant with long stem under normal (Figure 7.8) and loose fit conditions (Figure 7.9), the present study lends qualitative support to the argument that adding a stem helps to reduce interfacial motion (King and Scott 1985), particularly in the presence of imperfect surgical cuts.

It is important to note that stem length and fixation may also impact upon this conclusion. In the present study for example it was observed that the short fully frictional stem led to motions comparable to that of the PS implanted femur, whereas, the long stemmed implant, on the other hand, resulted in the smallest interfacial motions which only marginally increased with imperfect surgical cuts (overall motions remained well below the normal fit PS implanted femur).

One limitation of the current models is with respect to the low flexion angles tested. In short, these flexion angles were not extreme enough to fully compress the defect. Had higher flexion angles been considered, it is likely that a more dramatic difference would have been observed between implants, such as where defects to the surgical cuts on the posterior condyles have been reported clinically to shift the femoral component into flexion during high flexion activities (King and Scott 1985).

Only the effect of frictional stems was investigated in this study, had the short or long stem models been fixed along the stem the resulting interfacial motions would have reduced significantly. As such it must be considered that the stemmed models presented here represent a worst case scenario where fixation of the prosthesis is not fully achieved. Furthermore, for simplicity only two stem configurations were considered in the present study. These two stems were selected on the basis of representing opposite ends of the available product range in terms of both stem diameter and length. It is therefore expected that all other stems in the range would lie somewhere between the performance of these two, though future studies should be conducted to verify the performance of other configurations.

In conclusion, based on the findings in this study, internal implant features are found to have little influence on the peak interfacial motions. However, internal implant features play a significant role in the surface area associated with peak motion values. Similar to that observed *in vitro* by Bollars et al. (2011), in the present study it was observed that femoral components with two distal femoral pegs were less susceptible to interfacial motions. This trend was observed under both normal and

loose fit conditions, indicating pegs to be a desirable design feature for resisting loosening (both translational and rotational).

Similar to the findings of Completo et al. (2009), this study also concluded that the use of a long canal filling stem over shorter non-diaphyseal engaging stem provides the greatest level of stability. In practice, however, full fixation of long stems is hard to achieve due to the length of the prosthesis and the natural bow in the shaft of the femur. In the absence of complete fixation of the stem, the subsequent motion at the stem tip may cause high localised stresses and lead to end of stem pain (Barrack et al. 1999, Brown et al. 2002, Barrack et al. 2004) or place undue stress on the prosthesis junctions.

In this chapter, FE models of the distal femur following primary and revision knee arthroplasty were developed. These models incorporated frictional interactions at the bone-implant interface to allow investigation of how implant geometry and fit may influence component stability. In the next chapter, the role of stems and fixation is explored further *in vitro* using a custom relative motion test rig.

# VIII

# Experimental Evaluation of Femoral Component Motion

## VIII.1 Introduction

The role of fixation (cemented vs. uncemented) in both primary and revision TKA remains a widely debated if not controversial topic (Laskin 2001). The majority of the orthopaedic community has strong preferences "in support of" or "against" the use of cemented components. A number of studies highlight the benefit of uncemented fixation (Rand 1991, Nilsson et al. 2006) and a similar number suggest that cemented fixation remains the gold standard for implantation (Duffy et al. 1998, Park and Kim 2011). Based on the current body of knowledge, some suggest neither technique has an overall advantage over the other (Toksvig-Larsen et al. 1998, Park and Kim 2011) and that the technique used should ultimately be dependent on the situation and patient specific factors. Proponents of uncemented fixation suggest that this technique is particularly well suited to younger more active patients as it reduces surgical time, prevents thermal damage to the surrounding bone tissue and preserves bone stock (Nilsson et al. 2006, Meneghini and Hanssen 2008), a factor which is significant at the time of revision surgery.

The issue of fixation becomes even more complex in the setting of revision TKA, where surgeons must choose between a variety of prosthesis designs and fixation techniques in order to achieve the best possible fixation. Though there is a general consensus in the orthopaedic community that stems are required to obtain initial

mechanical stability in the presence of deficient metaphyseal bone (van Loon et al. 2000, Fehring 2005, Whittaker et al. 2008), little to no consensus exists regarding the appropriate selection of stem size, length or method of fixation. Surgeons choose between cemented fixation, cementless fixation and "hybrid" fixation of a cementless stem coupled with a cemented metaphyseal component. Based on the overwhelmingly contradictory evidence currently available to surgeons on the topics of prosthesis selection and fixation, it is no surprise that a recent review of the literature was unable to recommend one form of fixation over the other (Beckmann et al. 2011). Many variables contribute to the contradictory conclusions observed in the literature, particularly in the case of uncemented fixation, where factors such as skill of the surgeon and experience with different techniques, design of the implant, patient geometry/bone quality and successful alignment/placement of the prosthesis all heavily influence the outcome (Toksvig-Larsen et al. 1998).

Surgeons are increasingly relying on *in vitro* laboratory testing to supplement current knowledge through controlled investigation of stresses and strains post implantation, examination of the influence different fixation methods exert on component stability and monitoring of interfacial motions for different implant systems. However, due to the complexity of loading and boundary conditions on the femoral side of the knee joint relatively few studies have been conducted on the distal femur (Wackerhagen et al. 1992, van Loon et al. 2000, Moran 2005, Completo et al. 2007, Cristofolini et al. 2008, Cristofolini et al. 2009). Studies which have focused on the distal femur have often been limited to loading in extension only (van Loon et al. 2000, Completo et al. 2007). Work carried out by Wackerhagen et al. (1992) investigated femoral component motion through the use of a custom built dynamic knee rig capable of a range of flexion angles from 0°-90°. Moran (2005) employed the use of a custom knee rig which included representations of the quadriceps and hamstrings muscles to test the influence of femoral component anteroposterior slope on interfacial motions along three degrees of freedom. Later work by Cristofolini et al. (2008, 2009) employed a modified knee wear simulator to investigate the long term loosening behaviour of both cobalt chromium and ceramic primary knee implants with loading

based on ISO 14243-1 and ISO 14243-3 testing regimes (ISO 2004, ISO 2009). In these studies motions of the femoral component along only a few degrees of freedom (typically anteroposterior translation and rotation in the sagittal plane) were recorded at the bone-implant interface (Wackerhagen et al. 1992, Moran 2005, Cristofolini et al. 2008, Cristofolini et al. 2009). Critically, another limiting factor of previous *in vitro* studies has been their focus on primary stemless prostheses. *In vitro* studies which have investigated revision implants on the other hand, only considered the effects of stemmed prosthesis on the strain distribution in the femur post implantation (Completo et al. 2008a, Completo et al. 2008b) under simplified loading regimes. Only one previous study investigated the influence stemmed prostheses exert on femoral component motion (van Loon et al. 2000) in the setting of revision TKA. In this study, van Loon and colleagues evaluated how the presence of a stem altered the translational and rotational motions at the interface in the presence of an unconfined condylar defect. The authors concluded that stemmed prostheses resulted in greater stability than stemless prosthesis and had a greater contribution to stability than the bone graft.

The two main aims to be achieved in this chapter were, firstly to develop a test apparatus capable of discerning small changes in relative motion at the bone implant interface for both primary and revision TKA prostheses at a high level of accuracy. The second aim was to investigate the influence of stem length on the overall pattern and level of relative motions at a range of functional flexion angles for both cemented and uncemented interface conditions.

## VIII.2 Methods

This section details the development of the micromotion test rig and the protocols for femoral component implantation and testing. Other aspects covered include the coordinate transformation theory employed in the evaluation of all translational and rotational components of relative motion based on the assumption of rigid body kinematics.

### VIII.2.1 Micromotion rig development

The micromotion measurement rig developed in this study was based on similar concepts employed by Berzins et al.(1993) and Maher et al.(2001, 2002) in the study of hip implant subsidence and micromotion and more recently by McLean (2007) in the study of tibial component micromotion. Adaptation of the system to the distal femur presented a number of challenges due to the complex geometry and the nature of loading at the knee joint (i.e. position of loading changes with flexion).

The initial design developed in this study consisted of four main components: a target bracket, a sensor housing which contained six differential variable reluctance transducers (DVRTs; Microstrain Inc., USA), adjustable coupling bolts and a femoral clamping device (Figure 8.1).

#### VIII.2.1.1 Design of the target bracket

The target bracket as shown in Figure 8.2 consisted of three spheres attached to a U-shaped frame. Previous studies at other joint locations employed a fully rigid or fully closed target frame (Maher and Prendergast 2002, Britton and Prendergast 2005, McLean 2007). However, due to the changing position of the tibia relative to the femur with flexion it was necessary to adopt an open or U-shaped frame approach to provide the necessary clearance for tibial loading in flexion. The frame was constructed of mild steel and to a thickness of 10mm which was found to be adequate to ensure that it did not bend. Additionally, the frame incorporated a large radius ( $R = 25mm$ ) so as to ensure adequate stiffness of the frame in the medial/lateral direction and to maintain its shape under loading (Appendix C, section C.4); this was an important consideration as any deformation of the target bracket or rig relative to the sensors could be registered by the system as relative motion of the implant to the bone. Two slots (Figure 8.2b) were precision machined into the top surface of the bracket to accommodate the incorporation of two adjustable wedges. The adjustable wedges as shown in Figure 8.2c provided an interference fit between the standard implant tool grooves and the target bracket to ensure there was no relative motion

between implant and target spheres. The use of adjustable wedges during attachment of the target bracket ensured compatibility of the measurement system with a wide range of implant types and sizes. The final part of the target bracket assembly consisted of two stiff plates which attached to the upper surface of the target frame. These plates were used to secure the adjustable wedges in position and prevent any upwards translation of the wedges when attached to the implant.

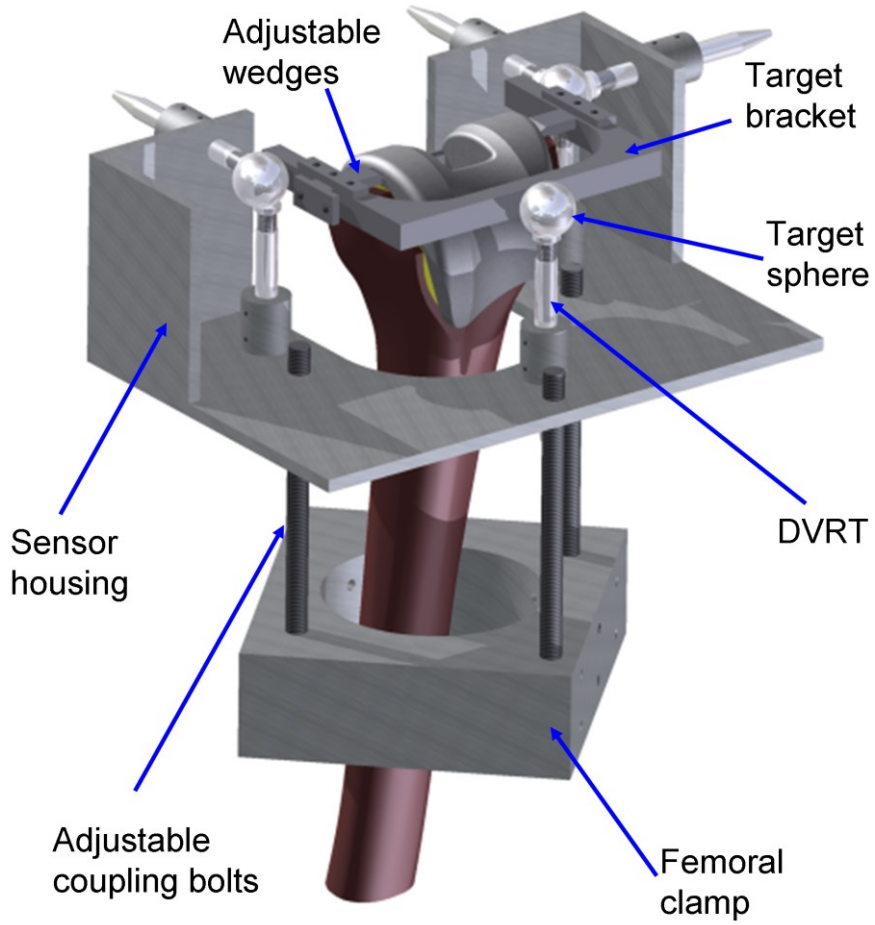


**Figure 8.1:** Rendered CAD model of prototype rig assembly with all major components labelled.

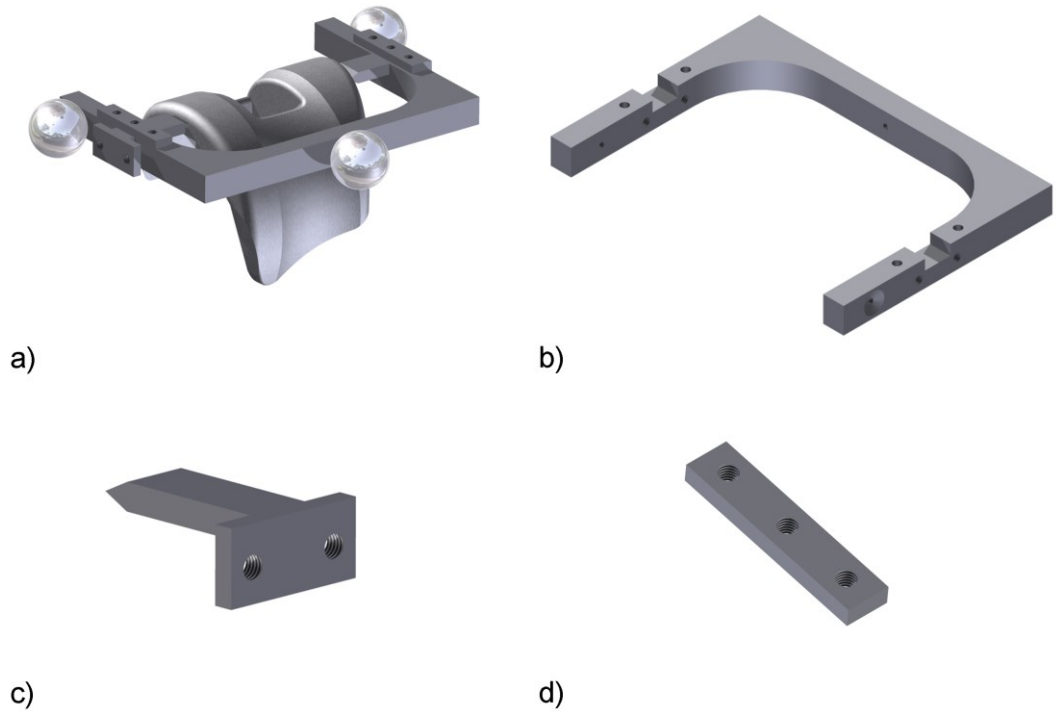


**Figure 8.2:** CAD drawings showing: a) the implant-target bracket assembly, b) the main frame of the target bracket without target spheres attached, c) adjustable wedge and d) target bracket clamp.

#### VIII.2.1.2 Sensor housing

The sensor housing assembly comprised of two distinct parts: the main body (Figure 8.3a) and the individual sensor holders (Figure 8.3b). The individual sensor holders were attached to the main body by means of an M14 screw thread on the end of each holder. Precision machining of both the main body and sensor holders was required to ensure the correct alignment of the flat heads of each DVRT with its respective target spheres once assembled.

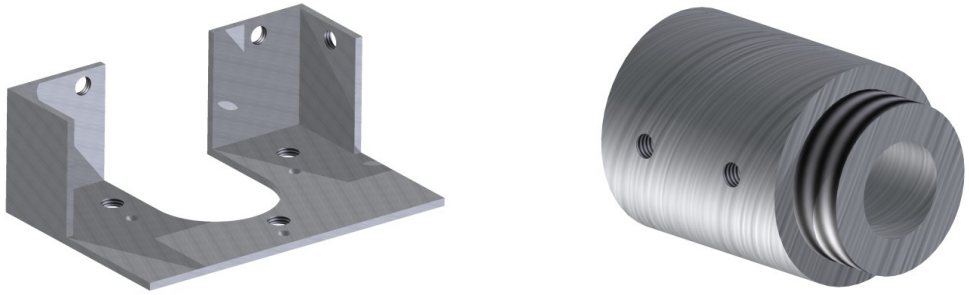

a) b)

**Figure 8.3:** CAD drawings showing the different components of the sensor housing assembly.

### VIII.2.1.3 Femoral clamping device

This part of the test rig was designed to attach to the femur through the use of 12 adjustable pointed screws, two rows of three equally spaced screws 45° either side of the central screw position, symmetrically on both parts of the femoral clamping device (Figure 8.4). The sensor housing was in turn secured to the femoral clamping device through the use of three adjustable coupling bolts. Adjustable bolts were used so that fine adjustment of the sensor housing could be carried out to ensure correct alignment of the flat head of each DVRT with the relevant target sphere. The open back of the sensor housing and the split part design of the femoral clamping device were to ensure a quick turnaround time between specimens, allowing the complete test rig to be removed prior to changing of the bone specimen in the bone holder.

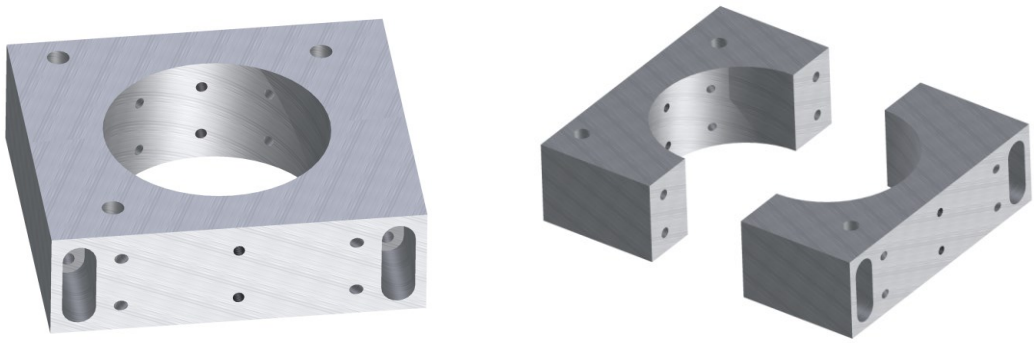

**Figure 8.4:** CAD drawings showing the different components of the target bracket assembly.

### VIII.2.2 Sensors

Current literature (Pilliar et al. 1986) suggests that values of motion in the range of 40μm – 150μm or above may lead to the formation of fibrous tissue instead of bone. Motions in this range are therefore important as they may be indicators of the early stages of implant loosening. To ensure relevant relative motions between the prosthesis and bone are adequately captured this study, as in similar studies of this nature (Moran 2005, McLean 2007), employed the use of six DVRTs, positioned in the arrangement outlined in Figure 8.1. All DVRTs had a working range of +/- 2mm and an accuracy of 1% using a straight line fit for voltage to micron conversion. According to the manufacturer, each gauge has a theoretical resolution of 1μm.

In the current study, the standard pointed probes of the DVRTs were replaced with precision machined flat plate like heads to ensure orthogonal contact was achieved with each of the target spheres (Appendix C, section C.5).

### VIII.2.3 Coordinate transformation theory

Consider a Cartesian coordinate system fixed in space (x, y, z) and a rigid body moving in space with another Cartesian coordinate system fixed to that body (X, Y, Z). If in the initial reference position both the local (X, Y, Z) and global (x, y, z) systems' axes and directions are aligned, then the motion of the rigid body can be describe in terms of the relative motion between the fixed global coordinate system and the rigid body local coordinate system.

This relative motion can be described mathematically as:

$$\bar{r} = M \times \bar{r}_o + \bar{d} \tag{8.1}$$

where the new position ($\bar{r}$) of a point $\bar{r}_o$ in the rigid body after a displacement can be determined through a transformation using a matrix $M$ and a vector $\bar{d}$. For example, consider a positive rotation of a vector OP $(x_o, y_o, z_o)$ through an angle $\theta$ about a single coordinate axis (z) as shown in Figure 8.5.

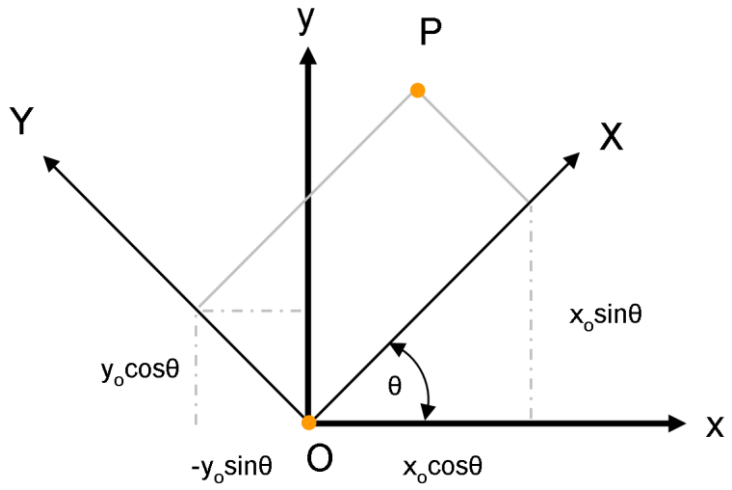


**Figure 8.5:** Rotation of the rigid body coordinate system (X, Y, Z) about the Z axis where z=Z through an angle of θ.

The position of this vector $(x_\theta, y_\theta, z_\theta)$ in the global coordinate system after rotation through an angle of $\theta$ can be determined as follows:

$$\begin{aligned} x_\theta &= x_o \cos\theta - y_o \sin\theta \\ y_\theta &= x_o \sin\theta + y_o \cos\theta \\ z_\theta &= z_o \end{aligned} \tag{8.2}$$

Rewriting equation 2 in matrix form to determine *M* we get:

$$\begin{Bmatrix} x_\theta \\ y_\theta \\ z_\theta \end{Bmatrix} = \begin{bmatrix} \cos\theta & -\sin\theta & 0 \\ \sin\theta & \cos\theta & 0 \\ 0 & 0 & 1 \end{bmatrix} \begin{Bmatrix} x_o \\ y_o \\ z_o \end{Bmatrix} \tag{8.3}$$

It must be noted that the coordinates of the vector in the rigid body coordinate system remain unchanged by the above transformation.

### VIII.2.3.1 Expanding to account for multiple rotations

If a rotation occurs about a fixed origin O, firstly about the z – axis ($\theta_z$), then about the y – axis ($\theta_y$) and lastly about the x – axis ($\theta_x$), then a point ($x_o, y_o, z_o$) will translate to a point ($x_\theta, y_\theta, z_\theta$) such that the rotation matrix is a composite of the three consecutive rotations applied to the rigid body coordinate system (Equation 8.4).

$$\begin{Bmatrix} x_\theta \\ y_\theta \\ z_\theta \end{Bmatrix} = \begin{bmatrix} \cos\theta_y \cos\theta_z & -\cos\theta_y \sin\theta_z & \sin\theta_y \\ \sin\theta_x \sin\theta_y \cos\theta_z + \cos\theta_x \sin\theta_z & -\sin\theta_x \sin\theta_y \sin\theta_z + \cos\theta_x \cos\theta_z & -\sin\theta_x \cos\theta_y \\ -\cos\theta_x \sin\theta_y \cos\theta_z + \sin\theta_x \sin\theta_z & \cos\theta_x \sin\theta_y \sin\theta_z + \sin\theta_x \cos\theta_z & \cos\theta_x \cos\theta_y \end{bmatrix} \begin{Bmatrix} x_o \\ y_o \\ z_o \end{Bmatrix} \tag{8.4}$$

Based on the assumption of "small" angles (Selvik 1989), the above matrix *M* can be simplified as follows:

$$\begin{Bmatrix} x_\theta \\ y_\theta \\ z_\theta \end{Bmatrix} = \begin{bmatrix} 1 & -\theta_z & \theta_y \\ \theta_z & 1 & -\theta_x \\ -\theta_y & \theta_x & 1 \end{bmatrix} \begin{Bmatrix} x_o \\ y_o \\ z_o \end{Bmatrix} \tag{8.5}$$

where for infinitesimally small angles $\sin\theta \approx \theta$, $\cos\theta \approx 1$ and the products of angles (i.e. $\sin\theta \times \sin\theta$) being approximately two orders of magnitude smaller, are disregarded.

It can also be shown through matrix multiplication that the simplified matrix *M* is commutative, and thus independent of the order in which the rotations take place.

If (*x, y, z*) is the change in position of a point, then Equation 8.5 becomes:

$$\begin{Bmatrix} x \\ y \\ z \end{Bmatrix} = \begin{bmatrix} 1 & -\theta_z & \theta_y \\ \theta_z & 1 & -\theta_x \\ -\theta_y & \theta_x & 1 \end{bmatrix} \begin{Bmatrix} x_o \\ y_o \\ z_o \end{Bmatrix} + \begin{Bmatrix} u \\ v \\ w \end{Bmatrix} - \begin{Bmatrix} x_o \\ y_o \\ z_o \end{Bmatrix} \tag{8.6}$$

where (*u, v, w*) is the displacement of the origin.

### VIII.2.3.2 Application of rigid body kinematics to DVRT rig

By treating the implant – target bracket assembly as the rigid body in space and the attachment site of the sensor housing to the bone as the fixed coordinate reference system, the principles of rigid body kinematics discussed previously can be applied to the DVRT test rig to allow the relative motion of the implant to the bone to be determined. In this study the origin of the rigid body coordinate system was defined as an imaginary point at the centre of the implant. This reference point was determined as the point at which a line drawn from the centre of sphere B crosses a line parallel to and offset 25mm from the centres of spheres C and A in the y

direction (Figure 8.6) at approximately the centre of the implant tool grooves (as seen in Figure 8.1).

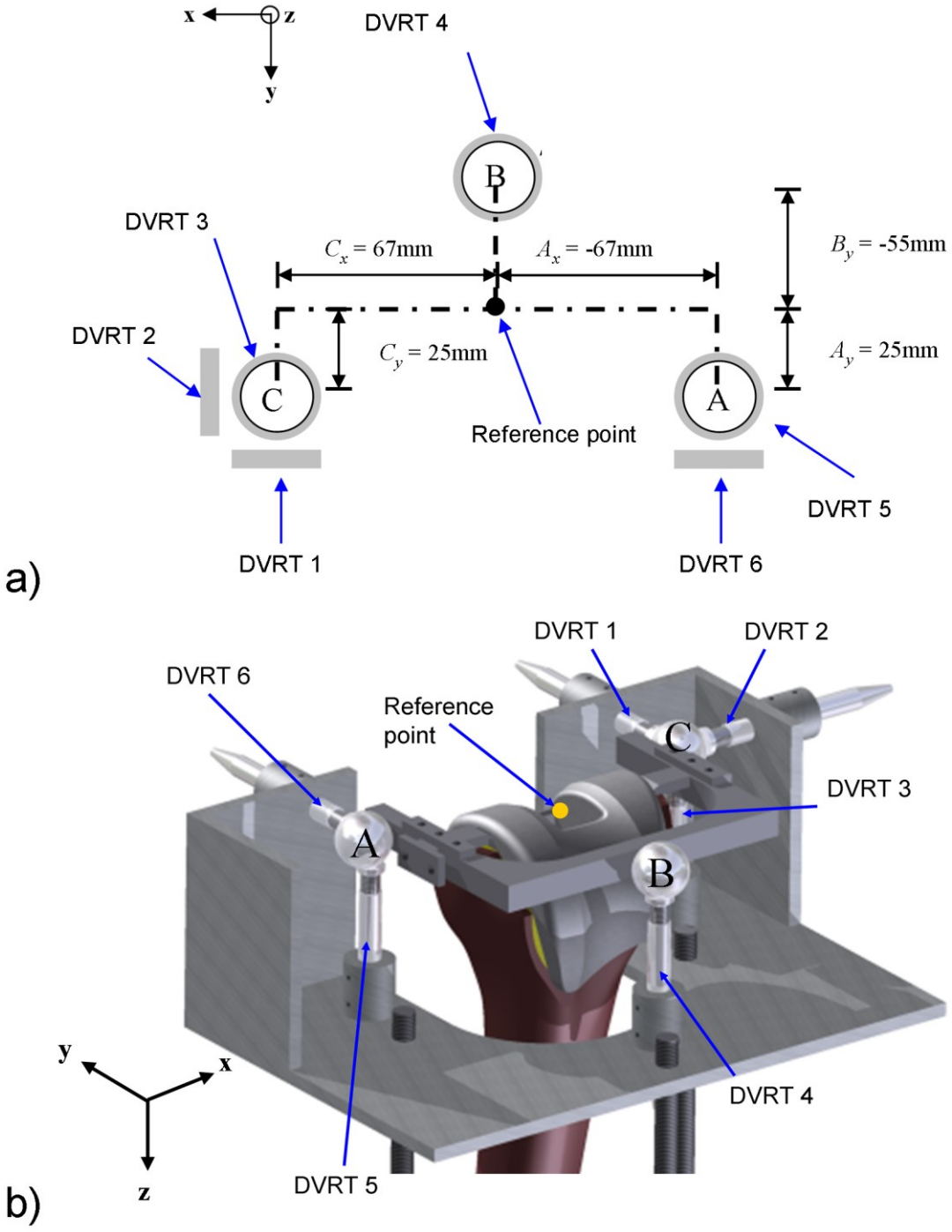


**Figure 8.6:** a) Schematic of sensor arrangement identifying the reference point used to determine relative motion of the implant and the relative offset in the x and y directions of the target spheres from this reference point and b) rendered CAD model showing the

arrangement of the sensors and the position of the reference point in 3D space.

A matrix representing the location of the centre of each of the target spheres relative to the rigid body origin was constructed, where ($A_x$, $A_y$, $0$) is the centre of sphere A, ($0$, $B_y$, $0$) is the centre of sphere B and ($C_x$, $C_y$, $0$) is the centre of sphere C. In matrix form this can be written as:

$$\begin{bmatrix} A_x & 0 & C_x \\ A_y & B_u & C_y \\ 0 & 0 & 0 \end{bmatrix} \tag{8.7}$$

Substituting Equation 8.7 into Equation 8.6 we get the following:

$$\begin{Bmatrix} U_a & U_b & U_c \\ V_a & V_b & V_c \\ W_a & W_b & W_c \end{Bmatrix} = \begin{bmatrix} 1 & -\theta_z & \theta_y \\ \theta_z & 1 & -\theta_x \\ -\theta_y & \theta_x & 1 \end{bmatrix} \begin{Bmatrix} A_x & 0 & C_x \\ A_y & B_y & C_y \\ 0 & 0 & 0 \end{Bmatrix} + \begin{Bmatrix} u & u & u \\ v & v & v \\ w & w & w \end{Bmatrix} - \begin{Bmatrix} A_x & 0 & C_x \\ A_y & B_y & C_y \\ 0 & 0 & 0 \end{Bmatrix} \tag{8.8}$$

The terms $A_x$, $A_y$, $B_y$, $C_x$, $C_y$ represent the distance each target sphere is offset from the reference point. The translations in the x, y and z directions, $u$, $v$ and $w$, and the rotations about the x, y, and z axes $\theta_x$, $\theta_y$, and $\theta_z$ are unknown. Rearranging the above equation and solving for these unknowns gives the relative motion of the implant to the bone as:

$$u = U_c + \left( \frac{V_a - V_c}{A_x - C_x} \right) C_y \tag{8.9}$$

$$v = V_c - \left( \frac{V_a - V_c}{A_x - C_x} \right) C_x \tag{8.10}$$

$$w = W_b - \left( \frac{C_x(W_b - W_a) + A_x(W_c - W_b)}{C_x(B_y - A_y) + A_x(C_y - B_y)} \right) B_y \tag{8.11}$$

$$\theta_x = \frac{C_x(W_b - W_a) + A_x(W_c - W_b)}{C_x(B_y - A_y) + A_x(C_y - B_y)} \tag{8.12}$$

$$\theta_y = \frac{w + \theta_x A_y - W_a}{A_x} \tag{8.13}$$

$$\theta_z = \frac{V_a - V_c}{A_x - C_x} \tag{8.14}$$

Referring to Figure 8.6a and Figure 8.6b it can be seen that $U_c$, $V_c$ and $W_c$ are the displacements measured by DVRT 2, DVRT 1 and DVRT 3 respectively; $V_a$ and $W_a$ are the displacements measured by DVRT 6 and DVRT 5 respectively; and $W_b$ is the displacement measured by DVRT 4.

### VIII.2.3.3 Calibration

To ensure the accuracy of experimental readings, prior to fitting of the sensor into the sensor housing each sensor was calibrated using the setup detailed in Figure 8.7a. During calibration trials, the polished head of a micrometer was brought into contact with the custom flat head of the DVRT sensor. Once contact was made, the voltage at zero displacement was recorded. The main barrel of the micrometer was then incremented by a set distance (1mm) and the corresponding value of voltage recorded. A number of such increments were carried out over the course of each trial and the results for three trials averaged. In this manner, calibration equations for each individual sensor could be determined relating change in voltage to change in displacement using a linear least squares fit. Figures 8.7b and 8.7c show an example of the voltage vs. time output from the sensors recorded during the trials and the corresponding calibration graph of voltage to displacement generated using this setup.

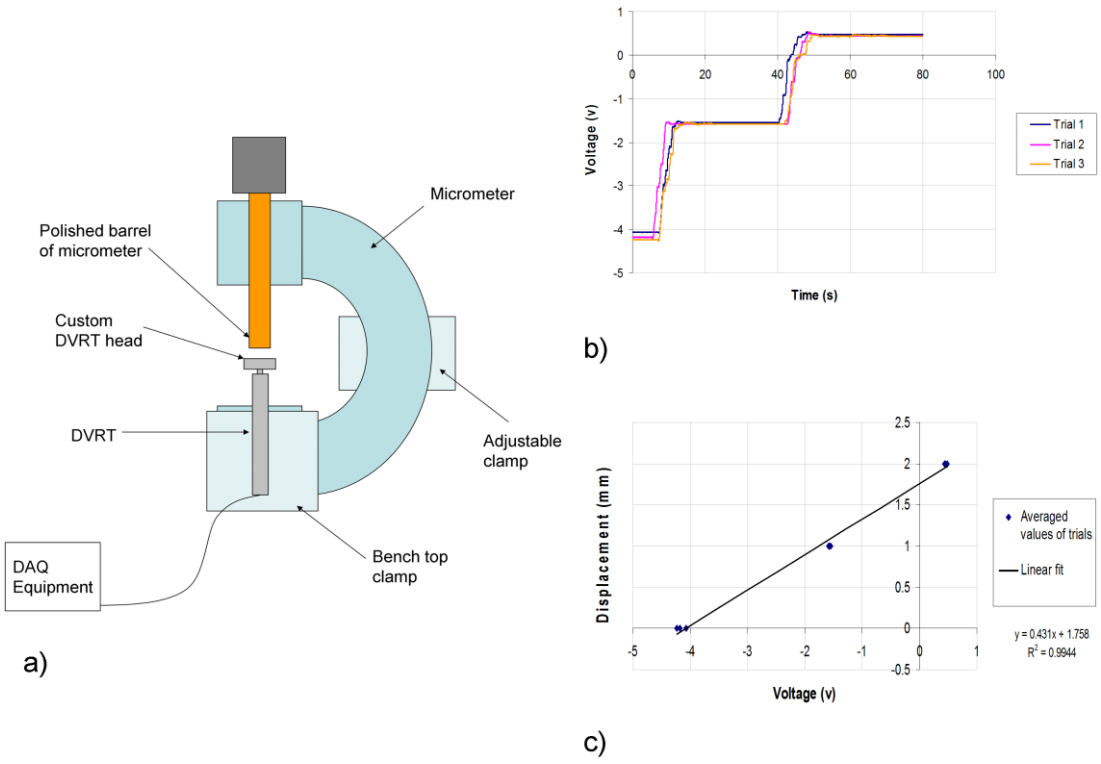


**Figure 8.7:** Schematic of a) sensor calibration rig, b) voltage output and c) example of corresponding calibration equation.

### VIII.2.4 Femoral test specimen

This study used fourth generation composite femurs (Sawbones, Pacific Research Laboratories, Vashon, WA, USA). This human bone analogue consists of a rigid polyurethane foam core surrounded by a pressure injected mixture of short glass fibres and epoxy resin, where the glass fibre/epoxy resin and rigid polyurethane foam represent the cortical and cancellous bone structure respectively, as shown in Figure 8.8.

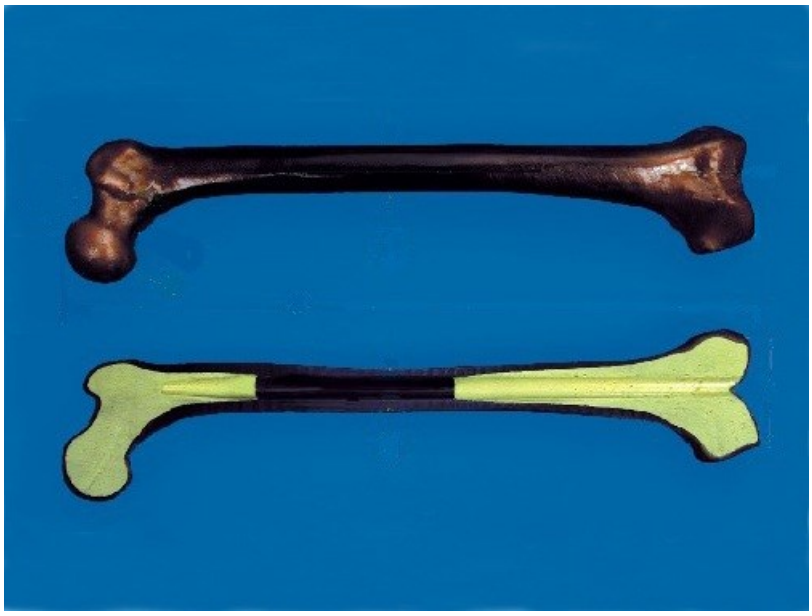

**Figure 8.8:** Image showing external (top) and internal (bottom) cortical and cancellous bone regions of the fourth generation composite femur, image adapted from (http://www.sawbones.com/-products/product.aspx?1937), retrieved 02/12/2008.

These composite femurs have been widely used to assess stability of stemmed femoral components used in total hip arthroplasty (Cristofolini et al. 2003, Britton and Prendergast 2005, Cristofolini et al. 2007). A number of studies have shown the composite femur to be a suitable substitute that replicates the strength and material properties of bone adequately while permitting higher levels of repeatability than their biological equivalent for smaller sample sizes due to the standardised nature of their geometry (Cristofolini et al. 1996).

### VIII.2.5 Implant variations investigated

Three different femoral components were investigated in this study: a posterior stabilising (PS), a total stabilising (TS) implant with short stem (12x50mm) and a TS implant with long offset stem (19x150mm stem with 4mm lateral offset), all from the Stryker (UK) Triathlon series (Figure 8.9). Due to the design of the implant system used in this study and geometry of the composite bone a 4mm lateral offset was necessary to allow the long stemmed implant to be implanted into the femoral canal, as is often the case clinically (Fehring 2005, Brilhault and Ries 2012). This implant line ranges in sizes from 1-8 based on anthropometric studies (Hitt et al. 2003) to provide a best possible fit for the patient. Size 5 implants were selected for use in this study based on AP and ML measurements of the test specimen.

### VIII.2.6 Femoral preparation protocols

Tests were divided into two main groups as listed in Table 8.1. The first group consisted of all components implanted into the femur without cement. In the second group PS implants were cemented at the metaphysis, TS short stemmed implants were cemented both distally and up past the stem to the cement restrictor (Hardinge, DePuy, UK) and Long stemmed TS implants employed a "hybrid" cementing technique, with cement on the metaphysis only. Figure 8.10 presents a schematic diagram of the three cementing techniques employed. The cement used in all cemented tests was polymerised methyl methacrylate (PMMA) commercially available as surgical Simplex-P (Stryker, UK). To ensure consistency of fixation, a protocol for the mixing and cement application to the test specimens was developed. The cement was mixed in a standardised manner using a Mixevac (Stryker, UK) in a constant temperature fume-cupboard. A timer was used to ensure cementing and component impaction was performed with the cement at the same viscosity for all samples. Impaction was carried out using a femoral impactor and mallet (Stryker, UK); cemented specimens were then left for a set period of time to cure before testing. To minimise potential errors introduced by variation in surgical cuts and for consistency, all femoral component implantation and cementing was carried out by a

qualified and experienced orthopaedic surgeon in accordance with each implant's surgical protocol using the appropriate cutting guides and instrumentation (Triathlon TS, System 5, Stryker, UK). An overview of the main step in the femoral implantation protocol can be seen in Figure 8.11 and an example of the cementing procedure in Figure 8.12. A more detailed step by step approach for both the femoral and cementing protocol is included in Appendix C.4.

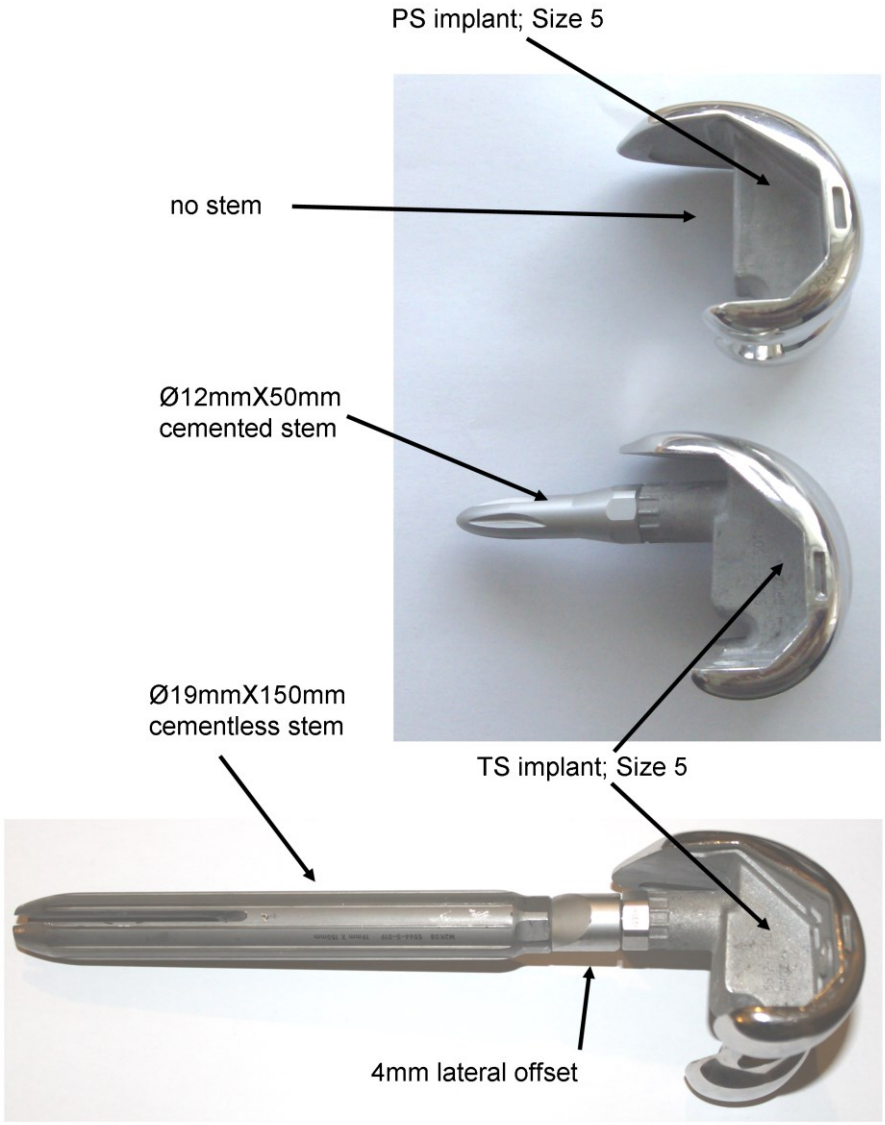


**Figure 8.9:** Implants investigated; A PS implant (top), a TS implant with short stem (middle) and a TS implant with long offset stem (bottom).

**Table 8.1:** Outline of experimental test groups.

| | Group 1 | Group 2 |
|---|---|---|
| PS implant | Uncemented | Cemented |
| TS implant short stem | Uncemented | Cemented (pressurised) |
| TS implant long offset stem | Uncemented | Hybrid cemented (implant cemented distally, stem remains uncemented) |

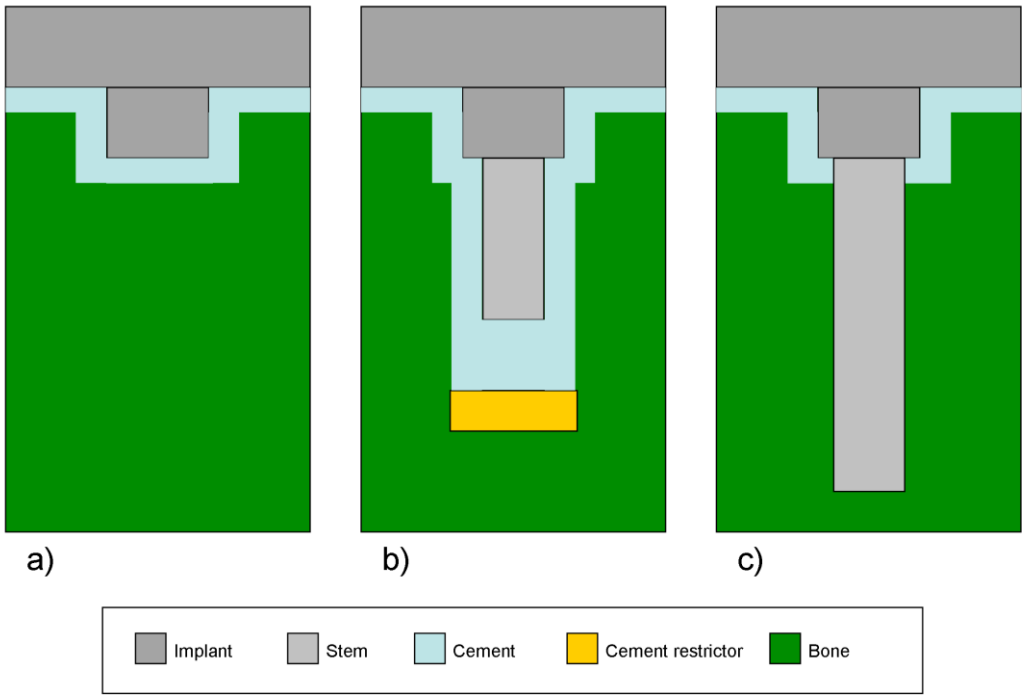


**Figure 8.10:** Frontal plan schematic of cementing protocol applied to the composite femurs; a) Metaphyseal cementing, b) full cementing of the implant and stem at the metaphysis and proximally past the stem to the cement restrictor and c) "hybrid" cementing, where the metaphysic only is cemented and the stem remains uncemented.

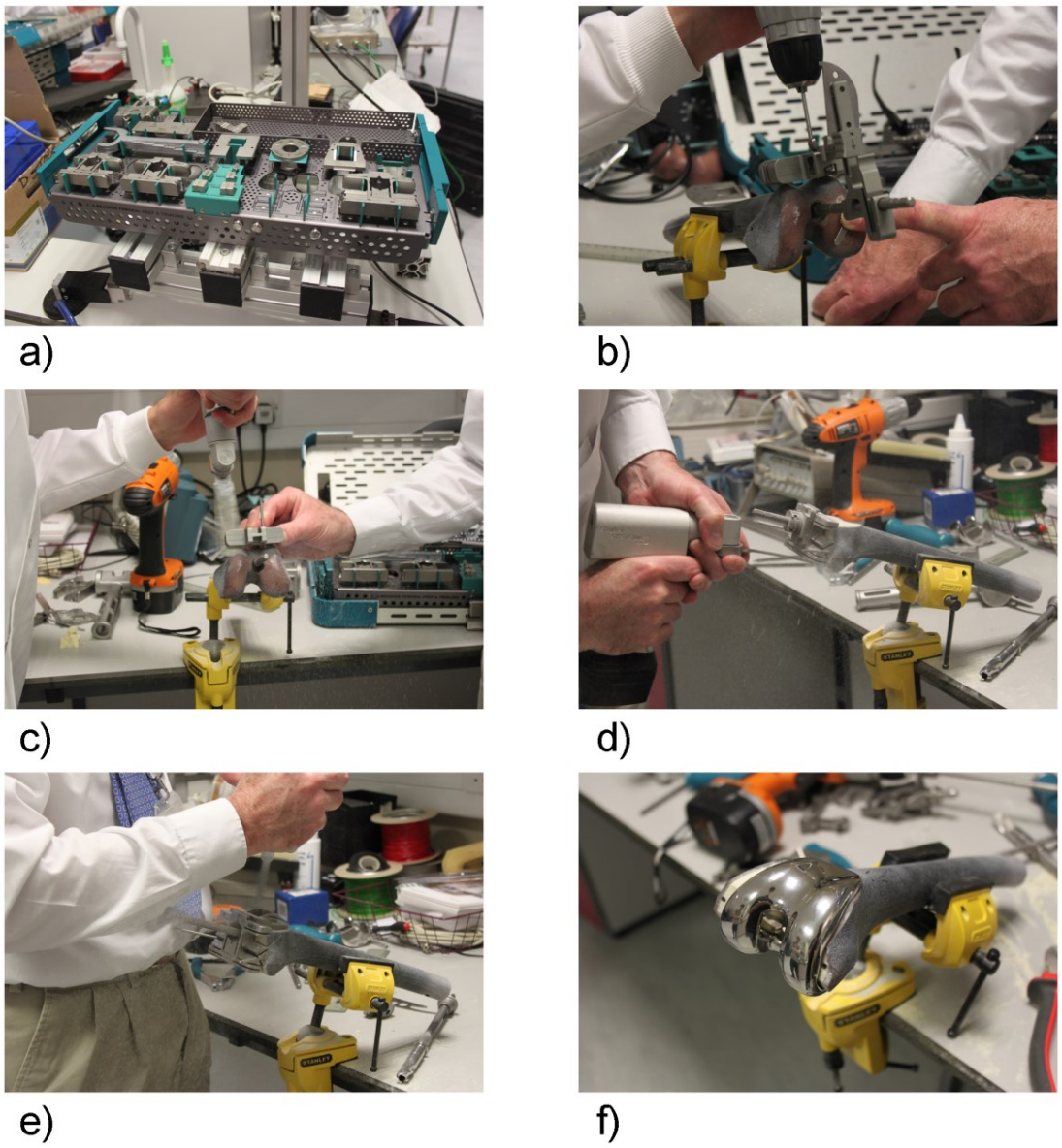


**Figure 8.11:** Images highlighting some of the tools used and key steps in the implantation protocol. a) shows an instrument tray with cutting blocks, b) attachment of alignment guide, c) use of alignment guide to perform distal cuts with sagittal saw, d) anterior, posterior and chamfer cuts carried out using cutting block, e) femoral box cut using smaller saw blade and box cut guide and f) finished implanted femoral component. Instrument kit (triathlon series implant line, Stryker, UK) and sagittal saw (System 5, Stryker, UK).

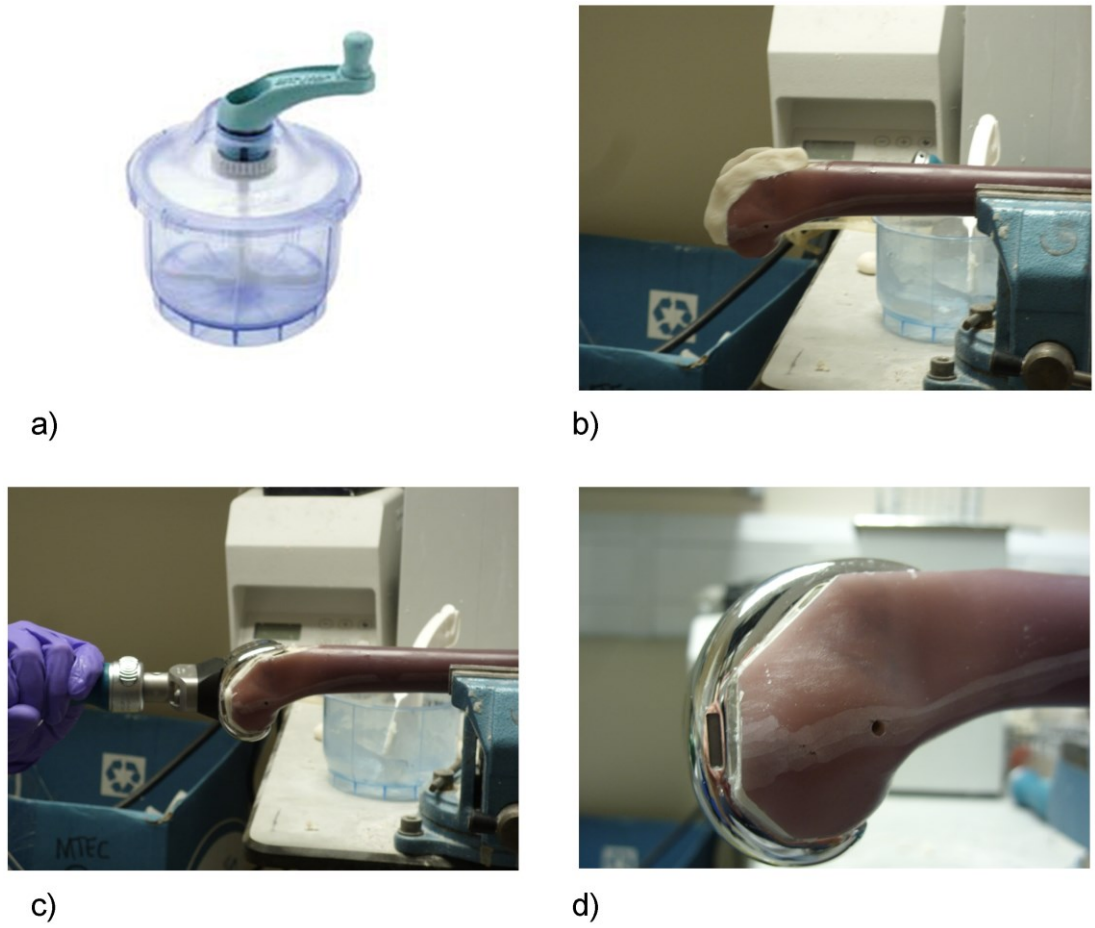


**Figure 8.12:** a) shows the Mixevac (Stryker, UK) apparatus used to mix the cement, b) shows the cement applied to the anterior and distal portions of the distal femur, c) shows the femoral component being impacted onto the femur using a mallet and impactor (Stryker, UK) and d) shows the final cemented component with visible cement mantle.

### VIII.2.7 Experimental setup

A custom bone holder was developed in house, which allowed the test specimen to be translated in the medial/lateral and anteroposterior directions to ensure correct alignment with the loading axis of the test machine. The bone holder permitted variation in orientation of the bone in the sagittal plane from 0° to 90° flexion relative to the machine loading axis (Figure 8.13). The bone was secured in the holder during testing by means of a 10mm diameter bolt, and further fixation was achieved through the use of three pointed adjustable screws spaced at regular intervals around the circumference of the holder cylinder at a location 50mm above

the bolt hole. This method served to secure the bone in all rotations and translations, while also allowing a relatively short turnaround time between test specimens in comparison to studies where the bone is potted using cement or other substances which require time to set.

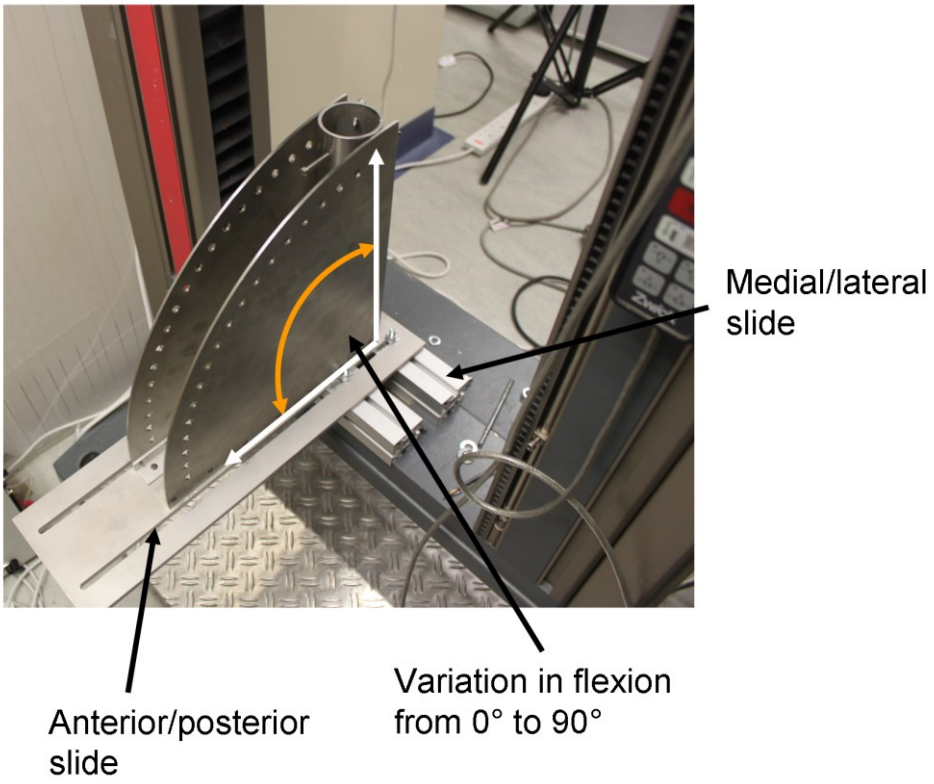


**Figure 8.13:** Test specimen holder used to permit variation in flexion angle from 0° to 90°.

### VIII.2.8 Loading protocol

Once fixed at the desired angle using the bone holder, a cyclical compressive load was applied through a matching tibial component (Figure 8.14) using a Zwick/Roell testing machine and companion software package TestXpert 9.01 (Zwick, Ulm, Germany). To ensure correct alignment and contact was achieved between the femoral component and tibial bearing surface for the three flexion angles investigated, a method of fine adjustment was incorporated into the design of the

attachment for the Zwick/Roell machine which allowed the angle of the tibial bearing surface to be modified slightly.

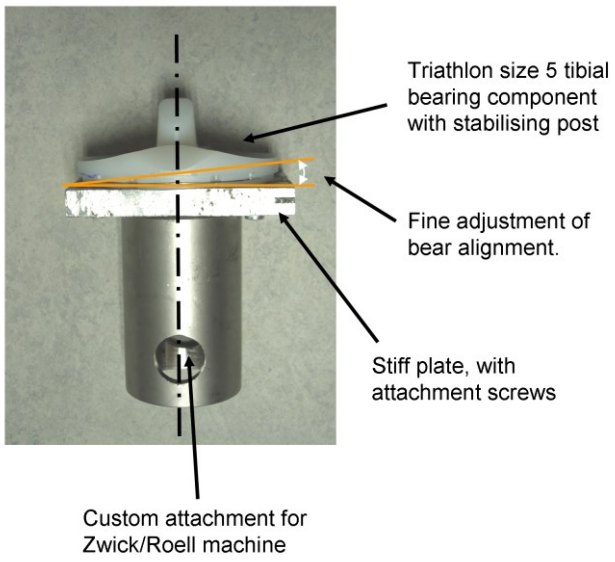


**Figure 8.14:** Tibial component with custom attachment for fitting to Zwick/Roell testing machine.

Loading was based on three peaks 728.5N, 1186N and 1643N (Figure 8.15) corresponding to 0°, 10° and 20° flexion during the stance phase of gait from a normal walking cycle (Bergmann 2008) for an assumed body weight of 775N. During the test the load was applied at a constant rate of 42N/s up to the maximum indicated for each step, the maximum load was applied for 10 seconds after which it was reduced back to a reference load of 20N (to maintain contact) for a further 10 seconds. Each test consisted of 40 cycles at each of the three flexion angles investigated. Previous studies have shown that a stabilised value of relative motions of uncemented implants can be determined within relatively few cycles of load application (Schneider et al. 1989).

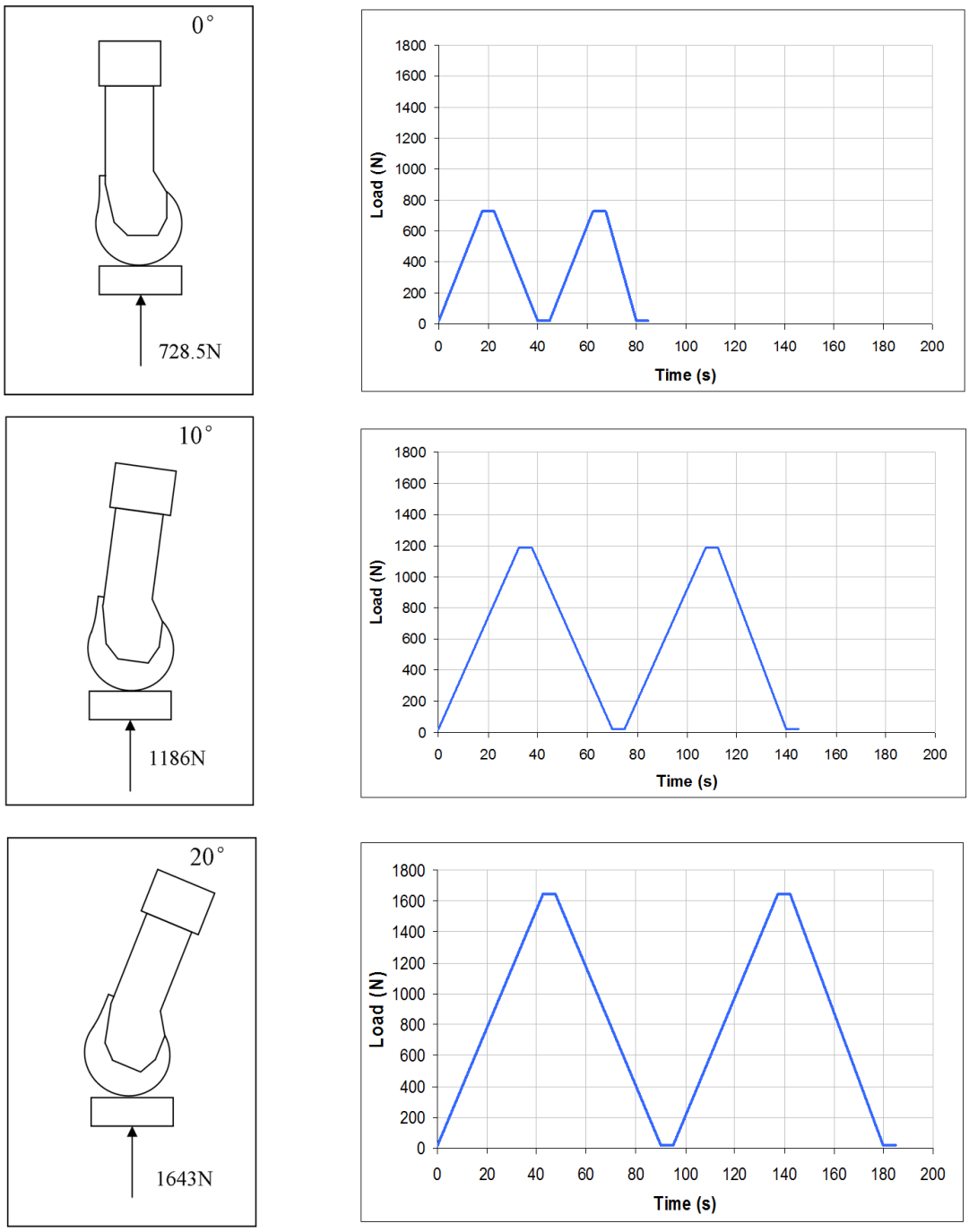


**Figure 8.15:** The left column shows schematic drawings of the loading setup for each of the three flexion angles investigated and highlights the maximum load applied. The right column represents the characteristic loading profile for two of the 40 cycles (for clarity) conducted at each flexion angle.

## VIII.3 Results

The following subsections detail the *in vitro* data acquisition protocol and the findings of preliminary tests, as well as, the final results obtained.

### VIII.3.1 Data acquisition and micromotion evaluation

Data acquisition was carried out using a National Instruments DAQpad-6070E (National Instruments, Austin, TX) and virtual instrumentation software LabVIEW™ 7.0 (National Instruments, Austin, TX). Custom programs were developed by the author in LabVIEW™ to log the data from each DVRT sensor during testing, convert it from voltage to displacement, filter the signal to reduce noise, and finally extract the amplitude of each sensors displacement curve over the entire 40 cycles of load application. To ensure all relative motions were captured during each test the signal was logged at a rate of 10 samples per second. Prior to each test the connections between equipment and computer were inspected, the DVRT sensors were then switched on and allowed to "warm up" for 15mins (as recommended by the manufacturer) to ensure that a constant voltage was achieved in each sensor before testing began.

A flowchart outlining the DAQ protocol and results processing is presented in Figure 8.16, further details on the processes involved and the custom programs employed can be found in Appendix C.

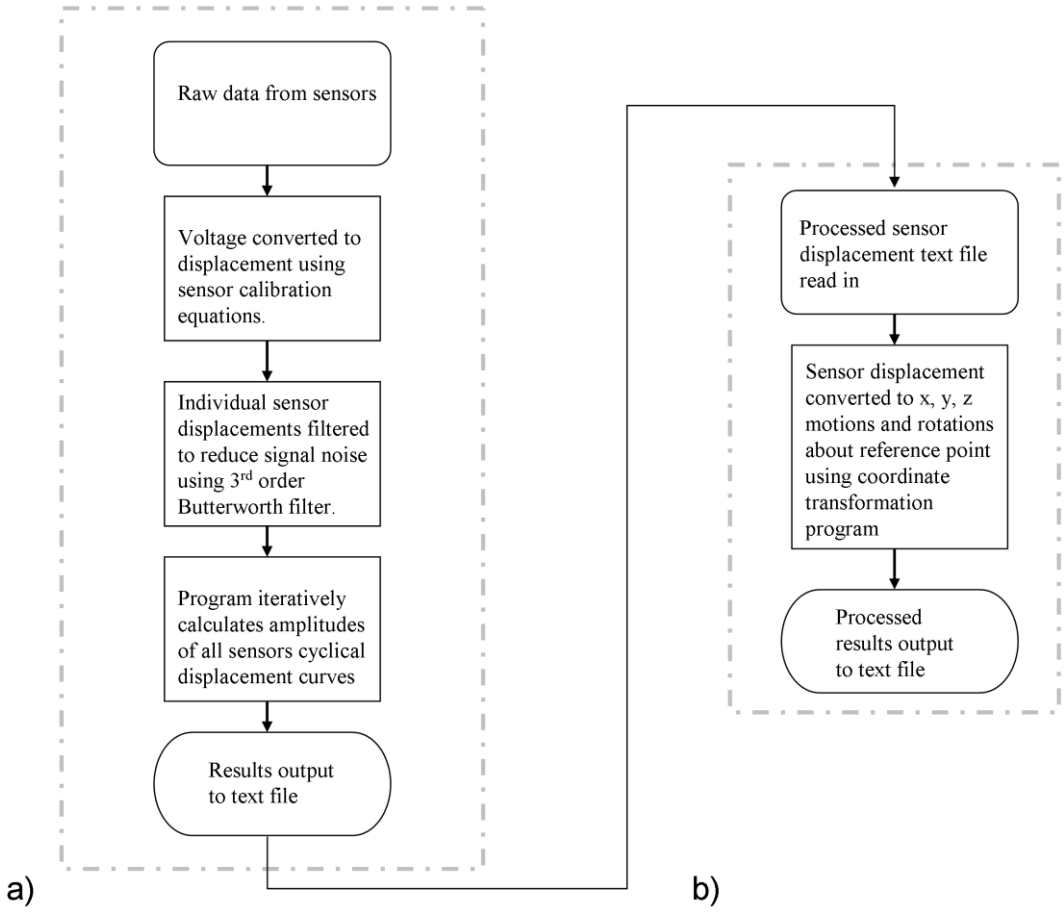


**Figure 8.16:** Summary of a) data acquisition process and b) results post processing using coordinate transformation theory. Both aspects of the above workflow were carried out in *LabVIEW*™ 7.0, using custom code developed by the author.

Referring to Figure 8.16a, the first stage involved in the DAQ process was to read in the values obtained for change in voltage during testing for each sensor. These individual sensor signals were then converted from voltage to microns using each DVRT sensors' custom calibration curve (Appendix C.1) and filtered using a 3$^{rd}$ order Butterworth filter (low pass) with a cut off frequency of 0.4 Hz to reduce noise. The resulting displacement curve obtained for each sensor varied over time corresponding to the loading and unloading of the femoral component. An iterative program was then implemented to determine the amplitude of each sensors displacement curve at one cycle intervals over the 40 cycles. The amplitude of these curves being the value of inducible displacement at the sensor. A brief graphical

representation of these steps for a single DVRT sensor is given in Figure 8.17. A more detailed explanation of the process involved can be found in Appendix C.2,

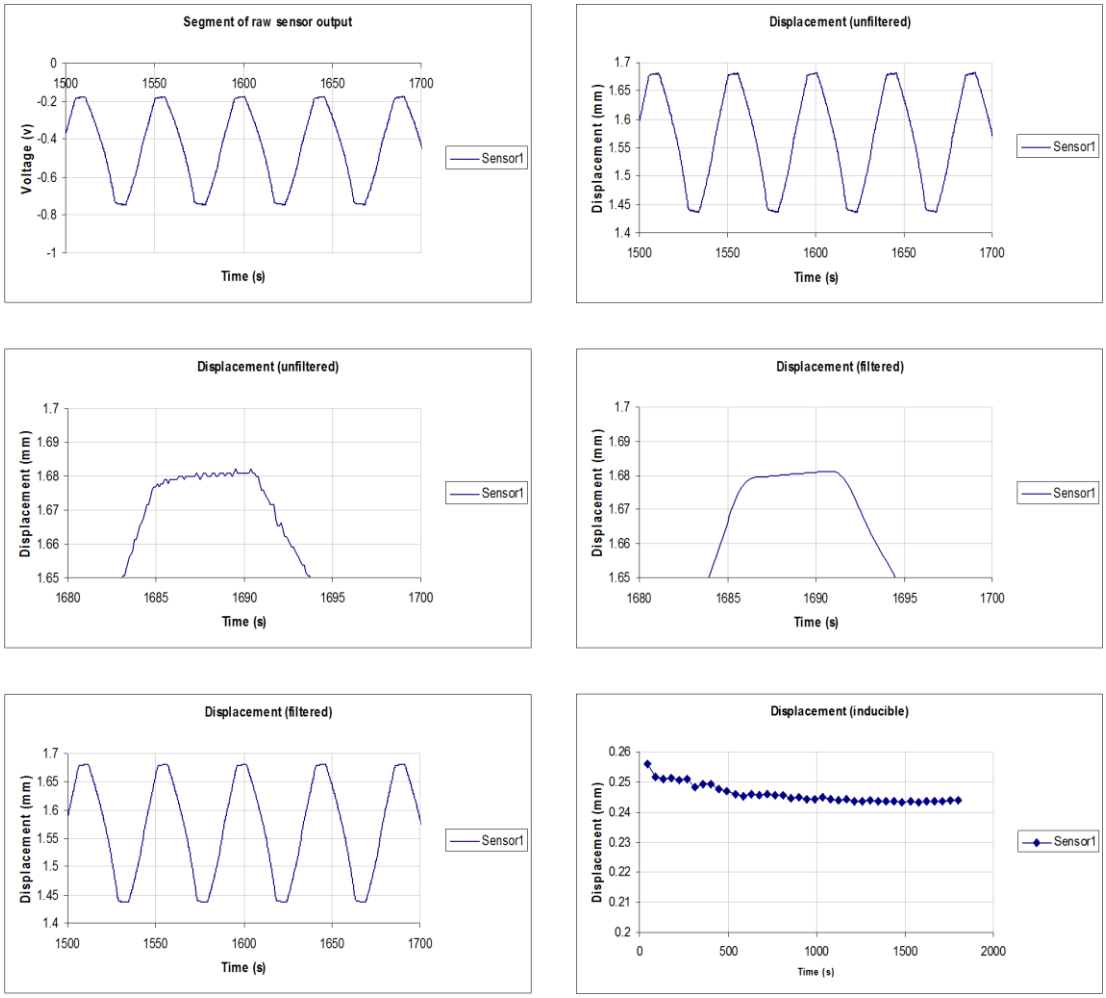


**Figure 8.17:** Example of data processing protocol applied in all tests. Raw input from sensor showing change in voltage due to loading (top left), voltage converted to displacement using each individual sensors calibration equations (top right), close up of displacement curve before and after data is filtered using a 3rd order Butterworth filter (middle left and middle right), the resulting filtered sensor displacement curve is then given (bottom left), and finally a graph of the inducible displacements for sensor 1 created by determining the amplitude of the displacement curve at one cycle intervals (bottom right).

Once inducible displacements for each sensor were obtained, the motion of the implant relative to the bone in all six degrees of freedom could then be evaluated following the procedure outlined in Figure 8.16b. To streamline the process of carrying out calculations on multiple trials across multiple datasets this process was also implemented using a semi-automated custom code and graphical user interface (GUI) developed by the author in LabVIEW™, as detailed in Appendix C.2. To summarise, this final program took sensor displacements as an input and performed the necessary coordinate transformations using the previously derived equations (Equations 8.9 to 8.14) and output the ($u$, $v$, $w$) translational and ($\theta_x$, $\theta_y$, $\theta_z$) rotational motions for the implant reference point relative to the point of fixation on the bone (Figure 8.6).

### VIII.3.2 Preliminary results

Referring to Figure 8.18, all results are reported in terms of $u$, $v$, $w$ and $\theta_x$, $\theta_y$, $\theta_z$ corresponding to the calculated relative motions and rotations using Equations 8.9 to 8.14 along the x, y and z global axes.

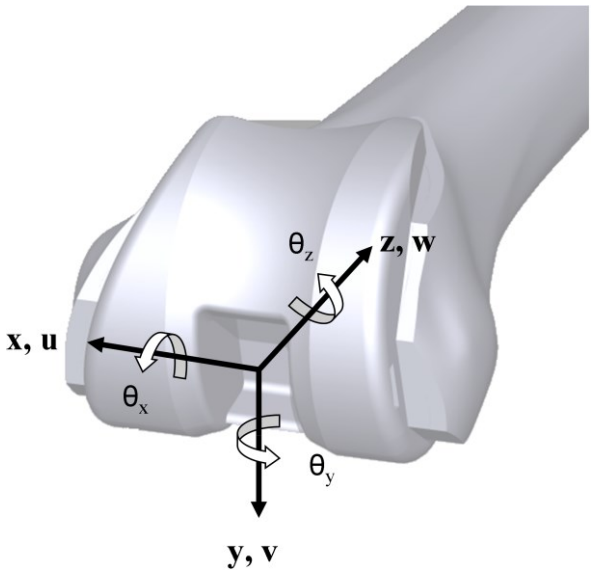


**Figure 8.18:** Illustration of coordinate system used to describe motions and rotations relative to the implant reference point.

A series of trials were conducted with the prototype rig for both uncemented and cemented conditions for each of the three implants investigated, an example of the average results of a set of uncemented trials using the prototype micromotion rig is presented in Figure 8.19.

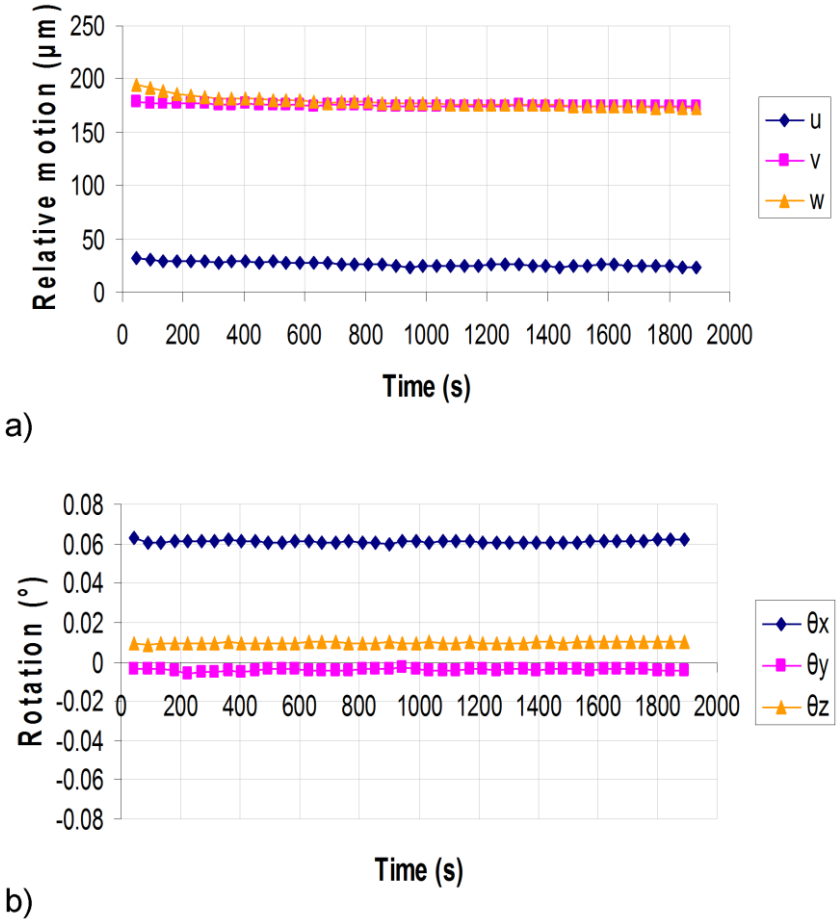


**Figure 8.19:** Sample results from prototype test rig showing a) translational and b) rotational relative motions averaged over three trials for an uncemented PS implanted femur at 0° flexion.

It can be seen from Figure 8.19a that as expected the largest relative motions occur in the z-direction, i.e. direction of applied load, additionally motion in the anteroposterior direction is found to be quite high in this particular set of trails. Observed rotations are seen to be smallest about the anteroposterior axis, followed by the long axis of the femur (Figure 8.19b). On examining the overall magnitude of translational relative motions for all implants (Figure 8.20) it can be seen that the

addition of a stem served to reduce the level of relative motion. Similarly once cemented the level of motion observed was found to reduce relative to the same implant under uncemented conditions. While initially the observed individual implant trends seemed reasonable, on comparison of the multiple implant types and fixation methods, it became apparent that other factors must be influencing the reported values of motion. Referring to Figure 8.20, it is clear that the overall levels of motion observed are quite high and that there is very little difference between cemented and uncemented fixation in the same implant. It can also be seen that the PS cemented implant case appears to be subject to larger relative motions than a fully uncemented TS implant with short stem. While it can be seen that the magnitude of these inducible displacements were within the range previously reported by several RSA studies (Ryd 1986, Broström et al. 1989, Ryd 1992, Nilsson et al. 1995, Ryd et al. 1995) for inducible displacement of knee prosthesis (200µm – 1000µm), it must be noted, however, that these values far exceeded those predicted by previous *in vitro* studies (Wackerhagen et al. 1992, Moran 2005, Cristofolini et al. 2008, Cristofolini et al. 2009).

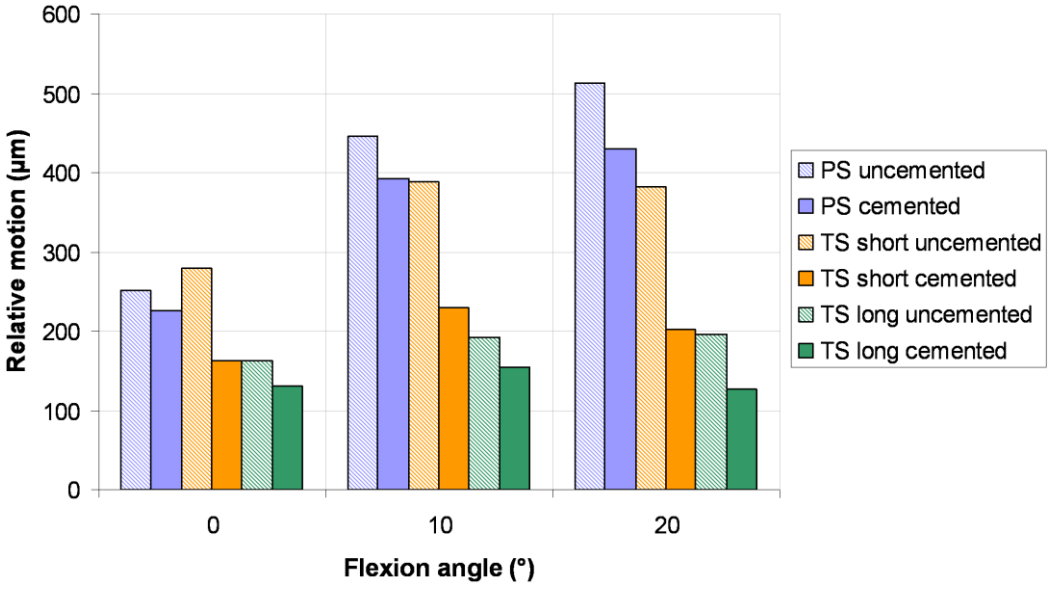


**Figure 8.20:** Sample results from prototype test rig showing overall magnitude of relative motion for cemented and uncemented tests.

After a thorough investigation of the sensors and test setup, it was concluded that the distance between point of fixation on the femur and the target spheres attached to the implant was too great (originally 120mm), thus causing the system to register a combination of motion and deformation (due to bending) as relative motion of the implant (i.e. the large motion observed in the anteroposterior direction in Figure 8.19). Initial attempts to minimise this distance through modification of the rig failed to dramatically improve the result and thus required a complete redesign of the main rig structures to overcome the issue of combined motion and deformation.

### VIII.3.3 Test rig redesign

As stated above, the key focus of the redesign phase was to minimise the distance between the attachment to the femur and the distal surface to prevent large deformations as a result of bending from obscuring the difference between the implants tested. Another factor considered during this phase was the overall weight of the prototype test rig (2.01 kg). The combined weight of both the sensor housing and femoral clamping device made the original rig quite heavy and cumbersome to position accurately despite efforts in the design phase to minimise weight through appropriate material selection (aluminium). The new test rig design was simplified greatly to allow for rapid manufacture and to promote ease of setup between test specimens. The distance between attachment site and the distal surface was reduced to a fraction of the original distance in the new design (35mm). This second prototype consisted of two main structures as shown in Figure 8.21; the sensor housing and the target bracket. The target bracket remained unchanged from the original design and fixed to the implant through the use of two adjustable wedges. The sensor housing, however, was changed significantly to reduce the effects of combined motion/deformation evident in the results from the first rig prototype. In this setup the sensor housing was designed to attach to the bone directly (eliminating the need for the femoral clamp and adjustable coupling bolts) through the use of 3 adjustable screws in the following arrangement; one into the medial epicondyle, one into the lateral epicondyle and one into the posterior distal femoral surface proximal

to the femoral box cut. Each DVRT was attached to the new sensor housing in a similar manner to the first rig prototype: Again DVRT 3, 4 and 5 were positioned to record displacement in the distal/proximal (z) direction; DVRT 1 and 6 in the anteroposterior (y) direction; and DVRT 2 in the medial/lateral (x) direction. It can be seen from Figure 8.22, that the new rig design is significantly smaller than the first rig prototype, the overall weight of the new test rig measured 0.377 kg representing a reduction in mass of approximately 81%. This lightweight design coupled with a significantly decreased distance between the femoral clamping device and the distal surface was desirable for reducing the likelihood of the weight of the test apparatus causing excessive bending of the femur.

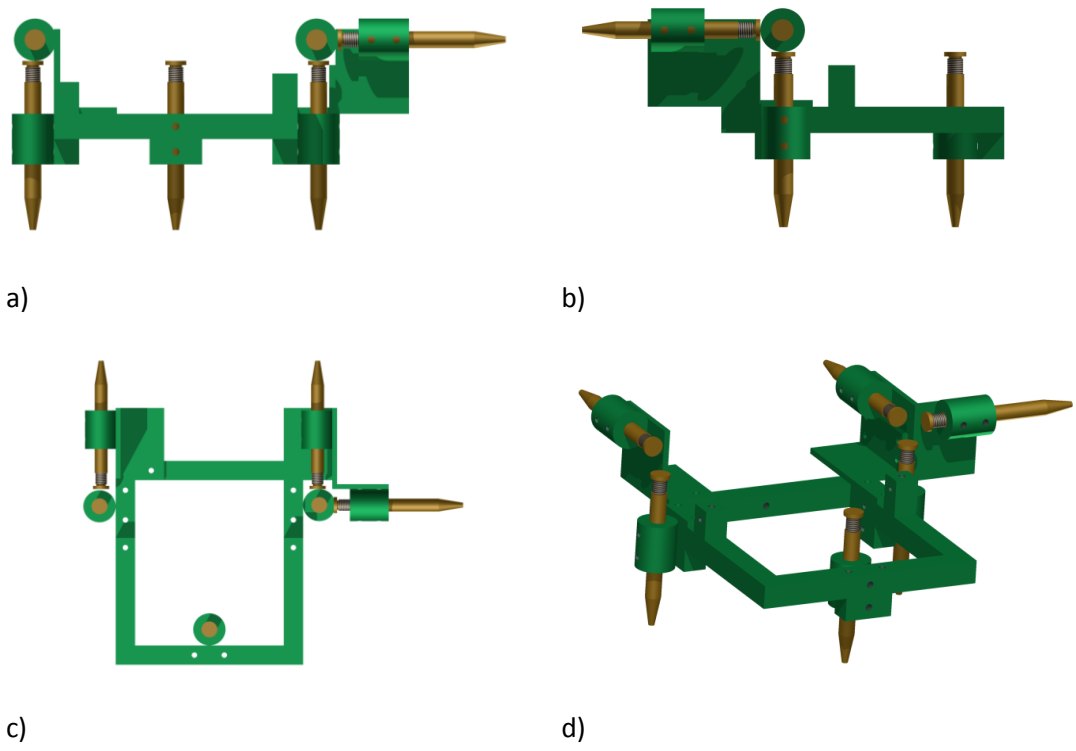


**Figure 8.21:** CAD models of new test rig design shown from a) frontal elevation, b) end elevation, c) plan views and d) isometric view of sensor housing.

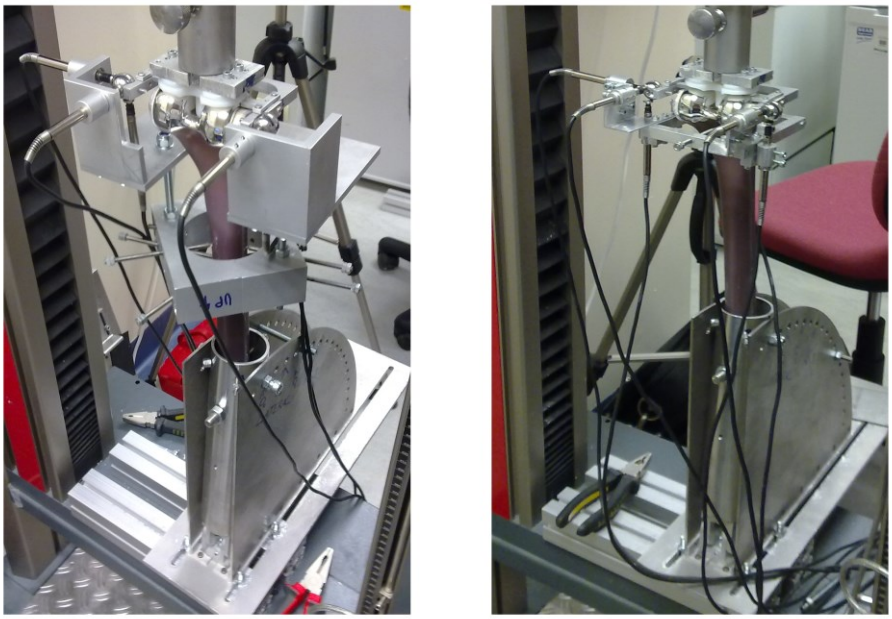

a) b)

**Figure 8.22:** Comparison of a) original rig prototype and b) new rig prototype.

### VIII.3.4 Results using redesigned rig

The previously outlined tests (Table 8.1) were then repeated using the new test rig. Figure 8.23a and 8.23b highlights the arrangement of the DVRT sensors in the new test rig sensor housing. The schematic presented in Figure 8.6 to identify the reference point remains valid as the target bracket and arrangement of sensors was unchanged from the original prototype rig design.

The average values of translational and rotational relative motion were calculated across all trials conducted with the new test rig and are presented in Figures 8.24-8.26. These figures show that all translational relative motions generally increase with flexion angle. The largest relative motions were found to occur in the z direction (distal/proximal) for all implant types. For all three flexion angles tested the component of loading in the z direction was the largest. It can be seen that the addition of a short stem (Figure 8.25a) for both cemented and uncemented cases leads to a reduction in translational relative motions in comparison to PS implants

with no stem (Figure 8.24a). The TS implant with long stem (Figure 8.26a) shows significantly reduced relative motions in comparison to the other two implants. The translational relative motions reduce with cementing as expected in almost all cases.

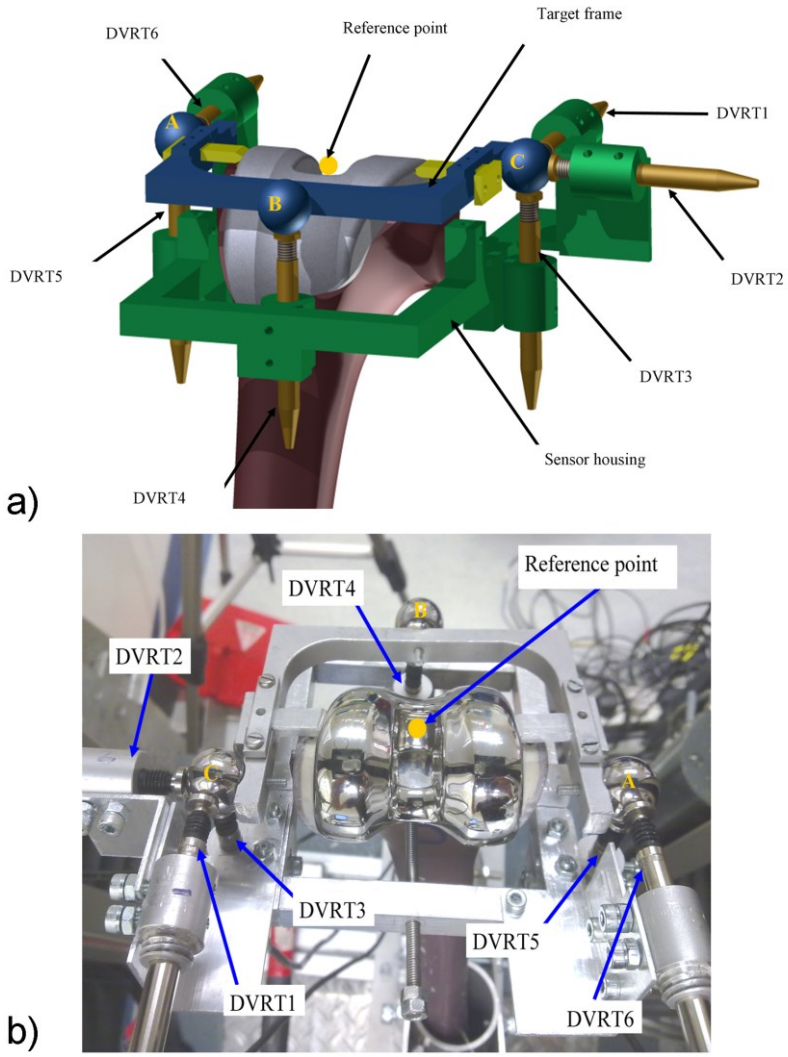


**Figure 8.23:** a) Rendered view and b) photo of new test rig assembly with reference point and all relevant components highlighted.

The trends with respect to relative rotations are considerably more complex (Figure 8.24b-8.26b). The largest relative rotations are found to occur with the uncemented PS implant. For long stem cases the relative rotations can be seen to be extremely

small in comparison to the other two implants. Cementing in general was found to reduce relative rotations. The component of relative rotations found to be the smallest in general was rotation in the transverse plane ($\theta_z$). Numerical values for mean translational and rotational relative motions along with standard deviations (SD) can be found in Appendix C (Table C.1 and C.2). Additional graphs showing both translational and rotational relative motions over the course of the 40 cycles are also included in Appendix C (Figures C.6 – C.11).

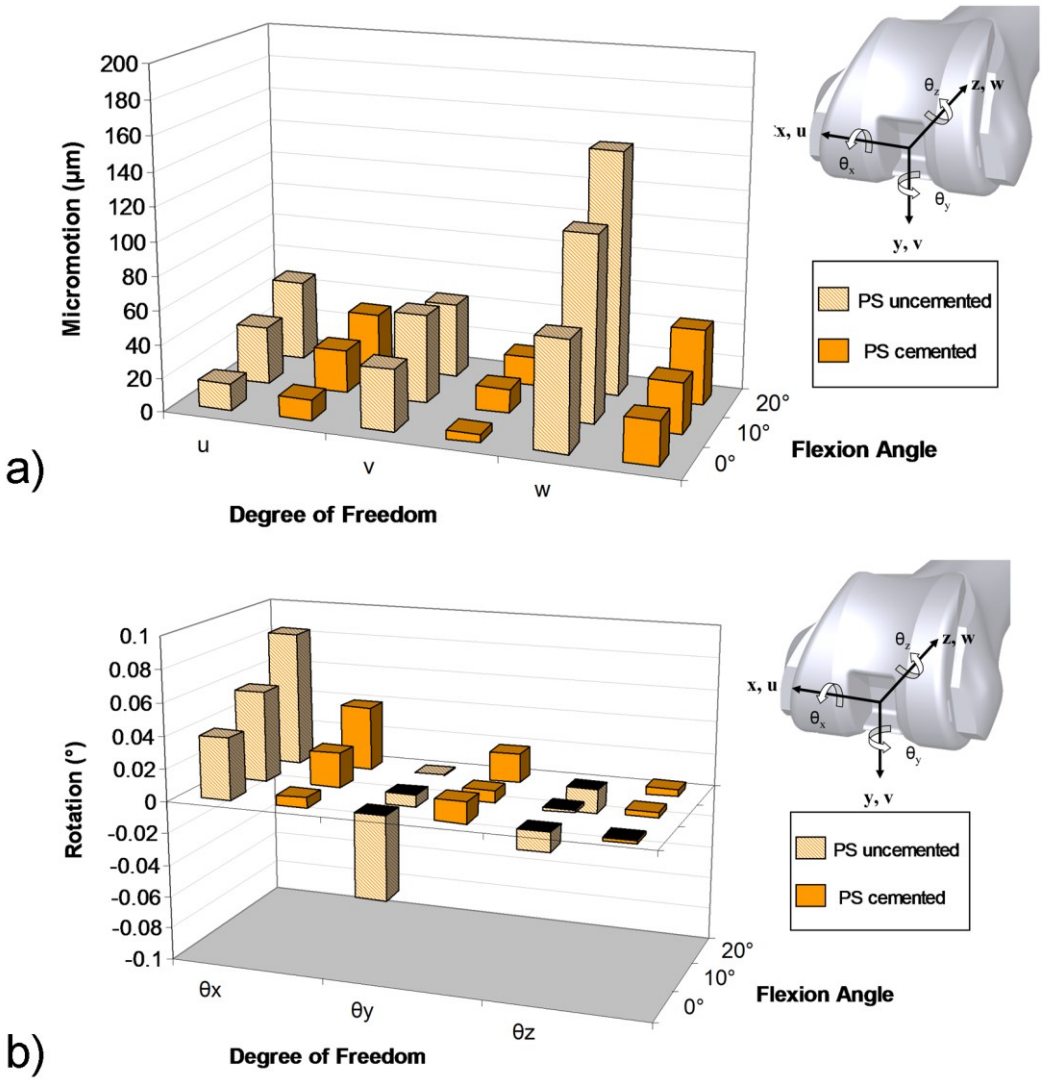


**Figure 8.24:** Comparison of a) translational and b) rotational relative motions for a PS implanted femur for both cemented and uncemented cases.

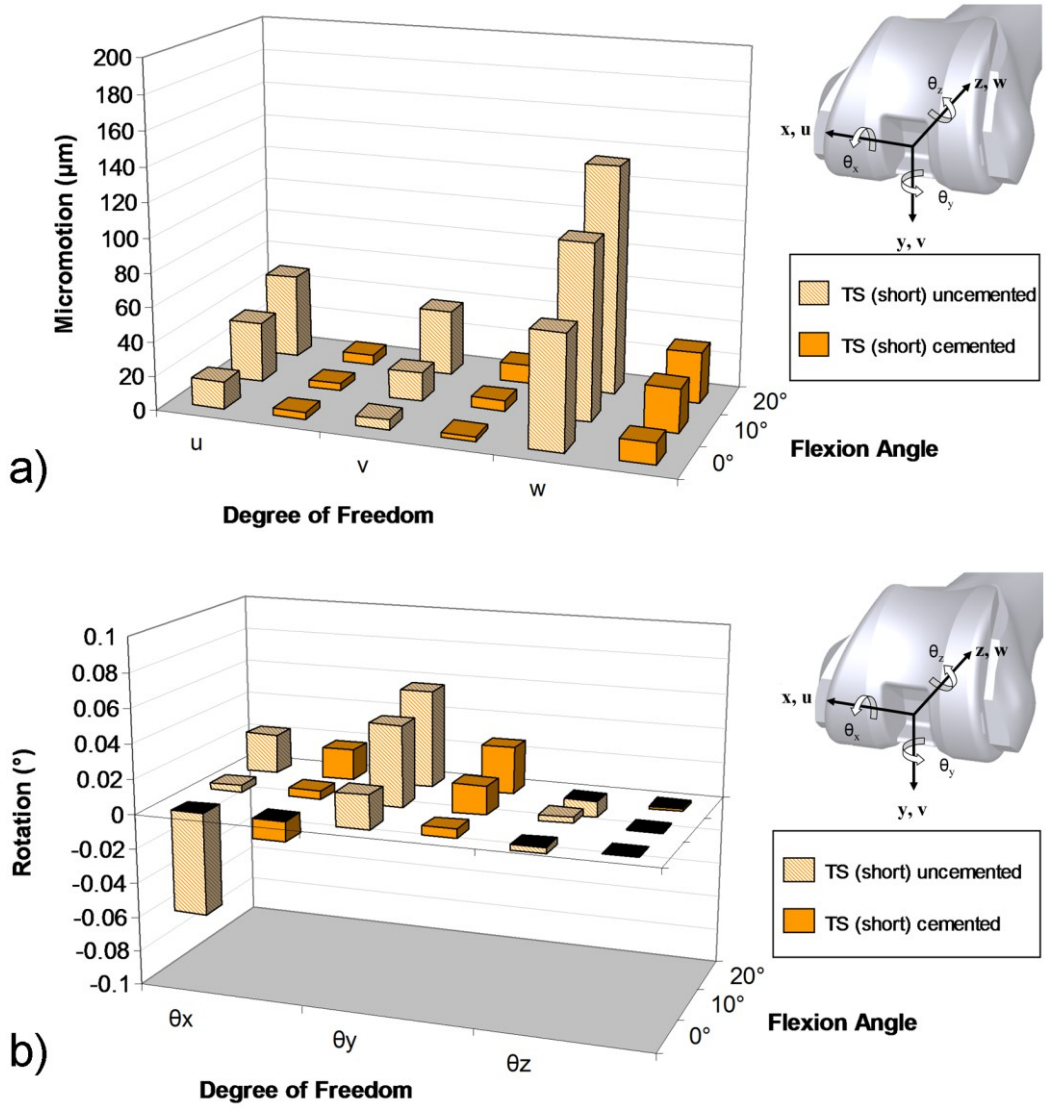


**Figure 8.25:** Comparison of a) translational and b) rotational relative motions for a TS implanted femur with short stem for both cemented and uncemented cases.

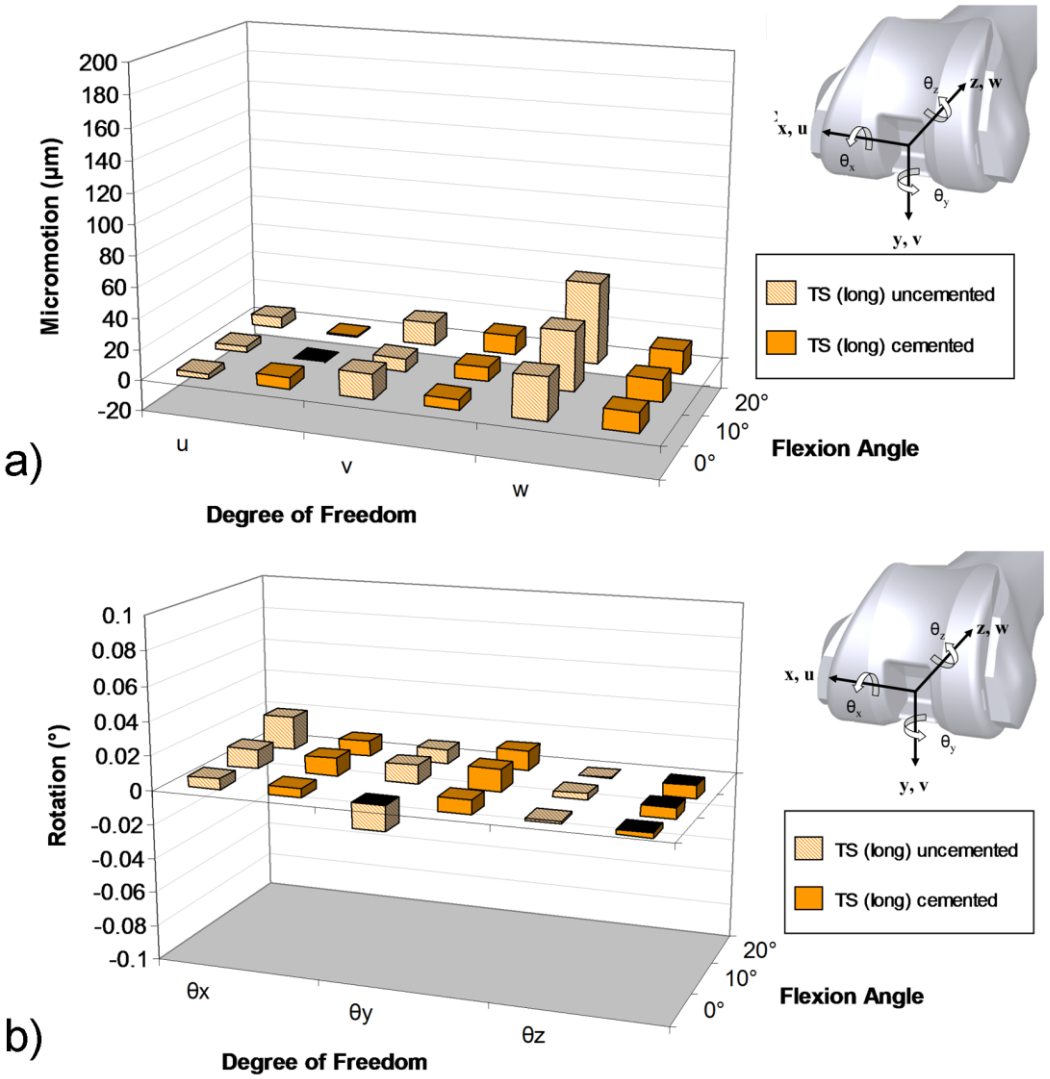


**Figure 8.26:** Comparison of a) translational and b) rotational relative motions for a TS implanted femur with long offset stem for both cemented and uncemented cases.

### VIII.3.5 Summary of results

The overall magnitude of relative motions for each of the uncemented and cemented implant cases were plotted in a single figure (Figure 8.27). This shows an overall increasing trend of motion with flexion angle for all implants tested. It can also be seen that the addition of a stem serves to reduce the levels of femoral component relative motion, with the long offset stem exhibiting the lowest relative motion. The difference in implants and fixation method (i.e. cemented or uncemented) is particularly noticeable in flexion.

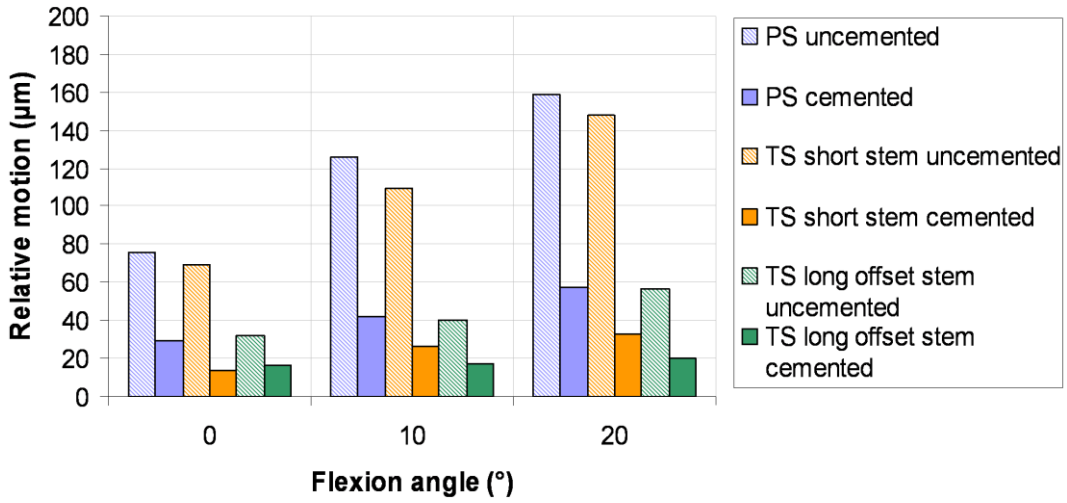


**Figure 8.27:** Overall magnitude of relative motions for the three flexion angles investigated for both uncemented and cemented conditions.

## VIII.4 Discussion

Based on currently available clinical and experimental evidence, there continues to be a significant amount of debate in the orthopaedic community as to the correct method of fixation and appropriate selection of stems in the setting of revision TKA. In this chapter, a test rig was developed which employed an array of highly sensitive DVRT sensors adjacent to the bone-implant interface, with the goal of determining what role stem length and method of fixation play in initial femoral component stability and how this changes over multiple flexion angles.

In this study, relative motion was measured along all six degrees of freedom for femoral components. Previous *in vitro* studies tend to report motion along fewer degrees of freedom (Wackerhagen et al. 1992, Moran 2005, Cristofolini et al. 2008, Cristofolini et al. 2009) typically axial motion or rotation in the sagittal plane, however, previous studies can provide cross validation where components of motion measured in these studies align to components of motion measured in the current study. The average inducible displacements in the direction of the long axis of the femur as reported by Cristofolini et al. (2008) are comparable to those recorded by DVRTs 3, 4 and 5 in this study. Furthermore, the range of inducible relative motion found in this study for both cemented (0-45µm) and uncemented (4-145µm) are similar to the range of relative motions (14-250µm) reported previously by Wackerhagen et al. (1992) and (9-130µm) by Cristofolini et al. (2008) for similar flexion angles.

A number of clinical studies employed RSA techniques to determine motion of the implant *in vivo* (Ryd 1986, Nilsson et al. 1991, Ryd 1992, Walker and Sathasivam 1992, Nilsson et al. 1995, Ryd et al. 1995, Nilsson and Kärrholm 1996); it must be noted, however, that the resolution of such techniques (100µm) is at the upper bounds of the range associated with fibrous tissue formation (Pilliar et al. 1986, Bragdon et al. 1996) and eventual failure of the prosthesis (40µm – 100µm) and therefore may not be sensitive enough to discern important difference between implants and fixation methods. RSA still provides a valuable tool for comparing qualitatively *in vivo* trends with *in vitro* measurements. Additionally as RSA studies predominantly focus on permanent migration rather than inducible displacement, values from such studies can act as an upper limit within which measured motions can be considered sensible, e.g. recorded motions for inducible displacement of a correctly implanted prosthesis should remain well below values of permanent migration, from literature RSA studies typically report translational motions in the range of 200µm – 1000µm and rotational motions in the range of 0.25° – 1° (Ryd 1986, Nilsson et al. 1991, Ryd 1992, Nilsson et al. 1995, Ryd et al. 1995, Nilsson and Kärrholm 1996).

In the current study, cemented relative motions were found to reduce to approximately 1/3 of their uncemented levels; these findings are within the range reported by a previous cemented study on cadaveric bone (Wackerhagen et al. 1992). Furthermore, this behaviour is consistent with trends from previous clinical studies which reported a relative reduction in inducible motion for patients implanted with cemented prostheses in comparison to patients implanted with uncemented prostheses (Ryd 1992). It can be observed from Figure 8.26 that PS implants once cemented exhibit similar levels of relative motions to uncemented TS implants with long offset stem. TS implants with a short cemented stem were found to have comparable relative motions to the hybrid cemented long stemmed implants. Again as with the uncemented tests the long offset stem was seen to result in the lowest relative motions in almost all cases.

Though RSA is capable of determining rotational as well as translational motions at the bone prosthesis interface, reporting of the former is far more common, e.g. (Ryd 1992). In a study by Nilsson et al. (1995), the authors reported that the values of rotational motion about the flexion/extension axis (sagittal plane rotation) and the longitudinal axis (internal/external rotation) were very similar (possibly due to the presence of distal femoral pegs). In the same study, all components of rotational motion were found to be within the same range (0.2° - 0.5°) for both cemented and uncemented interface conditions. In the present study, rotational relative motions were found to be significantly lower with values for an uncemented PS implant ranging from 0.01° – 0.05° at 0° flexion to 0.015° - 0.09° at 20° flexion. These values further reduced with the addition of a stem and cementing of the interface. In the current study it was also noted that the inclusion of a stem had an influence on pattern of rotations (i.e., the stem served to restrain rotational motion in $\theta_x$ and $\theta_y$). It must be noted, however, that long term migration of the implant was not considered in the current study and therefore rotations were calculated on the basis of inducible displacements alone. This could explain, in part, the significant difference between the magnitude of rotations in the present study and previous clinical RSA studies.

In the past, biomechanical studies have been performed to analyse primary stability and shear forces for the various fixation techniques using both cadaveric simulation and finite element analysis (Jazrawi et al. 2001, Completo et al. 2008a, Completo et al. 2010). These studies have largely been performed upon the tibia and tibial components. Unlike the tibia, the contact area and direction of loading across the distal femur changes significantly with flexion and extension of the knee during the gait cycle (Bergmann 2008). In the present study, as in Chapter VII, it was observed that relative motions increased with increasing flexion angle for all components and fixation methods tested, which is consistent with previous studies (Wackerhagen et al. 1992, Moran 2005). This serves to highlight the complexity of the distal femur and how changes to load magnitude and direction can greatly influence the levels of motion observed. As a result simulation or analysis in the anatomical position of extension does not accurately reflect the conditions for the majority of gait cycle and may lead to an overestimation of component stability, as can be seen from Figure 8.27.

In revision knee replacement stems transfer load from the metaphysis to the diaphysis. The use of longer stems increases surgical complexity and raises the concern of metaphyseal stress-shielding (van Lenthe et al. 2002, Completo et al. 2008a, Completo et al. 2008b, Completo et al. 2008c) and resultant fractures in the long-term (Scott and Biant 2012). Stem size, offset adaptors, stress shielding and the presence of either cement or bony in-growth can also complicate further revision surgery (Toksvig-Larsen et al. 1998). Beckmann et al. (2011) recently published a review of literature on revision knee replacement fixation. In this review it was indicated that the majority of recent research has dealt with the comparison of "hybrid" and cemented fixation, reporting comparable rates of loosening and clinical outcomes for both methods. Fewer studies were available for uncemented fixation. Overall, Beckmann and co-authors could not make a final statement recommending one form of fixation over the other based on the available evidence from clinical outcomes and *in vitro* studies. The results from the current study suggest that in uncemented reconstructions, stemmed implants perform better than stemless

implants, with the long offset stem seen to provide the greatest resistance to relative motion. However, it was found that, once cemented all implants with and without stems had comparable levels of relative motion. These findings indicate that the use of stems provides no obvious advantage for cemented implants unless there is a need to bypass a condylar defect. For the implants used in this study (PS or TS design) the central box housing can be regarded as a short stem in engineering terms. In situations where stems are necessary, metaphyseal defects requiring augments, these findings support the use of a short cemented stem, which has been shown in this study to provide comparable results to long offset stems (cemented and uncemented). A previous finite element study by van Lenthe et al. (2002) showed that the use of short stems produced a more favourable pattern of stress distally in comparison to long stems, which leads to less severe instances of stress shielding over time, this finding coupled with the results of the current study would seem to lend support for the use of short cemented stems over long press-fit stems. Another key practical factor is the relative ease of insertion when using short stems. In comparison, fitting of a long stem can be complicated by the natural AP bow in the femur, variations in the valgus angle, distal metaphyseal anatomical variants and other conditions which may affect the geometry of the shaft.

There are a number of limitations to the current study which must be considered when interpreting the results. Only three flexion angles in a walking gait cycle (0°, 10° and 20°) were investigated. Depending on the activity, higher flexion angles may be present during gait and following the observed trends one would expect even greater relative motions at higher flexion angles, as has been seen in previous studies (Wackerhagen et al. 1992, Moran 2005), particularly during physiological activities such as climbing stairs or rising from a chair. The current test rig was designed to allow flexion angles from 0°-90° to be investigated. In practice, due to the large bending moment introduced at higher flexion angles ($\geq 30^{o}$) and the absence of ligaments or muscles to redistribute the load and protect the bone (Phillips et al. 2007, Sverdlova and Witzel 2010, Wilkie et al. 2012), the results became heavily influenced by excessive bending/deformation of the bone. In tests conducted with the

initial prototype rig design, the added weight and large bending moment created due to fixation led one test specimen to fracture in the bone holder at the level of the bolt. This unrealistic bending moment introduced by the over simplification of femoral boundary conditions employed in the lab is a common limitation faced in the fielding of biomechanics and in this instance, is exacerbated by the alignment of the femur particularly in flexion which predisposes it to bending. A number of recent studies have attempted to overcome this issue by inclusion of a system of pulleys and belts representative of the lower limb "muscles" (Moran 2005, Innocenti et al. 2011) in combination with dynamic knee rigs. However, this type of setup requires access to specialist equipment and would have necessitated a further iteration of the test rig to allow clearance for muscle and ligament attachments about the knee joint and was therefore considered to be outside the scope of the current project. Future *in vitro* test setups should make efforts to include these anatomical features (e.g. cruciate ligaments, quadriceps and hamstrings), as well as being more physiological, inclusion of these features in the context of a full femur model would help to minimise the influence of bending particularly in flexion and reduce the risk of test specimen fracture. The use of a more complex loading setup in conjunction with a modified version of the micromotion test rig developed in this thesis, to allow appropriate clearance for the patella an muscle structures crossing the knee joint, could provide valuable information on the interface behaviour of various total knee prostheses under more physiologically realistic loading conditions (e.g. stairs, chair rise and squat).

This study does not measure the true levels of motion at the interface; it instead measures motions of the implant relative to the point of fixation of the DVRT rig to the bone. By comparing the overall magnitude of motions presented in Figures 8.20 and 8.27, it can be seen that minimising the distance from fixation leads to a significant decrease in the levels of apparent motion recorded. This highlighted the importance of minimising the distance from point of fixation to the surface of interest to prevent the artefacts such as bending from obscuring important trends between implants. Future iterations of the rig could also improve measurement accuracy

through incorporation of additional sensors in two possible configurations. The first modification would support the current arrangement through the addition of two extra sensors in the x direction and one extra sensor in the y direction to improve averaging in those directions. The second modification would incorporate the additional sensors into a secondary array aimed at the bone, then by tracking the apparent motion of both the bone and the implant relative to the point of fixation an estimate of the motion due to specimen bending could be made, thus improving accuracy of the results.

Finally, the addition of a locator device to allow accurate and consistent positioning of the sensor housing relative to the femoral target frame would allow testing to be extended to cadaver bone specimens. In the current setup, such a device was not required due to the existence of pre-defined holes in the sawbones femur specimen which allowed for consistent placement of the test rig across all specimens tested.

In this study, relative motions were calculated based on the assumption of rigid body kinematics. Though the implant due to its high stiffness can be assumed to be rigid the same assumption does not hold for the bone structures. The large mismatch in stiffness between cancellous bone regions and the implant in particular predisposes the assembly to a certain level of elastic deformation under loading. This has been recognised as a limitation in some previous studies of a similar nature (Berzins et al. 1993, Maher and Prendergast 2002, Britton and Prendergast 2005, McLean 2007, Cristofolini et al. 2008, Cristofolini et al. 2009). This combination of motion and deformation may therefore result in experimental values overestimating the level of "true" motion at the interface. It has been suggested by a previous study (Gilbert et al. 1992) that the contribution of elastic deformation is quite low (3-15μm) in comparison to values of motion observed. In a more recent study on the knee (Moran 2005), however, the value of elastic deformation was found to be significantly higher than previously reported (<50μm), though the author conceded that this reading may have been influenced by the lack of cortical support surrounding the prosthesis (only cancellous bone was modelled). In a canine model Berzins et al. (1994) showed that the cortex played a significant role in restraining transverse expansion of the

cancellous bone structure, therefore in the case of Moran (2005) it is likely that the lack of a cortical rim to provide support and resist deformation may have contributed to the larger than expected elastic deformations in the cancellous bone structure reported during testing.

Though elastic deformations, if large, may obscure true levels of interfacial motion, it must be considered that the magnitude of combined motion and deformation also hold importance to component stability and survival. If elastic deformations become too large then there is a possibility of loosening as a result of cumulative fatigue damage to the underlying cancellous bone structure which supports the prosthesis (Taylor and Tanner 1997). Cumulative fatigue of the underlying bone due to elastic deformations could also have implications in component loosening of cemented cases, and may increase the likelihood of cement mantle failure.

In the present study some components of relative motion for the cemented implants in particular were approaching or below the levels of "motion" attributed to elastic deformation (Gilbert et al. 1992) and in some cases were approaching the level of the sensor resolution (1μm). The contribution of elastic deformations to measured motions will attempt to be addressed through a combined FE and experimental approach detailed in the following Chapter. However, to overcome the issue of small motions approaching sensor resolution, future tests may need to employ the use of more sensitive nano-resolution gauges, though it must be considered that improvements in sensor resolution may come at the cost of overall working range.

Relatively few loading cycles ($n = 40$) were carried out during each test. While a small number of cycles have been shown to be adequate for determining the loosening behaviour of uncemented components (Schneider et al. 1989), cemented components have been seen to fail only after millions of cycles. Due to the comparative nature of this work (cemented vs. uncemented) it is believed that the behaviour observed in these short term findings is a good predictor of possible long term results, though further testing for a greater number of cycles may be necessary

to verify if the short term behaviour observed in the current study applies to long term scenarios.

In conclusion, this study detailed the development and testing of a custom test rig capable of measuring all six degrees of freedom of femoral components used in TKA. This test rig was used to investigate the relative motion of primary and revision TKA prostheses for cemented and uncemented interface conditions. Contrary to some earlier reports e.g. (Wackerhagen et al. 1992) it was determined that motions of femoral prosthesis are a complex combination of translations and rotations in all planes at the knee joint and should not be simplified to fewer degrees of freedom (Wackerhagen et al. 1992, Moran 2005, Cristofolini et al. 2008, Cristofolini et al. 2009). Moreover, the geometry of the implant (Moran 2005) and the presence of a stem (van Loon et al. 2000) can greatly influence the patterns of motion observed at the interface for both cemented and uncemented prostheses.

In the present study it was found that cemented short stems conferred as much stability as uncemented long stems. As these are clinically easier to fit they should be a preferred option. The condition of 0° flexion was found to result in the smallest difference between implants and fixation methods, indicating this commonly examined load case may lead to overestimation of component stability, and as a result future laboratory testing should be conducted at a range of flexion angles to give a more complete understanding of relative motions between prosthesis and bone.

Though the findings of this chapter are unlikely to definitively settle the long running debate over what is the appropriate stem length and which method of fixation is best, it does serve to supplement and advance the current state of knowledge on this topic and provide surgeons with additional evidence on which to make a more informed decision at the time of operation. Additionally, the information derived through the development and testing of the micromotion rigs in this study, as well as the issues encountered, will be useful in the development of future testing methodologies for orthopaedic implant micromotion evaluation.

In the next chapter, the experimental setup presented here will be reproduced *in silico*, for the purpose of estimating the influence of elastic deformations of the cancellous bone structure and to extract the true levels of motion which occur at the bone-implant interface.

# IX

# Finite Element Evaluation of Femoral Component Motion

## IX.1 Introduction

This study employs FE models of the distal femur with boundary conditions and load representative of the *in vitro* setup presented in Chapter VIII.

In Chapter VIII relative motion of the prosthesis to the bone was measured in all six degrees of freedom using a custom DVRT test rig. Such setups, as discussed previously, which infer interfacial motions indirectly from sensors positions at a distance from the interface, are subject to the inclusion of a number of flexibilities which may lead to an overestimation of the relative motions at the bone-prosthesis interface. The presence of flexibilities other than motion has been recognised as a limitation in some previous studies of a similar nature (Berzins et al. 1993, Maher and Prendergast 2002, Britton and Prendergast 2005, McLean 2007, Cristofolini et al. 2008, Cristofolini et al. 2009). Further flexibilities in the system may arise due to the manner in which test rigs are constructed or assembled. The level of cortical support near the bone-prosthesis interface has also been cited as a factor in determining its response under loading (Berzins et al. 1994). The combination of motion and deformation may therefore result in experimental values overestimating the level of "true" motion at the interface. Thus far, however, only a limited number of studies have attempted to directly quantify the impact of such elastic deformations on reported results (Monti et al. 1999, Britton and Prendergast 2005, Moran 2005, Tarala et al. 2011).

On the other hand, some studies choose more robust long term indicators such as permanent migration to predict inter-implant variability, which has been found to be less sensitive to such flexibilities (Britton and Prendergast 2005, Cristofolini et al. 2008, Cristofolini et al. 2009).

Little consensus exists on the exact contribution of elastic deformations to *in vitro* measurements. It has been suggested by a previous study (Gilbert et al. 1992) that the contribution is quite low ($3-15\mu m$) in comparison to values of micromotion observed. Research by Monti et al. (1999) into prosthesis motion following THA reported elastic deformations of $2.3\mu m$ at the interface through the use of LVDT sensors attached to trans-cortical pins. However, the authors noted that elastic deformations increased almost linearly with increasing distance from the interface (reaching a maximum of $5\mu m$ at the external surface).

The complex shape of the distal femur and the changing contact area with flexion limit the ability to attach devices directly to the surface. As a consequence, more indirect measurement methods need to be employed, lending to a higher potential error due to increasing distance from the interface (Monti et al. 1999, Tarala et al. 2011). A recent study by Moran (2005) found that elastic deformations alone could account for measured motions of up to $50\mu m$ in cancellous bone structures following TKA.

The main goal of this study was to predict the relative motion of the implants to the bone in all six degrees of freedom about a central reference point using FE and compare these findings to the *in vitro* tests discussed in Chapter VIII. Then, by examining how motion about the central reference point varies from "true" interfacial motion, it will be possible to quantify the error associated with experimental measurements of inducible motion.

## IX.2 Method

The quantification of the elastic deformations which may occur during laboratory testing required the development of an FE model with comparable setup and loading conditions to that previously presented in Chapter VIII. This necessitated significant simplification of the pattern of loading and alterations to the model boundary conditions to more closely approximate the *in vitro* setup. The key features of which will be outlined in the following sections.

### IX.2.1 Geometry

To incorporate the same loading and boundary conditions as applied in the lab necessitated the inclusion of two further parts in the bone-prosthesis assembly (Figure 9.1). These parts consisted of a stiff steel plate through which the machine load is applied and a UHMWPE tibial bearing insert with central post and an articulating surface conforming to the outer surface of the femoral component. In addition the posterior stabilising box section of the femoral component was closed off in the posterior region to complete the post-cam mechanism. Further modifications to the implant medial/lateral width were carried out to more closely match that of the lab test specimen and reduce the likelihood of medial/lateral overhang leading to an artificial reduction in axial elastic deformations.

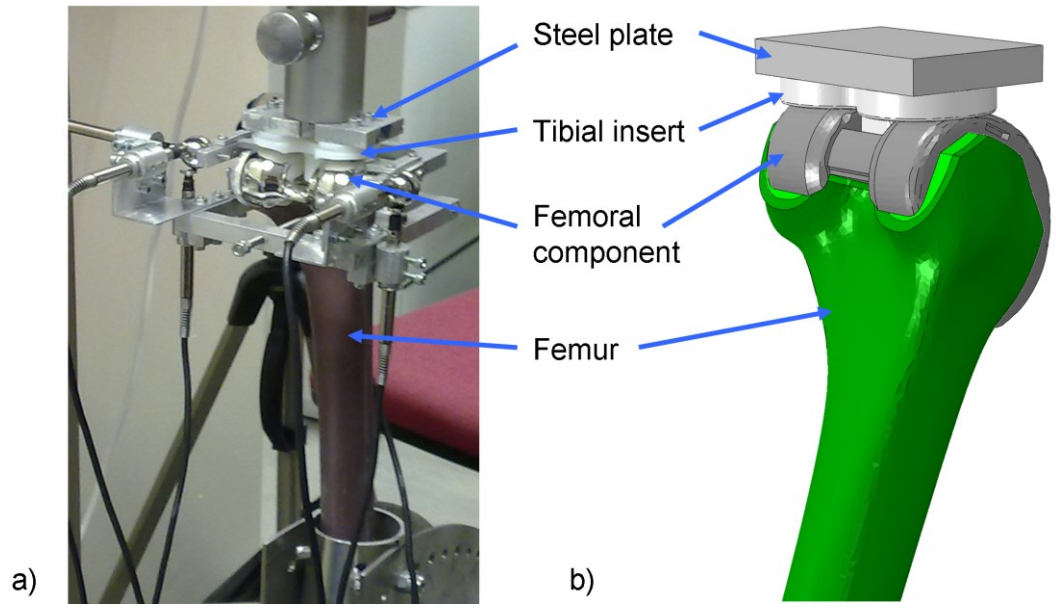


**Figure 9.1:** a) Image of *in vitro* experimental setup and b) corresponding model setup showing steel plate, tibial insert and femoral component.

Three different femoral components were investigated with the virtual micromotion rig setup (Figure 9.2); a posterior stabilising (PS), a total stabilising (TS) implant with short stem (12x50mm) and a TS implant with long offset stem (19x150mm stem with 4mm lateral offset). To remain consistent with the *in vitro* experiments conducted in Chapter VIII, all femur models were prepared in a consistent manner, e.g. all models were reamed to the size of the long stem with offset adapter as had been done in the *in vitro* laboratory tests to maintain consistency of preparation across all specimens.

### IX.2.2 Interface properties

Frictional interactions were applied to both bone-prosthesis and prosthesis-prosthesis interfaces to replicate the uncemented *in vitro* trials, with the frictional properties applied as per Chapter VII section VII.2.4. Additionally a second set of models were created to simulate the effects of femoral component cementing. For simplicity and to allow the same models to be used for both cemented and uncemented simulations, these models employed tied constraint at the bone-prosthesis interface rather than explicitly modelling the cement layer.

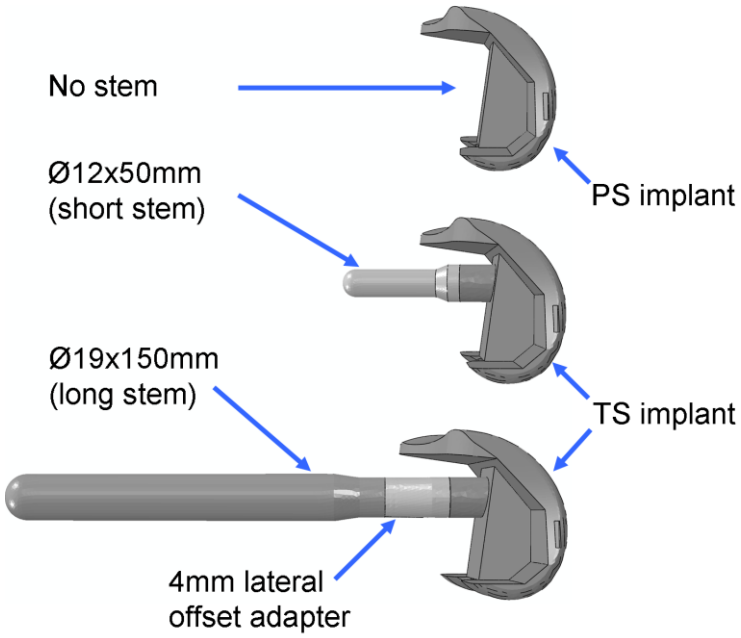


**Figure 9.2:** Rendered CAD models of a PS implant (top), a TS implant with short stem (middle) and a TS implant with long offset stem (bottom).

### IX.2.3 Material properties

As in Chapter IV, all materials were assumed to behave in a linear elastic, isotropic manner. The values of Young's modulus and Poisson's ratio applied to these structures were as presented in Table 4.1. The Young's moduli of the femoral stems were applied as per Chapter VI, Table 6.1. Properties assigned to the steel plate, tibial insert (Bei et al. 2004) and femoral offset adapter are presented in Table 9.1.

**Table 9.1:** Material properties for *in vitro* setup FE model.

| Model | Young's modulus E ($N/mm^2$) | Poisson's ratio (v) |
|---|---|---|
| Steel plate | 210000 | 0.3 |
| Offset adapter | 110000 | 0.3 |
| Tibial insert | 463 | 0.46 |

### IX.2.4 Boundary conditions

As in all previous models, the femur was truncated at the mid-shaft and fully fixed in all degrees of freedom on the proximal most surface. Additionally the steel plate was restrained such that only the degree of freedom relating to compression of the plate on the femur was free.

### IX.2.5 Loading protocol

To remain consistent with the experimental loading protocols for 20° flexion a cyclical load was applied to the centre of the steel plate (representative of the load cell attachment site), this load was set to vary from 0N to 1643N during the first cycle and 20N to 1643N during subsequent 39 cycles to maintain contact between tibial insert and femoral component, as in the *in vitro* testing protocol.

All 40 cycles were carried out during a single static load step in Abaqus. This was achieved by varying the load through a custom amplitude curve and then defining output of all interface parameters and displacements at each full time increment using a series of predefined time points to ensure all stages of each loading peak would be captured during the analysis (Figure 9.3), to replicate the conditions in the *in vitro* testing described in Chapter VIII.

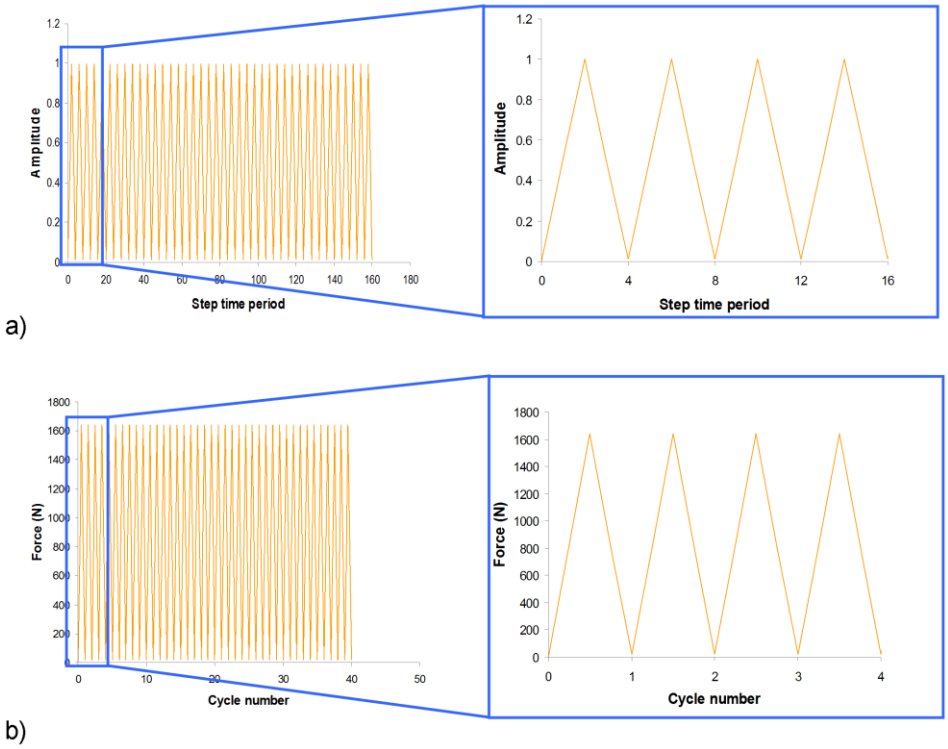


**Figure 9.3:** Graphs showing a) the variation of amplitude with step time period for a total step time of 160, and b) the resulting force amplitude curve in terms of cycle number. The profile of four typical amplitude and force curves are highlighted in the blue boxes on the right for clarity.

### IX.2.6 Micromotion measurement system

When comparing measurements taken during *in vitro* experiments to those in an FE model it is essential that the same parameters be measured in the same manner, to this end it was necessary to recreate the sensor placement and setup used in the *in vitro* experiments. Rather than adding to model complexity and runtime by explicitly modelling the entire three dimensional test rig, the location of each sensor and its corresponding target were recreated virtually using a system of reference points and coupling constraints, as shown in Figure 9.4. In this manner, the displacement of the sensor could be approximated by calculating the relative change in position of the target reference point to its corresponding sensor reference point (Figure 9.4).

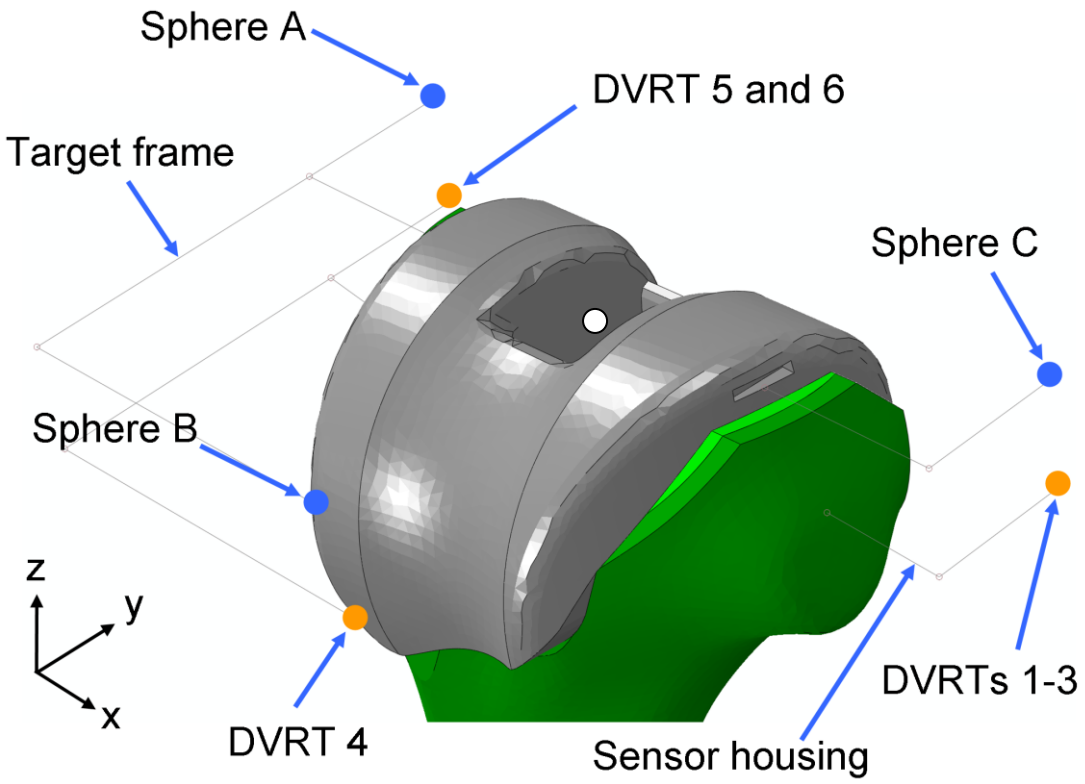


**Figure 9.4:** Showing the virtual recreation of the *in vitro* test rig through points representative of the DVRT sensors and the target spheres. In this instance the target sphere locations are represented by the blue dots which attach back to the implant tool groove using coupling constraints and the DVRT sensors are represented by the orange dots which attach to the bone at the approximate location of the sensor housing in the in vitro setup. The reference point about which all motions and rotations are calculated is indicated by the white dot.

### IX.2.7 Analysis of FE model results

It can be seen from Figure 9.4 that the displacement profile of DVRTs 1-3 are approximated by calculating the relative nodal displacement of the Sphere C reference point and corresponding sensor housing reference point in the global x, y, z coordinates over the course of the 40 cycles. Similarly DVRTs 5 and 6 displacements are determined by comparing relative nodal displacement in the y and z directions and DVRT 4 by comparing relative nodal displacement in the z direction only. A typical plot of "sensor" displacements following processing of relative motions of the reference points in excel is shown in Figure 9.5.

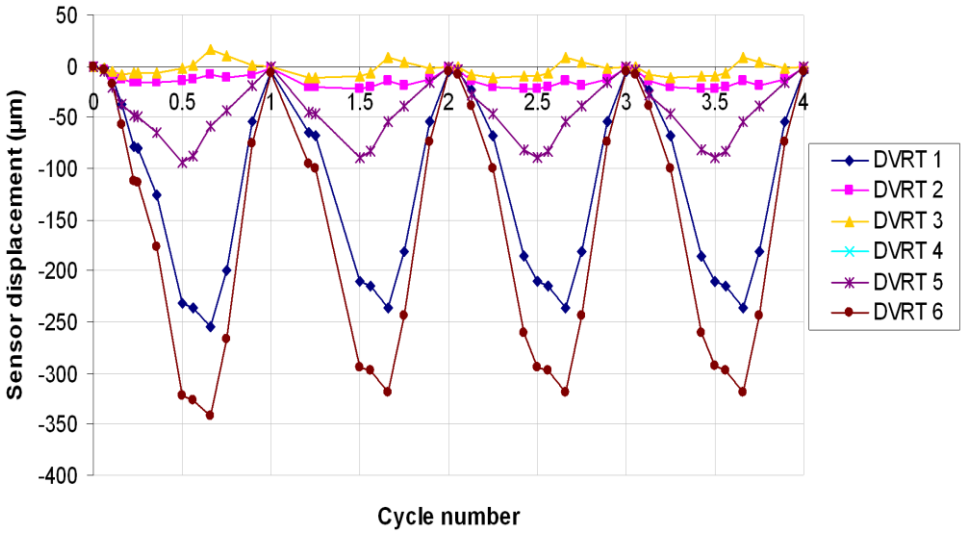


**Figure 9.5:** Example of the sensor displacement curves for the first four cycles of a PS implanted femur at 20° flexion.

Once the characteristic displacement curve for each sensor was extracted from the FE model this data was collectively exported to a text file in column format, where the first column represented the time and the remaining columns the individual displacement curves of each sensor over the entire 40 cycle period. The purpose of formatting the data in this manner was to allow the amplitude of each displacement curve to be extracted and subsequently to perform the necessary coordinate transformations using the custom LabVIEW programs presented in Chapter VIII. An overview of the results processing workflow is presented in Figure 9.6.

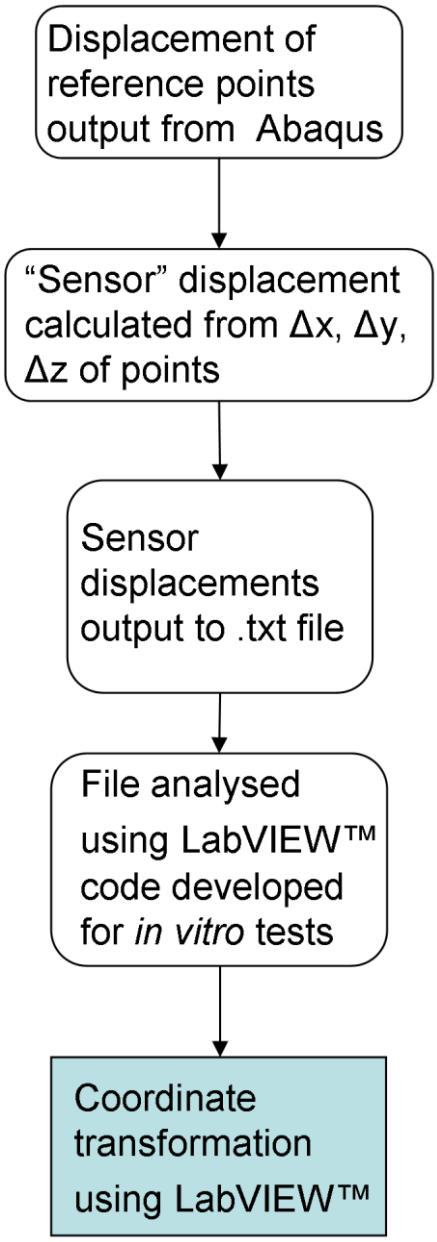


**Figure 9.6:** Major steps in analysis of FE model results about reference point.

## IX.3 Results

This first set of results shows the measured motions and rotations about the micromotion reference point highlighted in Figure 9.4. As in Chapter VIII, the relative motion of the implant to the bone is describe using three translational components of motion $u, v, w$ along the x, y and z global axes respectively and three

rotations $\theta_x, \theta_y, \theta_z$ about the x, y and z axes respectively. Referring to Figures 9.7 – 9.9, it can be seen that the smallest component of motion in general is displacement $u$ in x-direction. It should also be noted that the component of rotational motion found to be the smallest is $\theta_z$. These findings are consistent with those observed experimentally in Chapter VIII.

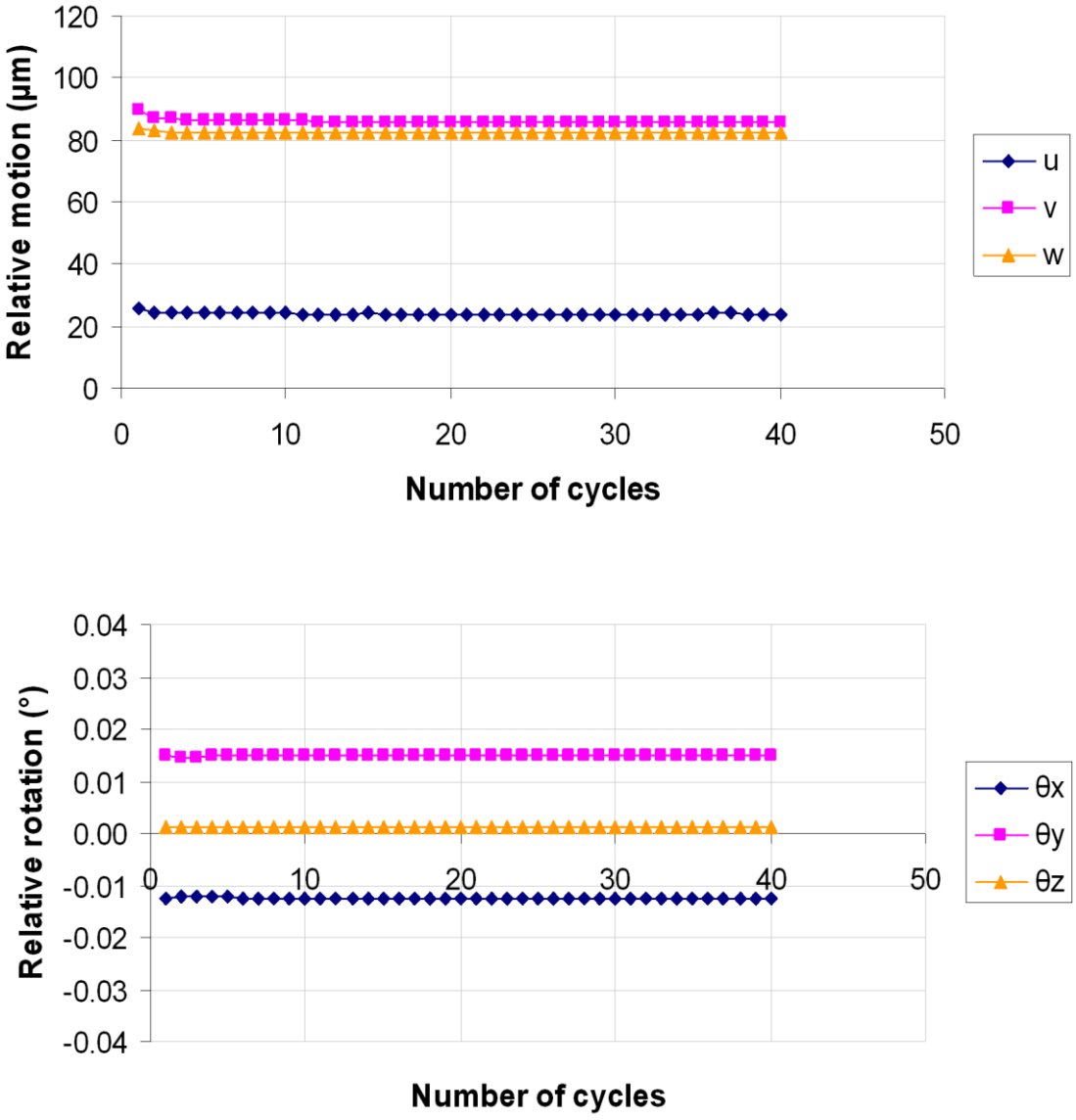


**Figure 9.7:** Cyclical graphs showing the translational (top) and rotational (bottom) relative motions of a PS implanted femur at 20° flexion.

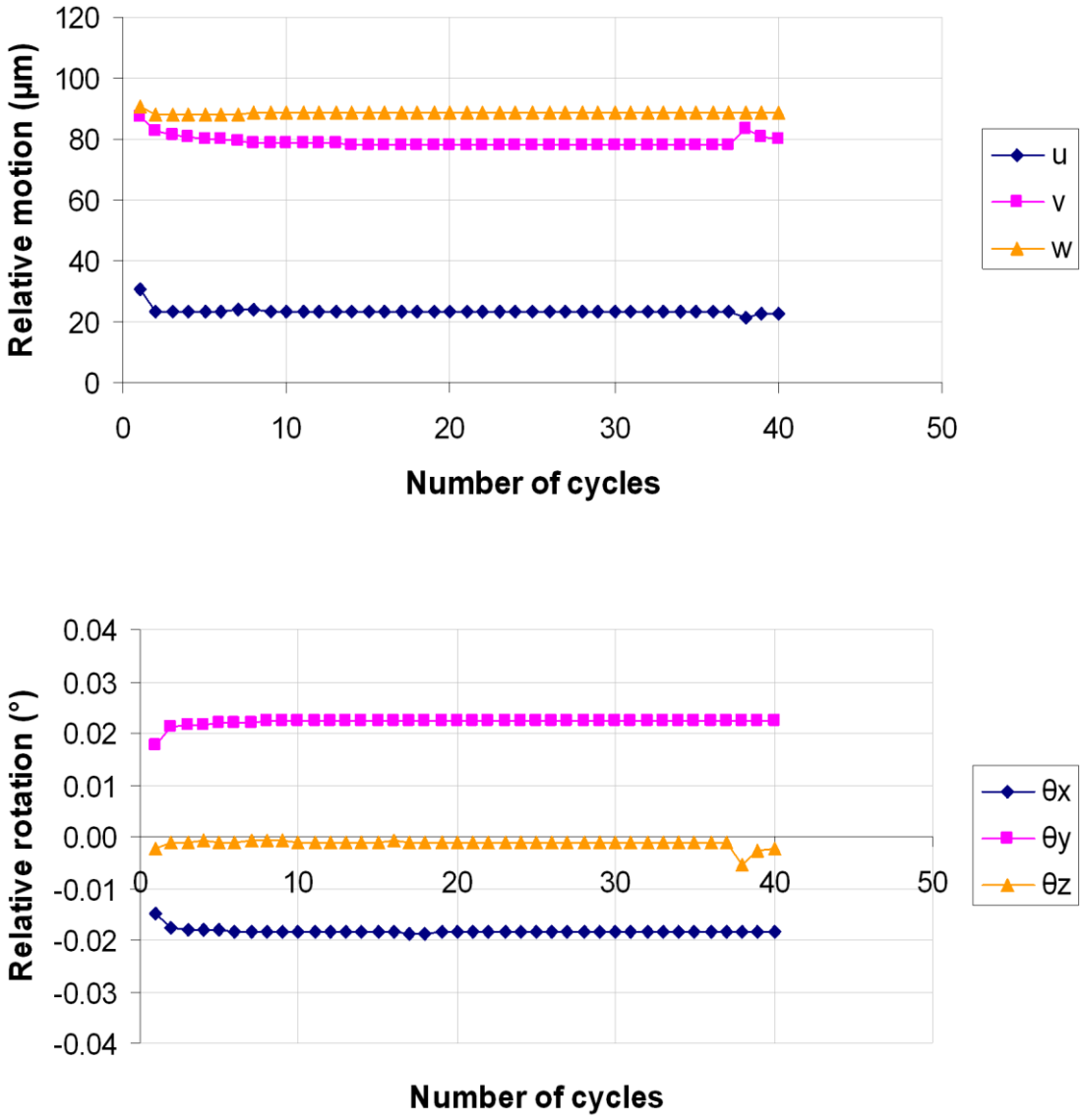


**Figure 9.8:** Cyclical graphs showing the translational (top) and rotational (bottom) relative motions of a short stemmed TS implanted femur at 20° flexion.

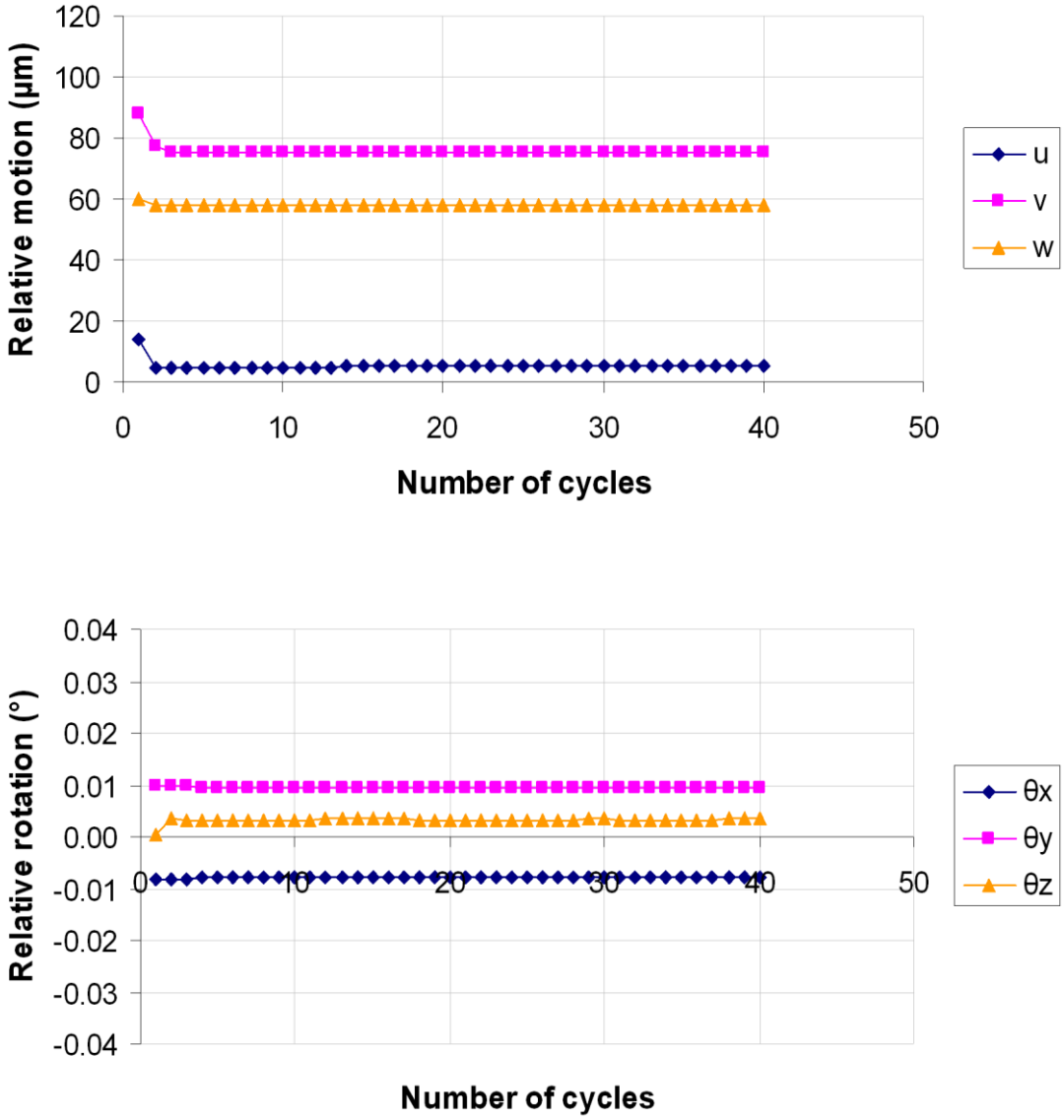


**Figure 9.9:** Cyclical graphs showing the translational (top) and rotational (bottom) relative motions of a long offset stemmed TS implanted femur at 20° flexion.

Table 9.2 to 9.4 highlight the average values of relative motion and rotation experienced by all three implants investigated in this study and indicate the corresponding averaged results from the *in vitro* trials described in Chapter VIII. In the *in vitro* investigation, the TS implanted femur with long offset stem was found to exhibit the smallest translational and rotational relative motions. In general, this trend

was maintained in the FE study with two exceptions; firstly, in the y-direction motions were overestimated by up to $60\mu m$ in comparison with the experimental results, and secondly, $\theta_z$ was found to be largest in the TS implant with long offset stem in the FE investigations in contrast to experimental findings. However, it is important to note that in the other two directions rotational relative motions were significantly lower than in the PS and TS with short stem implanted femurs and in all three of the principal directions translational relative motions were smallest in the TS implanted femur with long offset stem. Though the translational and rotational relative motions vary considerable between certain components of FE and *in vitro* setups both sets of motions are within the same order of magnitude. Interestingly though the displacement *v* in the y-direction is significantly larger in the FE setup by approximately 50%, possibly indicating a difference in fit between numerical and experimental setups.

**Table 9.2:** Comparison of FE and *in vitro* results for PS implanted femur at 20° flexion.

| Component of motion | FE results | *In vitro* results | Difference |
|---|---|---|---|
| u (μm) | 24 | 48 | -24 (μm) |
| v (μm) | 86 | 44 | +42 (μm) |
| w (μm) | 83 | 145 | -62 (μm) |
| $\theta_x$ (°) | -12.4E-03 | 84.15E-03 | -96.6E-03(°) |
| $\theta_y$ (°) | 14.8E-03 | 0.469E-03 | +14.3E-03(°) |
| $\theta_z$ (°) | 1.3E-03 | -15.06E-03 | +16.4E-03(°) |

**Table 9.3:** Comparison of FE and *in vitro* results for TS implanted femur with short stem at 20° flexion.

| Component of motion | FE results | *In vitro* results | Difference |
|---|---|---|---|
| u (μm) | 24 | 49 | -25 (μm) |
| v (μm) | 79 | 38 | +41 (μm) |
| w (μm) | 88 | 134 | -46 (μm) |
| $\theta_x$ (°) | -18.5E-03 | 22.9E-03 | -41.4E-03(°) |
| $\theta_y$ (°) | 22.0E-03 | 56.5E-03 | -34.5E-03(°) |
| $\theta_z$ (°) | -1.2E-03 | -9.5E-03 | +8.3E-03(°) |

**Table 9.4:** Comparison of FE and *in vitro* results for TS implanted femur with long offset stem at 20° flexion.

| Component of motion | FE results | *In vitro* results | Difference |
|---|---|---|---|
| u (μm) | 5 | 7 | -2 (μm) |
| v (μm) | 76 | 16 | +60 (μm) |
| w (μm) | 58 | 54 | -4 (μm) |
| $\theta_x$ (°) | -8.0E-03 | 20.2E-03 | -28.2E-03(°) |
| $\theta_y$ (°) | 9.50E-03 | 8.12E-03 | +1.4E-03(°) |
| $\theta_z$ (°) | 3.2E-03 | 0.2E-03 | +3.0 E-03(°) |

The overall magnitude of femoral component relative motion for both the FE and *in vitro* results is presented in Figure 9.10. In the *in vitro* experiments a decreasing trend with respect to motions was observed with stem use relative to the stemless PS

implanted femur. Similarly in the FE investigation the lowest overall magnitude of relative motion was observed to occur in the TS implanted femur with laterally offset stem, however, in contrast to the experimental trends the TS implanted femur with short stem was observed to result in a slightly higher level of relative motion than the PS implanted femur. Moreover, it is observed that the overall magnitude of relative motion is predicted to be within the upper range of fibrous tissue formation for both PS and TS short stem models and at the lower end for TS long stem implanted femurs (as indicated by the orange lines).

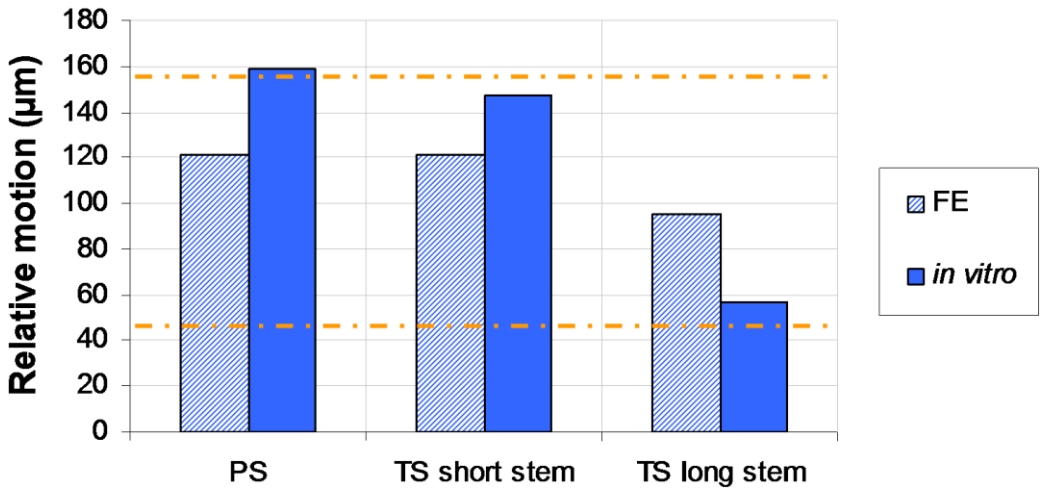


**Figure 9.10:** Comparison of the overall magnitude of relative displacement for both the FE and in vitro setups at 20° flexion. The upper and lower boundaries for fibrous tissue formation are indicated by the dashed orange line.

This second set of results investigates how fully tied interface conditions influenced the observed relative motion and rotation about the reference point. It can be seen (Figure 9.11-9.13) that all components of motion measured about the reference point reduce significantly when the bone-implant interface is fully tied. Comparable behaviour in terms of translations and rotations is observed for both PS and TS (short stem) implanted femurs, however, the TS implanted femur with long offset stem is again found to exhibit the smallest levels of "apparent" motion about the reference point. In this instance as the interface is fully tied, e.g. no relative motion of the implant to the bone is permitted, it is likely that the motions and rotations presented in the following tables and figures represent other quantities such as bending and

elastic deformation of the bone-implant complex under loading. These results were found to be comparable to the findings of the cemented tests conducted in Chapter VIII.

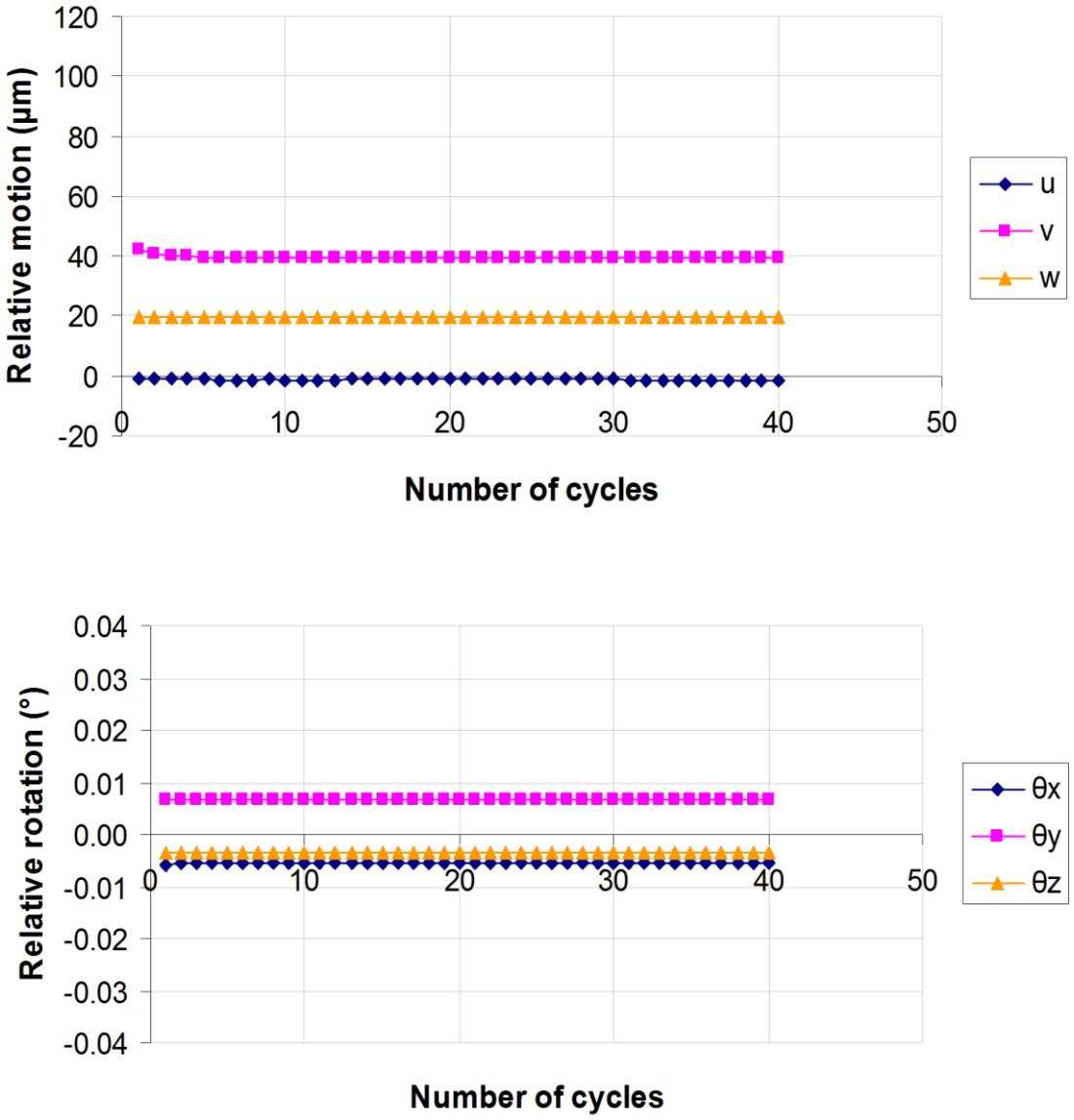


**Figure 9.11:** Cyclical graphs showing the translational (top) and rotational (bottom) relative motions of a fully tied PS implanted femur at 20° flexion.

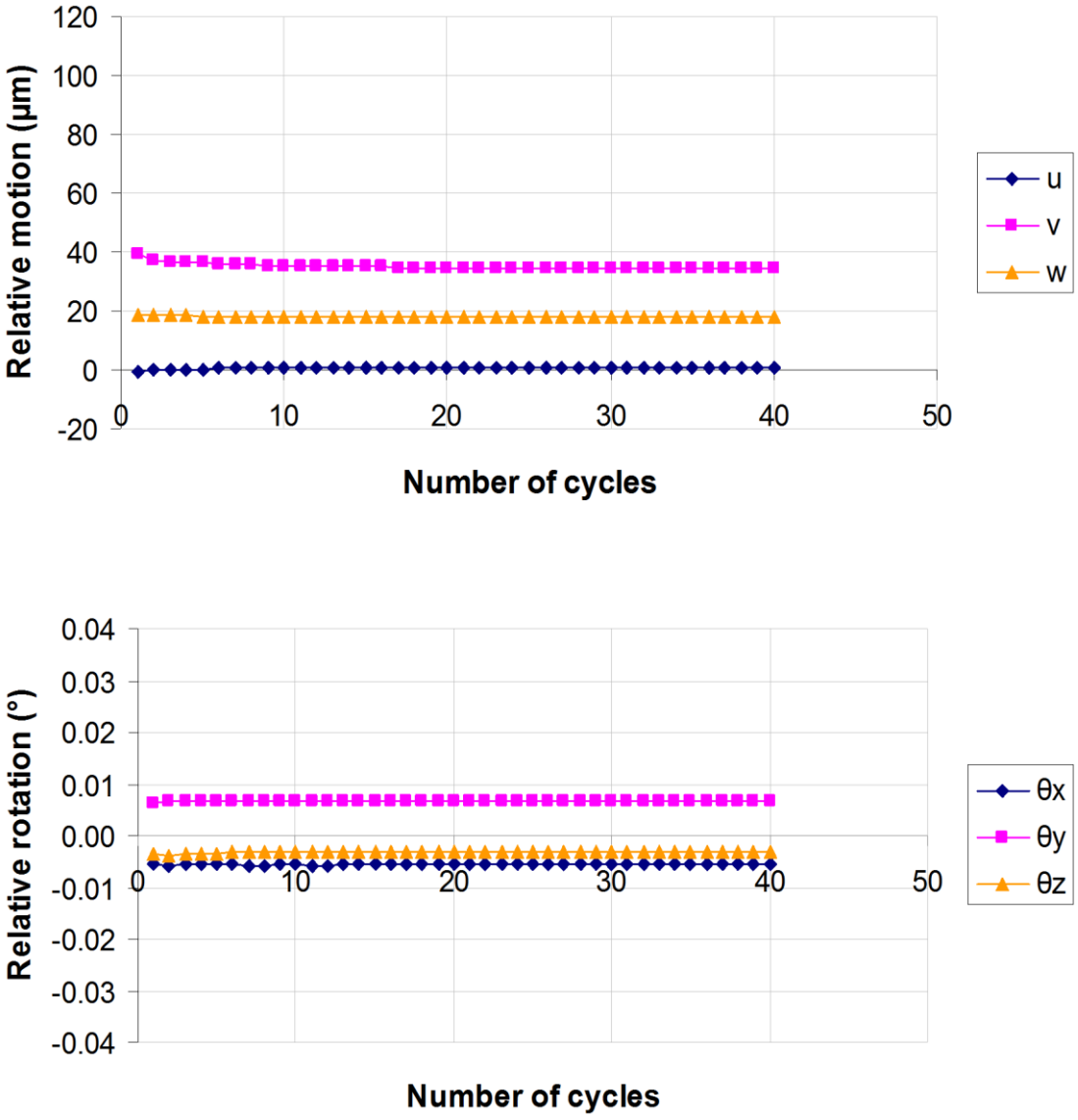


**Figure 9.12:** Cyclical graphs showing the translational (top) and rotational (bottom) relative motions of a fully tied short stemmed TS implanted femur at 20° flexion.

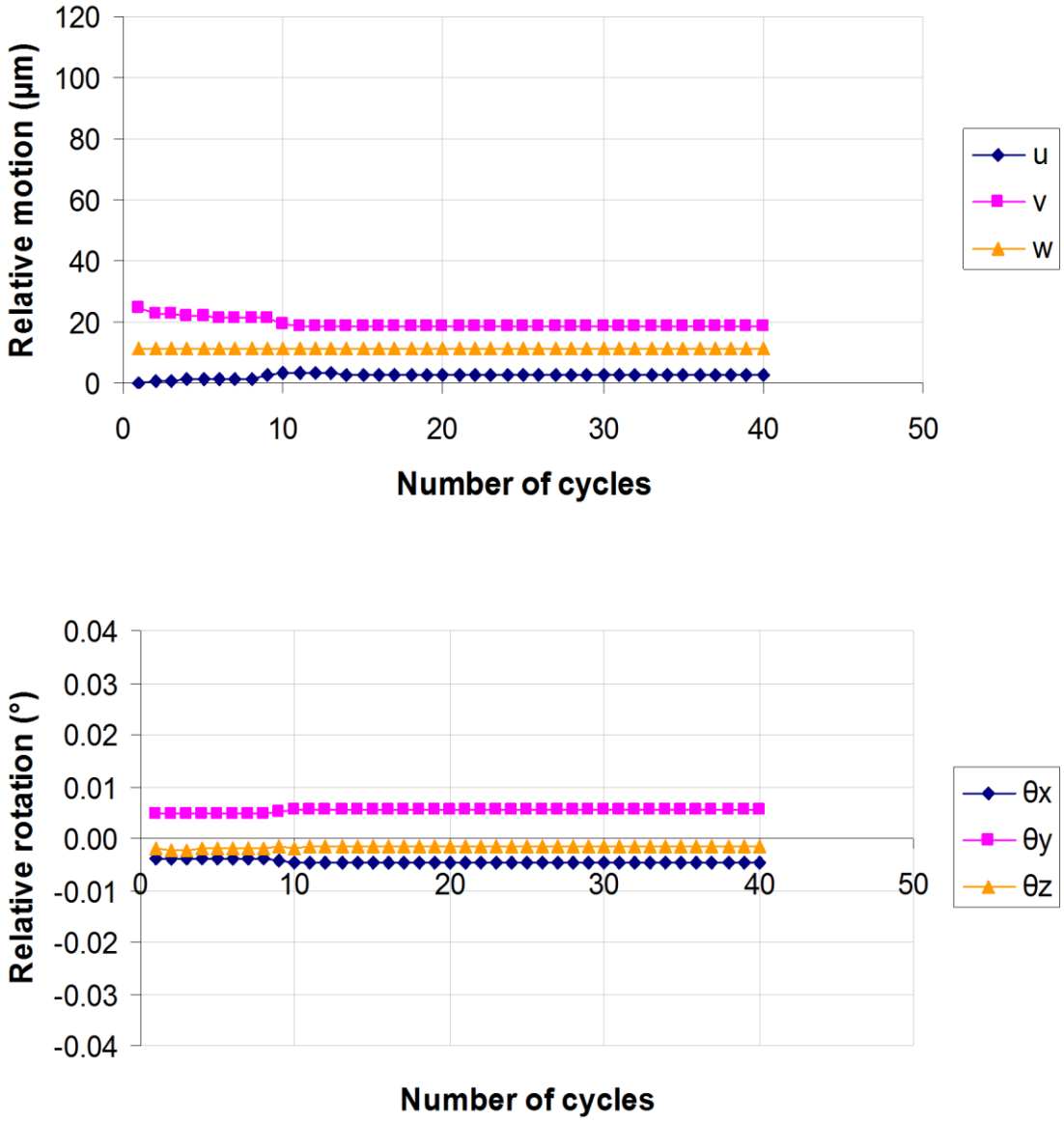


**Figure 9.13:** Cyclical graphs showing the translational (top) and rotational (bottom) relative motions of a fully tied long offset stemmed TS implanted femur at 20° flexion.

Table 9.5 to 9.7 highlight the average values of relative motion and rotation experienced by all three implants under tied interface conditions and indicate the corresponding averaged results from the *in vitro* trials with cemented fixation as described in Chapter VIII.

**Table 9.5:** Comparison of FE and *in vitro* results for PS implanted femur at 20° flexion.

| Component of motion | FE results | *In vitro* results | Difference |
|---|---|---|---|
| u (µm) | -1 | 32 | -33 (µm) |
| v (µm) | 39 | 17 | +22 (µm) |
| w (µm) | 19 | 45 | -26 (µm) |
| $\theta_x$ (°) | -5.6E-03 | 39.9E-03 | -45.5E-03(°) |
| $\theta_y$ (°) | 6.7E-03 | 18.2E-03 | -11.5E-03(°) |
| $\theta_z$ (°) | -3.3E-03 | 4.4E-03 | -7.7E-03(°) |

**Table 9.6:** Comparison of FE and *in vitro* results for TS implanted femur with short stem at 20° flexion.

| Component of motion | FE results | *In vitro* results | Difference |
|---|---|---|---|
| u (µm) | 1 | 6 | -5 (µm) |
| v (µm) | 35 | 11 | +24 (µm) |
| w (µm) | 18 | 30 | -12 (µm) |
| $\theta_x$ (°) | -5.6E-03 | 17.8E-03 | -23.4E-03(°) |
| $\theta_y$ (°) | 6.7E-03 | 27.3E-03 | -20.6E-03(°) |
| $\theta_z$ (°) | -3.3E-03 | -1.5E-03 | -1.8E-03(°) |

**Table 9.7:** Comparison of FE and *in vitro* results for TS implanted femur with long offset stem at 20° flexion.

| Component of motion | FE results | *In vitro* results | Difference |
|---|---|---|---|
| u (μm) | 2 | 0.4 | +1.60 (μm) |
| v (μm) | 19 | 13 | +6.00 (μm) |
| w (μm) | 11 | 15 | -4.00 (μm) |
| $\theta_x$ (°) | -4.4E-03 | 9.0E-03 | -13.4E-03(°) |
| $\theta_y$ (°) | 5.3E-03 | 11.8E-03 | -6.5E-03(°) |
| $\theta_z$ (°) | -1.7E-03 | -7.9E-03 | 6.2E-03(°) |

The difference in predicted and reported "apparent" motions for all implant types is found to be significantly reduced compared to the observed differences with fully frictional interfaces.

Predicted motions and translations of the reference point for both PS and TS (short stem) implanted femurs are observed to be much closer to the measured *in vitro* values for cemented trials. The TS implanted femur with long offset stem is found to exhibit the smallest difference in motion between FE and *in vitro* setups, possibly due to a greater resistance to bending and deformation as a result of presence of a large diameter canal filling stem. It should be noted, however, that the largest component of motion in both studies still varies in direction.

Interestingly, once fully tied interfaces are considered for all implant types investigated the difference between the "apparent" relative motions of the prosthesis to the bone are found to be very small (Figure 9.14). It can also be observed that once the interface is tied relative motions and rotations about the reference point are found to reduce to safer limits, e.g. $< 40 \mu m$.

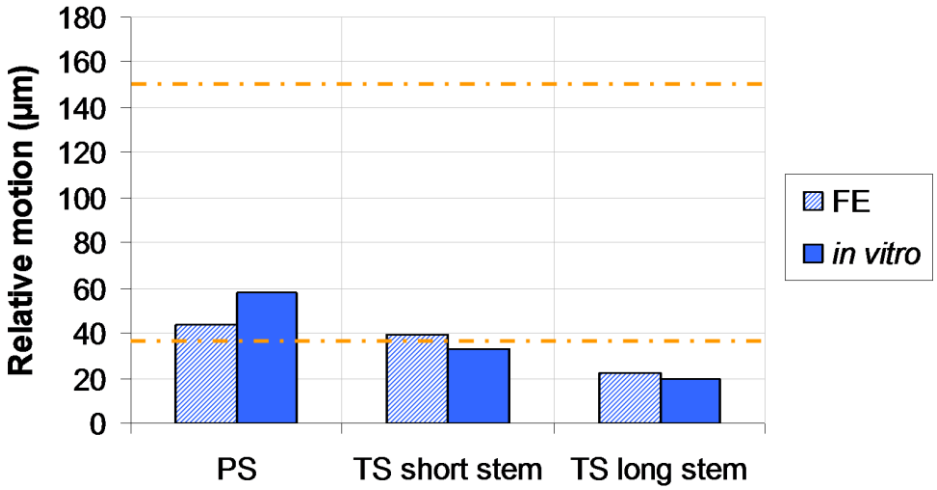


**Figure 9.14:** Comparison of the overall magnitude of relative displacement for both the FE (tied) and in vitro (cemented) setups at 20° flexion. The upper and lower boundaries for fibrous tissue formation are indicated by the dashed orange line.

In this last section, the difference between measured motion of the reference point and the relative motion at the interface was investigated. On the assumption that no interfacial motion should occur in cemented *in vitro* specimens and tied FE models (prior to fatigue or damage) then the motions measured under these interface conditions may reflect contributions from elastic deformation and bending of the femur. Therefore, the true level of relative motion of the implant to the bone without influence from elastic deformations and bending may be approximated by subtracting the values of motion found using tied models from the values found under frictional conditions. Individual components of relative translational motion before and after removal of these contributions are presented in Figure 9.15a and Figure 9.15b respectively.

It can be seen from Figure 9.15b, that after adjusting for deformities such as bending and elastic deformation, considerable relative translational motion is still reported at the reference point in all directions, thus confirming motion does occur between bone and prosthesis for frictional and uncemented cases. Similar trends were observed for both *in vitro* and FE investigations of the PS implanted femur following adjustment (Figure 9.15b), though slight variations exist in the magnitude of motions. Trends with respect to stemmed implants were less obvious.

Due to possible differences in the deformed behaviour of tied and frictional models under loading, this represents only an approximation of the possible factors which may contribute to errors in reported findings.

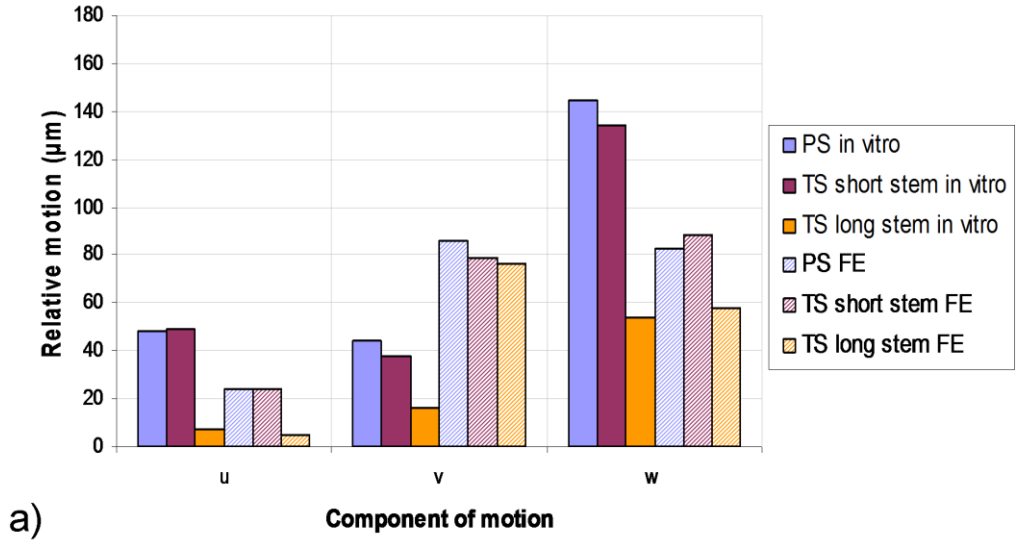


a)

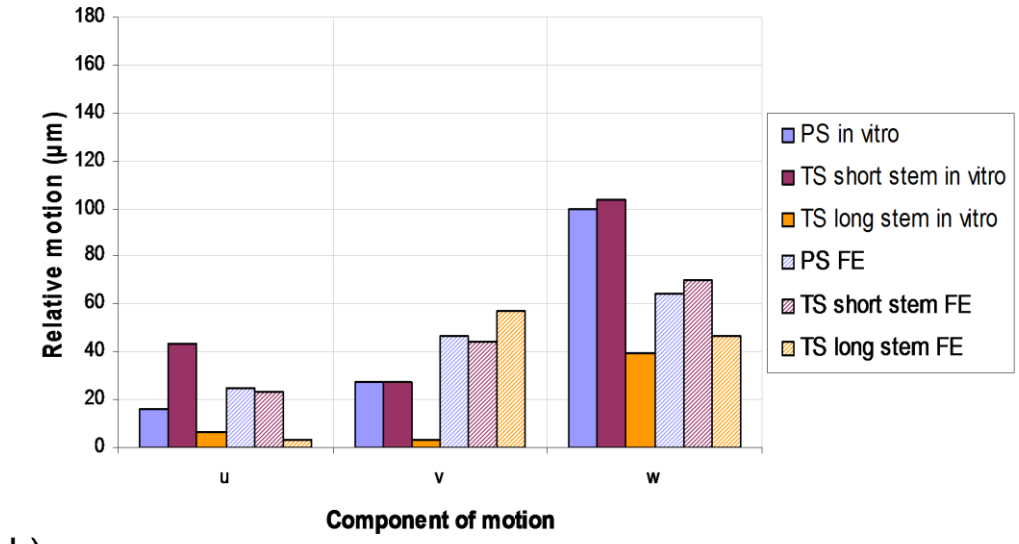


b)

**Figure 9.15:** Comparison of the average individual components of translational motions (u, v, w) a) before and b) after subtraction of contributions due to elastic deformation and bending (as characterised by tied interfaces) for both FE and in vitro setups.

By comparing Figure 9.15a to Figure 9.15b it is apparent that trends with respect to individual components of translational motion vary after removal of contributions

due to elastic deformation and bending, thus highlighting the importance of proper quantification of sources of error prior to establishing inter-implant trends.

On investigation of the "true" predicted relative motion at the interface using contour plots (Figure 9.16), results are observed to be lower again than that predicted about the reference point, typically $< 20\mu m$ on the distal surface, but rising much higher on the anterior and posterior surfaces.

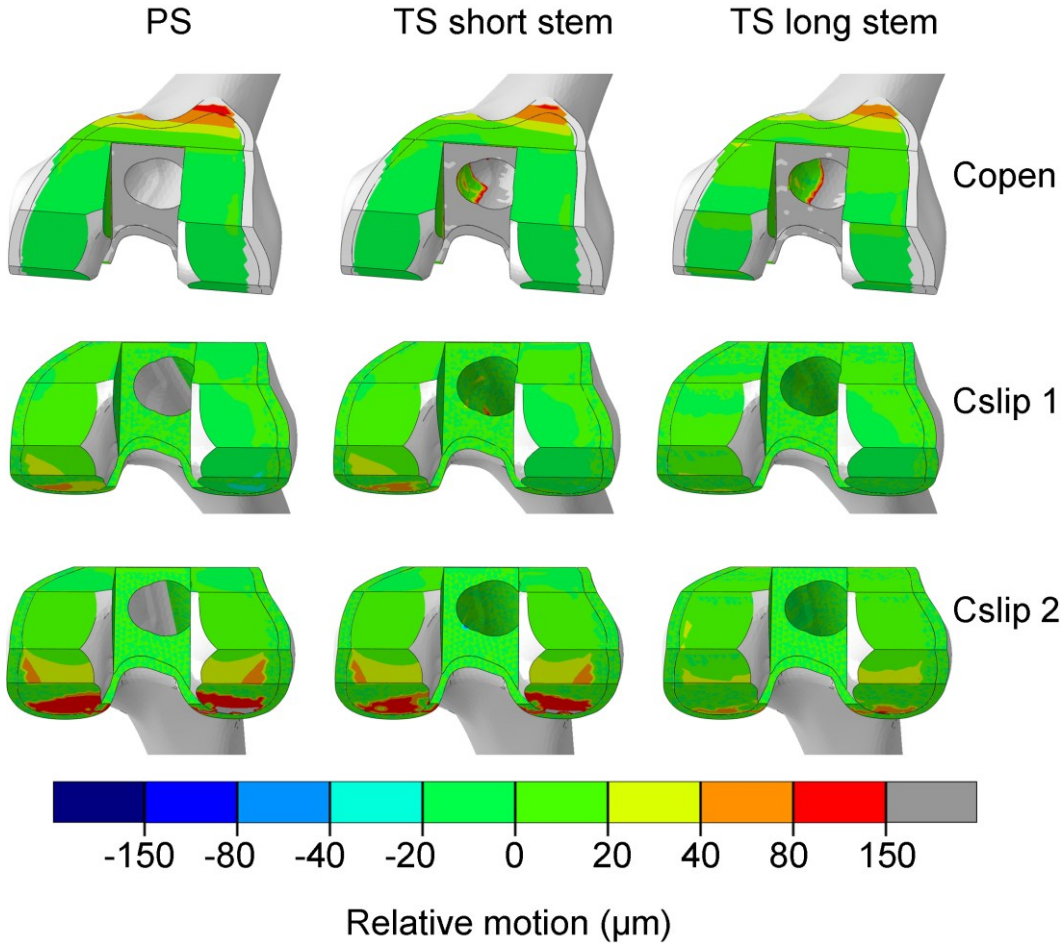


**Figure 9.16:** Femoral component micromotion expressed as contact separation and tangential motion in two orthogonal directions for a PS implanted femur (first column) and a TS implanted femur with short stem (second column) and a TS implanted femur with 4mm laterally offset stem (final column).

The findings from the contour plots support the overall *in vitro* trend presented previously (Chapter VII and Chapter VIII) where addition of a stem served to reduce motion, with the long canal filling stem providing the greatest implant stability.

Interestingly though the pattern and distribution of motion differs significantly from that experienced under more physiological loading conditions, i.e. the region of greatest motion shifts posteriorly in the *in vitro* setup FE models, possibly due to simplified loading conditions.

## IX.4 Discussion

This study detailed the creation and analysis of FE models of the distal femur following implantation with a PS implant, a TS implant with short stem, and a TS implant with 4mm laterally offset long stem, each model incorporated a virtual representation of the micromotion test rig developed in Chapter VIII (this was essential to allow comparison of similar quantities). The two main goals of this study were to predict the relative motion of the implants to the bone in all degrees of freedom about a central reference point and then to examine how this measured behaviour varies from the "true" motion at the interface.

As in the *in vitro* study presented in Chapter VIII, translational and rotational components of relative motion were predicted to be smallest in the TS implant with long offset stem. Differences in PS and TS (short stem) implanted femurs under frictional conditions were very small. The component of rotation found to be smallest in general was $\theta_z$. The percentage reduction in motion observed going from a fully frictional to fully tied interface was found to be similar to *in vitro* conclusions on uncemented and cemented implant motions, as presented in Chapter VIII. The overall trends evident by comparing Figure 9.10 and 9.14 lend support to the idea that comparable implant performances can be achieved without the use of stems provided full fixation of the implant is achieved at the metaphysis.

Comparisons of frictional models with fully tied interface models revealed that motion does occur at between implant and bone, as predicted *in vitro*. However, this investigation also revealed that the *in vitro* setup can be greatly influenced by bending and elastic deformations, despite close positioning of the test rig to interface. In the present study such quantities are estimated to account for readings ranging

from $1\mu m - 39\mu m$ depending on implant and direction of motion. These values are within the range previously reported by Moran (2005) and significantly higher than that observed in the hip (Gilbert et al. 1992, Monti et al. 1999).

It is important to note that no motion is permitted at the interface in tied models, as such relative motion reported in these models represent contributions from bending and deformation and this quantity itself may be an important factor to monitor during long term tests (Cristofolini et al. 2008). Any increase in the combined motion and deformation of the bone-prosthesis assembly may indicate an increased risk of fatigue damage to the underlying cancellous bone structure (Taylor and Tanner 1997).

Predicted (FE) and measured (*in vitro*) translational and rotational relative motions for both frictional (Table 9.2 – 9.4) and tied (Table 9.5 – 9.7) interface conditions were found to be within a reasonable range, however, directional differences between the largest components of motion measured in the *in vitro* experiments and that of the FE models were observed in the present study, as has been the case in similar studies of this nature (Pettersen et al. 2009, Chong et al. 2010). Differences in magnitude of translational and rotational relative motions may be explained by both geometrical differences (e.g. ideal Boolean fit in FE vs. press-fit in the lab) and the range of numerical parameters required during a frictional analysis increase the difficulty associated with accurately predicting exact *in vitro* values. Moreover, based on the findings presented in Appendix C, changes to the frictional coefficient alone can account for a change in relative motion of up to $40\mu m$. To minimise error future tests should closely calibration bone-implant interface frictional properties based on benchmark tests with samples from physical lab specimens of all relevant materials. In addition it must also be considered that a wide array of factors may adversely influence the outcome of experimental tests, e.g. imperfect surgical cuts due to saw blade motion.

Furthermore, it has been suggested that the specified and actual material properties of the sawbones composite femurs may be very different (Clarke et al. 2012), possibly

due to the arrangement of fibers in the short fiber filled epoxy that makes up the hard cortical shell, thus leading to another potential source of variability between the *in vitro* experiments discussed in the previous chapter and the results of the current study. A lower Young's modulus in the experimental study may lead to increased bending, and therefore a reduced interfacial relative motion. It may also heavily influence the predicted contribution of the elastic deformations. As with frictional considerations, future tests should investigate samples from the physical specimens to determine material properties prior to running comparative analyses in FE to help minimise this potential source of variability.

Trends from the investigations of overall magnitudes matched well between FE models and *in vitro* setup at the reference point, both before and after adjusting for elastic deformations. However, motion of the reference point does not reflect the complex behaviour of interface. On investigation of the "true" predicted interfacial motions using contour plots (Figure 9.16), results are observed to be lower again than that predicted about the reference point, typically $< 20\mu m$ on the distal surface, but rising much higher ($80-150\mu m$ on the anterior and posterior surface).This indicates that while *in vitro* investigations using the current DVRT setup may be useful for providing a general comparison of overall component stability, they are not fully able to characterise the complex interactions taking place at the interface. Similar limitations with respect to investigation of motion following THA of the femur and TKA of the tibia have been previously reported (Chong et al. 2010, Tarala et al. 2011).

In conclusion, though translational and rotational relative motions compared well between FE and *in vitro* with minor variations in magnitude and direction, it should also be noted that the relative motion of the reference point was not representative of "true" motion at the interface. However, general trends relating to the overall performance of an implant may still be drawn from such *in vitro* investigations. It is the recommendation of this study that data from this type of experimental setup be used as a calibration step for corresponding FE models, in this manner detailed information on the interfacial behaviour of various implant types can be determined

using the FE model, while overall validity of the model can be assessed by comparing measured trends about the same reference point as the experimental setup.

This chapter has reinforced the importance of accurately modelling physiological loading conditions when analysing a problem of biomechanics in FE, e.g. very different patterns and distributions of motion observed under the simplified loading presented in the current chapter and the resulting motions under the near physiological loading presented in Chapter VII. Equally important is correct modelling of the bone-implant interfaces and implant fit, as evident from the differences in results between the FE and *in vitro* studies. In the next chapter, commonly encountered bone pathologies and conditions are incorporated into the FE models of the distal femur in order to determine how implant failure may be influenced by inclusion of commonly encountered diseases and conditions which affect the structure and material properties of the bone.

# X

# Modularity and Stem Junction Stress

## X.1 Introduction

In the previous chapters, consideration has been given to the influence of internal implant features, implant fit during surgery, the role of accurately modelling the bone-implant interface and the influence of patient specific parameters such as age and osteoporosis. All these factors have been found to influence stresses in the femur and motions at the interface. In almost all cases the distal femur was modelled with a predominantly intact metaphyseal segment. However, during revision surgery poor quality bone stock (van Loon et al. 2000, Completo et al. 2009) acting in combination with large scale bony defects can make successful implantation and long term survival of the prosthesis very challenging.

When faced with poor bone stock in the form of stress shielding or large contained/uncontained condylar defects, surgeons have a limited range of treatment options available based on the severity of the loss encountered. If the bone loss or defect is confined to one region of the femoral condyles and the cortex is largely intact, then treatment with bone cement or tantalum cones may provide sufficient stability to ensure adequate fixation of the femoral component. If the defect is large or uncontained, a greater proportion of bone may need to be removed in order to achieve an adequate level of fixation. It must be noted however, that any bone the surgeon removes during this procedure needs to be replaced in order to maintain the joint line and correct alignment/functionality of the knee joint.

In these more complex cases, surgeons choose between augmentation of the prosthesis and supplementation of remaining viable bone with bone graft. Augmentation of the femoral component involves the attachment of metal blocks to the back of the femoral component, these blocks are precision machined to be compatible with the implant and are selected based on the size of the lost bone. Surgeons can also choose from a number of different bone graft types and techniques to repair defects, such as structural allografts (Ghazavi et al. 1997) or morselised cancellous bone (MCB) grafts. These biological alternatives offer some obvious advantages over simple treatment with metal augments. For example, a well fixed bone graft has the potential to eventually remodel and be fully integrated into the host bone. Bone grafts, however, require an initial period of protection while the graft fully integrates before patients can resume full weight bearing activities (Engh et al. 1997, Ghazavi et al. 1997), otherwise there is a potential risk of graft failure. The treatment method of interest in the current study is repair of bony defects through the use of distal femoral augmentation.

Revision surgery invariably involves modular implants which can be assembled to suite the specific needs of the patient. They also provide the surgeon with a greater level of flexibility at the time of operation should some unexpected issues be encountered. Modularity helps in ensuring an adequate level of fixation is achieved at the bone-implant interface to promote implant stability and long term survival. Modular components, on the other hand, are subject to additional risks and potential hazards not present in their more restrictive non-modular counterparts. The increase in number of junctions and joints per complex implant assembly for example create more potential sites for loosening or failure. A number of recent studies have documented such failures (Issack et al. 2007, Nikolopoulos et al. 2012). In these studies, failures ranged from complications due to loosening of locking screws and femoral stem disengagement (Lim et al. 2001, Issack et al. 2007) to full catastrophic failure of the prosthesis at the stem-implant interface (Nikolopoulos et al. 2012). In each instance failure or fracture of the stem-implant junction was theorised to be as a

result of weak osseous support or loosening of the prosthesis distally combined with a good proximal fitted stem.

Femoral implants must withstand not only compressive axial loading but also rotational and shearing components of load. In implanted femurs with healthy bone stock, load is shared between the femoral component-stem assembly and the bone (Completo et al. 2009). However, in the presence of weak osseous support or where distal loosening of the femoral component has occurred, this load sharing capacity is reduced. In the absence of load sharing, the majority of load is therefore transmitted solely through the femoral component-stem assembly leading to a significant increase in junction stress (Chu et al. 2000).

From the literature, it is clear that there exists a lack of information in relation to factors affecting the survival of these modular prostheses, particularly in the setting of revision TKA or in the presence of defects or bone loss. Therefore, the key aim of this chapter is to determine critical factors which may influence the long term outcome of complex revision scenarios. Of particular interest are the influence of condylar defects, the level of osseous support on the stresses at the junctions of the modular prostheses, and how complex clinical scenarios may influence failure of the modular components.

## X.2 Methods

In this chapter, the previously developed linear (4 node) models of the distal femur, implanted with a TS femoral component and 4mm laterally offset long stem, were modified to investigate factors that influence junction stress. Different levels of bony defect ranging from minor bone loss due to errors in surgical cuts to large scale bony defects developed according to the AORI defect classification system (Engh 2006) were considered as well as osteoporosis of the metaphyseal segment. Table 10.1 provides an overview of all cases investigated in the current study. Cases ‘Control’, ‘Con_tied’, ‘Con_PF’ and ‘Con_DF’ are for the no defect situation; they vary only in the manner in which the bone-implant interface is modelled. All the remaining cases

are related to F2 or F3 type of defects. Additionally, 'Con_OP' incorporates deteriorated elastic properties of the bone, as presented in Figure 10.4 and Table 10.2. Further details for each model are provided in the following sub sections.

**Table 10.1:** Summary of cases considered in this study.

| Model name | Bone-implant interface | Augment size used to treat defect | Metaphyseal fit | Supporting bone removed | Reduced osseous support |
|---|---|---|---|---|---|
| Control | All frictional | N/A | No gap | N/A | N/A |
| Con_tied | All tied | N/A | No gap | N/A | N/A |
| Con_PF | Tied at stem tip | N/A | No gap | N/A | N/A |
| Con_DF | Femoral component tied distally | N/A | No gap | N/A | N/A |
| F2A | All frictional | 15mm medial augment | No gap | N/A | N/A |
| F3 | All frictional | 30mm medial augment | No gap | No, bone as in Figure 10.3a | N/A |
| F3SB | All frictional | 30mm medial augment | No gap | Removed as shown in Figure 10.3b | N/A |
| Con_GAP | All frictional | N/A | 0.5mm gap | N/A | N/A |
| Con_OP | All frictional | N/A | N/A | N/A | Bone properties as in Figure 10.4 and Table 10.2 |

### X.2.1 Incorporation of F2A and F3 condylar defects

As discussed in Chapter II, defects in the distal femur can be categorised into three main classifications (Engh 2006) based on increasing severity and whether they are confined to a single condyle or affect the entire metaphysis. In the current study, the specific defects of interest fall in the F2 and F3 categories (Figure10.1).

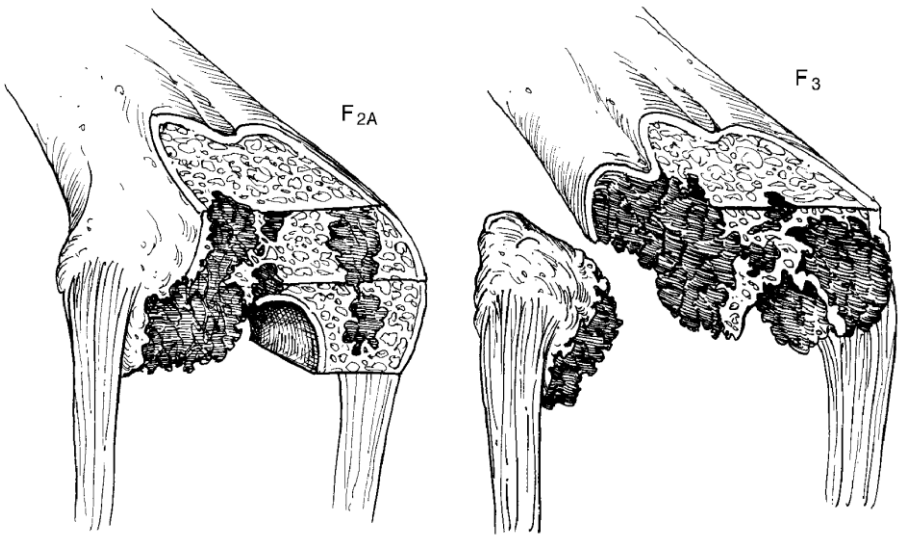


**Figure 10.1:** Femoral defects of increasing severity as characterised by the AORI, reproduced from (Scuderi and Tria 2006).

Modifications to the models to incorporate the desired defects were characterised by removal of bone from the distal femoral condyles, simulating the surgical removal of diseased or damaged tissue in preparation for replacement with prosthesis. Removal of bone was carried out at two different levels depending on the severity of defect to be modelled. To model the F2A defect, bone parallel to the distal surface up to a distance of 15mm in the proximal direction was removed from the medial condyle (Figure 10.2b). In the case of the F3 defect bone was removed to a distance of 30mm (Figure. 10.2c).

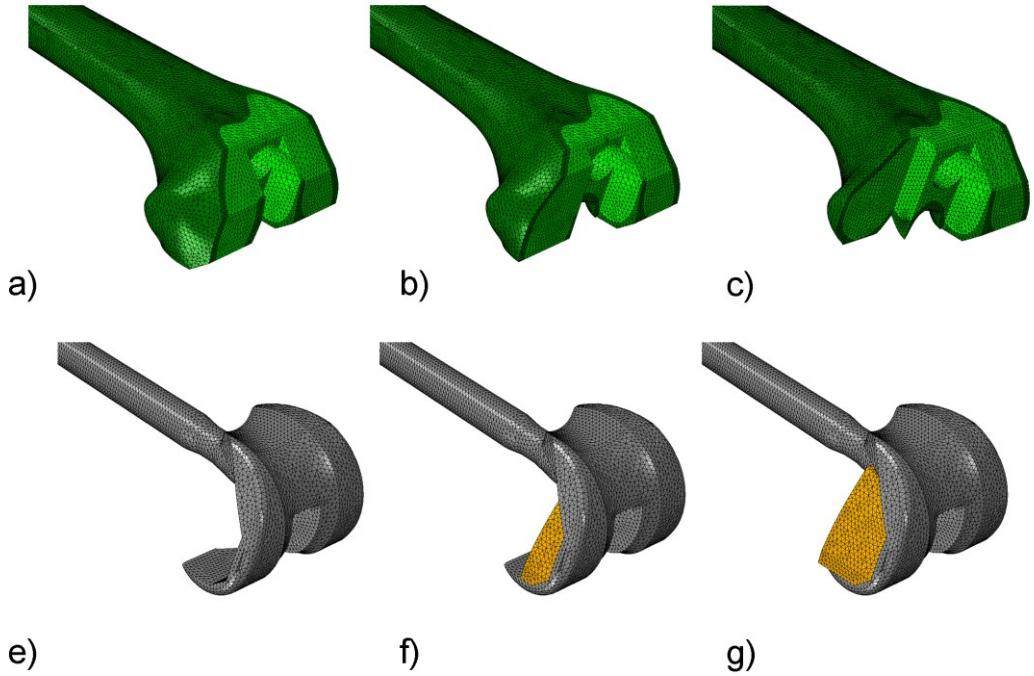


**Figure 10.2:** Mesh view of a) a healthy distal femur, b) a distal femur incorporating F2A defect and c) a distal femur incorporating an F3 condylar defect. Parts e)-f) show the corresponding implants for each model presented in the top row, where relevant the portions of the implant highlighted in orange represent attachment of f) 15mm and g) 30mm distal surface augments to the femoral component.

Two different distal augments 15mm and 30mm made of the same material as the implant were considered. For modelling, these were created using CAD software. The 15mm augment (Figure 10.2f) was based on the largest commercial distal medial femoral augment size produced as part of the Triathlon® series (Stryker, UK). The 30mm augment (Figure 10.2g) also followed the implant's internal contours to ensure compatibility and was created to model an extreme case of bone loss.

### X.2.2 Metaphyseal fit

Changes to metaphyseal fit were introduced to the control model by removal of 0.5mm from the distal surface of the medial femoral condyle. This value was chosen to be within the range of error in cut position possible during operation due to

oscillation of the reciprocal saw blade during the preparation of the femur to receive the femoral component (Otani et al. 1993, Plaskos et al. 2002, Bäthis et al. 2005).

### X.2.3 Supporting bone

The role of supporting bone in stem junction stress was investigated by removing the bone surrounding the junction at the level of the defect (Figure 10.3). This was done in the F3 defect model only as the F2A defect does not reach the level of the implant-stem junction.

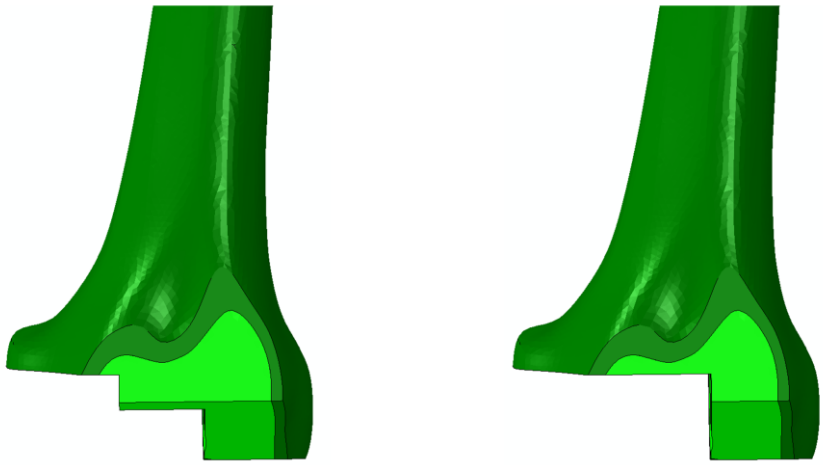


**Figure 10.3:** a) distal femur model incorporating an F3 defect with support at the implant-offset junction and b) distal femur model incorporating an F3 defect with supporting bone removed to the level of the defect.

### X.2.4 Material properties

As in previous chapters, isotropic elastic material properties were applied to cortical ($E = 16700$ N/mm$^2$ and $\nu = 0.3$) and cancellous ($E = 155$ N/mm$^2$ and $\nu = 0.3$) regions of the femur respectively. Similarly values corresponding to cobalt-chromium (CoCr) and titanium (ti-6al-4v) were assigned to implant ($E = 210000$ N/mm$^2$ and $\nu = 0.3$) and stem ($E = 110000$ N/mm$^2$ and $\nu = 0.3$) regions.

### X.2.4.1 Osteoporotic modelling of the femur

Many clinical studies have hypothesised that weak osseous support may have a role to play in failure of the stem-junction (Lim et al. 2001, Issack et al. 2007, Nikolopoulos et al. 2012). To test this hypothesis, extremely osteoporotic properties (Table 10.2) were applied to cancellous and cortical regions of the distal femur. In this instance to reduce model complexity[6], osteoporosis of the distal femur was modelled using regional sectional properties as shown in Figure 10.4. This technique has been previously used in the literature (Shi et al. 2007).

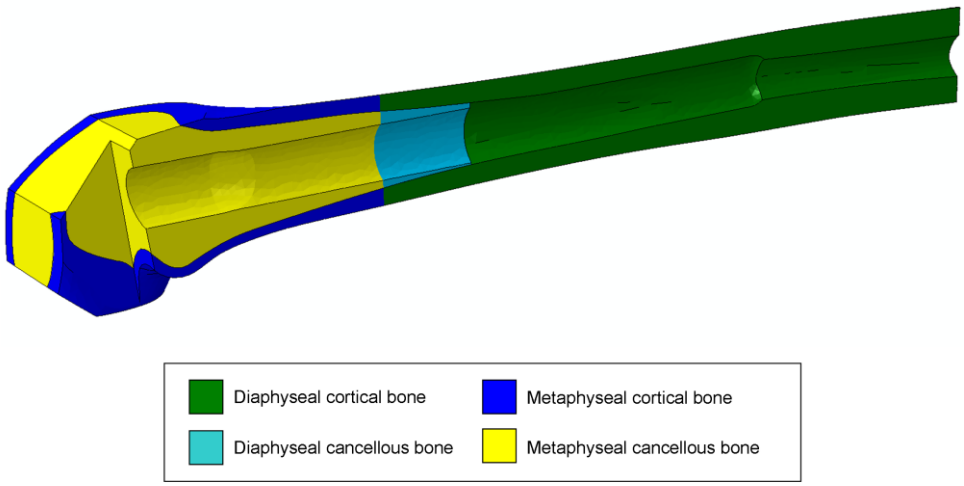


**Figure 10.4:** Sectioned view of the distal femur in the sagittal plane highlighting the different property sections applied to the femur to simulate osteoporosis of the metaphyseal region.

[6] The method used to model osteoporosis previously in Chapter V works well with higher order elements. However, to achieve the same even distribution of material through the thickness with linear elements requires a very high resolution mesh. Additionally, as stress in the femur is not the main focus of this chapter, regional section properties provide the most efficient means by which to incorporate osteoporotic effects at the stem junction.

**Table 10.2:** Material properties for osteoporotic femur model.

| | Young's modulus ($N/mm^2$) | Poisson's ratio (v) |
|---|---|---|
| Diaphyseal cortical bone | 16700 | 0.3 |
| Diaphyseal cancellous bone | 155 | 0.3 |
| Metaphyseal cortical bone | 8000 | 0.3 |
| Metaphyseal cancellous bone | 50 | 0.3 |

### X.2.5 Loading and boundary conditions

Applied loading consisted of six components of force (Fm, Fl, APm, APl, PF and IE) for three different flexion angles (0°, 22° and 48°) during the stance phase of gait for a normal walking cycle. Loading magnitudes and directions were applied as per Chapter IV (Figure 4.6 and Table 4.2). Similarly, the boundary conditions applied in the current chapter consisted of full fixation in all degrees of freedom at the mid-shaft of the femur.

### X.2.6 Interface modelling

In the current study where appropriate, the bone-implant interface was modelled using a combination of frictional and tied constraints.

The implant-augment interface in all instances was modelled as fully tied. Modular junctions, on the other hand, were constrained as shown in Figure 10.5; tied constraints were applied at the screw thread interface of both the stem and offset adapter, while frictional interfaces ($\mu$ = 0.3) were assumed at all other contacting faces. In this manner, contact separation of the implant-offset and offset-stem junction faces was permitted but no relative motion could occur at the threaded portion.

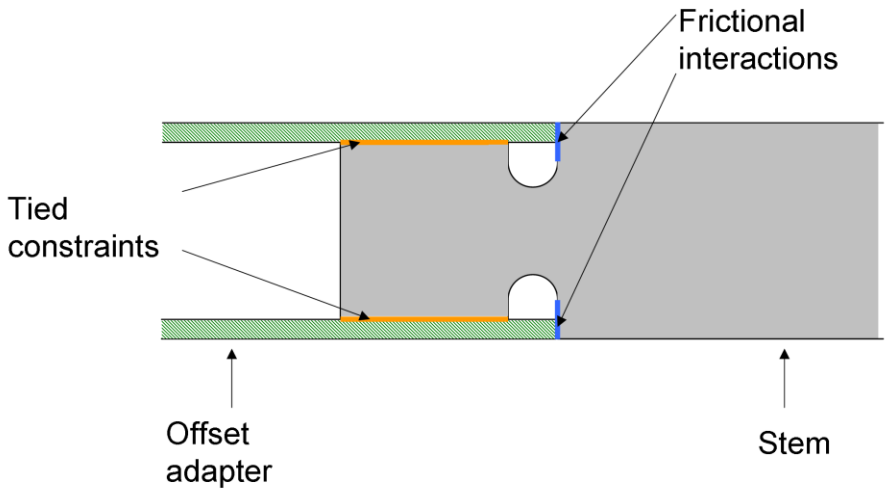


**Figure 10.5:** Illustration of interface contact definitions. Blue lines represent where friction contact conditions were applied to the faces of the stem and offset adapter, orange lines on the other hand indicate where both parts have been fully fixed at the interface modelling the fixation achieved in reality by the screw threads.

The bone-implant interfaces were modelled as tied and/or frictional depending on the cases considered as discussed later.

### X.2.7 Mesh convergence study

Due to the major role of contact in these analyses, linear tetrahedral elements were employed as in the previous chapter. In Chapter VII and IX, the region of interest was primarily the interface between bone and implant, whereas the region of interest in this chapter is largely confined to the radial undercut, where the threaded section of the stem meets the main stem body. This shift in focus from investigation of motion at the bone-implant interface to the investigation of changes in stress at the prosthesis-prosthesis interface due to various defects requires that convergence checks be carried out to determine if the mesh remains valid for this purpose. Referring to Figure 10.6, a series of mesh refinements were carried out on the radial undercut while all other parameters of the model were kept constant. Further details including average element edge length can be found in Table 10.3. The solution for the purposes of these analyses was considered as converged when the difference in all components of stress between successive refinements of the mesh dropped below

2%. These studies indicate that the previously used average element size of 0.9mm for the radial undercut is not suitable for stress prediction at the prosthesis-prosthesis interface. Based on this convergence study an average element edge size of 0.2mm was used.

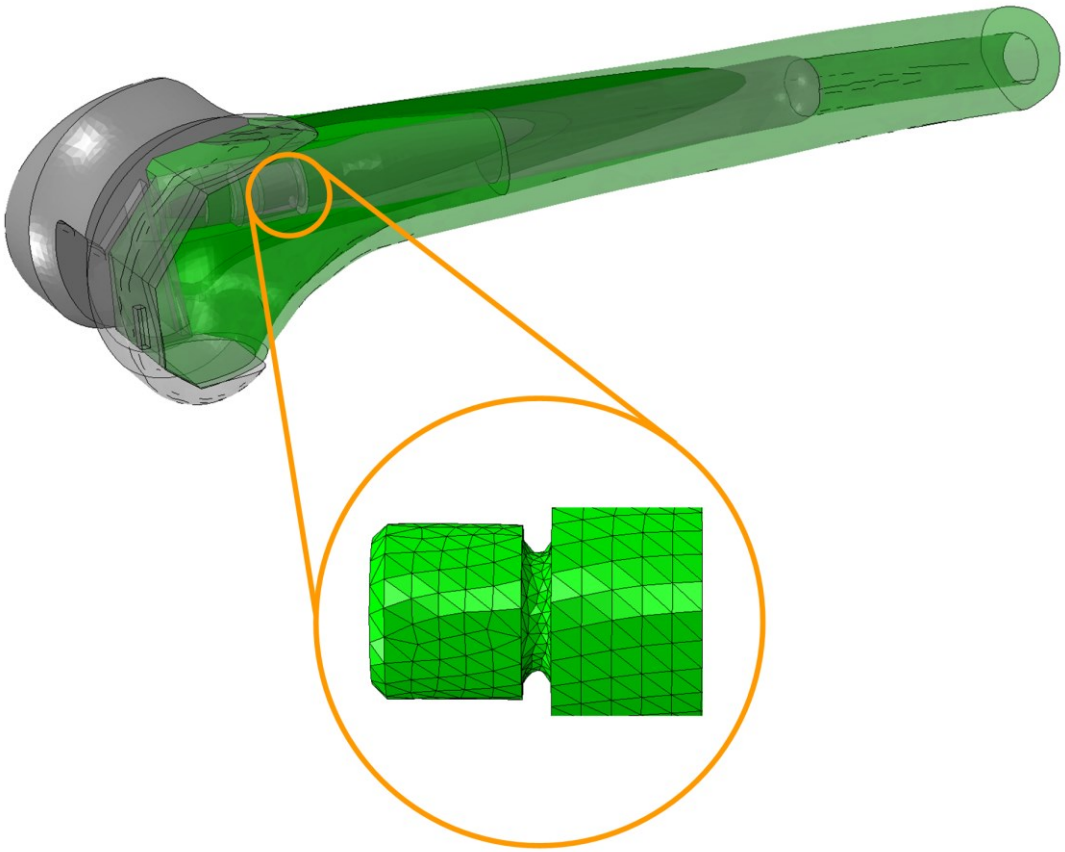

a)

b)

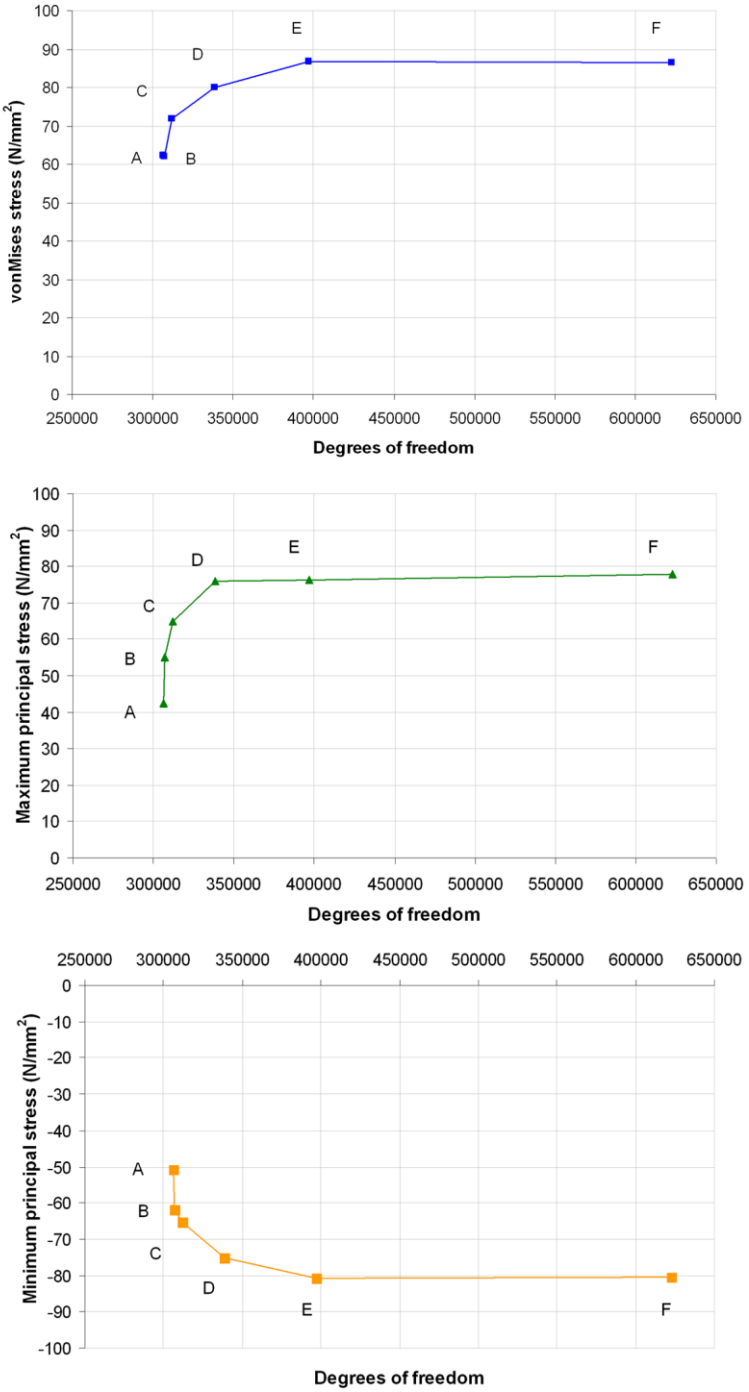


**Figure 10.6:** a) Image highlighting region of interest (stem junction) and b) convergence study graphs showing the values of peak stress with increasing level of mesh refinement at the stem junction (A-F) as detailed in Table 10.3.

**Table 10.3:** Stem junction mesh convergence data.

| | Average element size (mm) | Degrees of freedom | Number of nodes | von Mises stress ($N/mm^2$) | Maximum principal stress ($N/mm^2$) | Minimum principal stress ($N/mm^2$) |
|---|---|---|---|---|---|---|
| A | 2 | 306411 | 127637 | 62.1704 | 42.3784 | -50.8442 |
| B | 0.9 | 307005 | 127833 | 62.0593 | 55.0914 | -61.9236 |
| C | 0.5 | 312195 | 129676 | 71.8325 | 65.026 | -65.4336 |
| D | 0.3 | 338598 | 138882 | 80.047 | 76.0376 | -75.0604 |
| E | 0.2 | 397179 | 159052 | 86.7081 | 76.1648 | -80.6794 |
| F | 0.1 | 622707 | 236660 | 86.4729 | 77.7269 | -80.5109 |

## X.3 Results

The peak von Mises stress in the region of interest (stem junction) was extracted for each of the three flexion angles investigated (0°, 22° and 48°) for all the cases summarised in Table 10.1. Peak contact separation at the interfaces of the stem junction was also recorded for each case considered.

### X.3.1 Effect of interface conditions

The first set of models investigated the influence of bone-implant interface conditions. Figure 10.7 shows the peak von Mises stress at the stem junction for different interface conditions. It is apparent that the junction stresses increase with flexion angle. The ‘Con_tied’ and ‘Con_DF’ cases give similar von Mises stresses. Similarly the stresses from ‘Control’ and ‘Con_PF’ cases are comparable. The distally tied and the fully tied bone-implant interface optimise load sharing between the modular components and the bone, so as to reduce the load on the stem junction

and decrease the risk of fatigue failure. Largely frictional interfaces ('Con_PF' and 'Control') result in the implant carrying larger loads and thereby larger stresses at the junction. Similar trends were observed with regard to opening at the contact surfaces as shown in Figure 10.8: smaller peak contact opening with tied conditions and larger with frictional interfaces.

### X.3.2 Influence of defect size

The influence of bone loss as characterised by an F2A and F3 distal femoral condylar defects on peak von Mises junction stresses are shown in Figure 10.9. These are all cases characterised by frictional interfaces. It is interesting to note that 'Control' (no defect and no gap), 'F2A' (small defect and no gap) and 'Con_GAP' (no defect and a small gap) give almost identical results. The 'F3' case (30mm defect) showed a relative increase of 58% in comparison to frictional models without a defect for the 48º flexion angle. Comparing models 'F3' and 'F3SB' (without and with removal of supporting bone Figure 10.3b) shows that the latter leads to a 13% higher stress at the stem junction for the 48° flexion angle. Peak contact separate (Figure 10.10) shows trends which are similar to those of peak junction stress shown in Figure 10.9.

### X.3.3 Influence of bone properties

The influence of osteoporotic bone properties characterised by a reduction in Young's moduli of both cancellous and cortical bone regions in the distal femur on peak von Mises junction stress is shown in Figure 10.11. The figure shows that stem junction stresses increase significantly with osteoporosis for all flexion angles. Osteoporotic material properties also result in an increase in peak contact separation as shown in Figure 10.12.

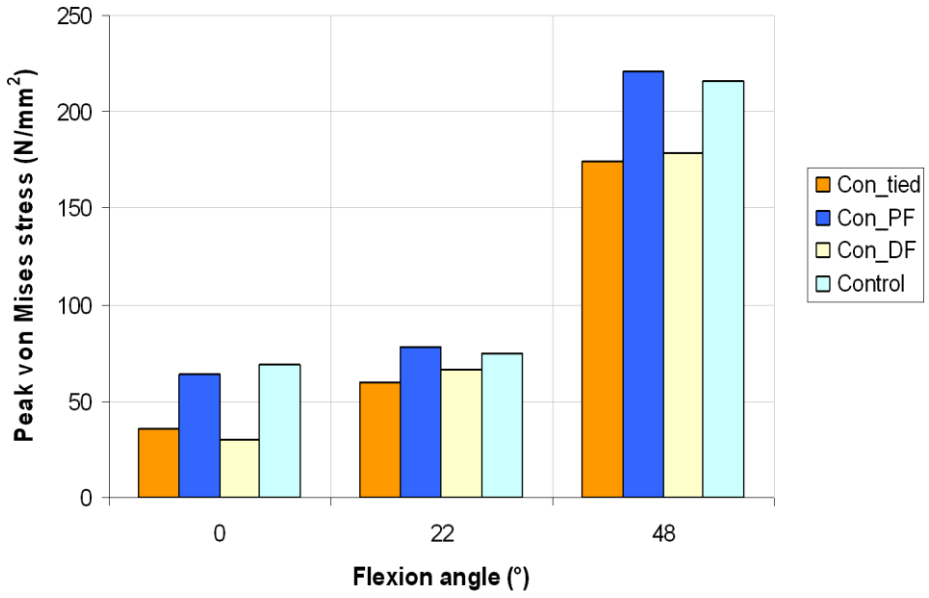


**Figure 10.7:** The value of peak von Mises stress at the stem junction for different interface conditions in no defect cases.

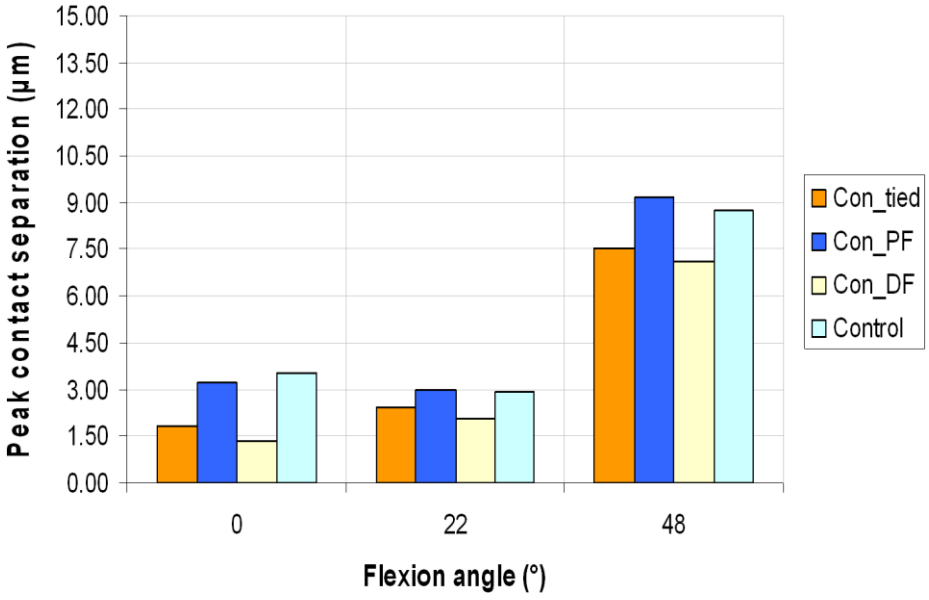


**Figure 10.8:** The value of peak contact opening at the stem junction for different interface conditions.

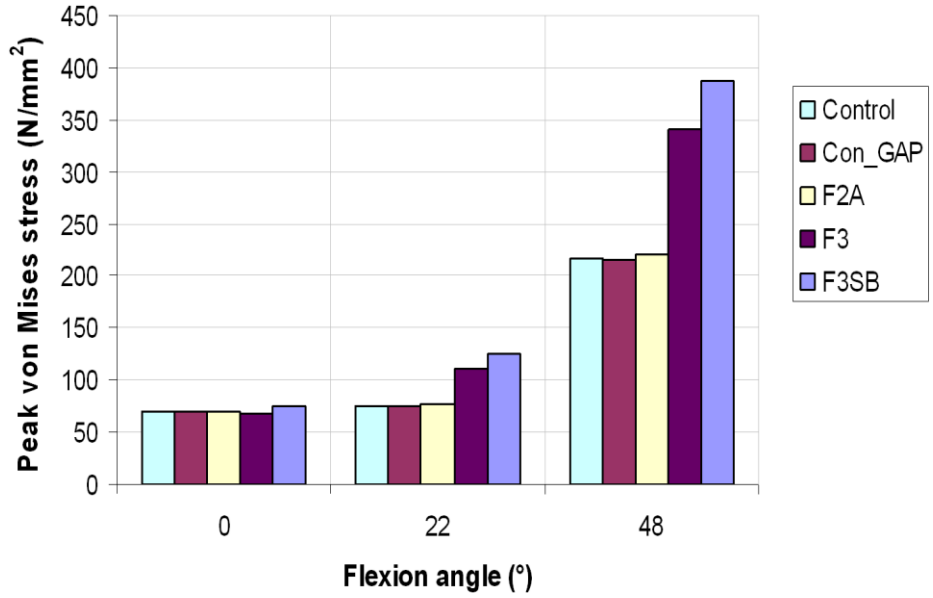


**Figure 10.9:** The value of peak von Mises stress in the stem junction of increasing size of condylar defect.

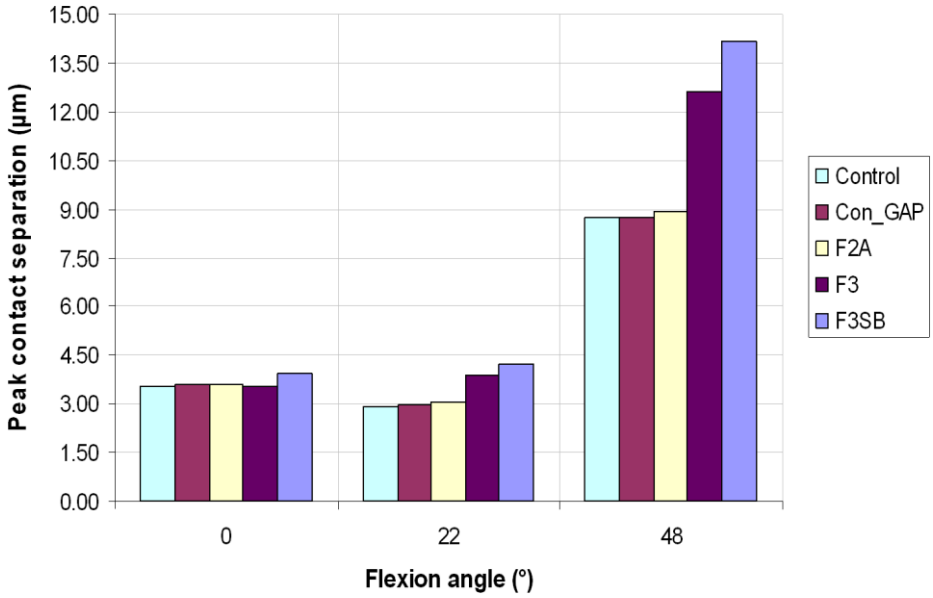


**Figure 10.10:** The value of peak contact opening at the stem junction for different sizes of condylar defects.

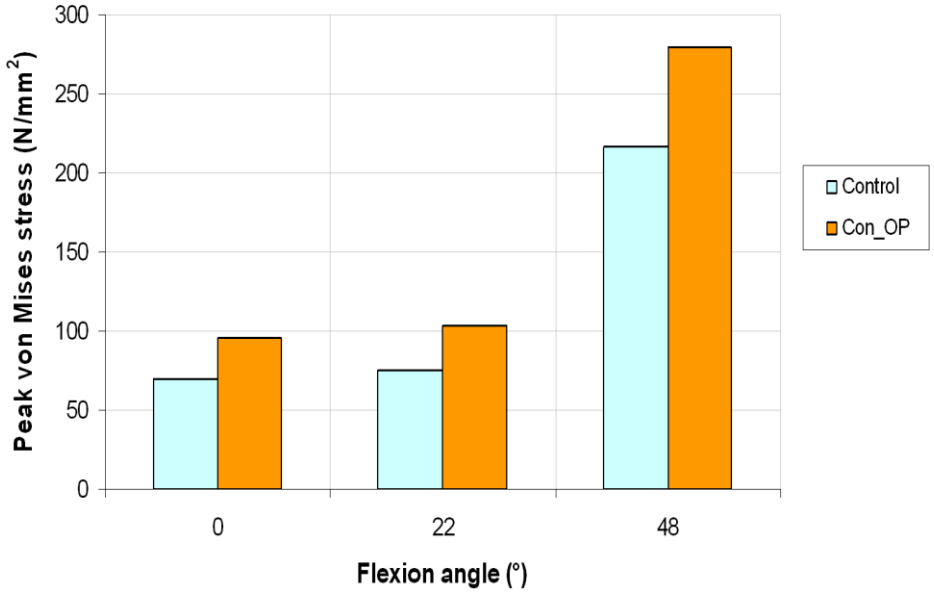


**Figure 10.11:** The value of peak von Mises stress in the stem junction for different levels of osseous support.

.

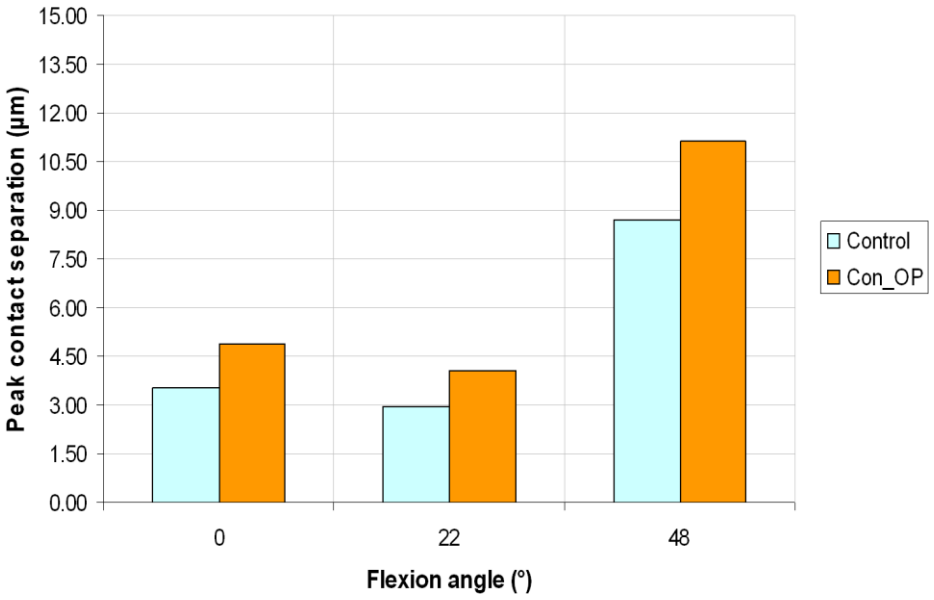


**Figure 10.12:** The value of peak contact opening at the stem junction interface for different levels of osseous support.

### X.3.4 Calculation of static safety factor

A safety factor ($n_f$) against static failure (Chu et al. 2000, Budynas and Nisbett 2007) was evaluated for each case as a ratio of the yield strength of the titanium (ti-6al-4v) stem ($S_y$) and the peak von Mises stress ($\sigma_{von}$) computed at the junction as:

$$n_f = \frac{S_y}{\sigma_{von}} \tag{10.1}$$

The calculated values for each case are given in Table 10.4.

**Table 10.4:** Calculated factor of safety for each model at 48° flexion. Yield strength of titanium ($S_y$ = 800 N/mm$^2$).

| Model name | Peak von Mises stress, $\sigma_{von}$ (N/mm$^2$) | Factor of safety, $n_f$ |
|---|---|---|
| Con_tied | 175 | 4.6 |
| Con_PF | 221 | 3.6 |
| Con_DF | 179 | 4.5 |
| Control | 216 | 3.7 |
| Con_GAP | 216 | 3.7 |
| F2A | 221 | 3.6 |
| F3 | 341 | 2.3 |
| F3SB | 387 | 2.1 |
| Con_OP | 279 | 2.9 |

From Table 10.4 it can be seen that the most significant reduction in factor of safety occurs due to a combination of frictional interface, large condylar defect and lack of supporting bone as seen in F3SB.

## X.4 Discussion

In this chapter, key factors affecting the long term outcome of complex clinical cases were investigated for both healthy and diseased bony geometry, implanted with a modular revision femoral component which employed a 4mm laterally offset diaphyseal engaging long stem. Inclusion of a 4mm lateral offset is often necessary to account for variations in the femoral shaft curvature (Fehring 2005, Brilhault and Ries 2012). This particular implant type is designed to share the load between the distal surfaces of the femur and the femoral shaft surrounding the stem. It also serves the purpose of protecting the distal segment from over loading in situations where damaged or diseased bone has been treated with bone grafts, until remodelling occurs and the graft is fully incorporated into the host bone.

The use of modular components in revision total knee arthroplasty has increased in popularity in recent years[7]. Part of this popularity can be attributed to the intra operative flexibility these components afford the surgeon for the variable range of cases encountered. However, a few studies have raised concerns, suggesting potential links between component modularity and fatigue failure of the prosthesis (Bobyn et al. 1994, Westrich et al. 1997). At high flexion angles the stem experiences stresses due to bending and axial forces, which lead to separation at the implant interfaces and stresses at modular junction. It is apparent that the load sharing between the bone and prosthetic components reduces when interfaces are not tied resulting in the prosthesis carrying higher stresses. The presence of defects and deteriorated bone quality also affects load sharing, with the implant carrying a larger load. The results obtained in this study support the above mechanical considerations and quantify the effect a range of parameters have on junction stress and contact separation.

According to several recent clinical case studies (Lim et al. 2001, Issack et al. 2007, Nikolopoulos et al. 2012), aseptic loosening of the femoral component combined with distal bone loss due to prosthesis induced stress shielding can leave the stem junction exposed to the full load crossing the knee joint. As these junctions are

[7] This is readily apparent from the majority of major orthopaedic implant manufacturing companies now offering modular solutions in their revision knee arthroplasty product lines.

designed to carry only a portion of the total joint reaction load in combination with the bone (Chu et al. 2000), this can lead to catastrophic failure of the modular prosthesis at its weakest point (i.e. the stem junction), as observed by (Lim et al. 2001, Issack et al. 2007, Nikolopoulos et al. 2012). The initial phase of this study employed the healthy distal femur model (Figure 10.1a) subject to four different interface conditions. The interfaces modelled as frictional allow motion which may occur in the absence of osseointegration or as a result of loosening.

Alterations to the bone-implant interface were found to significantly influence stem junction stress. Going from an all frictional bone-implant interface ('Control') to a fully bonded interface ('Con_tied') greatly reduced stem junction stress, highlighting the importance of osseointegration of the prosthesis (Figure 10.7). On average, distally tied components with frictional stems ('Con_DF') also presented lower levels of junction stress than the all frictional models, though to a lesser extent than the fully bonded models. Additionally, motion of the stem tip in distally fixed components has been indicated as a potential cause for end of stem pain. Proximal fixation on the other hand was found to result in a slight increase in junction stress relative to the fully frictional model (in flexion). These findings are in line with clinical conclusions that loss of metaphyseal fixation combined with a strong proximal fix of the stem can lead to greater proportion of the load being transmitted through the stem junction.

The role of metaphyseal defects in stem junction stress was also investigated in this chapter. Three types of defect were compared, ranging from a simple 0.5 mm surgical error due to saw blade oscillation to F2A and F3 condylar defects based on the AORI classification system (Engh 2006). The surgical error was left untreated ('Con_GAP'), while both defects (F2A and F3) were repaired with correctly sized medial distal femoral augments. Defect size was found to have little influence on peak stresses for the case of 0° flexion. In flexion the differences between these models became more apparent. On average, the saw blade induced error caused a relatively small change in stress (0.5 %) in comparison to no defect ('Control'), similarly the F2A defect resulted in an average increase of only 1.5% over the course

of the loading cycle. The large F3 defect on the other hand showed a significant increase in stem junction stress (average of 35% over the three load steps). Comparing peak values from cases 'F3' and 'F3SB' at 48° flexion shows that when this supporting bone is removed stem junction stress increases on average by 12.4% with the overall average increase relative to the 'Control' model being 52.3%. It is therefore apparent that size of defect is an important factor particularly when it passes the depth of the femoral box and approaches the level of the modular junction.

Osseous support has been suggested as one of the key factors linked to failure of modular components, in combination with loss of metaphyseal fix (Lim et al. 2001, Issack et al. 2007, Nikolopoulos et al. 2012). In a recent retrieval study, Issack et al. (2007) reported two cases of failure at the modular taper lock of constrained condylar prostheses with large diameter stems and distal femoral augments (Optetrak, Exactech, Gainesville, Florida ). Based on the evidence in both cases, failure at the modular junction was attributed to aseptic loosening of the femoral component distally in combination with a weakening of osseous support as suggested by the apparent bone loss under the implants visible from patient radiographs. Similarly, Nikolopoulos et al. (2012) reported a single case of modular junction failure in a cemented stemmed revision prosthesis (P.F.C. Sigma TC3, DePuy Inc., Warsaw, IN ) attributed to loss of fixation through poor cementing of the prosthesis and a lack of cancellous bone support at the time the of revision implantation.

In this chapter, loss of osseous support was modelled at two levels: firstly the role of supporting bone in large defects ('F3SB') was addressed (Figure 10.9 and 10.10) and secondly the influence of osteoporotic or "weak osseous" support was examined ('Con_OP') in the absence of any defects. Results from these investigations indicate that supporting bone particularly in large defects helps to protect the junction from stress. Comparisons of 'Con_OP' with 'Control' also revealed that osteoporotic bone was one of the main contributors to stem junction stress with an average increase of 35.4%. The findings of the current study confirm that deterioration of distal femoral material properties can contribute to significant increases in load transmitted through

the junctions of modular components, thereby increasing the risk of modular component failure.

It is important to state that there are reasons other than mechanical which can cause failure of the junction. These include poor design of implants, defects in the manufacturing process and biological reactions to the prosthesis. Surgical errors or poor choice of implants can also result in failure.

High stresses due to loss of load sharing at the bone implant interface not only increase the risk of cumulative fatigue damage, but may also increase the risk of fretting/ wear due to the repeated opening and closing of contact surfaces at the interface of modular components as observed in all models in the current study. Opening and closing of contact surfaces may also pose an increased risk of corrosion at the modular junction due to inflow of biological fluids (Chu et al. 2000, Issack et al. 2007).

One limitation of the current study is that it focused on only one particular type of modular junction characterised by a screw thread connection, further research should be conducted to validate these conclusions for a wider range of implants, modular connection types and stem geometries.

In conclusion, several different factors were found to dramatically increase the magnitude of stem junction stress. Consider the most extreme load case of 48° flexion, based on the calculated factor of safety against static fatigue failure presented in Table 10.4, the greatest risk of modular component failure is found to be as a result of a large femoral defect with loss of fixation and lack of supporting bone as indicated by its low factor of safety ($n_f = 2.1$), followed by the same defect with supporting bone. The next significant factor identified by these calculations was poor bone quality due to osteoporosis ($n_f = 2.9$). Less significant factors were proximal fixation of the prosthesis and incorporation of F2A defects, where both models were found to be within 2% of the 'Control' value. Opening at the contact interface followed similar trends, with peak values of approximately 14μm being observed in

'F3SB' case, with other cases having values in the range of 6.4µm to 12.5µm (as shown in Figure 10.8, 10.10 and 10.12). It must be noted however, that the 30mm F3 defect modelled in this study is somewhat of an extreme case. In reality such a large condylar defect would likely lead to loss of the MCL attachment site and surgeons may therefore opt to go straight to a distal femoral replacement with more constrained hinge type prostheses. Taking this factor into consideration would mean that the most clinically significant increase in stem junction stress was observed in the loose osteoporotic model. This conclusion is consistent with retrieval analysis conduction on failed modular components (Lim et al. 2001, Issack et al. 2007, Nikolopoulos et al. 2012).

In the current study, increased risk of modular component failure was indicated through a calculated factor of safety under static loading conditions, however, the knee joint undergoes cyclical loading as a result of different daily activities such as walking and ascending/descending stairs. In reality, these junctions are likely to fail under much lower forces as a result of fatigue due to the alternating stress caused by changes in direction and magnitude of loading during gait. This suggests the calculated safety factors presented here may be conservative. It has already been stated that opening and closing of the modular interfaces exposes these connections to bodily fluids and increases the risk of corrosive failure (Chu et al. 2000, Gill et al. 2012), however, these repetitive motions at contacting surfaces can also lead to a type of wear known as "fretting" (Baptista et al. 2007, Fadag et al. 2008). This process not only degrades the mechanical fixation of the implant assembly over time, but may also contribute to further weakening of the surrounding bone as a result of metal debris from the junction initiating particle induced osteolysis, as observed clinically (Nikolopoulos et al. 2012). Each of these factors potentially increases the likelihood of modular junction failure.

Based on the findings of this study, it is recommended that use of modular long stemmed prosthesis should be carried out with caution and reviewed on a case by case basis. This study has found that good metaphyseal fit aids in the protection of modular component junctions against fatigue through load sharing with the femur, as

identified by Table 10.4 (fully tied has highest safety factor). Particularly at risk patients e.g. patients with condylar defects or severe osteoporosis of the distal femur, however, have an extremely reduced load sharing capacity. In these situations, it is therefore suggested that a non-modular approach be adopted or if necessary a complete distal femoral replacement so as to reduce the risk of component failure and the need for future “re-revisions”.

# XI

# Conclusions & Recommendations

This thesis has investigated the mechanical environment in the distal femur following primary and revision total knee arthroplasty using both numerical and experimental techniques. The particular focus of this research was on to the role of component design and how this influences internal stresses and relative motions at the bone-prosthesis interface. This study also incorporated variable bone properties through the cortical thickness of the FE models for the purpose of simulating the effects of both age and osteoporosis on the femur pre- and post-implantation. Furthermore, FE models of the distal femur incorporating F2A and F3 femoral defects were developed to investigate how complex clinical scenarios may influence failure of modular components.

The following sections detail the key conclusions which can be drawn from this work as well as a number of relevant clinical implications. Recommendations for the direction of future investigations are also given, and the extension of the presented modelling techniques and *in vitro* methods to the wider field of biomechanics considered.

## XI.1 Summary of findings

### XI.1.1 Stress distribution and the influence of internal implant features

Both the hip and knee joints experience stress shielding following joint arthroplasty. In this study, the mechanisms at work in relation to stress shielding following TKA

were closely examined. Based on the findings presented in Chapter IV, it is suggested that post-implantation stress shielding occurs in the distal femur as a result of the joint contact force being redistributed over a greater surface area, leading to a removal of the concentrated joint contact forces (stress bulbs). This is particularly noticeable in flexion.

Since internal stresses must be in equilibrium with externally applied loads, shielding in some regions will lead to an increase in stress in other regions. In this study, it was observed that the implant, in some respects, serves as a bridge spanning the anteroposterior length of the femur and transmitting the joint contact forces to the cortex immediately above the implant. Stress shielding for both cruciate retaining (CR) and posterior stabilising (PS) implant types was found to increase with increasing flexion angle and changing load direction. This indicates the importance of testing the functionally of implants over a wide range of angles and loading conditions, and also lends support to the argument that femoral components may fail in flexion due to increases in periprosthetic stress.

Based on the investigations conducted in Chapter IV, the overall magnitude of stress shielding experienced by the femur was observed to be independent of the internal implant features (e.g. pegs or box). On the other hand, internal implant features were found to influence the pattern and magnitude of stress concentrations following implantation. CR implants induced stress at the tip of the pegs, and PS implants at the corners of the femoral box cuts. Differences in localised stress concentrations become more important as secondary conditions such as osteoporosis become established and enhance the fracture risk around the prosthesis. Furthermore, as the box in the PS implant spans almost the entire anterior-posterior region, stress concentrations accompanied by bone loss due to stress shielding may potentially lead to a more complex fracture pattern than a CR implant.

### XI.1.2 Conclusions on incorporation of age related changes

In this study, the novel application of temperature dependent material properties as an artifice for modelling inhomogeneity and geometrical changes to the femur was considered. Models representative of both young and old patients for healthy and osteoporotic conditions were developed.

Contrary to some previous studies (Anderson 2010, Zdero et al. 2010), age related changes to the femur were found to have a considerable impact on periprosthetic stress in the cortex of both intact and implanted femurs; on average, increases of up to 15% were observed. This finding in particular, may have serious implications with respect to periprosthetic fracture risk following TKA in elderly patients, where the cortical bone structure may be further compromised by implant induced stress shielding. Endosteal thinning or trabecularisation of the endosteal surface was also observed to result in a marked increase in periprosthetic stress (26%). It must be noted, however, that the most significant increase in stress and strain was observed in models representative of older patients with osteoporosis (60%), e.g. models which incorporated both elderly patient material properties and severe thinning of the cortex.

These findings underscore the need to carefully consider implant choices and manner of fixation in patients with poor bone quality. The presented method for creation of models which incorporate the effects of ageing and osteoporosis is seen to allow rapid consideration of multiple clinical scenarios (e.g. young, old and osteoporotic patients) using the same model geometry by simply adjusting the relationship of temperature to Young's modulus. Furthermore, by comparing multiple clinical scenarios using the same core model and geometry, the influence of key parameters can be individually examined.

In Chapter VI, the use of a cemented stem as a means to reduce periprosthetic stress in the old osteoporotic femur was investigated. This study found that the reduction in stress above the implant was related to the length of stem used. A short cemented stem (50mm) caused a reduction of approximately 10% while longer stems (75mm

and 100mm) were seen to result in reductions of 26-29%. The reduction resulting from both the medium and long stems brings the periprosthetic stress close to that experienced by the older patients with healthy bone geometry (OH model from Chapter V).

### XI.1.3 Motion at the interface and considerations of fit

In Chapter VII, the role of internal implant features on relative motion at the bone prosthesis interface was assessed. These investigations revealed comparable peak motions for both CR and PS implanted femurs. Motions of $< 40 \mu m$ were observed at the lower flexion angles, however, at 48° flexion small regions of motion on the anterior chamfer (for the CR implanted femur) and the distal surface (for the PS implanted femur) were found to approach the limits for fibrous tissue formation.

Interestingly, it was found that peak interfacial motions acted across a larger surface area in PS implanted scenarios, and may therefore present a greater risk of loosening. Moreover, this study also revealed PS implanted femurs to be more sensitive to imperfect femoral bone cuts than CR implanted femurs. These findings tend to favour the use of internal implant features such as femoral pegs over intercondylar boxes, where possible, as the pegs may provide a better anchorage against translational and rotational motions at the interface and have a more favourable local stress distribution.

In Chapter VII, three dimensional models of the distal femur incorporating short and long stems were created, with the goal of addressing the role of femoral stems in component stability under normal and loose fit conditions. The addition of stems, in general, served to reduce the levels of motion at the bone-implant interface. The addition of a long diaphyseal engaging stem was found to significantly reduce interfacial motions, and was also observed to be less sensitive to errors in femoral bone cuts. However, it must be noted that this type of stem is harder to fit in practice, requires removal of more bone and is known to have less desirable stress distribution characteristics. Fully frictional short stem, on the other hand, were observed to only

marginally reduces motion compared to a fully frictional PS and are more sensitive to surgical cut errors.

Similar to the findings on stress shielding (Chapter IV), interfacial motions (Chapter VII models) were found to increase with increasing flexion angle and changing load direction. Reinforcing the importance of testing the functionally of implants over a wide range of flexion angles and conditions.

### XI.1.4 Considerations for combined FE and in-vitro investigations of motion

Relative motion of the implant to the bone for three different implant types was investigated, both *in vitro* (Chapter VIII) and through the use of matching FE models (Chapter IX). In the experimental portion of this study (Chapter VIII), it was observed that errors in recorded motion increased significantly with increased distance between attachment site of the micromotion rig and the distal surface of the femur. Care must be taken to ensure this distance and thus system error is minimized to ensure accuracy of results.

The results from the *in vitro* investigations suggest that in uncemented reconstructions, stemmed implants perform better than stemless implants, with the long offset stem seen to provide the greatest resistance to relative motion. However, it was found that once cemented all implants with and without stems had comparable levels of relative motion. These findings indicate that the use of stems provides no obvious advantage for cemented implants unless there is a need to bypass a condylar defect.

The results presented in Chapter IX contributed two further key pieces of information regarding the *in vitr*o setup. First and most importantly, these models proved that motion does occur at the interface in uncemented investigations and secondly, it is estimated that elastic deformations may contribute significantly to errors in measured relative motions (up to 40μm in this study).

It was found that while global trends between predicted and measured results (about the central reference point) showed good agreement (e.g. Figure 9.10 and 9.14), these motions did not correlate well with the motion observed at the interface using the FE model. This indicates that the multi-planar contact surface behaviour cannot be adequately characterised by a single point. As such, this kind of *in vitro* setup should be used for the purposes of discerning global trends, which can then be used in the calibration of FE models to provide more detailed information on the pattern and distribution of motions at the interface.

Motion at the interface has been observed numerically under both physiological loading conditions (Chapter VII) and loading conditions representative of the *in vitro* experiments (Chapter IX). Though similar trends were observed in both cases with respect to the global contribution of stems to femoral component stability, it must be noted that the magnitude and distribution of peak interface motions varied considerably between the simplified and physiological force setups. This finding has important implications for the design of *in vitro* measurement systems.

Sensors were arranged on the distal surface in the *in vitro* testing phase of the project on the basis that this region experienced the greatest level of motion as reported under physiological loading conditions. However, peak motions as revealed by the subsequent FE model based on the experimental loading protocol were located on the posterior condyles. While it is not known if this is truly representative of peak motions at the interface of the presented *in vitro* study in Chapter VIII (due to differences in components of measured and predicted motions), it at least indicates a sensitivity of motion distribution to the loading and geometry of the system. Careful consideration should therefore be given to replication of more physiological loading conditions during *in vitro* experiments to better approximate the behaviour of the implant under conditions more representative of the *in vivo* situation.

### XI.1.5 Conclusions on modularity and incorporation of bony defects

Previous studies on the role of modular stems, particularly in the presence of bone grafts or condylar defects following TKA have been limited (van Loon et al. 2000, Completo et al. 2009, Meijerink et al. 2010). To the author's knowledge, this is the first FE study to investigate the role of fixation method and osseous support in the presence of F2 and F3 femoral defects under the AORI classification system (Engh 2006). Osteoporosis next to defect size and loss of osseous support at the junction were revealed to lead to significant increases in stress at the stem junction. These findings correlate well with a number of retrieval studies (Lim et al. 2001, Issack et al. 2007, Nikolopoulos et al. 2012).

Other factors such as partial or full loss of fixation at the stem-bone interface and the presences of surgical cut errors were all found to play a role in increasing the risk of modular component failure.

## XI.2 Clinical implications

This section highlights some of the key recommendations, which have direct clinical applications, based on the findings of the preceding chapters:

- The results of this study suggests that stems may not confer any obvious advantage, with respect to component stability, provided the metaphysis remains intact and good fixation of the component can be achieved through cementing.
- In the event that stems are required, the findings of this study recommend the use of short cemented stems, which have been found to provide as much initial stability as long uncemented stems, produce a more favourable stress distribution in the periprosthetic region and are easier to fit.
- In at risk patients in particular, i.e. older patients with severe osteoporosis of the distal femur, this study suggests the use of a femoral component incorporating a medium length (75mm) cemented stem as an alternative to a

primary stemless femoral component to relieve periprosthetic stress and reduce the risk of fracture.

- Furthermore, should the patient lack sufficient osseous support at the distal metaphysis, it is recommended that a non-modular approach be adopted to reduce the risk of modular component fatigue failure at the junction.

These suggestions are made on the basis of findings from the preceding Chapters and as such are valid for the stated loading conditions and constraints applied both experimentally and numerically and under the identified limitations of the work. As such, further research may be warranted before clinical implementation of the above recommendations. In particular, long term testing of cemented and uncemented stems should be conducted to ensure the trends observed in short term tests are applicable to long term clinical scenarios. Moreover, on the topic of modularity testing should be extended to investigate the susceptibility of both modular and non-modular component to failure in severely osteoporotic patients, so that more definite conclusion can be drawn on this matter.

## XI.3 Recommendations

Based on the work carried out throughout the course of this thesis and its stated limitations, the following recommendations are made on aspects of both FE modelling and *in vitro* testing of the distal femur.

In this thesis, the impact of implant design and fixation on component stability was explored extensively with FE, however, a few key aspects should be considered for further development of these models.

The technique applied in this study to model ageing and osteoporosis could be further explored as an efficient means of investigating the influence of material property variations on fixation and stability of orthopaedic prosthesis for the same femur geometry. Wackerhagen et al. (1992) reported that the level of recorded micromotion at the bone implant interface varied significantly between hard and soft bone. The above mentioned methodology could be used in conjunction with friction

to determine if micromotions are likely to increase in 'soft' bone or if merely the level of elastic deformation increases.

Regional variations in bone properties and their influence on the mechanical environment under different loading regimes could also be modelled by assigning arbitrary (low or high) values of temperature in the region of interest and adjusting the temperature – stiffness relationship as appropriate, e.g. creating local site specific weakness or defects modelled on various clinical pathologies. A further improvement would be to incorporate variations in cancellous bone properties, either through the above methodology or through CT based properties, as inhomogeneity has been shown to be a key factor in simulation accuracy by several previous studies, e.g. (Au et al. 2010).

In this thesis, all models employed fully restrained boundary conditions at the mid-shaft. While this may adequately replicate many laboratory studies, it is not very representative of the true *in vivo* situation; as such on-going research is focused on the development and inclusion of more realistic boundary conditions to these FE models through incorporation of muscles and ligaments. Preliminary findings, as mentioned in Chapter IV, indicate that for areas close to the region of load application, in this case the distal femur where all external loads are applied, fixed boundary conditions at some distance have minimal influence on stresses and strains. A study by van der Ploeg et al. (2012) reported a similar findings on the influence of muscles and ligaments on micromotion following THA. Though slight differences in the observed local stress pattern may occur between the muscle supported and fixed boundary condition models as a result of the absence of some distally attaching muscles such as Gastrocnemius.

Preliminary investigations into FE boundary conditions, however, did highlight that end of stem stress varies significantly under fixed and muscle boundary conditions for diaphyseal engaging long stems, thus supporting why this area warrants further investigation (Conlisk et al. 2012).

A six degree of freedom micromotion measurement system was developed in this study and the short term loosening behaviour of three different types of implant with increasing stem length was investigated. It is known, however, that cemented implant loosening is based on its long term performance, with previous *in vitro* studies suggesting failure will occur only after a significant number of cycles, usually several million (Maher et al. 2001, Cristofolini et al. 2008), efforts should now be made to investigate if the short term trends observed in this initial study are applicable to the long term loosening behaviour of these implants.

To eliminate the issues discussed in Chapter VIII (e.g. bending in flexion), a modified dynamic knee rig based on the Kansas Knee Simulator as discussed in (Baldwin et al. 2012) could be incorporated into future experimental setups. The use of such equipment in conjunction with the micromotion test rig developed in this thesis could provide valuable information on the interface behaviour of various total knee prostheses under more physiologically realistic loading conditions.

Building on the work presented in Chapter X, interface motion tests could be extended to include cadaveric trials to directly assess how the presence of condylar defects impact upon stem junction stress. The role of the offset adapter for various interface conditions should also be examined.

## XI.4 Reflection and final considerations

As outlined in Chapter I, this thesis has contributed to the current body of knowledge on the topic of fixation and stability of femoral prostheses used in total knee arthroplasty. Through the course of this work numerous original FE models of the distal femur of increasing complexity were developed. Some highlights include; introduction of a novel method for incorporating the effects of endosteal thinning and variable material properties in the cortical bone, characterising the influence of internal implant features, and examining the influence of large bony defects on modular components. This work also detailed the creation of a combined *in vitro* and

FE approach to determining stability of different implant types under cemented and uncemented interface conditions.

In general through the course of this thesis several key factors have been highlighted which may be of importance to future researchers working in the field of biomechanics.

In respect to modelling, it is clear that loading conditions and correct modelling of the interface can greatly influence the resulting patterns of stress, and the interfacial motions between prosthesis and bone. When modelling biomechanical problems in FE, efforts should be made to ensure that all the relevant loads acting on the structure are accounted for and that the implant fit is reflective of the real life scenario. Furthermore, when modelling conditions such as osteoporosis, it is essential that changes to both the geometry and material properties be considered.

In respect to *in vitro* assessment of femoral component relative motion, the weight of the test apparatus should be kept to the minimum, so as to ensure this does not influence the results, another important factor is distance from surface of interest to point of fixation of apparatus, care should also be taken to ensure this value is as small as possible. As with computational modelling, replication of *in vivo* loading patterns is essential to producing reliable results. In terms of the knee joint, including an adequate representation of the patella-femoral joint is necessary in order to prevent unrealistically large deformations of the femur from occurring during higher flexion activities.

The *in vitro* and *in silico* models created during the course of this thesis allow the extraction of key information which would be difficult to obtain *in vivo* for ethical reasons. It is hoped that the information provided by these techniques (computational and experimental) may help inform orthopaedic surgeons and aid in the clinical decision making processes, where current clinical evidence is lacking or ambiguous.

However, many of the developments in this work are not strictly limited to the application of knee replacement in the distal femur. The efficient method of incorporating variable material properties to model osteoporosis and endosteal thinning, introduced in Chapter V, for example could find application in all other

bones in the human body which are encased by a cortical shell. Furthermore, this method could be used in any structure biological or otherwise where an inhomogeneous gradient of stiffness is desirable.

The design of the micromotion measurement rig could be easily adapted to monitor the performance of implants used in other joint replacement operations, such as total hip replacement (THA) and shoulder replacement (TSR). Moreover, the custom LabVIEW™ programs and graphical user interfaces (GUI) developed for data acquisition and coordinate transformation operations in this thesis, can be readily reused and adapted to suit other researchers' needs, such as new sensor setups and target sphere configurations, without having to modify extensive lines of code as a result of the incorporated GUI.

# References


AAOS. (2010a). "Distal Femur (Thighbone) Fractures of the knee." Retrieved 21/09/2012, 2012, from http://orthoinfo.aaos.org/topic.cfm?topic=A00526.

AAOS. (2010b). "Unicompartmental knee replacement." Retrieved 23/08/2012, 2012, from http://orthoinfo.aaos.org/topic.cfm?topic=A00585.

Aaron R. K. and Scott R. (1987). "Supracondylar fracture of the femur after total knee arthroplasty." Clinical Orthopaedics and Related Research(219): 136-139.

Abdul-Kadir M. R., Hansen U., Klabunde R., Lucas D. and Amis A. (2008). "Finite element modelling of primary hip stem stability: The effect of interference fit." Journal of Biomechanics **41**(3): 587-594.

Abu-Amer Y., Darwech I. and Clohisy J. (2007). "Aseptic loosening of total joint replacements: mechanisms underlying osteolysis and potential therapies." Arthritis Research & Therapy **9**(Suppl 1): S6.

Acker S. M., Cockburn R. A., Krevolin J., Li R. M., Tarabichi S. and Wyss U. P. (2011). "Knee Kinematics of High-Flexion Activities of Daily Living Performed by Male Muslims in the Middle East." The Journal of Arthroplasty **26**(2): 319-327.

Allen M. J. (2011). "Functional micromechanics: moving beyond migration in evaluation of implant fixation." J Am Acad Orthop Surg **19**: 242-244.

Anderson D. E. (2010). An examination of age-related differences in lower extremity joint torques and strains in the proximal femur during gait. Doctor of Philosophy, Virginia Polytechnic Institute and State University.

Andreaus U. and Colloca M. (2009). "Prediction of micromotion initiation of an implanted femur under physiological loads and constraints using the finite element method." Proceedings of the Institution of Mechanical Engineers, Part H: Journal of Engineering in Medicine **223**(5): 589-605.

Anonymous (1976). "Total Knee Replacement." The Lancet **307**(7967): 1002-1003.

AOA (2011). Annual Report. Adelaide, Australian Orthopaedic Association National Joint Registry.

Arthritis Research UK (2011). What is arthritis?

Ashman R. B. and Rho J. Y. (1988). "Elastic modulus of trabecular bone material." Journal of Biomechanics **21**(3): 177-181.

Au A. G., Liggins A. B., Raso V. J., Carey J. and Amirfazli A. (2010). "Representation of bone heterogeneity in subject-specific finite element models for knee." Computer Methods and Programs in Biomedicine **99**(2): 154-171.

Bahraminasab M., Sahari B. B., Edwards K. L., Farahmand F., Arumugam M. and Hong T. S. (2012). "Aseptic loosening of femoral components - A review of current and future trends in materials used." Materials & Design **42**: 459-470.

Baldwin M. A., Clary C. W., Fitzpatrick C. K., Deacy J. S., Maletsky L. P. and Rullkoetter P. J. (2012). "Dynamic finite element knee simulation for evaluation of knee replacement mechanics." Journal of Biomechanics **45**(3): 474-483.

Baptista C. A. R. P., Rossino L. S., Torres M. A. S. and Shigue C. Y. (2007). "Evaluation of the fretting fatigue behaviour of commercially pure titanium." Proceedings of the Institution of Mechanical Engineers, Part L: Journal of Materials Design and Applications **221**(3): 143-150.

Barink M., Kampen A. v., Malefijt M. d. W. and Verdonschot N. (2005). "A Three-Dimensional Dynamic Finite Element Model of the Prosthetic Knee Joint: Simulation of Joint Laxity and Kinematics." Proceedings of the Institution of Mechanical Engineers, Part H: Journal of Engineering in Medicine **219**(6): 415-424.

Barink M., Verdonschot N. and de Waal Malefijt M. (2003). "A different fixation of the femoral component in total knee arthroplasty may lead to preservation of femoral bone stock." Proceedings of the Institution of Mechanical Engineers, Part H: Journal of Engineering in Medicine **217**(5): 325-332.

Barrack R. L., Rorabeck C., Burt M. and Sawhney J. (1999). "Pain at the End of the Stem After Revision Total Knee Arthroplasty." Clinical Orthopaedics & Related Research October **367**: 216-225.

Barrack R. L., Stanley T., Burt M. and Hopkins S. (2004). "The effect of stem design on end-of-stem pain in revision total knee arthroplasty." The Journal of Arthroplasty **19**(7, Supplement 2): 119-124.

Bäthis H., Perlick L., Tingart M., Perlick C., Lüring C. and Grifka J. (2005). "Intraoperative cutting errors in total knee arthroplasty." Archives of Orthopaedic and Trauma Surgery **125**(1): 16-20.

Beckmann J., Lüring C., Springorum R., Köck F. X., Grifka J. and Tingart M. (2011). "Fixation of revision TKA: a review of the literature." Knee Surgery, Sports Traumatology, Arthroscopy **19**(6): 872-879.

Behrens B.-A., Nolte I., Wefstaedt P., Stukenborg-Colsman C. and Bouguecha A. (2009). "Numerical investigations on the strain-adaptive bone remodelling in the periprosthetic femur: Influence of the boundary conditions." BioMedical Engineering OnLine **8**(1): 7.

Bei Y., Fregly B. J., Sawyer W. G., Banks S. A. and Kim N. H. (2004). "The relationship between contact pressure, insert thickness, and mild wear in total knee replacements." Cmes-Computer Modeling in Engineering & Sciences **6**(2): 145-152.

Berend K. and Lombardi A., Jr. (2009). "Distal Femoral Replacement in Nontumor Cases with Severe Bone Loss and Instability." Clinical Orthopaedics and Related Research **467**(2): 485-492.

Bergmann G. (Ed.), Charite – Universitaetsmedizin Berlin (2008) "Orthoload." Retrived Jan. 10, 2010, from http://www.OrthoLoad.com.

Bergmann G., Graichen F., Siraky J., Jendrzynski H. and Rohlmann A. (1988). "Multichannel strain gauge telemetry for orthopaedic implants." Journal of Biomechanics **21**(2): 169-176.

Bernakiewicz M. and Viceconti M. (2002). "The role of parameter identification in finite element contact analyses with reference to orthopaedic biomechanics applications." Journal of Biomechanics **35**(1): 61-67.

Berzins A., Sumner D. R., Andriacchi T. P. and Galante J. O. (1993). "Stem curvature and load angle influence the initial relative bone-implant motion of cementless femoral stems." Journal of Orthopaedic Research **11**(5): 758-769.

Berzins A., Sumner D. R., Turner T. M. and Natarajan R. (1994). "Effects of fixation technique on displacement incompatibilities at the bone–implant interface in cementless total knee replacement in a canine model." Journal of Applied Biomaterials **5**(4): 349-352.

Bessho M., Ohnishi I., Matsumoto T., Ohashi S., Matsuyama J., Tobita K., Kaneko M. and Nakamura K. (2009). "Prediction of proximal femur strength using a CT-based nonlinear finite element method: Differences in predicted fracture load and site with changing load and boundary conditions." Bone **45**(2): 226-231.

Bhimji S. and Meneghini R. M. (2012). "Micromotion of Cementless Tibial Baseplates Under Physiological Loading Conditions." The Journal of Arthroplasty **27**(4): 648-654.

Bobyn J. D., Tanzer M., Krygier J., Dujovne A. R. and Brooks C. E. (1994). "Concerns With Modularity in Total Hip Arthroplasty." Clinical Orthopaedics & Related Research January **298**: 27-36.

Bollars P., Luyckx J. P., Innocenti B., Labey L., Victor J. and Bellemans J. (2011). "Femoral component loosening in high-flexion total knee replacement." Journal of Bone & Joint Surgery, British Volume **93-B**(10): 1355-1361.

Bougherara H., Nazgooei S., Sayyidmousavi A., Maršık F. and Mařík I. A. (2011). "Computation of bone remodelling after Duracon knee arthroplasty using a thermodynamic-based model." Proceedings of the Institution of Mechanical Engineers, Part H: Journal of Engineering in Medicine **225**(7): 669-679.

Bougherara H., Zdero R., Mahboob Z., Dubov A., Shah S. and Schemitsch E. H. (2010). "The biomechanics of a validated finite element model of stress shielding in a novel hybrid total knee replacement." Proceedings of the Institution of Mechanical Engineers Part H-Journal of Engineering in Medicine **224**(H10): 1209-1219.

Bousson V., Bergot C., Meunier A., Barbot F., Parlier-Cuau C., Laval-Jeantet A.-M. and Laredo J.-D. (2000). "CT of the Middiaphyseal Femur: Cortical Bone Mineral Density and Relation to Porosity1." Radiology **217**(1): 179-187.

Bousson V., Meunier A., Bergot C., Vicaut É., Rocha M. A., Morais M. H., Laval-Jeantet A.-M. and Laredo J.-D. (2001). "Distribution of Intracortical Porosity in Human Midfemoral Cortex by Age and Gender." Journal of Bone and Mineral Research **16**(7): 1308-1317.

Boyde A. (2012). "A scanning electron micrograph of healthy and osteoporotic bone from a vertebra ", from http://www.wellcome.ac.uk/Education-resources/Teaching-and-education/Big-Picture/All-issues/Exercise-energy-and-movement/Image-galleries/WTDV033065.htm.

Bragdon C. R., Burke D., Lowenstein J. D., O'Connor D. O., Ramamurti B., Jasty M. and Harris W. H. (1996). "Differences in stiffness of the interface between a cementless porous implant and cancellous bone in vivo in dogs due to varying amounts of implant motion." The Journal of Arthroplasty **11**(8): 945-951.

Brilhault J. M. and Ries M. D. (2012). "Influence of offset stem couplers in femoral revision knee arthroplasty: A radiographic study." The Knee **19**(2): 112-115.

Britton J. R. and Prendergast P. J. (2005). "Preclinical testing of femoral hip components: An experimental investigation with four prostheses." Journal of Biomechanical Engineering-Transactions of the Asme **127**(5): 872-880.

Broström L.-Å., Goldie I. and Selvik G. (1989). "Micromotion of the total knee." Acta Orthopaedica **60**(4): 443-445.

Brown T. A., Kohan L. and Ben-Nissan B. (2007). Assessment by finite element analysis of the impact of osteoporosis and

osteoarthritis on hip resurfacing. 5th Australasian Congress on Applied Mechanics, Brisbane, Austrailia.

Brown T. E., Larson B., Shen F. and Moskal J. T. (2002). "Thigh Pain After Cementless Total Hip Arthroplasty: Evaluation and Management." Journal of the American Academy of Orthopaedic Surgeons **10**(6): 385-392.

Budynas R. G. and Nisbett K. J. (2007). Shigley's Mechanical Engineering Design, SI version, McGraw-Hill Higher Education.

Burstein A. H. (1994). Fundamentals of Orthopaedic biomechanics. Baltimore, Williams & Wilkins.

Callaghan J. J., Rosenberg A. G., Rubash H. E., Simonian P. T. and Wickiewicz T. L. (2002). The Adult Knee, Lippincott Williams & Wilkins.

Callanan A., Morris L. G. and McGloughlin T. M. (2011). "Finite element and photoelastic modelling of an abdominal aortic aneurysm: a comparative study." Computer Methods in Biomechanics and Biomedical Engineering **15**(10): 1111-1119.

Carlson C. E., Mann R. W. and Harris W. H. (1974). "A Radio Telemetry Device for Monitoring Cartilage Surface Pressures in the Human Hip." Biomedical Engineering, IEEE Transactions on **BME-21**(4): 257-264.

Carr B. C. and Goswami T. (2009). "Knee implants – Review of models and biomechanics." Materials & Design **30**(2): 398-413.

Cawley D. T., Kelly N., Simpkin A., Shannon F. J. and McGarry J. P. (2012). "Full and surface tibial cementation in total knee arthroplasty: A biomechanical investigation of stress distribution and remodeling in the tibia." Clinical Biomechanics **27**(4): 390-397.

Charnley J. (1972). "The long-term results of low-friction arthroplasty of the hip performed as a primary intervention." Journal of Bone & Joint Surgery, British Volume **54-B**(1): 61-76.

Cheung G., Zalzal P., Bhandari M., Spelt J. K. and Papini M. (2004). "Finite element analysis of a femoral retrograde intramedullary nail subject to gait loading." Medical Engineering & Physics **26**(2): 93-108.

Chiu K. Y., Ng T. P., Tang W. M. and Yau W. P. (2002). "Review article: knee flexion after total knee arthroplasty." J Orthop Surg **10**(2): 194-202.

Choi K., Kuhn J. L., Ciarelli M. J. and Goldstein S. A. (1990). "The elastic moduli of human subchondral, trabecular, and cortical bone tissue and the size-dependency of cortical bone modulus." Journal of Biomechanics **23**(11): 1103-1113.

Chong D. Y. R., Hansen U. N. and Amis A. A. (2010). "Analysis of bone–prosthesis interface micromotion for cementless tibial prosthesis fixation and the influence of loading conditions." Journal of Biomechanics **43**(6): 1074-1080.

Chong D. Y. R., Hansen U. N., van der Venne R., Verdonschot N. and Amis A. A. (2011). "The influence of tibial component fixation techniques on resorption of supporting bone stock after total knee replacement." Journal of Biomechanics **44**(5): 948-954.

Chu Y.-H., Elias J. J., Duda G. N., Frassica F. J. and Chao E. Y. S. (2000). "Stress and micromotion in the taper lock joint of a modular segmental bone replacement prosthesis." Journal of Biomechanics **33**(9): 1175-1179.

CJRR (2009). Hip and Knee Replacements in Canada 2008-2009 Annual Report Ottawa, Canadian Joint Replacement Registry (CJRR).

Clarke S., Phillips A. and Bull A. (2012). "Validation of FE Micromotions and Strains Around a Press-Fit Cup: Introducing a New Micromotion Measuring Technique." Annals of Biomedical Engineering **40**(7): 1586-1596.

Completo A., Fonseca F., Relvas C., Ramos A. and Simões J. (2012). "Improved stability with intramedullary stem after anterior femoral notching in total knee arthroplasty." Knee Surgery, Sports Traumatology, Arthroscopy **20**(3): 487-494.

Completo A., Fonseca F. and Simoes J. A. (2008a). "Strain shielding in proximal tibia of stemmed knee prosthesis: Experimental study." Journal of Biomechanics **41**(3): 560-566.

Completo A., Fonseca F. and Simões J. A. (2007). "Experimental validation of intact and implanted distal femur finite element models." Journal of Biomechanics **40**(11): 2467-2476.

Completo A., Rego A., Fonseca F., Ramos A., Relvas C. and Simoes J. A. (2010). "Biomechanical evaluation of proximal tibia behaviour with the use of femoral stems in revision TKA: An in vitro and finite element analysis." Clinical Biomechanics **25**(2): 159-165.

Completo A., Simões J. and Fonseca F. (2008b). "Experimental Evaluation of Strain Shielding in Distal Femur in Revision TKA." Experimental Mechanics **48**(6): 817-824.

Completo A., Simões J. A. and Fonseca F. (2009). "Revision total knee arthroplasty: The influence of femoral stems in load sharing and stability." The Knee **16**(4): 275-279.

Completo A., Simões J. A., Fonseca F. and Oliveira M. (2008c). "The influence of different tibial stem designs in load sharing and stability at the cement–bone interface in revision TKA." The Knee **15**(3): 227-232.

Conlisk N., Pankaj P. and Howie C. R. (2012). The Mechanical Environment In The Distal Femur: Influence Of Boundary Conditions On FE Models 10th International Symposium Computer Methods in Biomechanics and Biomedical Engineering, Berlin, Germany.

Cooper D. M. L., Thomas C. D. L., Clement J. G., Turinsky A. L., Sensen C. W. and Hallgrímsson B. (2007). "Age-dependent change in the 3D structure of cortical porosity at the human femoral midshaft." Bone **40**(4): 957-965.

Cowin S. C., Ed. (2001). Bone mechanics handbook. Boca Raton, FL, London: CRC Press.

Cowin S. C. and Hegedus D. H. (1976). "Bone remodeling I: theory of adaptive elasticity." Journal of Elasticity **6**(3): 313-326.

Cowley K. and Neale M. (1998). Aspects of modelling skin and hair during shaving. Abaqus users conference, simulia.

Cristofolini L., Affatato S., Erani P., Leardini W., Tigani D. and Viceconti M. (2008). "Long-term implant-bone fixation of the femoral component in total knee replacement." Proceedings of the Institution of Mechanical Engineers Part H-Journal of Engineering in Medicine **222**(H3): 319-331.

Cristofolini L., Affatato S., Erani P., Tigani D. and Viceconti M. (2009). "Implant fixation in knee replacement: Preliminary in vitro comparison of ceramic and metal cemented femoral components." Knee **16**(2): 101-108.

Cristofolini L., Erani P., Savigni P., Bordini B. and Viceconti M. (2007). "Preclinical assessment of the long-term endurance of cemented hip stems. Part 2: in-vitro and ex-vivo fatigue damage of the cement mantle." Proceedings of the Institution of Mechanical Engineers, Part H: Journal of Engineering in Medicine **221**(6): 585-599.

Cristofolini L., Teutonico A. S., Monti L., Cappello A. and Toni A. (2003). "Comparative in vitro study on the long term performance of cemented hip stems: validation of a protocol to discriminate between "good" and "bad" designs." Journal of Biomechanics **36**(11): 1603-1615.

Cristofolini L., Viceconti M., Cappello A. and Toni A. (1996). "Mechanical validation of whole bone composite femur models." Journal of Biomechanics **29**(4): 525-535.

Currey J. D. (2002). Bone: structure and mechanics, Princeton University Press.

D'Lima D., Wong J., Patil S., Flores-Hernandez C., Colwell C., Steklov N. and Kester M. (2012). "Predicting Bone Damage and Implant Subsidence After Total Knee Arthroplasty." Journal of Bone & Joint Surgery, British Volume **94-B**(SUPP XXV): 35-35.

D'Lima D. D., Chen P. C. and Colwell C. W., Jr. (2001a). "Polyethylene contact stresses, articular congruity, and knee alignment." Clin Orthop Relat Res(392): 232-238.

D'Lima D. D., Patil S., Steklov N., Slamin J. E. and Colwell C. W., Jr. (2005). "The Chitranjan Ranawat Award: in vivo knee forces after total knee arthroplasty." Clin Orthop Relat Res **440**: 45-49.

D'Lima D. D., Patil S., Steklov N., Slamin J. E. and Colwell Jr C. W. (2006). "Tibial Forces Measured In Vivo After Total Knee Arthroplasty." The Journal of Arthroplasty **21**(2): 255-262.

D'Lima D. D., Steklov N., Fregly B. J., Banks S. A. and Colwell C. W. (2008). "In vivo contact stresses during activities of daily living after knee arthroplasty." Journal of Orthopaedic Research **26**(12): 1549-1555.

D'Lima D. D. M. D., Chen P. C. P. and Colwell C. W. J. M. D. (2001b). "Polyethylene Contact Stresses, Articular Congruity, and Knee Alignment." Clinical Orthopaedics & Related Research November **392**: 232-238.

D'Lima D. D., Patil S., Steklov N., Chien S. and Colwell Jr C. W. (2007). "In vivo knee moments and shear after total knee arthroplasty." Journal of Biomechanics **40, Supplement 1**(0): S11-S17.

Dahlkvist N. J., Mayo P. and Seedhom B. B. (1982). "Forces during Squatting and Rising from a Deep Squat." Engineering in Medicine **11**(2): 69-76.

Dassault Systèmes (2010a). 3.2.6 Triangular, tetrahedral, and wedge elements. Abaqus Theory Manual.

Dassault Systèmes (2010b). Abaqus Analysis User's Manual, Part IX: Interactions. Abaqus 6.10 Online Documentation.

Davis J. L., Dumont E. R., Strait D. S. and Grosse I. R. (2011). "An Efficient Method of Modeling Material Properties Using a Thermal Diffusion Analogy: An Example Based on Craniofacial Bone." PLoS ONE **6**(2): e17004.

Donaldson F. E., Pankaj P., Cooper D. M. L., Thomas C. D. L., Clement J. G. and Simpson A. H. R. W. (2011). "Relating age and micro-architecture with apparent-level elastic constants: a micro-finite element study of female cortical bone from the anterior femoral midshaft." Proceedings of the Institution of Mechanical Engineers, Part H: Journal of Engineering in Medicine **225**(6): 585-596.

Donaldson F. E., Pankaj P. and Simpson A. H. R. W. (2012). "Investigation of factors affecting loosening of ilizarov ring-wire external fixator systems at the bone-wire interface." Journal of Orthopaedic Research **30**(5): 726-732.

Duffy G. P., Berry D. J. and Rand J. A. (1998). "Cement Versus Cementless Fixation In Total Knee Arthroplasty." Clinical Orthopaedics & Related Research November **356**: 66-72.

Engh G. A. (2006). Classification of Bone Defects Femur and Tibia

Knee Arthroplasty Handbook. G. R. Scuderi and A. J. Tria, Springer New York**:** 116-132.

Engh G. A., Herzwurm P. J. and Parks N. L. (1997). "Treatment of major defects of bone with bulk allografts and stemmed components during total knee arthroplasty." Journal of Bone and Joint Surgery - Series A **79**(7): 1030-1039.

Fadag H. A., Mall S. and Jain V. K. (2008). "A finite element analysis of fretting fatigue crack growth behavior in Ti–6Al–4V." Engineering Fracture Mechanics **75**(6): 1384-1399.

Faraj A. A. and Rajasekar K. (2006). "The effect of two different types of cement restrictors on the femoral cement mantle." Acta Orthop Belg **72**(6): 702-708.

Fehring T. (2005). Use of Stems in Revision Total Knee Arthroplasty

Revision Total Knee Arthroplasty. J. V. Bono and R. D. Scott, Springer New York**:** 137-144.

Fehring T. K. and McAvoy G. (1996). "Fluoroscopic evaluation of the painful total knee arthroplasty." Clinical Orthopaedics and Related Research(331): 226-233.

Fehring T. K., Odum S., Olekson C., Griffin W. L., Mason J. B. and McCoy T. H. (2003). "Stem Fixation in Revision Total Knee Arthroplasty: A Comparative Analysis. ." Clinical Orthopaedics & Related Research November **416**: 217-224.

Fisher J. and Dowson D. (1991). "Tribology of Total Artificial Joints." Proceedings of the Institution of Mechanical Engineers, Part H: Journal of Engineering in Medicine **205**(2): 73-79.

Font-Rodriguez D. E., Scuderi G. R. and Insall J. N. (1997). "Survivorship of Cemented Total Knee Arthroplasty." Clinical Orthopaedics & Related Research **345**: 79-86.

Fox A. J. S., Bedi A. and Rodeo S. A. (2009). "The basic science of articular cartilage: structure, composition, and function." Sports Health **1**(6): 461-468.

Fox A. J. S., Bedi A. and Rodeo S. A. (2012). "The Basic Science of Human Knee Menisci: Structure, Composition, and Function." Sports Health: A Multidisciplinary Approach **4**(4): 340-351.

Fregly B. J., Bei Y. and Sylvester M. E. (2003). "Experimental evaluation of an elastic foundation model to predict contact pressures in knee replacements." Journal of Biomechanics **36**(11): 1659-1668.

Fregly B. J., Besier T. F., Lloyd D. G., Delp S. L., Banks S. A., Pandy M. G. and D'Lima D. D. (2012). "Grand challenge competition to predict in vivo knee loads." Journal of Orthopaedic Research **30**(4): 503-513.

Frosch P., Decking J., Theis C., Drees P., Schoellner C. and Eckardt A. (2004). "Complications after total knee arthroplasty: a comprehensive report." Acta Orthop Belg **70**(6): 565-569.

Gao F., Henricson A. and Nilsson K. G. (2009). "Cemented versus uncemented fixation of the femoral component of the NexGen CR total knee replacement in patients younger than 60 years: A Prospective Randomised Controlled RSA Study." The Knee **16**(3): 200-206.

Ghazavi M. T., Stockley I., Yee G., Davis A. and Gross A. E. (1997). "Reconstruction of massive bone defects with allograft in revision total knee arthroplasty." Journal of Bone and Joint Surgery - Series A **79**(1): 17-25.

Gilbert J. L., Bloomfeld R. S., Lautenschlager E. P. and Wixson R. L. (1992). "A computer-based biomechanical analysis of the three-dimensional motion of cementless hip prostheses." Journal of Biomechanics **25**(4): 329-340.

Gill H. S., Waite J. C., Short A., Kellett C. F., Price A. J. and Murray D. W. (2006). "In vivo measurement of volumetric wear of a total knee replacement." The Knee **13**(4): 312-317.

Gill I. P. S., Webb J., Sloan K. and Beaver R. J. (2012). "Corrosion at the neck-stem junction as a cause of metal ion release and pseudotumour formation." Journal of Bone & Joint Surgery, British Volume **94-B**(7): 895-900.

Goldberg V. M., Figgie M. P., Figgie H. E. and Sobel M. (1988). "The results of revision total knee arthroplasty." Clinical Orthopaedics and Related Research(226): 86-92.

Goldstein S. A. (1987). "The mechanical properties of trabecular bone: Dependence on anatomic location and function." Journal of Biomechanics **20**(11–12): 1055-1061.

Goldstein S. A., Goulet R. and McCubbrey D. (1993). "Measurement and significance of three-dimensional architecture to the mechanical integrity of trabecular bone." Calcif Tissue Int **53 Suppl 1**: S127-132; discussion S132-123.

Goudakos I. G., König C., Schöttle P. B., Taylor W. R., Hoffmann J.-E., Pöpplau B. M., Singh N. B., Duda G. N. and Heller M. O. (2010). "Regulation of the patellofemoral contact area: An essential mechanism in patellofemoral joint mechanics?" Journal of Biomechanics **43**(16): 3237-3239.

Halder A., Kutzner I., Graichen F., Heinlein B., Beier A. and Bergmann G. (2012). "Influence of Limb Alignment on Mediolateral Loading in Total Knee ReplacementIn Vivo Measurements in Five Patients." The Journal of Bone & Joint Surgery **94**(11): 1023-1029.

Hambli R., Bettamer A. and Allaoui S. (2012). "Finite element prediction of proximal femur fracture pattern based on orthotropic behaviour law coupled to quasi-brittle damage." Medical Engineering & Physics **34**(2): 202-210.

Hamill J. and Knutzen K. M. (2008). Biomechanical Basis of Human Movement, Lippincott Williams and Wilkins.

Harrison R. J., Thacker M. M., Pitcher J. D., Temple H. T. and Scully S. P. (2006). "Distal Femur Replacement Is Useful in Complex Total Knee Arthroplasty Revisions." Clinical Orthopaedics & Related Research May **446**: 113-120.

Harrysson O., Hosni Y. and Nayfeh J. (2007). "Custom-designed orthopedic implants evaluated using finite element analysis of patient-specific computed tomography data: femoral-component case study." BMC Musculoskeletal Disorders **8**(1): 91.

Hashemi A. and Shirazi-Adl A. (2000). "Finite Element Analysis of Tibial Implants — Effect of Fixation Design and Friction Model." Computer Methods in Biomechanics and Biomedical Engineering **3**(3): 183-201.

Healy W. L., Siliski J. M. and Incavo S. J. (1993). "Operative treatment of distal femoral fractures proximal to total knee replacements." The Journal of Bone & Joint Surgery **75**(1): 27-34.

Heinlein B., Kutzner I., Graichen F., Bender A., Rohlmann A., Halder A. M., Beier A. and Bergmann G. (2009). "ESB clinical biomechanics award 2008: Complete data of total knee replacement loading for level walking and stair climbing measured in vivo with a follow-up of 6–10 months." Clinical Biomechanics **24**(4): 315-326.

Helgason B., Perilli E., Schileo E., Taddei F., Brynjólfsson S. and Viceconti M. (2008). "Mathematical relationships between bone density and mechanical properties: A literature review." Clinical Biomechanics **23**(2): 135-146.

Hitt K., ShurmanIi J. R., Greene K., McCarthy J., Moskal J., Hoeman T. and Mont M. A. (2003). "Anthropometric Measurements of the Human Knee: Correlation to the Sizing of Current Knee Arthroplasty Systems." The Journal of Bone & Joint Surgery **85**(suppl_4): 115-122.

Hodgskinson R. and Currey J. D. (1992). "Young's modulus, density and material properties in cancellous bone over a large density range." Journal of Materials Science: Materials in Medicine **3**(5): 377-381.

Hodgskinson R., Njeh C. F., Currey J. D. and Langton C. M. (1997). "The ability of ultrasound velocity to predict the stiffness of cancellous bone in vitro." Bone **21**(2): 183-190.

Howie C. R. (2010). Stems and augments: Where and how much? Paterswolde Symposium 2010: New developments in revision total knee replacement. Netherlands.

Huang H.-T., Su J. Y. and Wang G.-J. (2005). "The Early Results of High-Flex Total Knee Arthroplasty: A Minimum of 2 Years of Follow-up." The Journal of Arthroplasty **20**(5): 674-679.

Inglis A. E. and Walker P. S. (1991). "Revision of failed knee replacements using fixed-axis hinges." Journal of Bone & Joint Surgery, British Volume **73-B**(5): 757-761.

Innocenti B., Pianigiani S., Labey L., Victor J. and Bellemans J. (2011). "Contact forces in several TKA designs during squatting: A numerical sensitivity analysis." Journal of Biomechanics **44**(8): 1573-1581.

ISO (2004). Implants for surgery — Wear of total knee-joint prostheses, Part 3: Loading and displacement parameters for wear-testing machines with displacement control and corresponding environmental conditions for test. ISO 14243-1. Switzerland, The International Organization for Standardization.

ISO (2009). Implants for surgery — Wear of total knee-joint prostheses, Part 1: Loading and displacement parameters for wear-testing machines with load control and corresponding environmental conditions for test. . ISO 14243-1. Switzerland, The International Organization for Standardization.

Issack P. S., Cottrell J. M., Delgado S., Wright T. M., Sculco T. P. and Su E. P. (2007). "Failure at the taper lock of a modular stemmed femoral implant in revision knee arthroplasty - A report of two cases and a retrieval analysis." Journal of Bone and Joint Surgery-American Volume **89A**(10): 2271-2274.

Jacobs J. J., Roebuck K. A., Archibeck M., Hallab N. J. and Glant T. T. (2001). "Osteolysis: Basic Science. ." Clinical Orthopaedics & Related Research December **393**: 71-77.

Jazrawi L. M., Bai B., Kummer F. J., Hiebert R. and Stuchin S. A. (2001). "The effect of stem modularity and mode of fixation on tibial component stability in revision total knee arthroplasty." The Journal of Arthroplasty **16**(6): 759-767.

Jensen C., Petersen M., Schrøder H. and Lund B. (2010). "Changes in bone mineral density of the distal femur after revision total knee arthroplasty with metaphyseal press-fit stem." Journal of Orthopaedics and Traumatology **11**(3): 143-148.

Jensen K. S., Mosekilde L. and Mosekilde L. (1990). "A model of vertebral trabecular bone architecture and its mechanical properties." Bone **11**(6): 417-423.

Julin J., Jämsen E., Puolakka T., Konttinen Y. T. and Moilanen T. (2010). "Younger age increases the risk of early prosthesis failure following primary total knee replacement for osteoarthritis." Acta Orthopaedica **81**(4): 413-419.

Kärrholm J. (1989). "Roentgen stereophotogrammetry: Review of orthopedic applications." Acta Orthopaedica **60**(4): 491-503.

Katsamanis F. and Raftopoulos D. D. (1990). "Determination of mechanical properties of human femoral cortical bone by the Hopkinson bar stress technique." Journal of Biomechanics **23**(11): 1173-1184.

Kaufman K. R., Kovacevic N., Irby S. E. and Colwell C. W. (1996). "Instrumented implant for measuring tibiofemoral forces." Journal of Biomechanics **29**(5): 667-671.

Keyak J. H., Rossi S. A., Jones K. A., Les C. M. and Skinner H. B. (2001). "Prediction of fracture location in the proximal femur using finite element models." Medical Engineering & Physics **23**(9): 657-664.

Kim K.-I., Egol K. A., Hozack W. J. and Parvizi J. (2006). "Periprosthetic fractures after total knee arthroplasties." Clinical Orthopaedics and Related Research **446**: 167-175.

King T. V. and Scott R. D. (1985). "Femoral component loosening in total knee arthroplasty." Clin Orthop Relat Res(194): 285-290.

Kluess D., Bergschmidt P., Mueller I., Mittelmeier W. and Bader R. (2012). "Influence of the distal femoral resection angle on the principal stresses in ceramic total knee components." The Knee **19**(6): 846-850.

Knight L. A., Pal S., Coleman J. C., Bronson F., Haider H., Levine D. L., Taylor M. and Rullkoetter P. J. (2007). "Comparison of long-term numerical and experimental total knee replacement wear during simulated gait loading." Journal of Biomechanics **40**(7): 1550-1558.

Komdeur P., Pollo F. E. and Jackson R. W. (2002). Dynamic knee motion in anterior cruciate impairment: a report and case study. BUMC.

Koskinen E., Eskelinen A., Paavolainen P., Pulkkinen P. and Remes V. (2008). "Comparison of survival and cost-effectiveness between unicondylar arthroplasty and total knee

arthroplasty in patients with primary osteoarthritis: A follow-up study of 50,493 knee replacements from the Finnish Arthroplasty Register." Acta Orthopaedica **79**(4): 499-507.

Kuhn J. L., Goldstein S. A., Choi R., London M., Feldkamp L. A. and Matthews L. S. (1989). "Comparison of the trabecular and cortical tissue moduli from human iliac crests." Journal of Orthopaedic Research **7**(6): 876-884.

Kuiper J. H. (2007). Disease, replacement and regeneration of joints, Keele University, UK.

Kuiper J. H. and Huiskes R. (1996). "Friction and stem stiffness affect dynamic interface motion in total hip replacement." Journal of Orthopaedic Research **14**(1): 36-43.

Kuster M. S. and Stachowiak G. W. (2002). "Factors affecting polyethylene wear in total knee arthroplasty." Orthopedics **25**(2 Suppl): s235-242.

Kuster M. S., Wood G. A., Stachowiak G. W. and Gächter A. (1997). "Joint load considerations in total knee replacement." Journal of Bone & Joint Surgery, British Volume **79-B**(1): 109-113.

Kutzner I., Heinlein B., Graichen F., Bender A., Rohlmann A., Halder A., Beier A. and Bergmann G. (2010). "Loading of the knee joint during activities of daily living measured in vivo in five subjects." Journal of Biomechanics **43**(11): 2164-2173.

Kwon O., Kamath A., Voleti P. and Garino J. (2012). "Isolated Lateral Ligament Laxity in Primary Total Knee Arthroplasty: Cohort Study of Stemmed Versus Unstemmed Implants." Journal of Bone & Joint Surgery, British Volume **94-B**(SUPP XXV): 124.

Laskin R. S., Ed. (2001). Controversies in Total Knee Replacement, OUP Oxford.

Lesh M. L., Schneider D. J., Deol G., Davis B., Jacobs C. R. and PelligriniJr V. D. (2000). "The Consequences of Anterior Femoral Notching in Total Knee Arthroplasty A Biomechanical Study*." The Journal of Bone & Joint Surgery **82**(8): 1096-1096.

Lim L.-A., Trousdale R. T., Berry D. J. and Hanssen A. D. (2001). "Failure of the stem–condyle junction of a modular femoral stem in revision total knee arthroplasty: A report of five cases." The Journal of Arthroplasty **16**(1): 128-132.

Liu G. R. and Quek S. S. (2003). Finite Element Method: A Practical Course, Elsevier Butterworth-Heinemann.

Lo S. H. and Ling C. (2000). "Improvement on the 10-node tetrahedral element for three-dimensional problems." Computer Methods in Applied Mechanics and Engineering **189**(3): 961-974.

Lombardi Jr A. V., Mallory T. H., Waterman R. A. and Eberle R. W. (1995). "Intercondylar distal femoral fracture: An unreported complication of posterior-stabilized total knee arthroplasty." The Journal of Arthroplasty **10**(5): 643-650.

Mabry T. M., Vessely M. B., Schleck C. D., Harmsen W. S. and Berry D. J. (2007). "Revision Total Knee Arthroplasty With Modular Cemented Stems: Long-Term Follow-Up." The Journal of Arthroplasty **22**(6, Supplement): 100-105.

Mackay D. C. and Siddique M. S. (2003). "The results of revision knee arthroplasty with and without retention of secure cemented femoral components." Journal of Bone & Joint Surgery, British Volume **85-B**(4): 517-520.

Maher S. A. and Prendergast P. J. (2002). "Discriminating the loosening behaviour of cemented hip prostheses using measurements of migration and inducible displacement." Journal of Biomechanics **35**(2): 257-265.

Maher S. A., Prendergast P. J. and Lyons C. G. (2001). "Measurement of the migration of a cemented hip prosthesis in an in vitro test." Clinical Biomechanics **16**(4): 307-314.

Marieb E. N. and Hoehn K. (2007). Human Anatomy and Physiology, Pearson.

McEwen H. M. J., Barnett P. I., Bell C. J., Farrar R., Auger D. D., Stone M. H. and Fisher J. (2005). "The influence of design, materials and kinematics on the in vitro wear of total knee replacements." Journal of Biomechanics **38**(2): 357-365.

McLean A. J. (2007). The Effect of Modular Stems and Cement Fixation Techniques on the Initial Stability of the Tibial Prosthesis and the Strain Distribution within the Proximal Tibia in Primary and Revision Total Knee Arthroplasty. Doctor of Philosophy, The University of Edinburgh.

Meek R. M. D., Norwood T., Smith R., Brenkel I. J. and Howie C. R. (2011). "The risk of peri-prosthetic fracture after primary and revision total hip and knee replacement." Journal of Bone & Joint Surgery, British Volume **93-B**(1): 96-101.

Meijerink H. J., van Loon C. J. M., de Waal Malefijt M. C., van Kampen A. and Verdonschot N. (2010). "A sliding stem in revision total knee arthroplasty provides stability and reduces stress shielding." Acta Orthopaedica **81**(3): 337-343.

Meneghini R. M. and Hanssen A. D. (2008). "Cementless fixation in total knee arthroplasty: past, present, and future." The Journal Of Knee Surgery **21**(4): 307-314.

Mente P. L. and Lewis J. L. (1989). "Experimental method for the measurement of the elastic modulus of trabecular bone tissue." Journal of Orthopaedic Research **7**(3): 456-461.

Merkel K. D. and Johnson E. W., Jr. (1986). "Supracondylar fracture of the femur after total knee arthroplasty." J Bone Joint Surg Am **68**(1): 29-43.

Milovanovic P., Potocnik J., Djonic D., Nikolic S., Zivkovic V., Djuric M. and Rakocevic Z. (2012). "Age-related deterioration in trabecular bone mechanical properties at material level: Nanoindentation study of the femoral neck in women by using AFM." Experimental Gerontology **47**(2): 154-159.

Mintzer C. M., Robertson D. D., Rackemann S., Ewald C., Scott R. D. and Spector M. (1990). "Bone Loss in the Distal Anterior Femur After Total Knee Arthroplasty. ." Clinical Orthopaedics & Related Research November **260**: 135-143.

Monti L., Cristofolini L. and Viceconti M. (1999). "Methods for Quantitative Analysis of the Primary Stability in Uncemented Hip Prostheses." Artificial Organs **23**(9): 851-859.

Moran M. F. (2005). Computational and experimental assessment of total knee motion. Doctor of Philosophy, The Pennsylvania State University.

Morris B. A., D'Lima D. D., Slamin J., Kovacevic N., Arms S. W., Townsend C. P. and ColwellJr C. W. (2001). "e-Knee: Evolution of the Electronic Knee Prosthesis Telemetry Technology Development." The Journal of Bone & Joint Surgery **83**(2_suppl_1): S62-66.

Morrison J. B. (1969). "Function of the knee joint in various activities." Biomedical Engineering **4**: 573-580.

Morrison J. B. (1970). "The mechanics of the knee joint in relation to normal walking." Journal of Biomechanics **3**(1): 51-61.

Mow V. C., Ratcliffe A. and Robin Poole A. (1992). "Cartilage and diarthrodial joints as paradigms for hierarchical materials and structures." Biomaterials **13**(2): 67-97.

Mündermann A., Dyrby C. O., D'Lima D. D., Colwell C. W. and Andriacchi T. P. (2008). "In vivo knee loading characteristics during activities of daily living as measured by an instrumented total knee replacement." Journal of Orthopaedic Research **26**(9): 1167-1172.

Murphy M., Journeaux S. and Russell T. (2009). "High-flexion total knee arthroplasty: a systematic review." International Orthopaedics **33**(4): 887-893.

Nadaud M. C., Fehring T. K. and Fehring K. (2004). "Underestimation of osteolysis in posterior stabilized total knee arthroplasty." The Journal of Arthroplasty **19**(1): 110-115.

NAR (2010). Norwegian Arthroplasty Register Annual Report. Haukeland, Norwegian Arthroplasty Register.

Naudie D. D. R., Ammeen D. J., Engh G. A. and Rorabeck C. H. (2007). "Wear and Osteolysis Around Total Knee Arthroplasty." Journal of the American Academy of Orthopaedic Surgeons **15**(1): 53-64.

NHS Scotland (2009). "Scottish Arthroplasty Project Annual Report." Information Services Division NHS Scotland.

NHS Scotland (2010). "Scottish Arthroplasty Project Annual Report." Information Services Division NHS Scotland.

NIH. (2012). "What Is Osteoporosis?" Retrieved 02/01/2012, 2012, from http://www.niams.nih.gov/Health_Info/Bone/Osteoporosis/osteoporosis_ff.asp.

Nikolopoulos D., Polyzois I., Magnissalis E., Bernard P. and Michos I. (2012). "Fracture at the stem–condylar junction of a modular femoral prosthesis in a varus–valgus constrained total knee arthroplasty." Knee Surgery, Sports Traumatology, Arthroscopy **20**(6): 1071-1074.

Nilsson K. G., Henricson A., Norgren B. and Dalen T. (2006). "Uncemented HA-coated implant is the optimum fixation for TKA in the young patient." Clinical Orthopaedics and Related Research(448): 129-138.

Nilsson K. G. and Kärrholm J. (1996). "RSA in the assessment of aseptic loosening." Journal of Bone & Joint Surgery, British Volume **78-B**(1): 1-3.

Nilsson K. G., Karrholm J., Ekelund L. and Magnusson P. (1991). "Evaluation of micromotion in cemented vs uncemented knee arthroplasty in osteoarthrosis and rheumatoid

arthritis. Randomized study using roentgen stereophotogrammetric analysis." The Journal of Arthroplasty **6**(3): 265-278.

Nilsson K. G., Kärrholm J. and Linder L. (1995). "Femoral component migration in total knee arthroplasty: Randomized study comparing cemented and uncemented fixation of the Miller-Galante I design." Journal of Orthopaedic Research **13**(3): 347-356.

Nisell R. (1985). "Mechanics of the knee. A study of joint and muscle load with clinical applications." Acta Orthop Scand Suppl **216**: 1-42.

NJR (2011). "8th Annual Report." National Joint Registry for England and Whales.

Nogler M., Hozack W., Collopy D., Mayr E., Deirmengian G. and Sekyra K. (2012). "Alignment for total knee replacement: a comparison of kinematic axis versus mechanical axis techniques. A cadaver study." International Orthopaedics **36**(11): 2249-2253.

O'Brien S., Luo Y., Wu C., Petrak M., Bohm E. and Brandt J.-M. (2012). "Prediction of backside micromotion in total knee replacements by finite element simulation." Proceedings of the Institution of Mechanical Engineers, Part H: Journal of Engineering in Medicine **226**(3): 235-245.

Otani T., Whiteside L. A. and White S. E. (1993). "Cutting errors in preparation of femoral components in total knee arthroplasty." The Journal of Arthroplasty **8**(5): 503-510.

Panayi G. (2003). "What is RA?" Retrieved May 05, 2013, from http://www.nras.org.uk/about_rheumatoid_arthritis/what_is_ra/what_is_ra.aspx.

Park J. W. and Kim Y. H. (2011). "Simultaneous cemented and cementless total knee replacement in the same patients." Journal of Bone & Joint Surgery, British Volume **93-B**(11): 1479-1486.

Payen D. J. and Bathe K.-J. (2011). "Improved stresses for the 4-node tetrahedral element." Computers & Structures **89**(13–14): 1265-1273.

Petersen M. M., Olsen C., Lauritzen J. B. and Lund B. (1995). "Changes in bone mineral density of the distal femur following uncemented total knee arthroplasty." The Journal of Arthroplasty **10**(1): 7-11.

Pettersen S. H., Wik T. S. and Skallerud B. (2009). "Subject specific finite element analysis of implant stability for a cementless femoral stem." Clinical Biomechanics **24**(6): 480-487.

Petty W., Miller G. J., Bartel D. L., Wright T. M. and Burstein A. H. (1999). Total knee contact pressures: the effect of congruity and alignment. Medscape General Medicine. **1**.

Phillips A. T. M. (2009). "The femur as a musculo-skeletal construct: A free boundary condition modelling approach." Medical Engineering & Physics **31**(6): 673-680.

Phillips A. T. M., Pankaj P. and Howie C. R. (2007). "Finite element modelling of the pelvis: inclusion of muscular and ligamentous boundary conditions." Medical Engineering & Physics **29**: 739-748.

Pilliar R. M., Lee J. M. and Maniatopoulos C. D. (1986). "Observations on the Effect of Movement on Bone Ingrowth into Porous-Surfaced Implants." Clinical Orthopaedics & Related Research July **208**: 108-113.

Plaskos C., Hodgson A. J., Inkpen K. and McGraw R. W. (2002). "Bone cutting errors in total knee arthroplasty." The Journal of Arthroplasty **17**(6): 698-705.

Poole A. R., Kobayashi M., Yasuda T., Laverty S., Mwale F., Kojima T., Sakai T., Wahl C., El-Maadawy S., Webb G., Tchetina E. and Wu W. (2002). "Type II collagen degradation and its regulation in articular cartilage in osteoarthritis." Annals of the Rheumatic Diseases **61**(suppl 2): ii78-ii81.

Primal Pictures (2007). Functional Anatomy. Primal Pictures Interactive Anatomy.

Ramos A. and Simões J. A. (2006). "Tetrahedral versus hexahedral finite elements in numerical modelling of the proximal femur." Medical Engineering & Physics **28**(9): 916-924.

Rancourt D., Shirazi-Adl A., Drouin G. and Paiement G. (1990). "Friction properties of the interface between porous-surfaced metals and tibial cancellous bone." Journal of Biomedical Materials Research **24**(11): 1503-1519.

Rand J. A. (1991). "Cement or Cementless Fixation in Total Knee Arthroplasty?" Clinical Orthopaedics & Related Research December **273**: 52-62.

Rayan F., Konan S. and Haddad F. S. (2008). "A review of periprosthetic fractures around total knee arthroplasties." Current Orthopaedics **22**(1): 52-61.

Reilly D. T. and Burstein A. H. (1974). "The Mechanical Properties of Cortical Bone." The Journal of Bone & Joint Surgery **56**(5): 1001-1022.

Reilly D. T. and Martens M. (1972). "Experimental Analysis of the Quadriceps Muscle Force and Patello-Femoral Joint Reaction Force for Various Activities." Acta Orthopaedica **43**(2): 126-137.

Rho J. Y., Ashman R. B. and Turner C. H. (1993). "Young's modulus of trabecular and cortical bone material: Ultrasonic and microtensile measurements." Journal of Biomechanics **26**(2): 111-119.

Rice J. C., Cowin S. C. and Bowman J. A. (1988). "On the dependence of the elasticity and strength of cancellous bone on apparent density." Journal of Biomechanics **21**(2): 155-168.

Ritter M. A., Faris P. M. and Keating E. M. (1988). "Anterior femoral notching and ipsilateral supracondylar femur fracture in total knee arthroplasty." The Journal of Arthroplasty **3**(2): 185-187.

Runkle J. C. and Pugh J. (1975). "The micromechanics of cancellous bone. II. Determination of the elastic modulus of individual trabeculae by a buckling analysis." Bulletin of the Hospital for Joint Diseases **36**(1): 2-10.

Russo C. R., Lauretani F., Seeman E., Bartali B., Bandinelli S., Di Iorio A., Guralnik J. and Ferrucci L. (2006). "Structural adaptations to bone loss in aging men and women." Bone **38**(1): 112-118.

Ryan S. D. and Williams J. L. (1989). "Tensile testing of rodlike trabeculae excised from bovine femoral bone." Journal of Biomechanics **22**(4): 351-355.

Ryd L. (1986). "Micromotion in knee arthroplasty." Acta Orthopaedica **57**(s220): 3-80.

Ryd L. (1992). "Roentgen Stereophotogrammetric Analysis of Prosthetic Fixation in the Hip and Knee Joint. ." Clinical Orthopaedics & Related Research March **276**: 56-65.

Ryd L., Albrektsson B. E., Carlsson L., Dansgard F., Herberts P., Lindstrand A., Regner L. and Toksvig-Larsen S. (1995). "Roentgen stereophotogrammetric analysis as a predictor of mechanical loosening of knee prostheses." Journal of Bone & Joint Surgery, British Volume **77-B**(3): 377-383.

Saari T., Uvehammer J., Carlsson L. V., Regnér L. and Kärrholm J. (2006). "Posterior stabilized component increased femoral bone loss after total knee replacement. 5-year follow-up of 47 knees using dual energy X-ray absorptiometry." The Knee **13**(6): 435-439.

Sawbones. (2008, 29/08/2008). "Biomechanical bones: 4th generation biomechanical composite femur." from http://www.sawbones.com/products/product.aspx?1937.

Schneider E., Kinast C., Eulenberger J., Wyder D., Eskilsson G. and Perren S. M. (1989). "A comparative-study of the initial stability of cementless hip prostheses." Clinical Orthopaedics and Related Research(248): 200-209.

Scott C. E. H. and Biant L. C. (2012). "The role of the design of tibial components and stems in knee replacement." Journal of Bone & Joint Surgery, British Volume **94-B**(8): 1009-1015.

Scuderi G. R. (2011). "Complications After Total Knee Arthroplasty How to Manage Patients with Osteolysis." The Journal of Bone & Joint Surgery **93**(22): 2127-2135.

Scuderi G. R., Insall J. N., Windsor R. E. and Moran M. C. (1989). "Survivorship of cemented knee replacements." Journal of Bone & Joint Surgery, British Volume **71-B**(5): 798-803.

Scuderi G. R. and Tria A. J., Eds. (2006). Knee Arthroplasty Handbook Techniques in Total Knee and Revision Arthroplasty, Springer New York.

Selvik G. (1989). "Roentgen stereophotogrammetry." Acta Orthopaedica **60**(s232): 1-51.

Shi J. (2007). Finite element analysis of total knee replacement considering gait cycle load and malalignment. Doctor of Philosophy, University of Wolverhamption.

Shi J. F., Wang C. J., Laoui T., Hart W. and Hall R. (2007). "A dynamic model of simulating stress distribution in the distal femur after total knee replacement." Proceedings of the Institution of Mechanical Engineers, Part H: Journal of Engineering in Medicine.

Singh J. A., Jensen M. and Lewallen D. (2013). "Predictors of periprosthetic fracture after total knee replacement." Acta Orthopaedica **84**(2): 170-177.

Soderberg G. L. (1986). Kinesiology: Application to Pathological Motion. Baltimore, Williams &Wilkins.

Soininvaara T. A., Miettinen H. J. A., Jurvelin J. S., Suomalainen O. T., Alhava E. M. and Kröger H. P. J. (2004). "Periprosthetic femoral bone loss after total knee arthroplasty: 1-year follow-up study of 69 patients." The Knee **11**(4): 297-302.

Speirs A. D., Heller M. O., Duda G. N. and Taylor W. R. (2007). "Physiologically based boundary conditions in finite element modelling." Journal of Biomechanics **40**(10): 2318-2323.

Spinelli M., Affatato S., Cristofolini L., Erani P., Tigani D. and Viceconti M. (2010). "Combined Wear Behavior and Long-Term Implant-Bone Fixation of Total Knee Replacement: A Novel In Vitro Set-up." Artificial Organs **34**(5): E177-E183.

Spittlehouse A. J., Getty C. J. and Eastell R. (1999). "Measurement of bone mineral density by dual-energy x-ray absorptiometry around an uncemented knee prosthesis." The Journal of Arthroplasty **14**(8): 957-963.

Stryker Orthopaedics. (2008a). "Anthropometrically-Based Design." Retrieved 17/12/2008, from http://www.stryker.com/myhsp/exercise/Orthopaedics/KneeReplacement/Primary/Triathlon/038944.

Stryker Orthopaedics. (2008b). "Triathlon Total Knee Replacement System." Retrieved 17/11/2008, 2008, from http://www.stryker.com/en-us/products/Orthopaedics/KneeReplacement/Primary/Triathlon/index.htm.

Stryker Orthopaedics (2011). Triathlon® TS Knee System Surgical Protocol. **2011**.

Suárez D. R., Nerkens W., Valstar E. R., Rozing P. M. and van Keulen F. (2012). "Interface micromotions increase with less-conforming cementless glenoid components." Journal of Shoulder and Elbow Surgery **21**(4): 474-482.

Sundberg M., Lidgren L., W-Dahl A. and Robertsson O. (2011). The Swedish Knee Arthroplasty Register : Annual Report.

Sverdlova N. S. and Witzel U. (2010). "Principles of determination and verification of muscle forces in the human musculoskeletal system: Muscle forces to minimise bending stress." Journal of Biomechanics **43**(3): 387-396.

Tarala M., Janssen D., Telka A., Waanders D. and Verdonschot N. (2011). "Experimental versus Computational Analysis of Micromotions at the Implant—Bone Interface." Proceedings of the Institution of Mechanical Engineers, Part H: Journal of Engineering in Medicine **225**(1): 8-15.

Taunton J. E., Clement D. B., Smart G. W., Wiley J. P. and McNicol K. L. (1985). "A triplanar electrogoniometer investigation of running mechanics in runners with compensatory overpronation." Can J Appl Sport Sci **10**(3): 104-115.

Taylor M. and Tanner K. E. (1997). "Fatigue failure of cancellous bone: a possible cause of implant migration and loosening." Journal of Bone & Joint Surgery, British Volume **79-B**(2): 181-182.

Taylor S. J. G. and Walker P. S. (2001). "Forces and moments telemetered from two distal femoral replacements during various activities." Journal of Biomechanics **34**(7): 839-848.

Taylor S. J. G., Walker P. S., Perry J. S., Cannon S. R. and Woledge R. (1998). "The forces in the distal femur and the knee during walking and other activities measured by telemetry." The Journal of Arthroplasty **13**(4): 428-437.

Taylor W. R., Heller M. O., Bergmann G. and Duda G. N. (2004). "Tibio-femoral loading during human gait and stair climbing." Journal of Orthopaedic Research **22**(3): 625-632.

Terrier A. (1999). Adaptation of bone to mechanical stress: theoretical model, experimental identification and orthopedic application. PhD, Swiss Federal Institute of Technology.

Thambyah A. (2008). "How critical are the tibiofemoral joint reaction forces during frequent squatting in Asian populations?" The Knee **15**(4): 286-294.

Tissakht M., Ahmed A. M. and Chan K. C. (1996). "Calculated stress-shielding in the distal femur after total knee replacement corresponds to the reported location of bone loss." Journal of Orthopaedic Research **14**(5): 778-785.

Toksvig-Larsen S., Ryd L. and Lindstrand A. (1998). "Early Inducible Displacement of Tibial Components in Total Knee Prostheses Inserted with and without Cement. A Randomized Study with Roentgen Stereophotogrammetric Analysis*." The Journal of Bone & Joint Surgery **80**(1): 83-89.

Townsend P. R., Raux P., Rose R. M., Miegel R. E. and Radin E. L. (1975a). "The distribution and anisotropy of the stiffness of cancellous bone in the human patella." Journal of Biomechanics **8**(6): 363-367.

Townsend P. R., Rose R. M. and Radin E. L. (1975b). "Buckling studies of single human trabeculae." Journal of Biomechanics **8**(3–4): 199-201.

Turner C. H. (1999). "Toward a Mathematical Description of Bone Biology: The Principle of Cellular Accommodation." Calcified Tissue International **65**(6): 466-471.

Turner M. J., Clough R. W., Martin H. C. and Topp L. J. (1956). "Stiffness and Deflection Analysis of Complex Structures." Journal of the Aeronautical Sciences (Institute of the Aeronautical Sciences) **23**(9): 805-823.

van der Ploeg B., Tarala M., Homminga J., Janssen D., Buma P. and Verdonschot N. (2012). "Toward a more realistic prediction of peri-prosthetic micromotions." Journal of Orthopaedic Research **30**(7): 1147-1154.

van Lenthe G. H., de Waal Malefijt M. C. and Huiskes R. (1997). "Stress shielding after total knee replacement may cause bone resorption in the distal femur." Journal of Bone & Joint Surgery, British Volume **79-B**(1): 117-122.

van Lenthe G. H., Willems M. M. M., Verdonschot N., de Waal Malefijt M. C. and Huiskes R. (2002). "Stemmed femoral knee prostheses: effects of prosthetic design and fixation on bone loss." Acta Orthopaedica Scandinavica **73**(6): 630.

van Loon C. J., de Waal Malefijt M. C., Buma P., Verdonschot N. and Veth R. P. (1999). "Femoral bone loss in total knee arthroplasty. A review." Acta orthopaedica Belgica **65**(2): 154-163.

van Loon C. J. M., Kyriazopoulos A., Verdonschot N., de Waal Malefijt M. C., Huiskes R. and Buma P. (2000). "The role of femoral stem extension in total knee arthroplasty." Clinical Orthopaedics and Related Research(378): 282-289.

van Loon C. J. M., Oyen W. J. G., de Waal Malefijt M. C. and Verdonschot N. (2001). "Distal femoral bone mineral density after total knee arthroplasty: a comparison with general bone mineral density." Archives of Orthopaedic and Trauma Surgery **121**(5): 282-285.

van Rietbergen B., Huiskes R., Eckstein F. and Rüegsegger P. (2003). "Trabecular Bone Tissue Strains in the Healthy and Osteoporotic Human Femur." Journal of Bone and Mineral Research **18**(10): 1781-1788.

van Rietbergen B., Weinans H., Huiskes R. and Odgaard A. (1995). "A new method to determine trabecular bone elastic properties and loading using micromechanical finite-element models." Journal of Biomechanics **28**(1): 69-81.

Vandamme K., Naert I., Geris L., Sloten J. V., Puers R. and Duyck J. (2007). "The effect of micro-motion on the tissue response around immediately loaded roughened titanium implants in the rabbit." European Journal of Oral Sciences **115**(1): 21-29.

Verhulp E., van Rietbergen B. and Huiskes R. (2008). "Load distribution in the healthy and osteoporotic human proximal femur during a fall to the side." Bone **42**(1): 30-35.

Viceconti M., Muccini R., Bernakiewicz M., Baleani M. and Cristofolini L. (2000). "Large-sliding contact elements accurately predict levels of bone–implant micromotion relevant to osseointegration." Journal of Biomechanics **33**(12): 1611-1618.

W.H.O. (2012). "Ageing." Retrieved 05/09/2012, 2012, from http://www.who.int/topics/ageing/en/.

Wackerhagen A., Bodem F. and Hopf C. (1992). "The effect of cement fixation on initial micromotion of the femoral component in condylar knee replacement." International Orthopaedics **16**(1): 25-28.

Walker P. S. and Sathasivam S. (1992). "A simplified radiographic method for measuring bone-component motion in total knees." Journal of Biomechanics **25**(9): 1059-1066.

Warfel J. H. (1993). The Extremities Muscles and Motor Points, Lippincott Williams & Wilkins.

Waugh A. and Grant A. (2010). Ross and Wilson Anatomy and Physiology in Health and Illness, Elsevier Health Sciences Churchill Livingstone.

Westrich G. H., Hidaka C. and Windsor R. E. (1997). "Disengagement of a Locking Screw from a Modular Stem in Revision Total Knee Arthroplasty. A Report of Three Cases*." The Journal of Bone & Joint Surgery **79**(2): 254-258.

Wheeless C. R. (1996a, 26/04/2012). "Mechanical Axis." Retrieved 20/09/2012, 2012, from http://www.wheelessonline.com/ortho/mechanical_axis.

Wheeless C. R. (1996b). "Wheeless' Textbook of Orthopaedics." Retrieved May 10, 2012, from http://www.wheelessonline.com/ortho/muscle_index.

Whittaker J. P., Dharmarajan R. and Toms A. D. (2008). "The management of bone loss in revision total knee replacement." Journal of Bone & Joint Surgery, British Volume **90-B**(8): 981-987.

Wilkie Y. M., Kerr C. D., Conlisk N. and Pankaj P. (2012). "Computational analysis of the mechanical environment in the femur - how sophisticated does a model need to be?" Journal of Bone & Joint Surgery, British Volume **94-B**(SUPP XVIII): 97-97.

Wolff J. (1892). Das Gesetz der Transformation der Knochen. Berlin, Hirschwald.

Yau W. P. and Chiu K. Y. (2008). "Cutting errors in total knee replacement: assessment by computer assisted surgery." Knee Surgery, Sports Traumatology, Arthroscopy **16**(7): 670-673.

Zdero R., Bougherara H., Dubov A., Shah S., Zalzal P., Mahfud A. and Schemitsch E. H. (2010). "The effect of cortex thickness on intact femur biomechanics: A comparison of finite element analysis with synthetic femurs." Proceedings of the Institution of Mechanical Engineers, Part H: Journal of Engineering in Medicine **224**(7): 831-840.

Zelle J., Janssen D., Van Eijden J., De Waal Malefijt M. and Verdonschot N. (2011). "Does high-flexion total knee arthroplasty promote early loosening of the femoral component?" Journal of Orthopaedic Research **29**(7): 976-983.

Zhao D., Banks S. A., D'Lima D. D., Colwell Jr C. W. and Fregly B. J. (2007). "In vivo medial and lateral tibial loads during dynamic and high flexion activities." Journal of Orthopaedic Research **25**(5): 593-602.

Zhou H., Wang D., Liu T., Zeng X. and Wang C. (2012). "Kinematics of hip, knee, ankle of the young and elderly Chinese people during kneeling activity." Journal of Zhejiang University- SCIENCE B (Biomedicine & Biotechnology) **13**(10).

Zienkiewicz O. C. and Taylor R. L. (2000a). Finite Element Method, Volume 1, Elsevier Butterworth-Heinemann.

Zienkiewicz O. C. and Taylor R. L. (2000b). Finite Element Method, Volume 2, Elsevier Butterworth-Heinemann.

Zienkiewicz O. C. and Taylor R. L. (2000c). Finite Element Method, Volume 3, Elsevier Butterworth-Heinemann.

Zysset P. K., Edward Guo X., Edward Hoffler C., Moore K. E. and Goldstein S. A. (1999). "Elastic modulus and hardness of cortical and trabecular bone lamellae measured by nanoindentation in the human femur." Journal of Biomechanics **32**(10): 1005-1012.

# A

# Benchmark Tests for Chapter IV

## A.1 Stress shielding benchmark tests

In Chapter IV the issue of femoral component stress shielding was investigated. To help illustrate one of the mechanisms which contribute to stress shielding in the distal femur, a series of simple benchmark tests were conducted. This appendix details the creation and solving of these simple models and highlights the key findings.

## A.2 Methods

Three principal models were created for the purposes of this study (Figure A.1). The first represented the intact case, the second represented an implanted case similar to knee arthroplasty (e.g. implant in series) and the third an implanted case similar to hip arthroplasty (e.g. implant in parallel).

### A.2.1 Material properties

In this study cortical bone properties ($E = 16700$ MPa and $\nu = 0.3$) were applied to bone regions and properties of stainless steel ($E = 210000$ MPa and $\nu = 0.3$) were applied to implant structures.

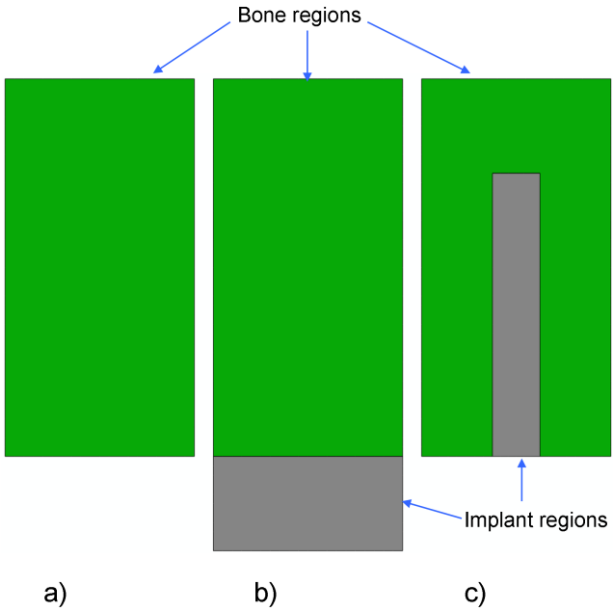


**Figure A.1:** Simple two-dimensional plane strain models used to examine post implantation stress shielding, where a) represents the intact bone, b) a bone with implant in series and c) a bone with implant in parallel. Bone regions are shown in green and implant regions in grey.

### A.2.2 Loading, boundary conditions and interface properties

In these simple benchmark tests the proximal most edge (top edge) of the rectangular structure representing bone was fixed in all degrees of freedom, as with the models presented in Chapter IV, all bone implant assemblies were considered to be fully tied at the interface.

Two methods of loading were considered, the first method was applied displacement and the second applied load. Under the applied displacement conditions a displacement of 0.1mm in the positive y direction was applied to the distal most edge (bottom edge) of the models as shown in Figure A.2. Under applied loading conditions (Figure A.3) a small region on the distal most surface representative of the joint contact was subjected to a uniformly distributed pressure load ( $P = 10\,\text{MPa}$). In this instance the geometry was modified slightly through the addition of a bone and prosthesis blocks to models a) and c) respectively, in this manner the region of loading was kept consistent across all models (as shown in Figure A.3).

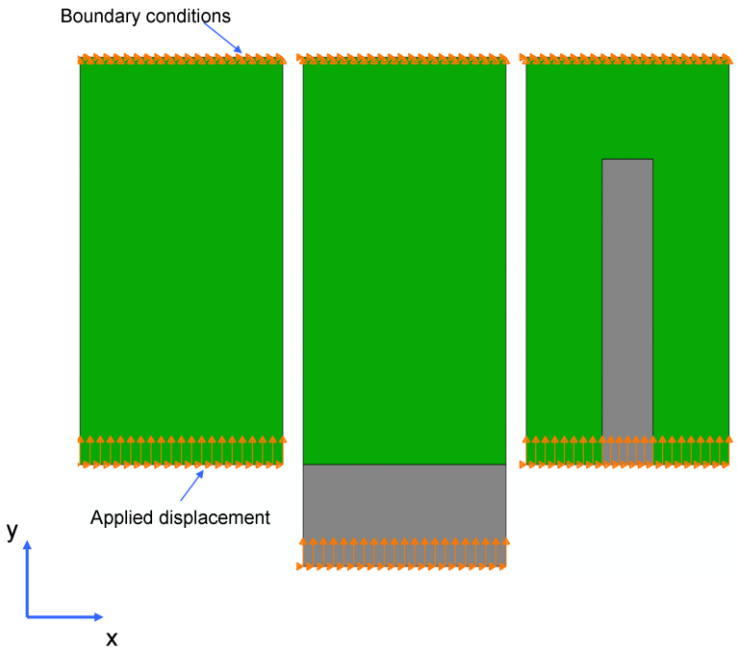


**Figure A.2:** Illustration of the model boundary conditions and applied displacement loading conditions for all three models.

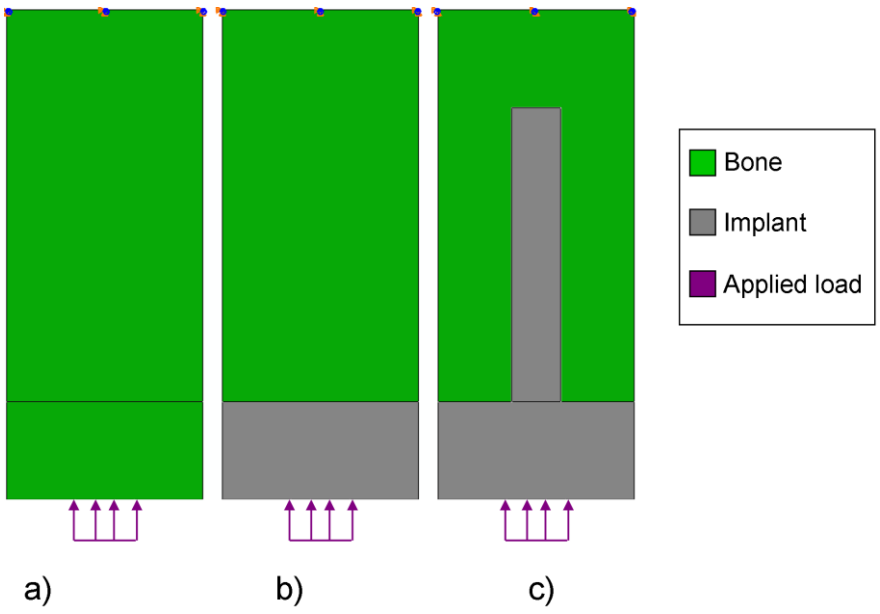


**Figure A.3:** Illustration of the applied load model setup for a) an intact bone, b) a bone with implant in series and c) a bone with implant in parallel and series.

## A.3 Results

The resulting von Mises stress distributions for each model under applied displacement loading conditions are shown in Figure A.4. It can be seen that the models representative of the intact bone and a bone with prosthesis implanted in series lead to very similar stress distributions throughout the bone regions of both models. On the other hand, the bone with prosthesis implanted in parallel can be seen to exhibit significantly lower stress at the bottom end of the bone and higher stress at the top end, e.g. the stem due to its higher stiffness is transmitting the majority of load to the bone immediately above the stem. Similar distributions of stress are often seen clinically at the hip after stemmed THA or distally at the knee after revision TKA with a long stemmed femoral component.

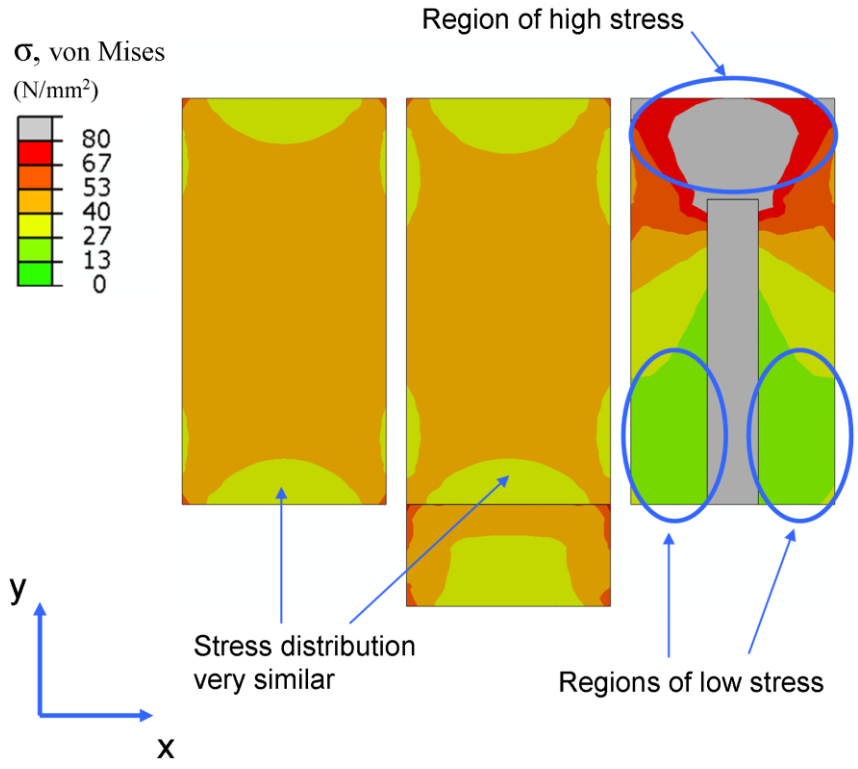


**Figure A.4:** von Mises stress distribution for applied displacement conditions.

The second set of results considers the influence of applied load on stress distribution within the bone regions for all three models (Figure A.5). It can be observed in this

instance that the intact bone model exhibits a bulb of stress extending upwards from the joint contact site. In the other two cases, however, due to the relative difference in stiffness between bone and the implant, the stress resulting from the joint contact force is distributed over a wider area leading to an absence of this stress bulb.

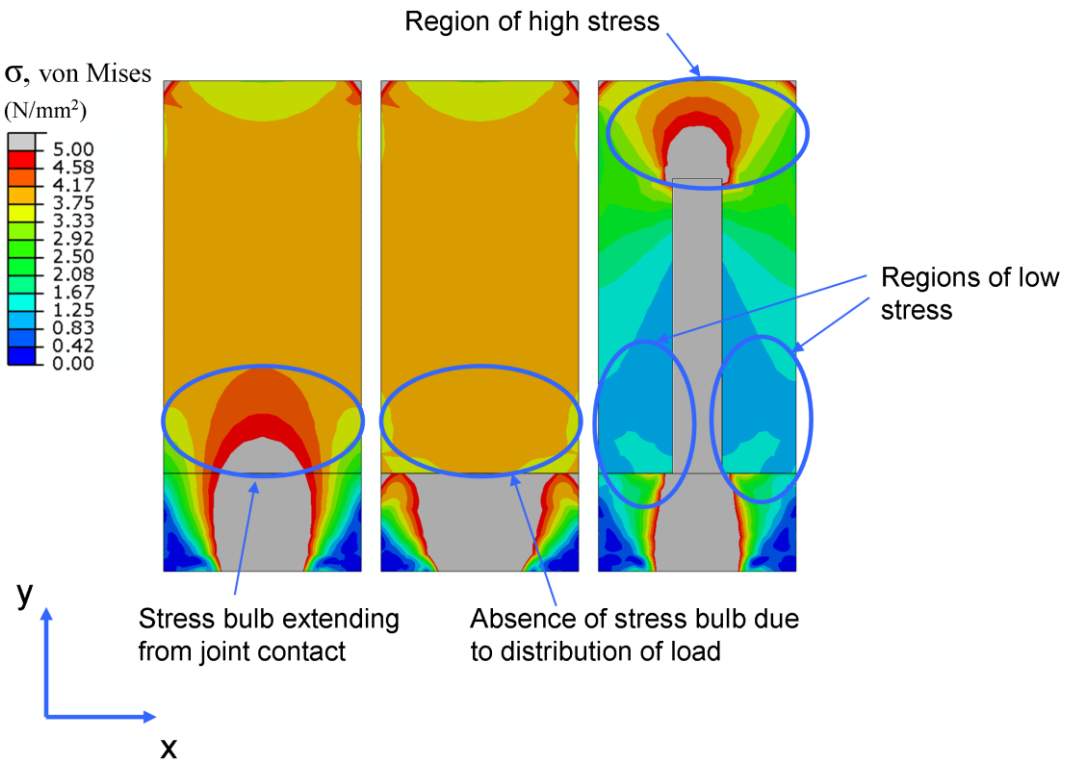


**Figure A.5:** von Mises stress distribution for applied load conditions.

## A.4 Conclusions

Both the hip and knee joints experience stress shielding following joint arthroplasty. In this benchmark study the mechanisms at work, pertaining to stress shielding following TKA, were more closely examined. These findings indicate two important points. Firstly, the models presented in this appendix suggest that the exact mechanism of shielding appears to be different in both THA and TKA scenarios. Secondly, the redistribution of concentrated forces due to the stiffness of the implant and not merely the presence of an implant itself is one possible contributing factor to the stress shielding observed clinically in the distal femur.

# B

# Computational Micromotion

## B.1 Frictional interface benchmark tests

In Chapter VII FE models of the distal femur employing frictional interfaces were used to capture the relative micromotions between bone and prosthesis due to physiological loading following joint arthroplasty.

In determining the validity of a frictional contact analysis in the field of orthopaedic biomechanics it is suggested that successive iterations of a model should result in a small change in predicted micromotions relative to 150µm (Bernakiewicz and Viceconti 2002). In any FE analysis the accuracy of the solution is dependent on correct assignment of material properties, geometry, boundary conditions and external loading. Furthermore the resolution of the mesh must be adequate enough to ensure that the solution is independent of element size, however, the inclusion of frictional interactions at the bone-implant interface requires the definition of a number of additional parameters which may also affect solution accuracy (e.g. coefficient of friction and allowable elastic slip).

## B.2 Benchmark tests

A series of benchmark tests were carried out to investigate how changes to interface properties influence the pattern of relative motion observed at the bone prosthesis interface. To avoid the large computational cost associated with varying frictional properties on the complex three-dimensional model of the distal femur; these benchmark tests employed the use of simple solid cubical domains. Referring to

Figure B.1, at the beginning of the analysis both cubical domains were perfectly aligned with a frictional interface applied at the contacting surfaces.

The top part (Part A) was assigned the properties of cancellous bone, while the bottom part was assigned properties of steel. The Young's moduli of cancellous bone and steel applied in these analyses were $2x10^3$ MPa and $2.1x10^5$ MPa respectively. A Poisson's ratio (ν) of 0.3 was assumed for both materials. Both simple cubical parts had an edge length of 10mm.

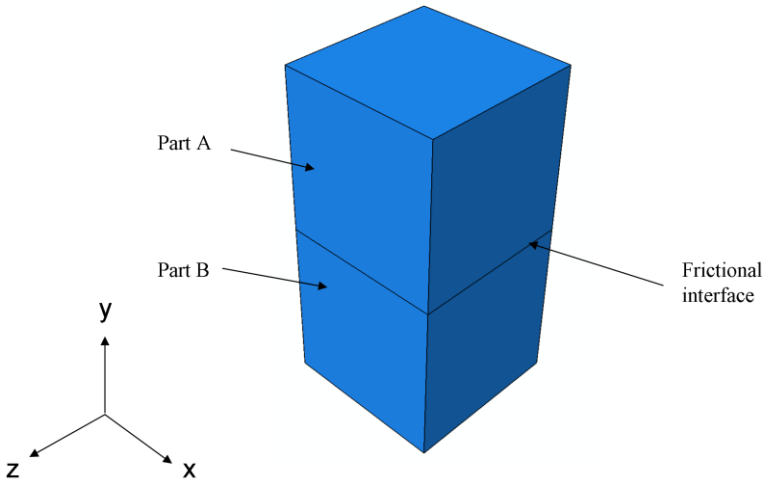


**Figure B.1:** Benchmark model setup used to test frictional parameters.

In this first test the bottom surface of part 2 (the steel block) was fully restrained in all degrees of freedom. Normal vertical loads were applied to the top surface of part 1 (cancellous bone). The bottom surface of part 1 was then subject to an applied displacement in the x-direction and the reaction forces at the fixed surface of part 2 were recorded. A frictional coefficient of $\mu = 0.3$ was assumed at the interface. The first set of tests conducted detail the effects of varying the slip tolerance on the behaviour at the frictional interface.

### B.2.1 Investigation of slip tolerance

In this test each part was meshed with a single 20 noded quadratic brick element. Force-displacement curves were then generated for an applied normal force of 10N and a maximum displacement of 1mm with varying slip tolerance values as indicated in Table B.1.

**Table B.1:** Slip parameter variations tested.

| Model | Slip tolerance $F_f$ |
|---|---|
| Model 1 | 0.00005 |
| Model 2 | 0.005 |
| Model 3 | 0.05 |
| Model 4 | 0.1 |

Referring to Figure B.2, it can be seen that the selection of the correct slip tolerance is an important factor when modelling frictional interactions between solid structures as it directly influence the level of motion which occurs at the interface.

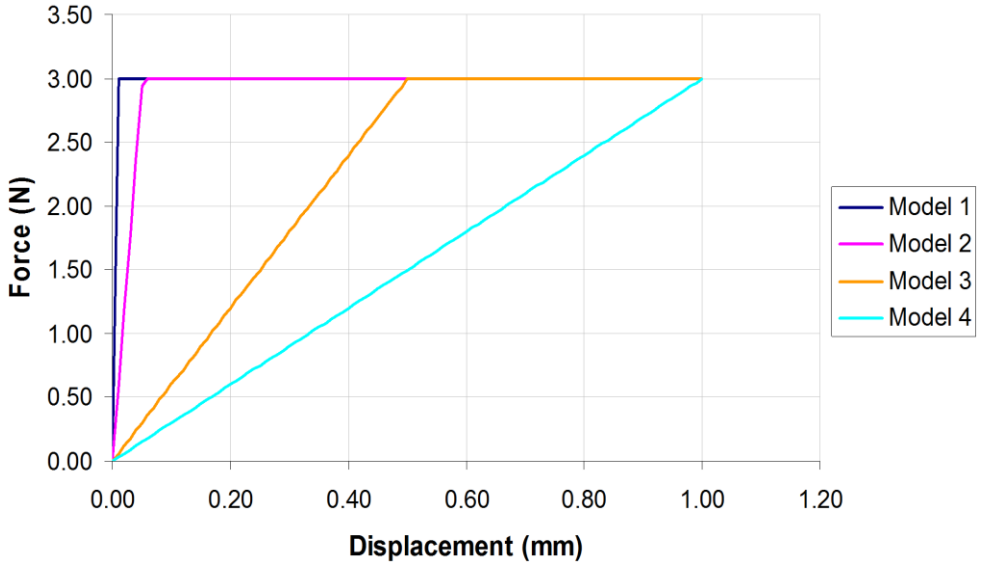


**Figure B.2:** Influence of slip tolerance $F_f$ on interfacial motion prior to the theoretical value for motion as defined by Coulomb friction theory.

### B.2.2 Investigation of mesh refinement

According to Equation 7.2, allowable slip is a function of characteristic element length. Therefore the next benchmark model focused on the role mesh refinement plays on reported motion at the interface. In this instance slip tolerance ( $F_f$ ) was maintained at 0.005 and the number of elements used to mesh each model was increased as shown in Figure B.3 and Table B.2.

**Table B.2:** Level of mesh refinement.

| Model | Total number of elements |
|---|---|
| Model 1 | 2 |
| Model 2 | 16 |
| Model 3 | 128 |
| Model 4 | 250 |

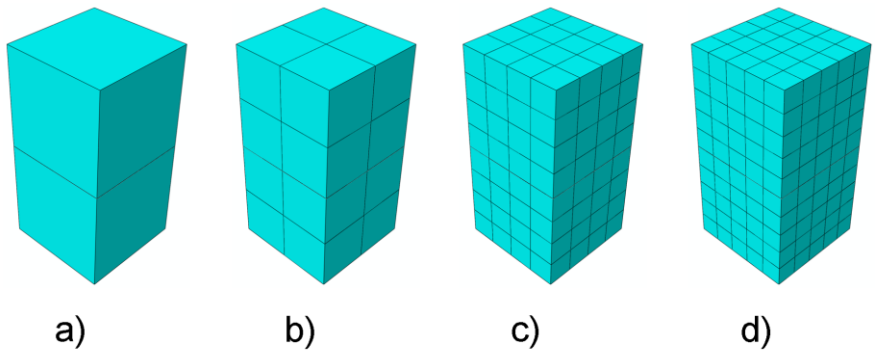


**Figure B.3:** Isometric view of models used to investigate effect of mesh refinement on motion at the interface, with numbers of elements define as per Table B.2 where a) 2 elements, b) 16 elements, c) 128 element and d) 250 elements.

It is observed that when specifying slip tolerance, the overall levels of motion reported become highly mesh sensitive (Figure B.4). On the other hand if we specify

the allowable elastic slip as defined by $y_i$ directly, then it can be seen that maximum recorded motions for these simple benchmark tests become "*largely*" independent of mesh refinement (Figure B.5), assuming proper care has been taken through convergence studies to ensure the base mesh is of adequate refinement to give an acceptable solution.

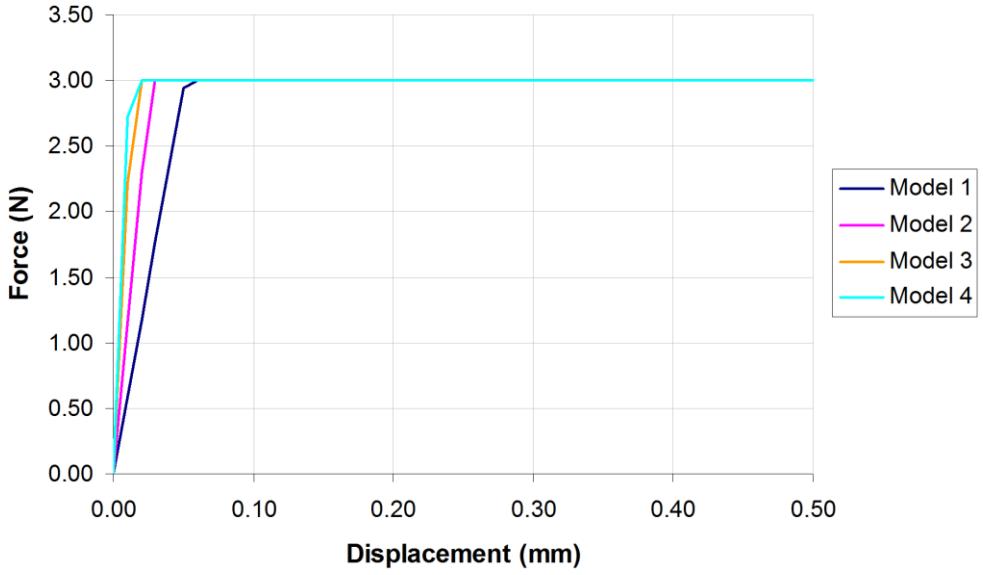


**Figure B.4:** Influence of mesh refinement on motion at the interface.

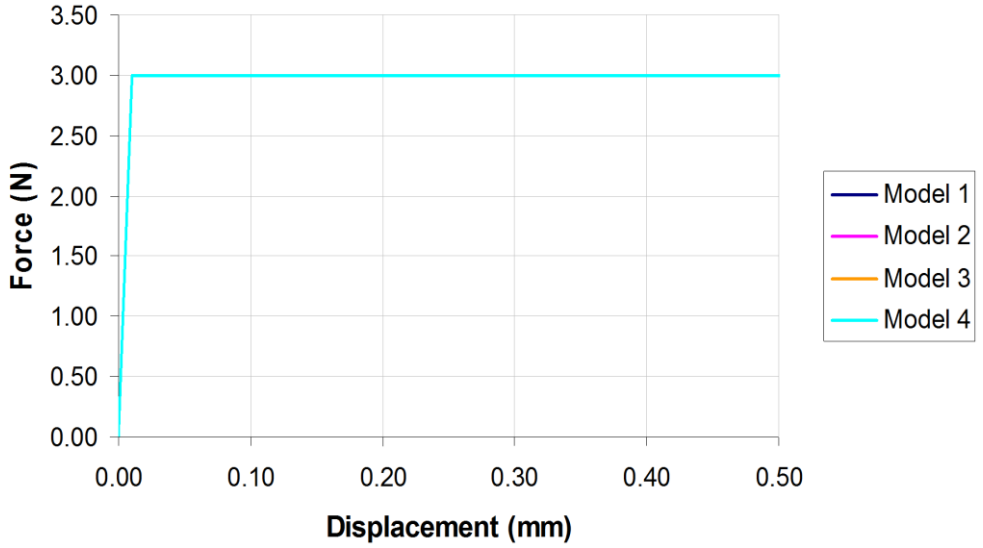


**Figure B.5:** Influence of mesh refinement when the allowable elastic slip $y_i$ is specified directly.

### B.2.3 Bidirectional frictional setup

The bone-implant interface must withstand variable magnitudes of loading from multiple directions simultaneously during gait. To test the influence of multi-directional loading on the allowable slip parameter a bi-directional horizontal displacement setup was adopted. In this case the allowable elastic slip was specified directly $y_i = 0.005$.

Referring to Figure B.6, the two tangential forces in the x and z directions are identical. Under bi-directional loading it was observed that the model reached the sliding limit at a lower tangential force. Upon investigation it was determined that this is due to the equivalent frictional stress acting on the cube at the interface. The case of friction for a bi-directional loading setup can therefore be described by the following equation (Equation B.1).

$$\tau_{eq} = \sqrt{\tau_1^2 + \tau_2^2} \qquad (B.1)$$

Where $\tau_{eq}$ represents the equivalent frictional stress acting on the surface, after which sliding will occur. $\tau_1$ is the tangential frictional stress in the global x-direction and $\tau_2$ the tangential frictional stress in the global z-direction.

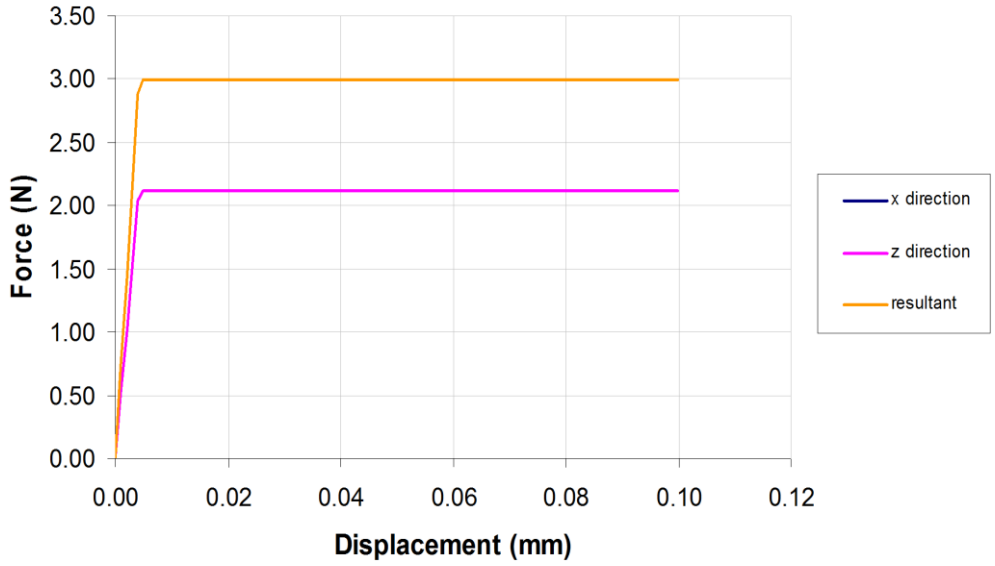


**Figure B.6:** Influence of bidirectional loading on force to overcome friction.

### B.2.4 Load controlled behaviour

All previous tests were conducted under application of an applied horizontal displacement. If in place of displacements horizontal loads were applied then as would be expected non convergence of the solution would be achieved once the horizontal load exceeds the maximum frictional force, i.e. the flat portion of the load displacement curves seen previously cannot be obtained through a load controlled FE analysis. The lack of convergence under load controlled analyses can be a serious problem in modelling of frictional interfaces of the knee, where the complexity of the loads acting on the knee joint don't lend themselves easily to being converted to displacement control.

### B.2.5 Conclusions on simple benchmark tests

It is important that the user is aware of how friction is being applied in numerical simulations, particularly if the simulation's main focus is the comparison of interfacial motions where two or more dissimilar meshes are involved. If two such meshes were compared under default conditions, differences in characteristic element length would lead to different elastic slip tolerances being applied and therefore would cause an uncertain level of error to be introduced to the results which would affect any attempt at comparison of results. It is also evident that changes to the slip tolerance parameter exert a more dramatic effect on interfacial motions than that due to variations in mesh density for the simplified models tested.

It is therefore recommended that in the more complex three-dimensional studies, as motion on the scale of microns between different implant types is to be considered (with varying mesh densities due to prosthesis features), direct specification of the allowable elastic slip ( $y_i = 0.005$ or $5\mu m$) is recommended to minimise influence of numerical parameters on the results of the analyses.

## B.3 Complex model tests

A series of tests were conducted to quantify the influence of both the coefficient of friction and level of mesh refinement on interfacial motions in the complex three-dimensional models. These studies employed the PS implanted femur model detailed in Chapter VII. All material properties, loading (at 48° flexion) and boundary conditions remained constant and are as described in the Chapter.

### B.3.1 Influence of frictional coefficient

It is suggested that a change in frictional coefficient when $\mu$ is in the range of 0.1-0.5 minimally influences the results of the simulation (Kuiper and Huiskes 1996, Viceconti et al. 2000). It is also suggested that a change in input parameter should result in a small change in motion relative to 150μm (Abdul-Kadir et al. 2008). In this study the PS implanted femur with average element edge length of 2mm was employed with different coefficients of friction as detailed in Table B.3.

**Table B.3:** Coefficients of friction investigated.

| Model | Coefficient of friction ($\mu$) |
|---|---|
| Frictionless model | 0 |
| Frictional model 1 | 0.1 |
| Frictional model 2 | 0.2 |
| Frictional model 3 | 0.3 |
| Frictional model 4 | 0.5 |
| Frictional model 5 | 0.5 |

The resulting peak values of motion in the normal and tangential directions at the interface are shown in Figure B.7. The results showed that going from a purely frictionless case to a frictional setup, where $\mu = 0.1$, caused an approximate reduction

in interfacial motion of 20%. Subsequent incrementation of $\mu$ in steps of 0.1 caused further reductions of approximately 10% per increment. In general this equates to a reduction of $15\mu m$ going from frictionless to frictional and a further $8-10\mu m$ for every subsequent incrementation of the coefficient of friction.

The variation between frictional coefficients is found to be half that of the variation between a frictionless and frictional case, while the inter model variability is quite small for the frictional cases (Frictional models 1 to 5) in comparison to the suggest value of $150\mu m$ (e.g. changes to friction result in a variation of <7%) the overall range of motion going from $\mu = 0.1$ to $\mu = 0.5$ accounts for an approximate reduction in interfacial motions of 27%. These findings indicate that careful selection of the frictional coefficient is necessary to ensure solution accuracy, particularly during replication of experimental setups.

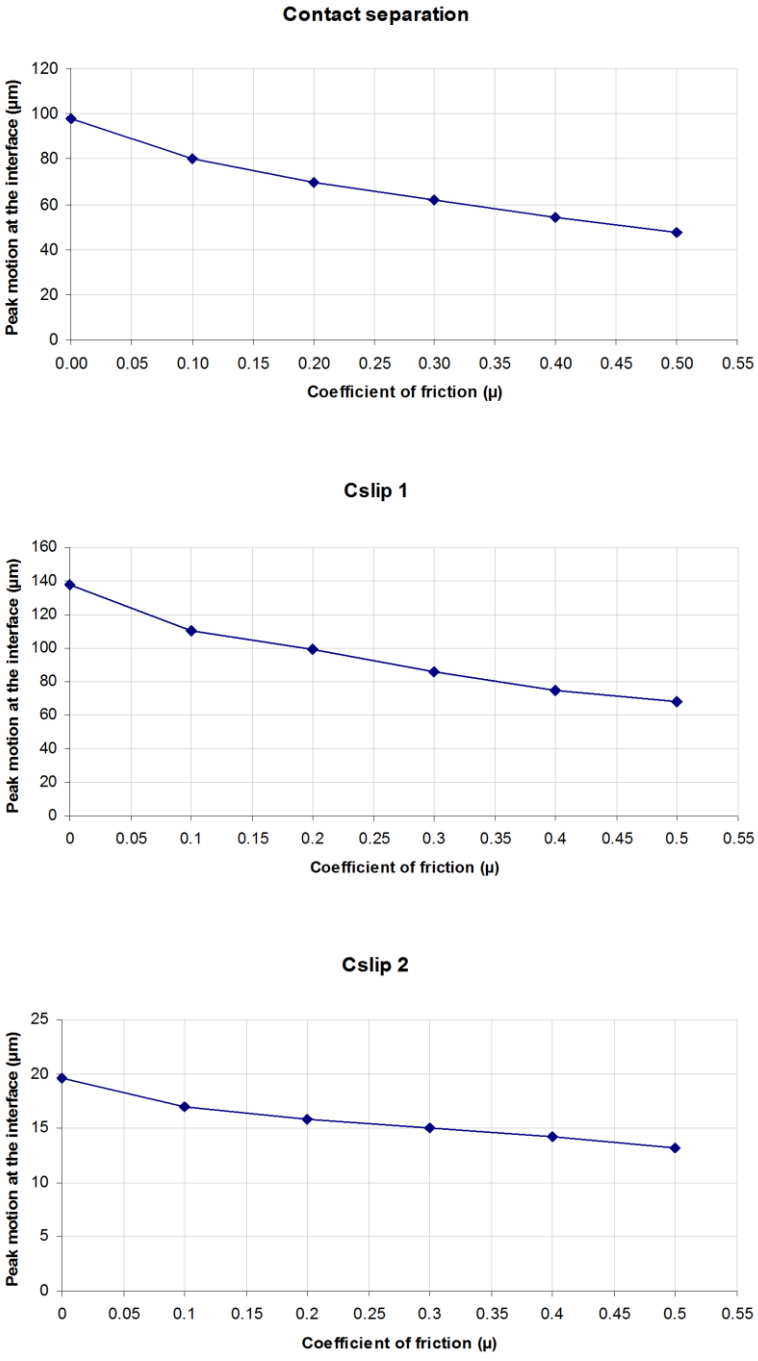


**Figure B.7:** Individual components of peak interface motion for varying coefficients of friction.

### B.3.2 Mesh refinement on peak motions

In this study the effect of seven different mesh densities, ranging from coarse to fine (e.g. 10mm to 1mm), on peak interfacial motion was investigated. Details of the overall element numbers and average element edge length for models of the distal femur used in this study are presented in Table B.4.

**Table B.4:** levels of mesh refinement investigated.

| Model | Number of elements | Average element edge length (mm) |
|---|---|---|
| Coarse mesh 1 | 61770 | 10 |
| Coarse mesh 2 | 64206 | 8 |
| Refined mesh 1 | 78043 | 5 |
| Refined mesh 2 | 92669 | 4 |
| Refined mesh 3 | 134763 | 3 |
| Refined mesh 4 | 293563 | 2 |
| Refined mesh 5 | 1537493 | 1 |

The results of these analyses are presented in Figure B.8. It can be seen that element edge length does have a slight impact on peak motion at the interface. However, it should be noted that by directly specifying the allowable elastic slip, as in the previously described benchmark tests, the variation of peak motions with changing mesh density is found to be less severe than the variation of peak motions with changing coefficient of friction, e.g. over the range of frictional coefficients tested peak motions varied by up to $40\mu m$, whereas changes to the level of mesh refinement as presented in this study resulted in an overall maximum variation in peak motions of just over half that ($< 24\mu m$). Though the variation in mesh typically resulted in a change of $< 4\mu m$ for the more refined meshes it is still recommended that the optimum mesh density be chosen to ensure solution accuracy.

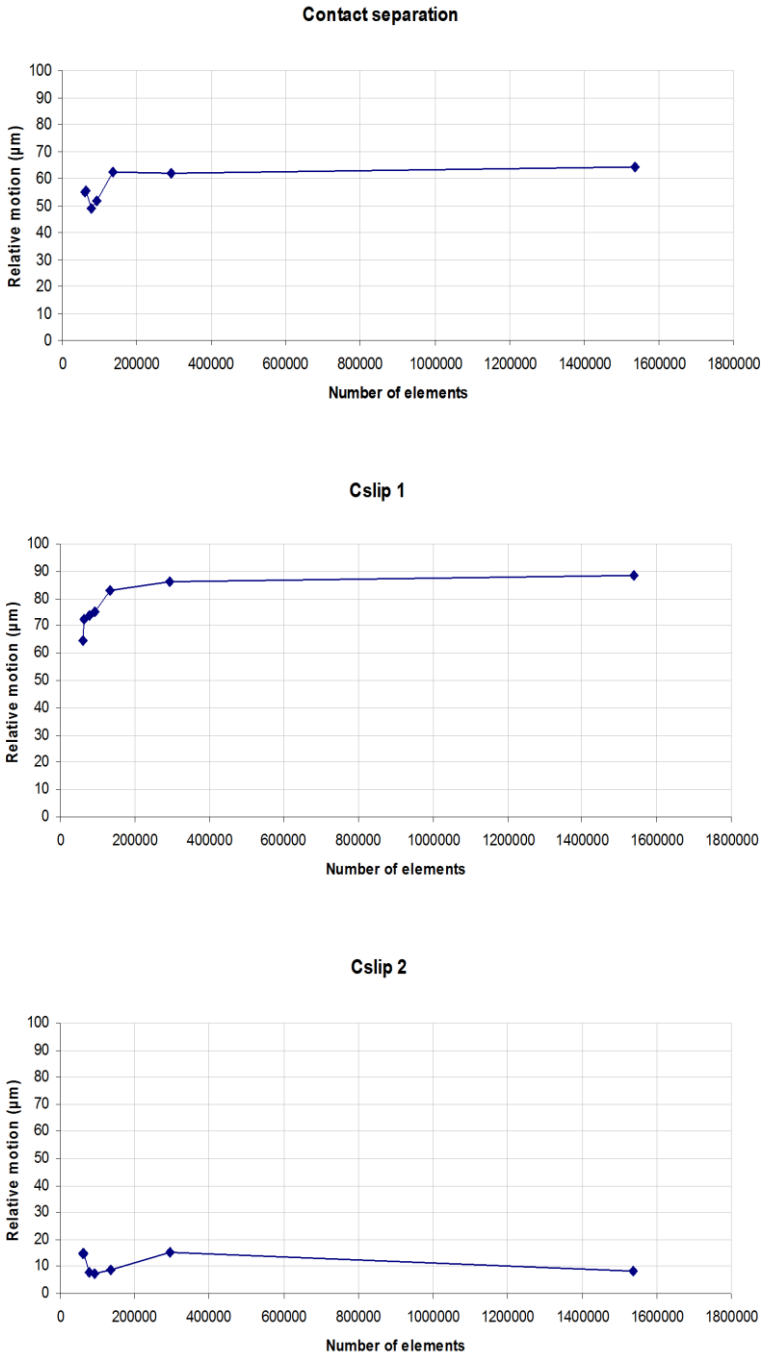


**Figure B.8:** Individual components of peak interface motion for varying levels of mesh refinement.

In this instance, the results from Figure B.8 also show that the model with an average element edge length of 2mm  model "Refined mesh 4" represents the best balance of overall model complexity and solution accuracy.

## B.4 Supplementary details of additional contact parameters

The previous section detailed the key contact settings used to implement coulomb friction in Abaqus for FE models with frictional interfaces. However, several additional software specific parameters are also required during frictional analyses. These parameters relate to how the contact interfaces are defined, the interactions are enforced and the contact itself is tracked. Tables B.5 to B.7 provide an overview of the parameters and their respective values as applied in the current analyses. Further information on each of these parameters can be found in the Abaqus manuals (Dassault Systèmes 2010b).

**Table B.5:** Summary of interaction module settings.

| Parameter | Value |
|---|---|
| Sliding formulation | Finite sliding |
| Discretisation method | Surface to surface |
| Slave adjustment | No adjustment |
| Surface smoothing | Do not smooth |
| Contact tracking | Two configurations (path) |

**Table B.6:** Summary of interaction properties module settings.

| Parameter | Value |
|---|---|
| Tangential behaviour: | |
| Friction formulation | Penalty |
| Directionality | Isotropic |
| Frictional coefficient | 0.3 |
| Shear stress | No limit |
| Normal behaviour: | |
| Elastic slip | Absolute distance (0.005) |
| Pressure overclosure | “Hard” Contact |
| Check box | Allow separation after contact |
| Contact enforcement method | Penalty (Standard) |
| Behaviour | Linear |
| Stiffness value | Use default |
| Stiffness scale factor | 1 |
| Clearance at which contact pressure is zero | 0 |

**Table B.7:** Summary of contact controls.

| Parameter | Value |
|---|---|
| Frictional onset | Immediate |
| Stabilisation | No stabilisation |

## B.5 Supplementary contour plots of relative motion

This section of Appendix B contains supplementary contour plots for the frictional interface FE models presented in Chapter VII at both 0° and 22° flexion.

The first set of plots compare the influence of a loose fit on interfacial motion for both the CR and PS implanted femur models (Figure B.9 and B.10). The second set of plots detail the comparison of TSSS and TSLS models under normal fit conditions (Figure B.11 and B.12) and the final set of plots examine the effect of a loose fit on stemmed femoral prostheses (Figure B.13 and B.14).

It can be seen from Figures B.9 to B.14 that the majority of motions which occurred at lower flexion angles were found to be well within the limits for osseointegration (typically $< 20\mu m$), with the exception of small regions on the distal surfaces and anterior chamfers of the CR, PS and TSSS implanted femurs under both normal and loose fit conditions which were observed to be approaching the lower boundary fibrous tissue formation (e.g. $20 - 40\mu m$). In general it was observed that motion increased going from a normal fit to loose fit. By comparing Figures B.14 and B.10 it can be seen that the TS implant with short stem appears more sensitive to the presence of imperfect femoral bone cuts than the PS implanted femur, and that the TS implant with long stem was the most stable under both interface conditions, for the flexion angles and loading patterns investigated.

### B.5.1 Cruciate retaining vs. posterior stabilising – loose fit

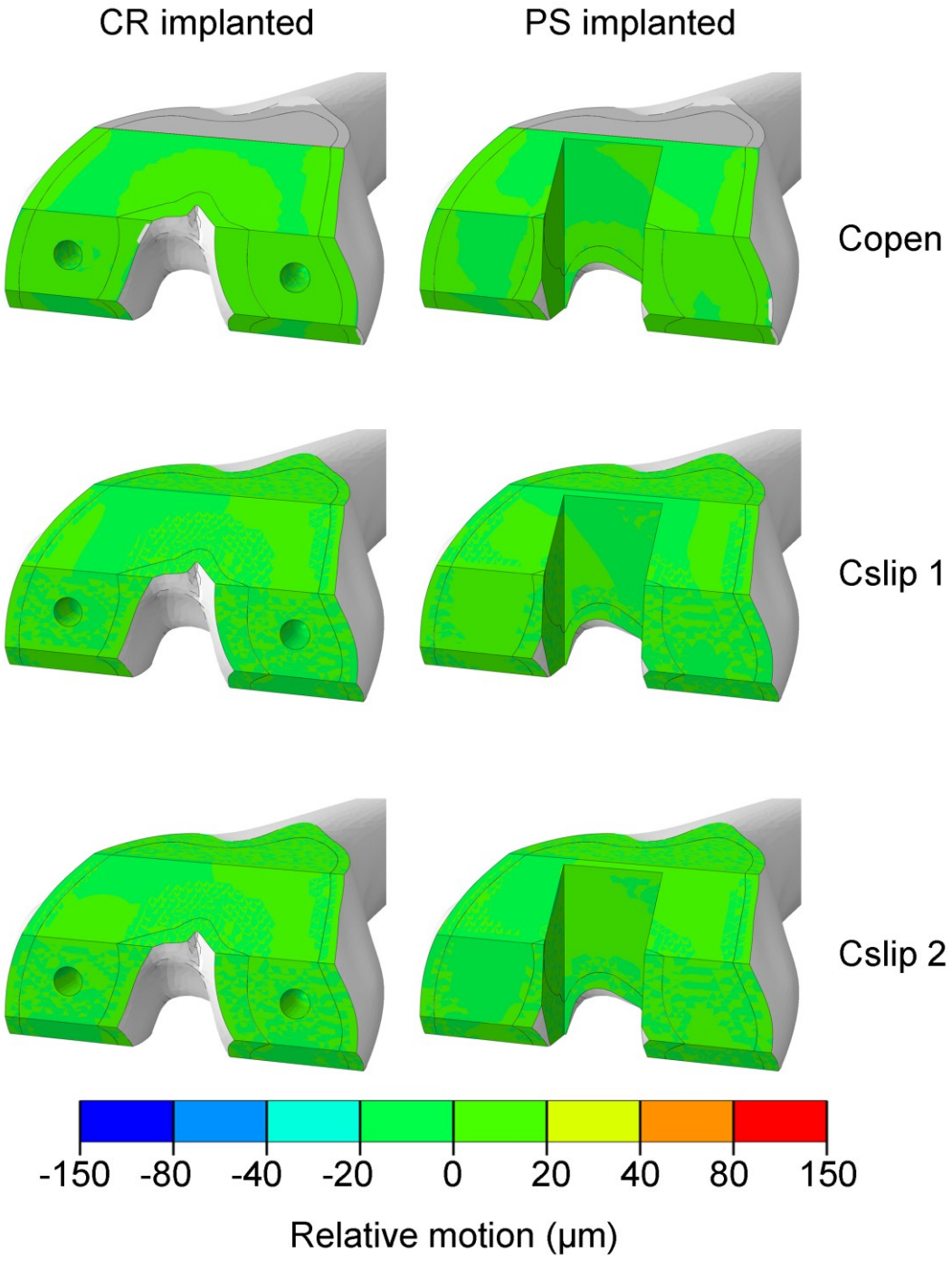


**Figure B.9:** Femoral component relative motion expressed as contact separation and tangential motion in two orthogonal directions for a PS implanted femur (first column) and a PS implanted femur at 0° flexion for loose fit conditions.

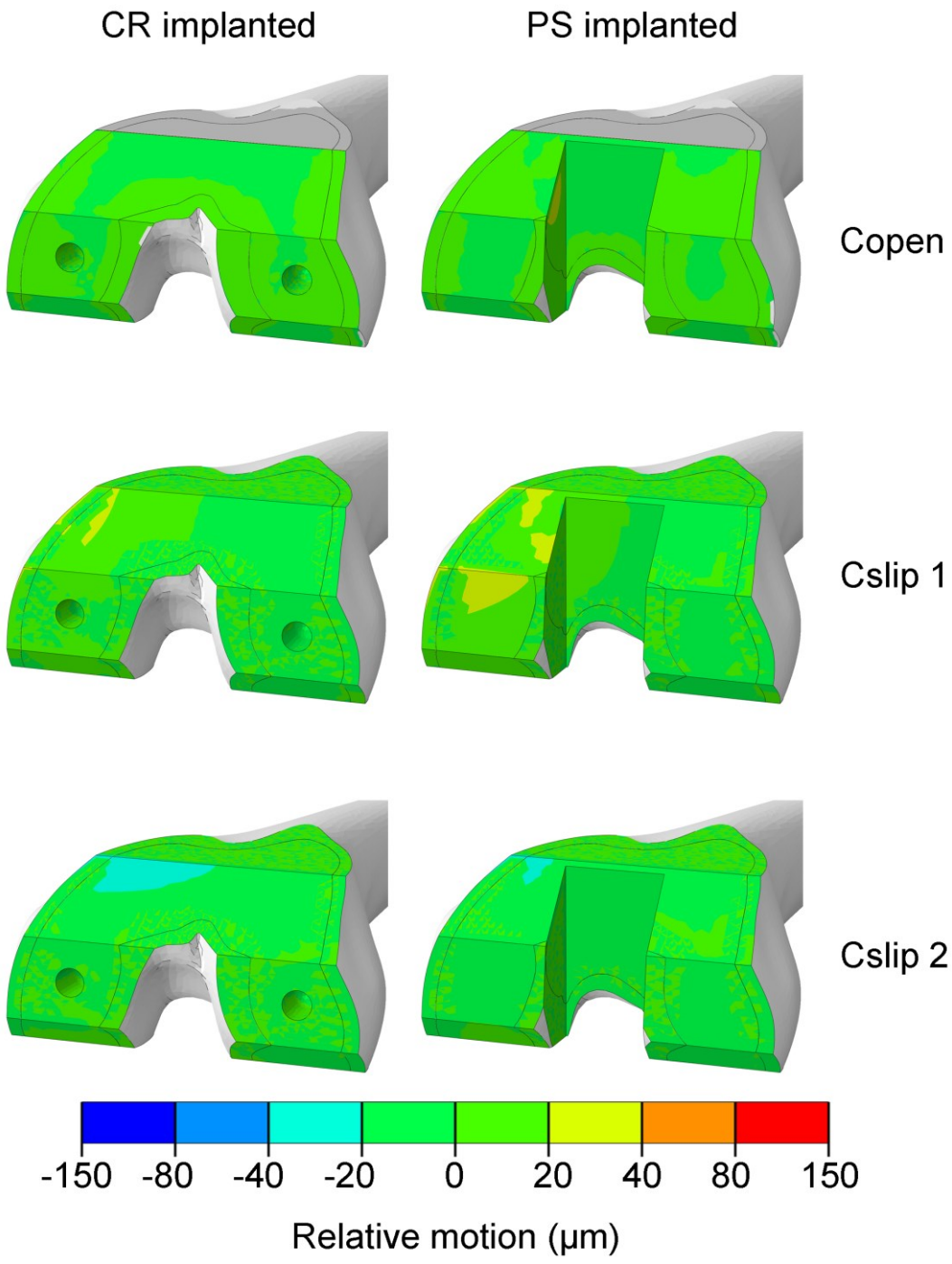


**Figure B.10:** Femoral component relative motion expressed as contact separation and tangential motion in two orthogonal directions for a PS implanted femur (first column) and a PS implanted femur at 22° flexion for loose fit conditions.

### B.5.2 Effect of stemmed femoral prosthesis on femoral component motion

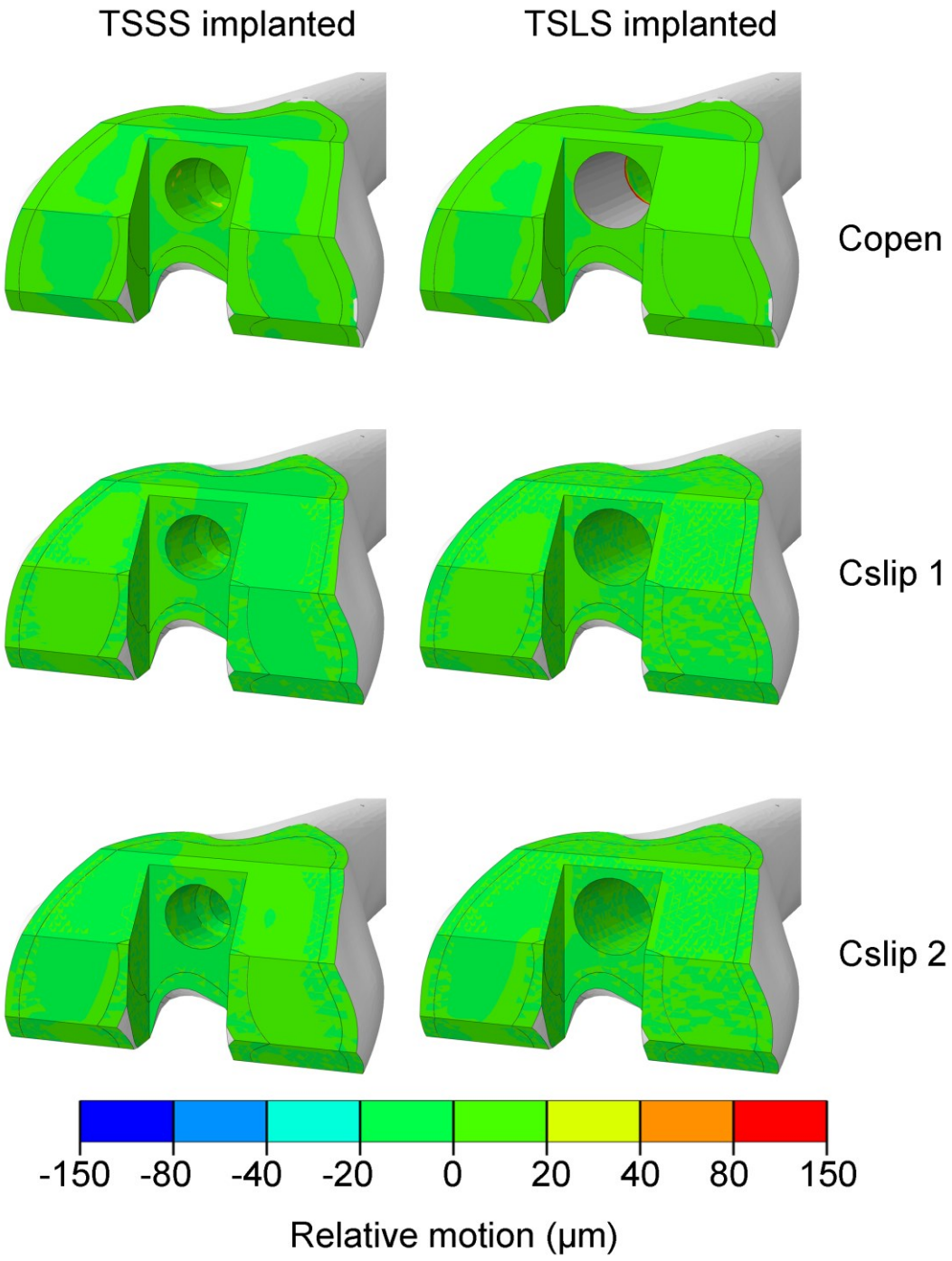


**Figure B.11:** Femoral component relative motion expressed as contact separation and tangential motion in two orthogonal directions for a TS implanted femur with short stem (first column) and a TS implanted femur with long stem at 0° flexion.

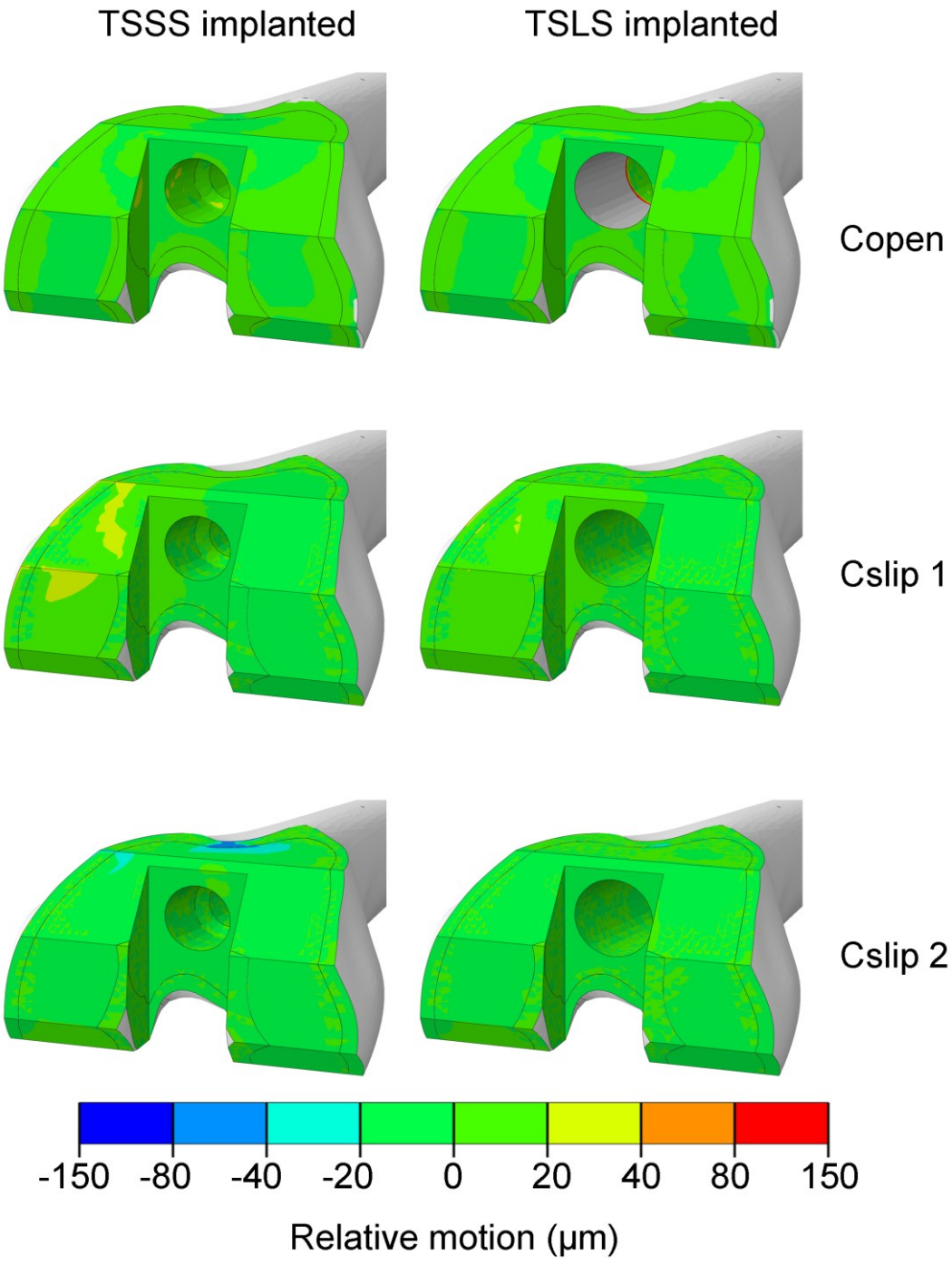


**Figure B.12:** Femoral component relative motion expressed as contact separation and tangential motion in two orthogonal directions for a TS implanted femur with short stem (first column) and a TS implanted femur with long stem at 22° flexion.

### B.5.3 Effect of loose fit on component motion for stemmed implants

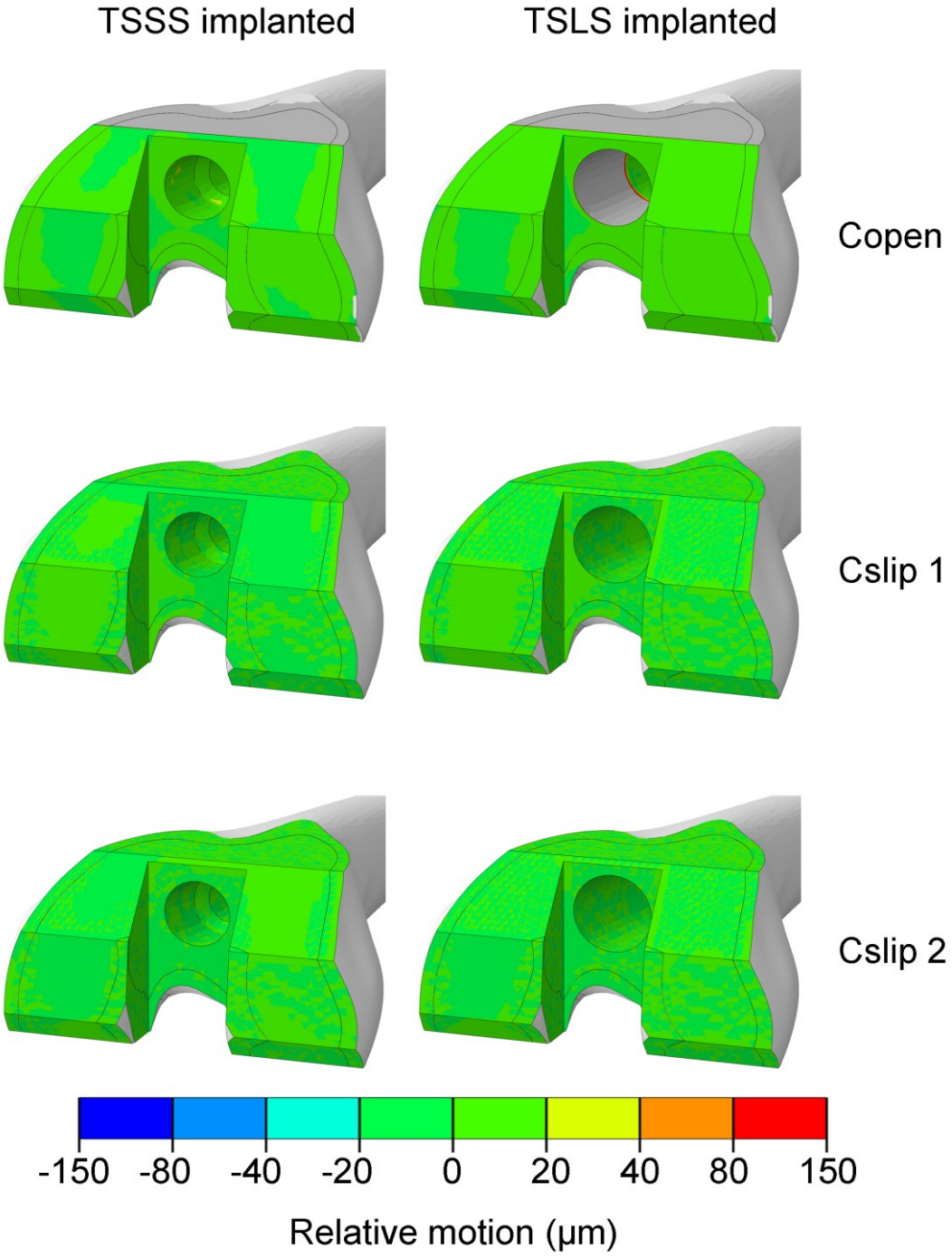


**Figure B.13:** Femoral component relative motion expressed as contact separation and tangential motion in two orthogonal directions for a TS implanted femur with short stem (first column) and a TS implanted femur with long stem at 0° flexion for loose fit conditions.

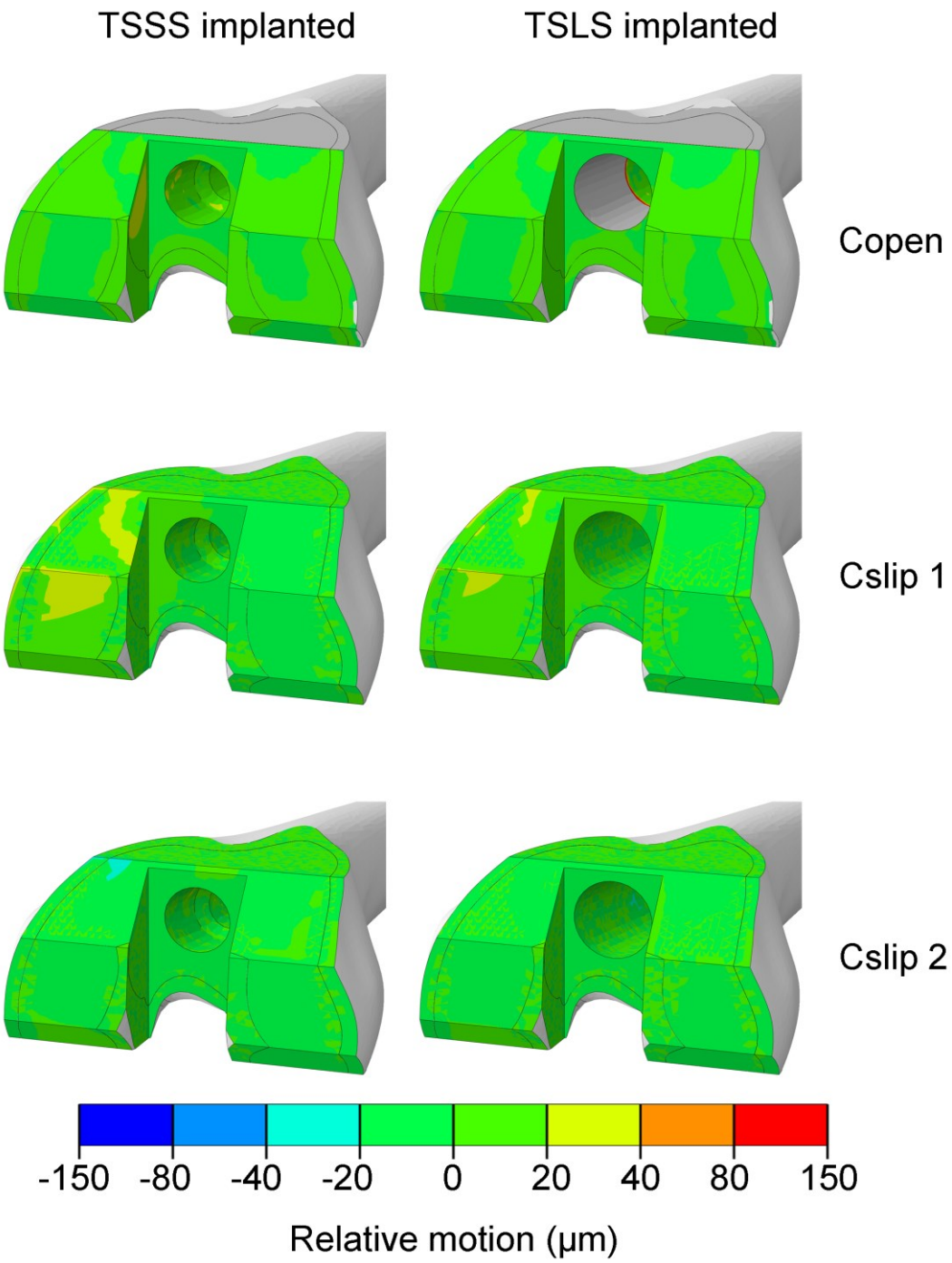


**Figure B.14:** Femoral component relative motion expressed as contact separation and tangential motion in two orthogonal directions for a TS implanted femur with short stem (first column) and a TS implanted femur with long stem at 22° flexion, for loose fit conditions.

# C

# Experimental Micromotion

In Chapter VIII data acquisition was carried out using a National Instruments DAQpad-6070E (National Instruments, Austin, TX) and virtual instrumentation software LabVIEW™ 7.0 (National Instruments, Austin, TX). This appendix contains the LabVIEW™ code used extensively throughout Chapter VIII.

LabVIEW™ programs are written in a special graphical format called G. Each program consists of a front panel graphical user interface (GUI) with all the required virtual instruments and a block diagram (the graphical program code). In this study three custom programs were developed by the author, in order to calibrate each sensor; log, convert and filter the experimental results and finally perform the coordinate transformation to determine all three translational and rotational motions of the implant relative to the bone for the fixed reference point.

Section C.1 presents the calibration graphs used for each sensor. Section C.2 details the main LabVIEW™ filtering and processing program as well as the custom program created to carry out coordinate transformation operations on the sensor displacement data. Additionally engineering drawings of the main components of the final prototype rig design are presented at the end of this appendix (C.3).

## C.1 – Sensor calibration

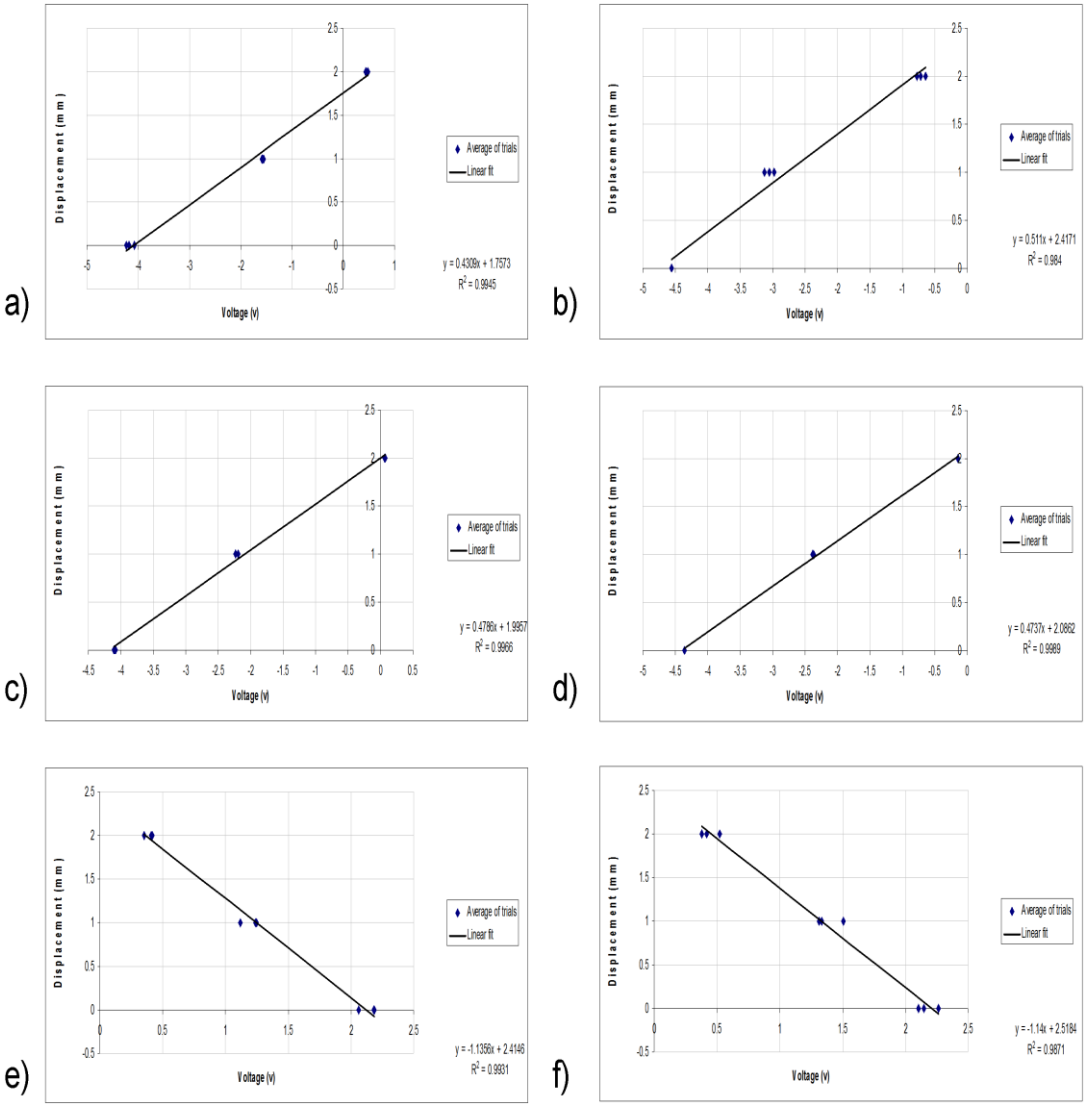


**Figure C.1:** Individual sensor calibration equations derived using the setup detailed in Chapter VIII, calibration graphs (a to f) corresponding to DVRT sensors 1-6.

## C.2 – Programme code

In Chapter VIII, Figure 8.17, a brief overview of the DVRT sensor post-processing protocol was given. In this section the LabVIEW™ graphical code used to analyse the sensor data is presented.

The first program logged the data from all DVRT sensors during each test, creating an output file of change in sensor voltage with time (Figure C.2).

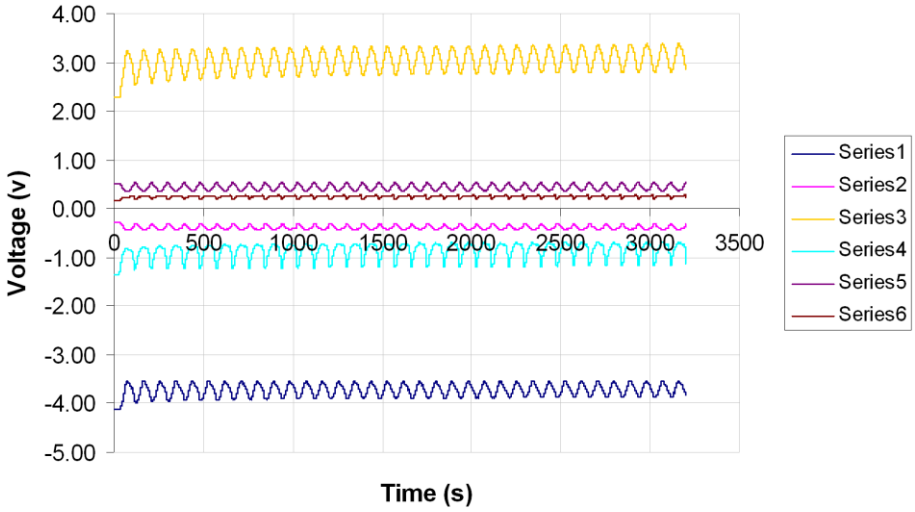


i)

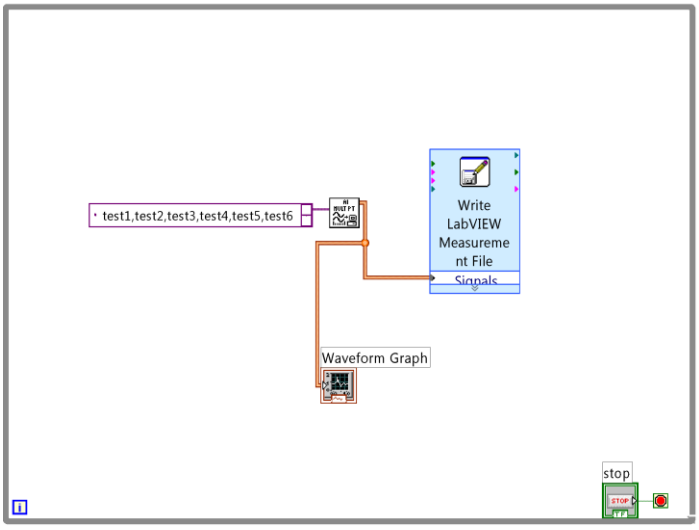


ii)

**Figure C.2:** i) example of raw sensor output and ii) block diagram code of DAQ program.

The second program (Figure C.3), using the previously generated LabVIEW™ measurement file as an input, separated each sensors voltage data by channel. The data from each channel was then converted from voltage to displacement using the individual sensors calibration equations shown previously (Figure C.1). A 3$^{rd}$ order Butterworth filter (low pass) was then applied to the data with a cut off frequency of 0.4 Hz to reduce noise. The final section of code in this program (Figure C.4) employed an iterative loop (based on cycle time at the specified flexion angle), to extract the amplitude of each individual sensors cyclical displacement curve at one cycle intervals over the 40 cycles. The value of amplitude extracted in this case being the relative displacement of the femoral component to the bone corresponding to the loading and unloading of the femur "inducible motion".

Once the "inducible motion" for each sensor had been determined these values were then taken as the input for the coordination transformation equations used to determine the relative motion of the implant to the bone in all degrees of freedom. Figure C.5 details the LabVIEW™ implementation of Equations 8.9 – 8.14 from Chapter VIII.

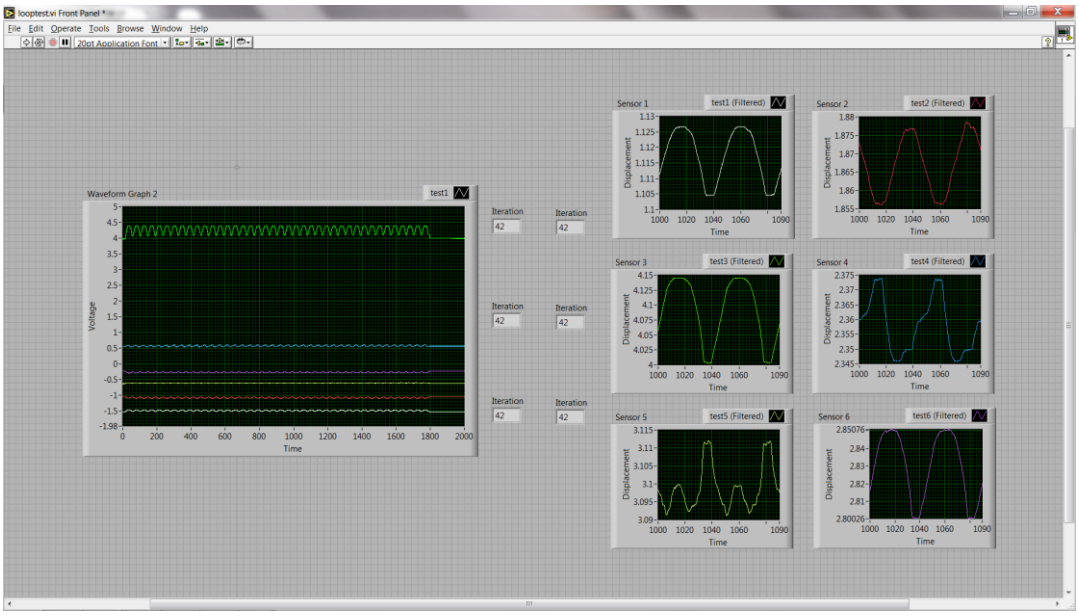


i)

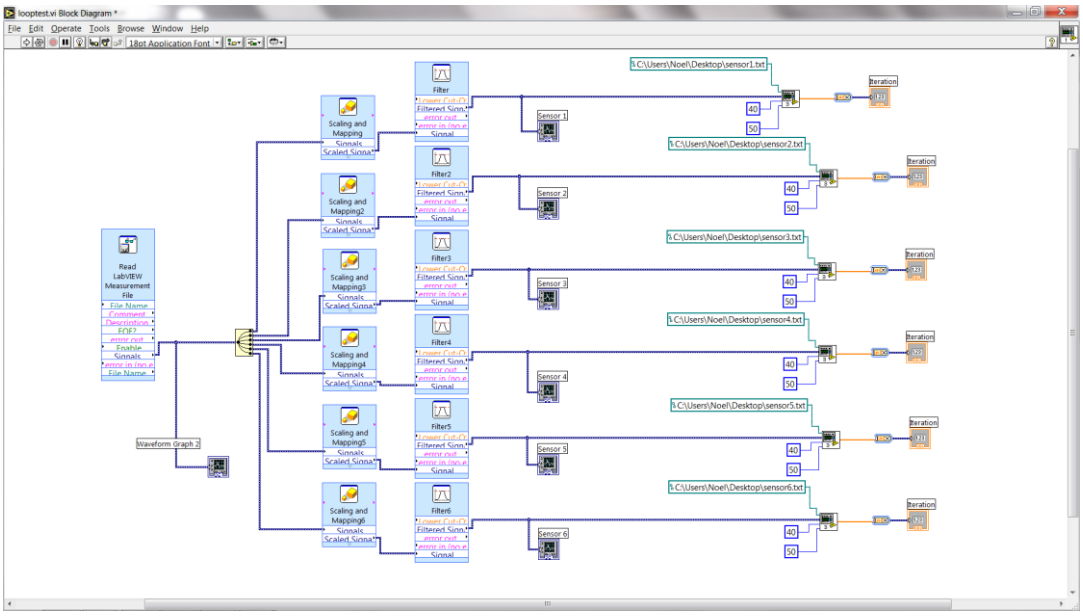


ii)

**Figure C.3:** i) Front panel (GUI) and ii) block diagram code of custom signal conversion and filtration program.

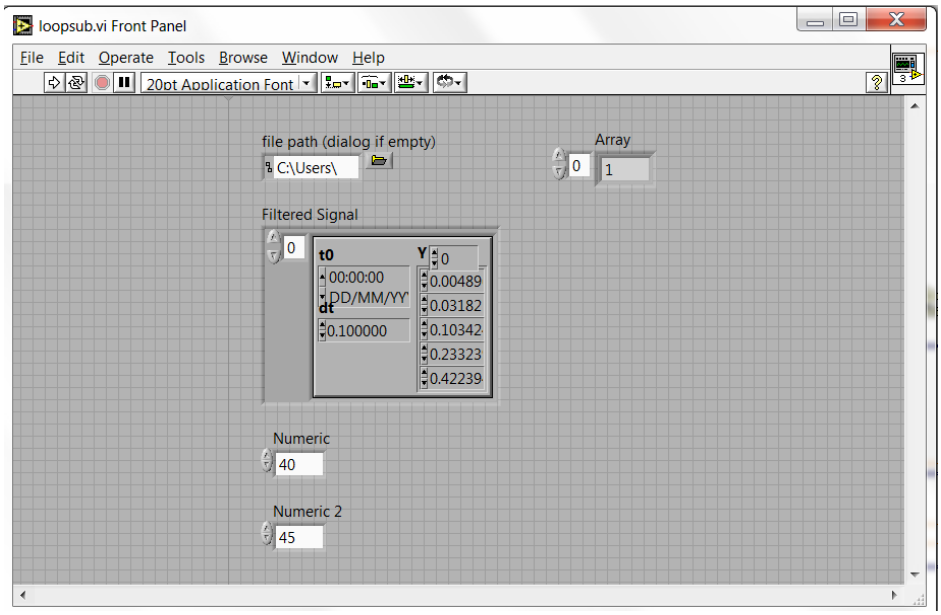


i)

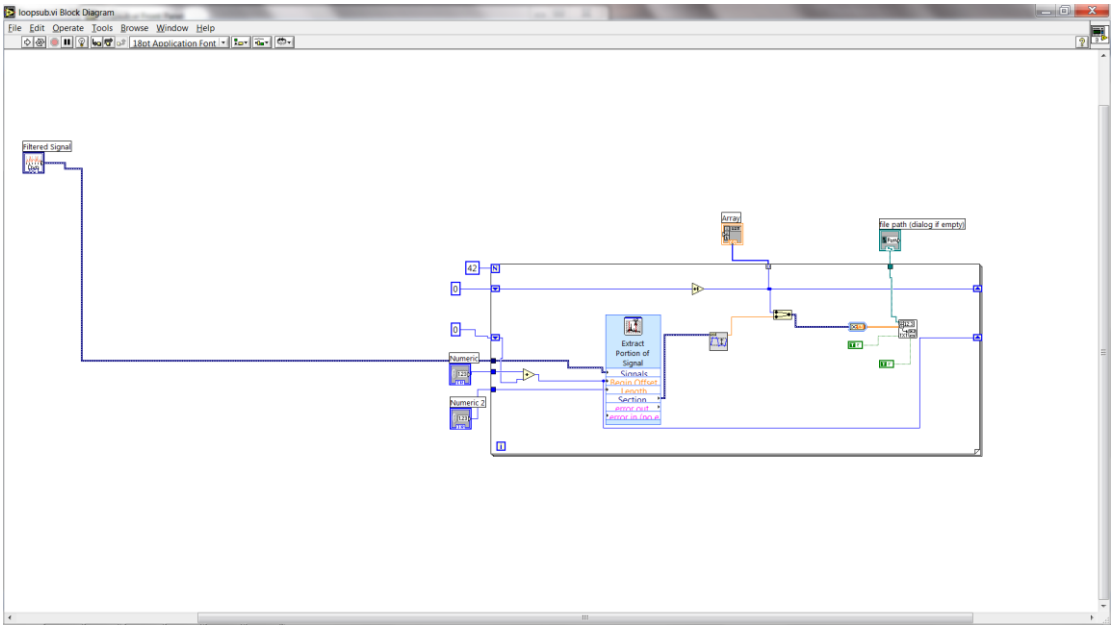


ii)

**Figure C.4:** i) Front panel (GUI) and ii) block diagram of iterative amplitude extraction subroutine for use in main program.

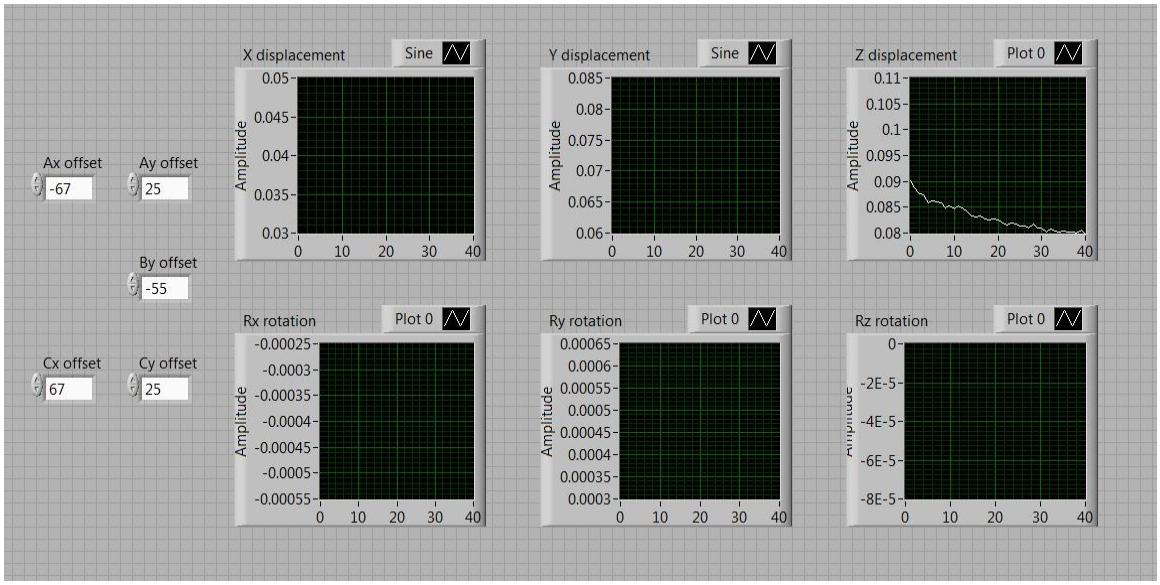


i)

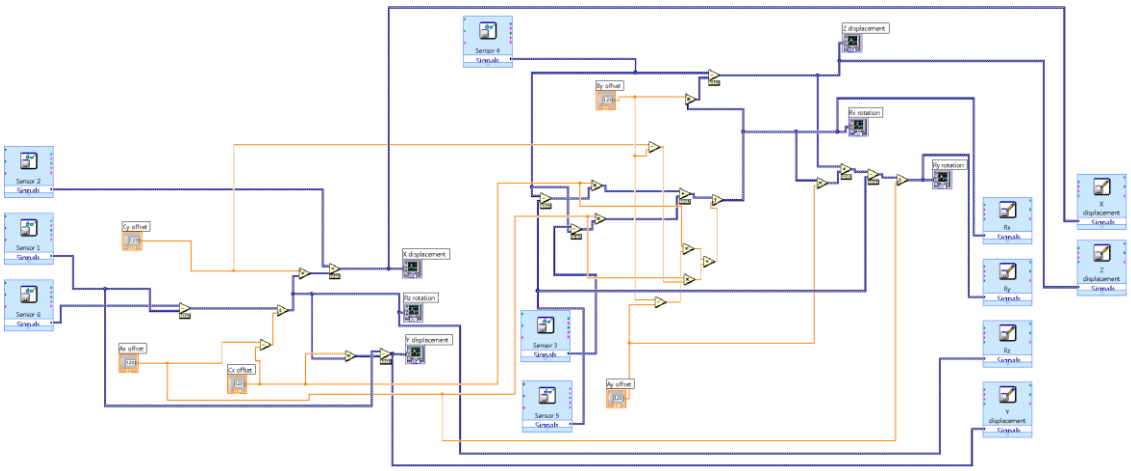

ii)

**Figure C.5:** i) Front panel (GUI) showing reference point offset values and ii) block diagram of implemented coordinate transformation equations.

## C.3 – Cyclical graphs and tables of mean translational and rotational micromotions

The following Figures (C.6 to C.11) show the levels of translational and rotational relative motion averaged over all trials, based on the tests outlined in Chapter VIII. The graphs show that a kind of steady state of inducible displacement occurs over the 40 cycles of loading and unloading for both uncemented and cemented interface conditions. This finding is consistent with previous studies (Schneider et al. 1989). In general it was found that the magnitude of motions and rotations increased with flexion.

It can be seen from Figure C.6a – C.6c that for an uncemented PS implanted femur the largest translational relative motion occurs in the distal/proximal (w) direction for all flexion angles investigated. In general the largest component of rotational relative motion was found to act about the x-axis (Figure C.6d – C.6f) in the sagittal plane ($\theta_x$), which is consistent with many previous in-vitro and clinical RSA studies (Nilsson et al. 1991, Wackerhagen et al. 1992, Nilsson and Kärrholm 1996, Cristofolini et al. 2008, Cristofolini et al. 2009, Spinelli et al. 2010).

From Figure C.7 it can be seen that the magnitude of translational and rotational relative motions for an uncemented TS implant with short stem initially appears to be very similar to the PS implant, particularly in the axial or w direction. However, the addition of a short stem serves to reduce translational motions (Figure C.7a-C.7c) in the other two directions (medial/lateral and anterior/posterior). It can also be seen that the addition of a short stem greatly reduces rotation about the x-axis in the sagittal plane for all flexion angles.

Referring to Figure C.8, it can be seen that the greatest reduction in motion and rotation of the femoral component is achieved through the use of the long offset stem. All translational and rotational relative motions were found to be reduced significantly at all flexion angles. The long offset stem was also found to prevent the large axial displacements observed in the other two implant types.

It is clear from these results that the addition of a stem serves to increase implant stability and reduce rotational and translational components of relative motion

particularly in the sagittal plane in comparison to stemless implants. Similarly a previous *in vitro* study by van Loon et al. (2000) on femoral stem extension noted that varus/valgus rotation of the femoral was greatly reduced in the presence of a modular stem.

This study also investigated the influence of cemented fixation on "apparent" levels of relative motion for the previously described implants. In PS implanted femurs cement was applied to the distal surfaces of the femur and posterior surfaces of the femoral component. The TS implanted femurs with short stem were cemented distally and along the length of the stem up to the cement restrictor (1cm past the stem). TS implants with a long offset stem, on the other hand, employed a "hybrid" cementing technique where cement was applied to the metaphysis only and the stem remained cementless.

It can be seen from Figures C.9 to C.11 that all components of motion and rotation have significantly reduced in comparison to the corresponding implant under uncemented conditions. In general, components of relative motion reduced to approximately 1/3 of their uncemented equivalent. This finding is in line with a previous study which investigated cemented and uncemented fixation of a primary implanted femur on cadaveric bone (Wackerhagen et al. 1992). It can be seen by comparing Figure C.8 (TS long offset stem uncemented) and Figure C.9 (PS cemented) that the maximum values of relative translational and rotational motion are quite similar for both implanted femurs.

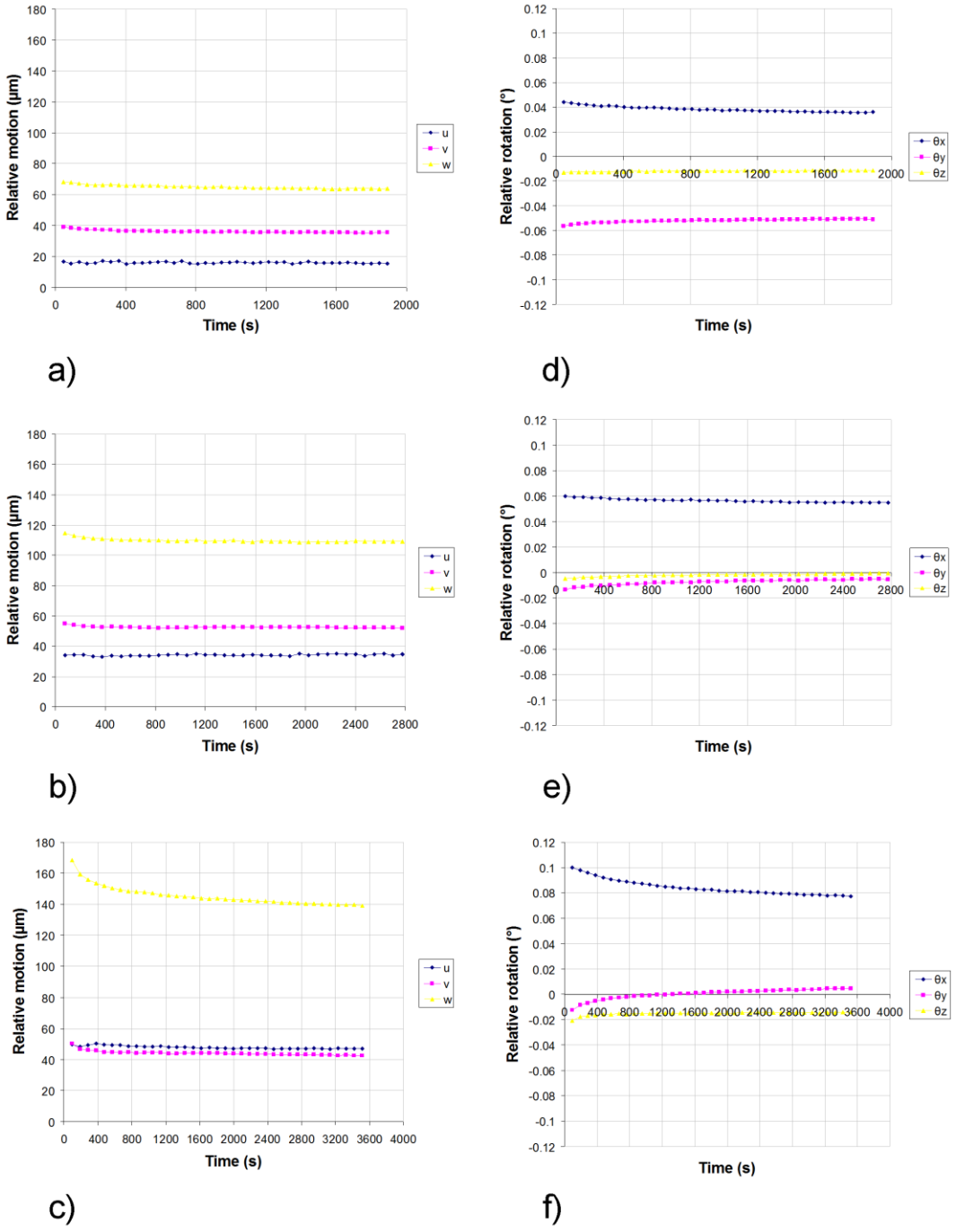


**Figure C.6:** Cyclical graphs showing the translational (a, b, c) and rotational (d, e, f) relative motions of an uncemented PS implanted femur at 0° flexion (a and d), 10° flexion (b and e) and 20° flexion (c and f).

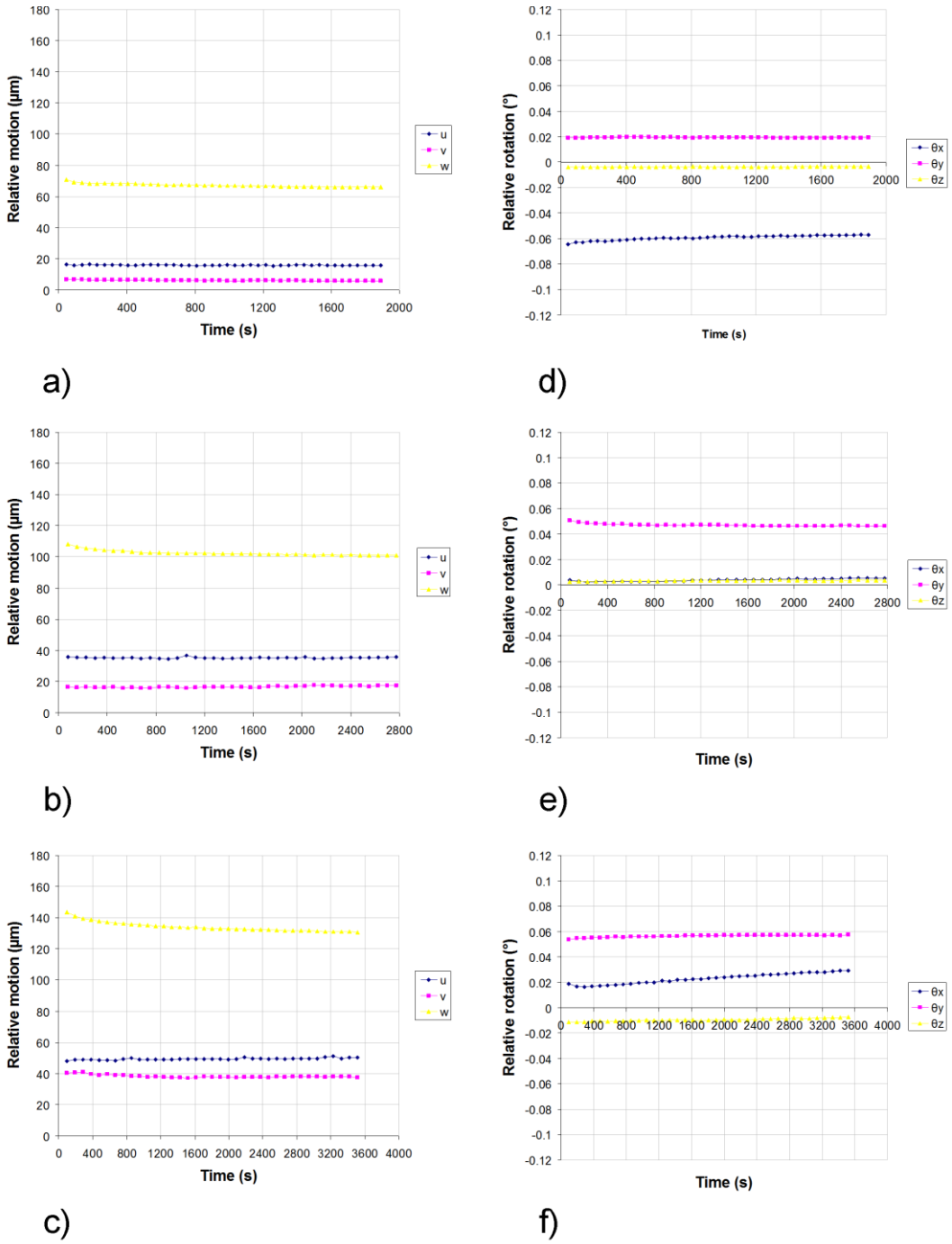


**Figure C.7:** Cyclical graphs showing the translational (a, b, c) and rotational (d, e, f) relative motions of an uncemented TS implanted femur with short stem at 0° flexion (a and d), 10° flexion (b and e) and 20° flexion (c and f).

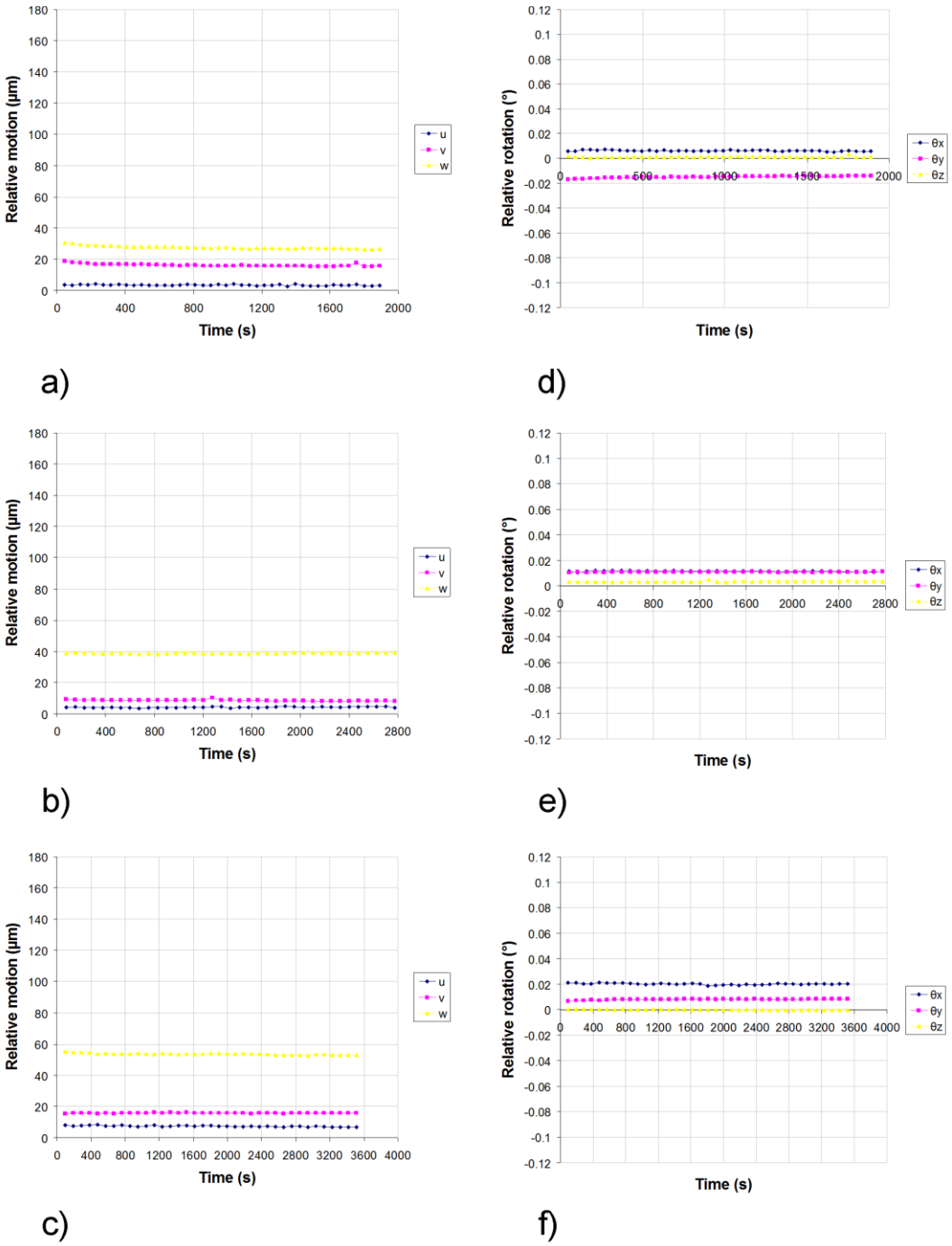


**Figure C.8:** Cyclical graphs showing the translational (a, b, c) and rotational (d, e, f) relative motions of an uncemented TS implanted femur with long offset stem at 0° flexion (a and d), 10° flexion (b and e) and 20° flexion (c and f).

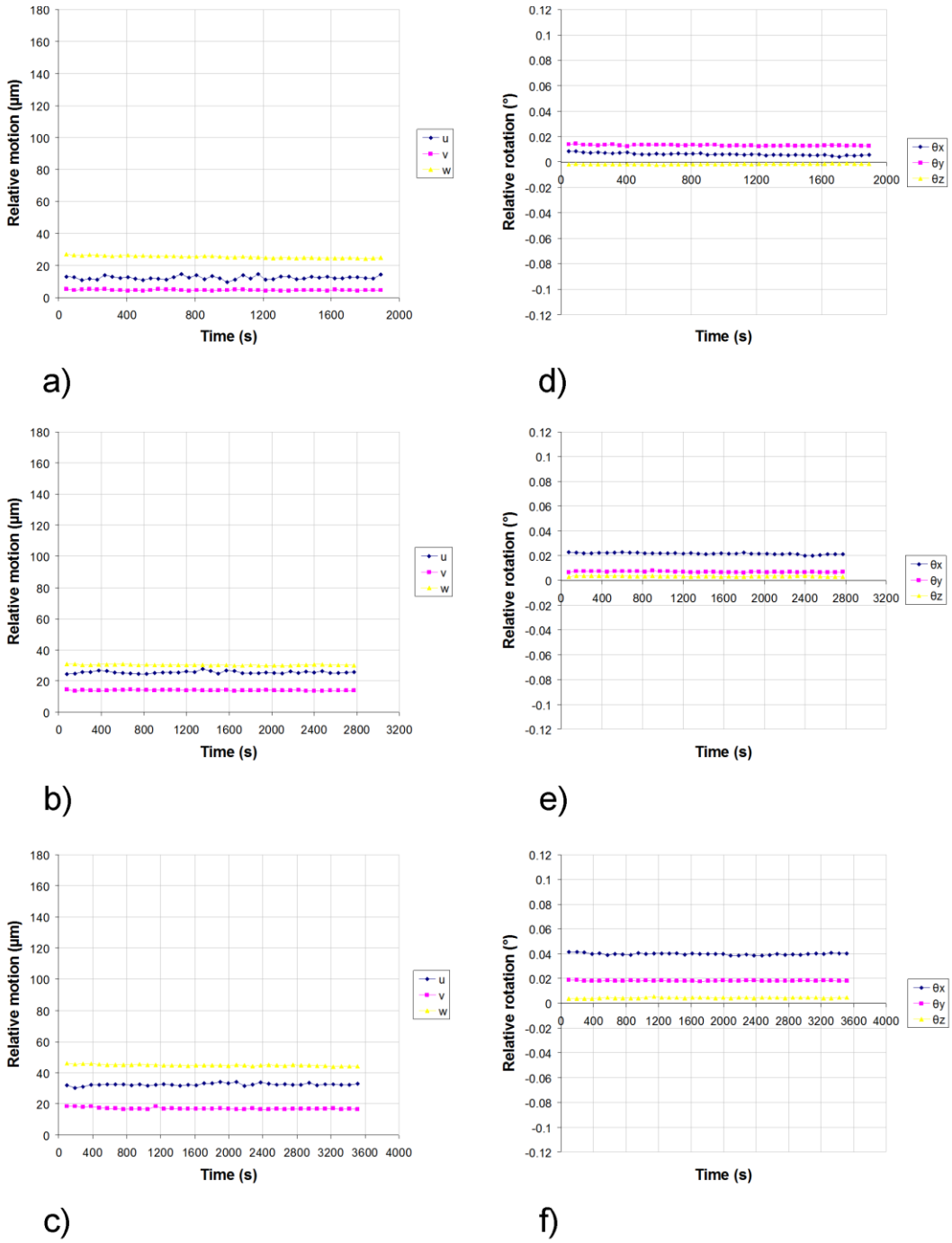


**Figure C.9:** Cyclical graphs showing the translational (a, b, c) and rotational (d, e, f) relative motions of a cemented PS implanted femur at 0° flexion (a and d), 10° flexion (b and e) and 20° flexion (c and f).

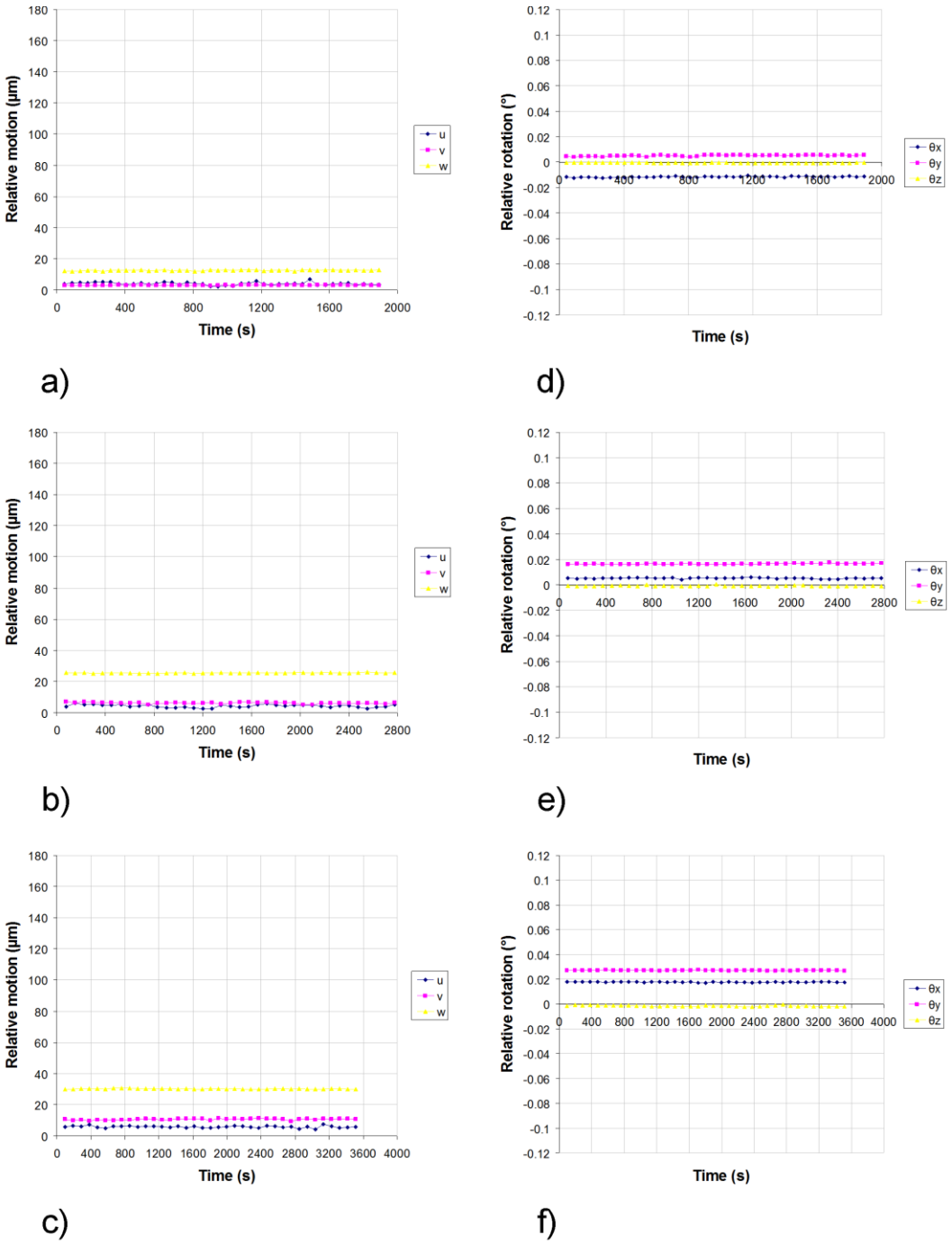


**Figure C.10:** Cyclical graphs showing the translational (a, b, c) and rotational (d, e, f) relative motions of an all cemented TS implanted femur with short stem at 0° flexion (a and d), 10° flexion (b and e) and 20° flexion (c and f).

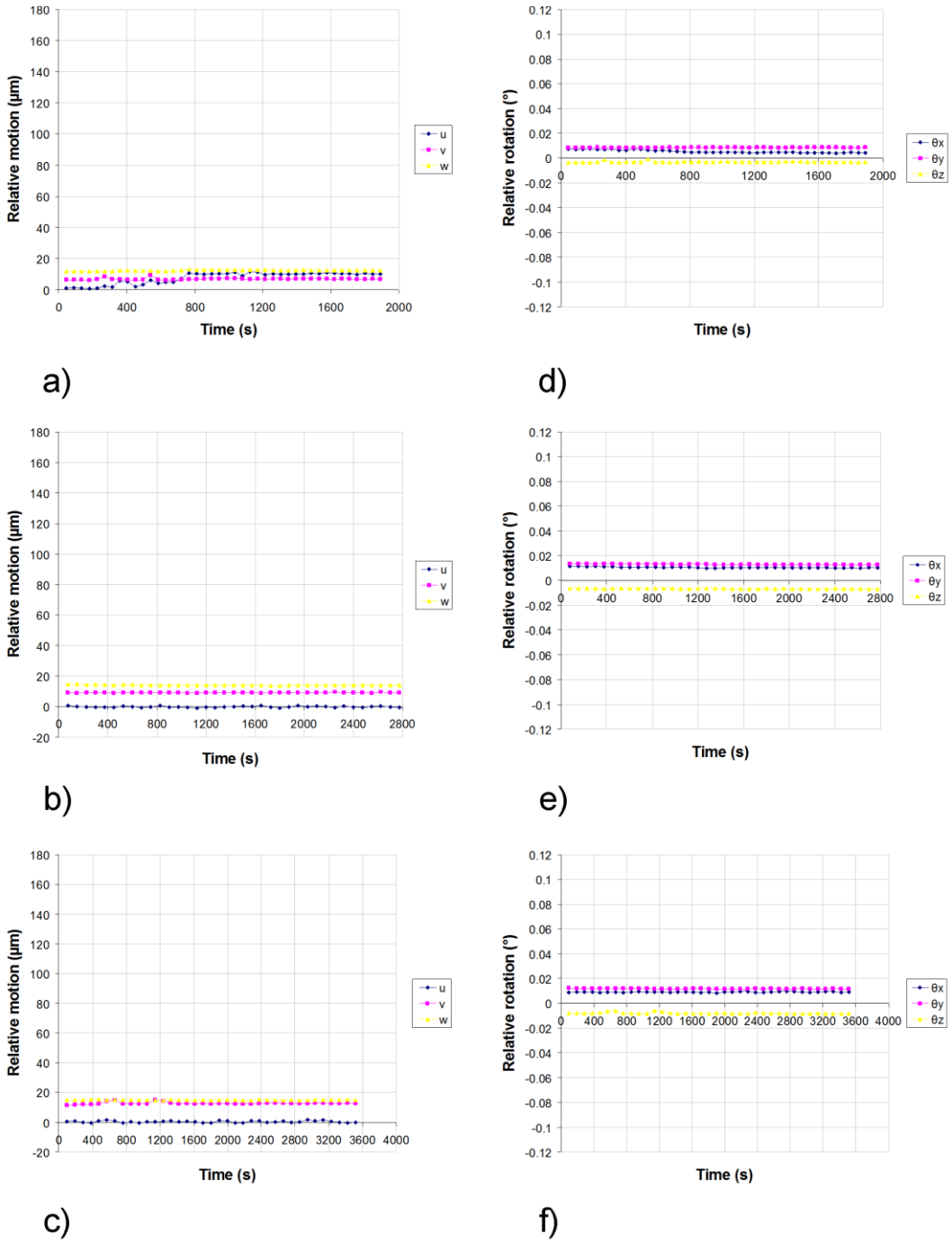


**Figure C.11:** Cyclical graphs showing the translational (a, b, c) and rotational (d, e, f) relative motions of a "hybrid" cemented TS implanted femur with long offset stem at 0° flexion (a and d), 10° flexion (b and e) and 20° flexion (c and f).

**Table C.1:** Mean translational and rotational relative motions for uncemented cases.

| u (μm) | | | | | | |
|---|---|---|---|---|---|---|
| Flexion (°) | PS | (SD) | TS short | (SD) | TS long | (SD) |
| 0 | 16 | (0.71) | 16 | (0.45) | 3 | (0.57) |
| 10 | 34 | (1.07) | 35 | (0.59) | 4 | (0.46) |
| 20 | 48 | (4.85) | 49 | (1.13) | 7 | (0.76) |
| $\theta_x$ (°) | | | | | | |
| Flexion (°) | PS | (SD) | TS short | (SD) | TS long | (SD) |
| 0 | 38.34E-03 | (2.69E-03) | -59.22E-03 | (3.12E-03) | 6.29E-03 | (0.63E-03) |
| 10 | 56.52E-03 | (1.79E-03) | 3.88E-03 | (1.59E-03) | 11.53E-03 | (0.45E-03) |
| 20 | 84.15E-03 | (24.33E-03) | 22.90E-03 | (8.77E-03) | 20.19E-03 | (0.99E-03) |

| v (μm) | | | | | | |
|---|---|---|---|---|---|---|
| Flexion (°) | PS | (SD) | TS short | (SD) | TS long | (SD) |
| 0 | 36 | (1.04) | 6 | (0.57) | 16 | (0.88) |
| 10 | 53 | (0.79) | 17 | (1.04) | 9 | (0.73) |
| 20 | 44 | (10.73) | 38 | (1.62) | 16 | (0.22) |
| $\theta_y$ (°) | | | | | | |
| Flexion (°) | PS | (SD) | TS short | (SD) | TS long | (SD) |
| 0 | -52.07E-03 | (1.65E-03) | 19.44E-03 | (0.82E-03) | -14.86E-03 | (0.79E-03) |
| 10 | -7.40E-03 | (2.41E-03) | 47.03E-03 | (1.37E-03) | 10.82E-03 | (0.30E-03) |
| 20 | 0.469E-03 | (25.57E-03) | 56.46E-03 | (0.98E-03) | 8.12E-03 | (0.59E-03) |

| w (μm) | | | | | | |
|---|---|---|---|---|---|---|
| Flexion (°) | PS | (SD) | TS short | (SD) | TS long | (SD) |
| 0 | 65 | (1.34) | 67 | (1.69) | 28 | (1.13) |
| 10 | 110 | (1.53) | 103 | (2.06) | 39 | (0.37) |
| 20 | 145 | (24.60) | 134 | (4.46) | 54 | (0.68) |
| $\theta_z$ (°) | | | | | | |
| Flexion (°) | PS | (SD) | TS short | (SD) | TS long | (SD) |
| 0 | -11.83E-03 | (0.61E-03) | -3.56E-03 | (0.25E-03) | 1.28E-03 | (0.49E-03) |
| 10 | -1.83E-03 | (1.65E-03) | 3.44E-03 | (0.45E-03) | 3.57E-03 | (0.42E-03) |
| 20 | -15.06E-03 | (12.12E-03) | -9.54E-03 | (2.58E-03) | 0.174E-03 | (0.61E-03) |

**Table C.2:** Mean translational and rotational relative motions for cemented cases.

| u (μm) | | | | | | |
|---|---|---|---|---|---|---|
| Flexion (°) | PS | (SD) | TS short | (SD) | TS long | (SD) |
| 0 | 12 | (1.14) | 4 | (1.42) | 8 | (4.07) |
| 10 | 26 | (0.71) | 4 | (1.35) | -0.13 | (0.65) |
| 20 | 32 | (0.75) | 6 | (1.47) | 0.40 | (0.83) |
| $\theta_x$ (°) | | | | | | |
| Flexion (°) | PS | (SD) | TS short | (SD) | TS long | (SD) |
| 0 | 6.25E-03 | (0.92E-03) | -11.44E-03 | (0.67E-03) | 5.36E-03 | (1.30E-03) |
| 10 | 21.79E-03 | (0.67E-03) | 5.27E-03 | (0.63E-03) | 10.53E-03 | (0.62E-03) |
| 20 | 39.86E-03 | (0.70E-03) | 17.79E-03 | (0.57E-03) | 9.04E-03 | (0.40E-03) |

| v (μm) | | | | | | |
|---|---|---|---|---|---|---|
| Flexion (°) | PS | (SD) | TS short | (SD) | TS long | (SD) |
| 0 | 5 | (0.24) | 3 | (0.37) | 7 | (0.94) |
| 10 | 14 | (0.24) | 6 | (0.60) | 9 | (0.19) |
| 20 | 17 | (0.56) | 11 | (0.97) | 13 | (1.54) |
| $\theta_y$ (°) | | | | | | |
| Flexion (°) | PS | (SD) | TS short | (SD) | TS long | (SD) |
| 0 | 13.20E-03 | (0.38E-03) | 5.08E-03 | (0.65E-03) | 8.44E-03 | (0.29E-03) |
| 10 | 7.11E-03 | (0.35E-03) | 16.67E-03 | (0.36E-03) | 12.97E-03 | (0.40E-03) |
| 20 | 18.15E-03 | (0.25E-03) | 27.25E-03 | (0.63E-03) | 11.77E-03 | (0.24E-03) |

| w (μm) | | | | | | |
|---|---|---|---|---|---|---|
| Flexion (°) | PS | (SD) | TS short | (SD) | TS long | (SD) |
| 0 | 26 | (0.67) | 13 | (0.41) | 12 | (0.47) |
| 10 | 30 | (0.28) | 26 | (0.30) | 14 | (0.26) |
| 20 | 45 | (0.49) | 30 | (0.33) | 15 | (0.25) |
| $\theta_z$ (°) | | | | | | |
| Flexion (°) | PS | (SD) | TS short | (SD) | TS long | (SD) |
| 0 | -1.59E-03 | (0.25E-03) | -0.35E-03 | (0.38E-03) | -2.93E-03 | (0.67E-03) |
| 10 | 3.46E-03 | (0.27E-03) | -0.68E-03 | (0.49E-03) | -6.48E-03 | (0.15E-03) |
| 20 | 4.44E-03 | (0.30E-03) | -1.45E-03 | (0.77E-03) | -7.88E-03 | (1.33E-03) |

## C.4 – CAD drawings of experimental test rig

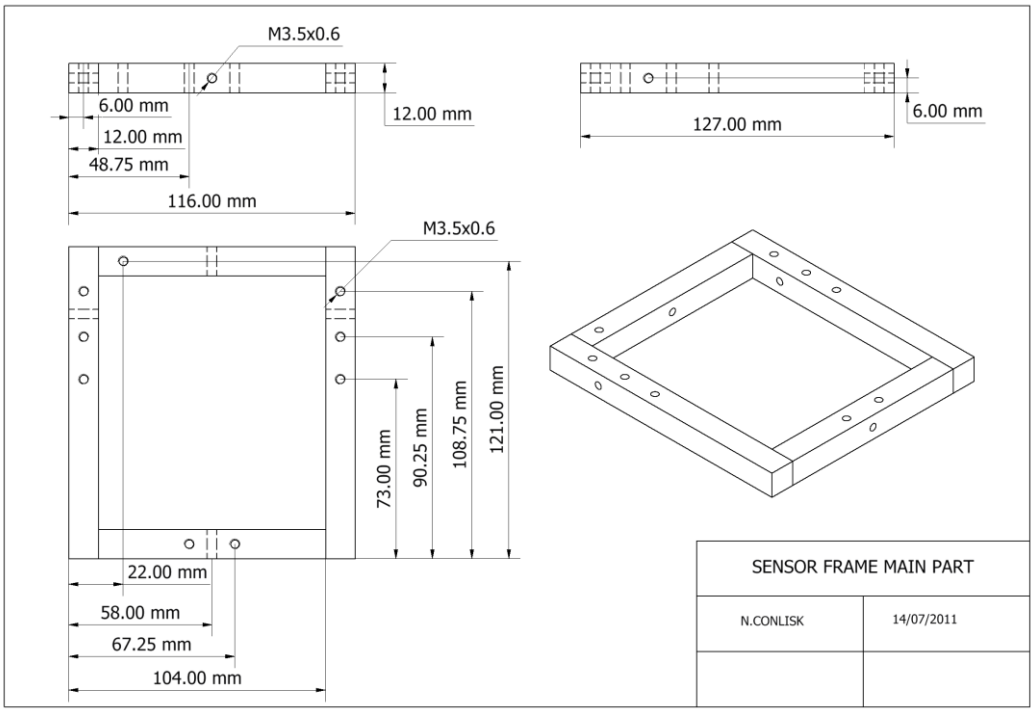
M3.5x0.6
6.00 mm
12.00 mm
48.75 mm
116.00 mm
12.00 mm
127.00 mm
6.00 mm
M3.5x0.6
73.00 mm
90.25 mm
108.75 mm
121.00 mm
22.00 mm
58.00 mm
67.25 mm
104.00 mm
SENSOR FRAME MAIN PART
N.CONLISK
14/07/2011

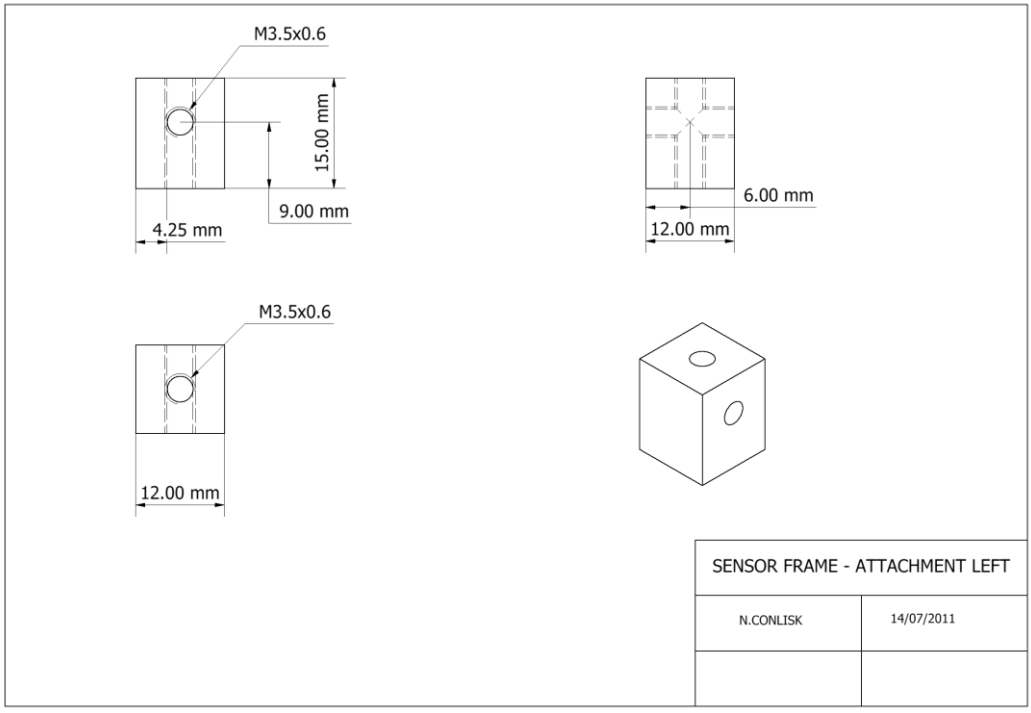
M3.5x0.6
15.00 mm
9.00 mm
4.25 mm
6.00 mm
12.00 mm
M3.5x0.6
12.00 mm
SENSOR FRAME - ATTACHMENT LEFT
N.CONLISK
14/07/2011

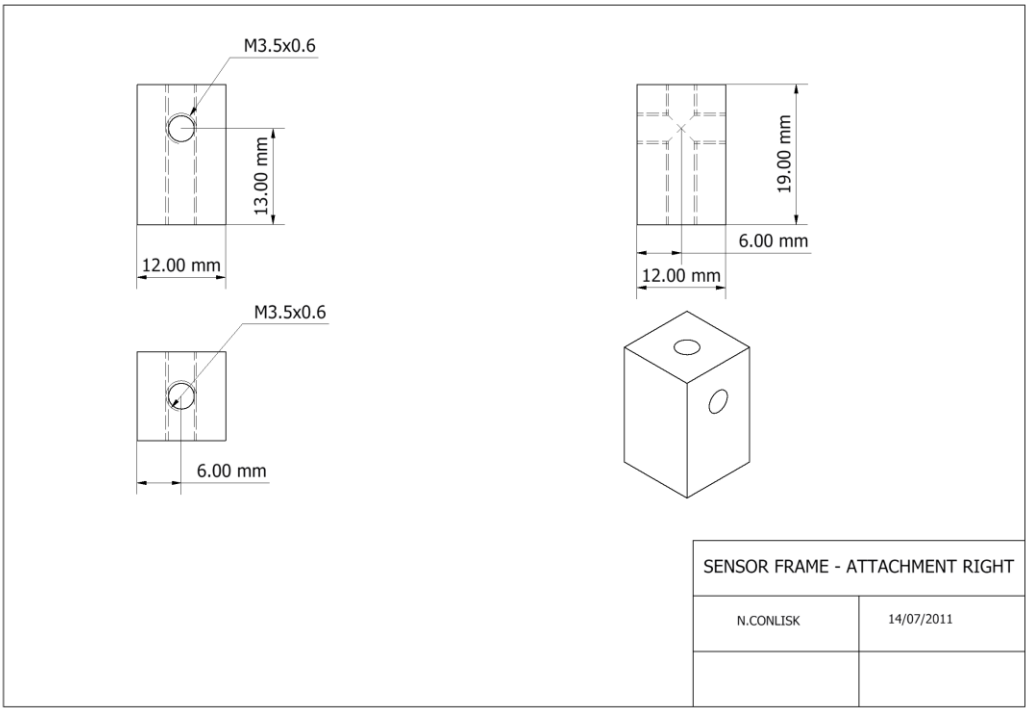
M3.5x0.6
13.00 mm
12.00 mm
M3.5x0.6
6.00 mm
19.00 mm
6.00 mm
12.00 mm
SENSOR FRAME - ATTACHMENT RIGHT
N.CONLISK
14/07/2011

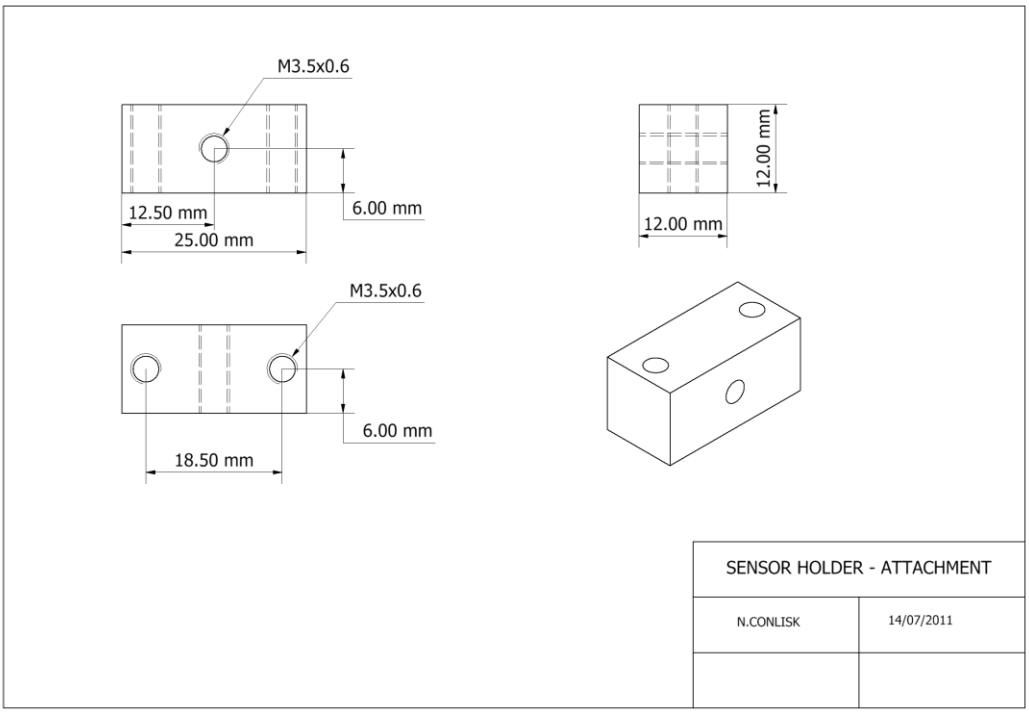
M3.5x0.6
12.50 mm
25.00 mm
6.00 mm
M3.5x0.6
18.50 mm
6.00 mm
12.00 mm
12.00 mm
SENSOR HOLDER - ATTACHMENT
N.CONLISK
14/07/2011

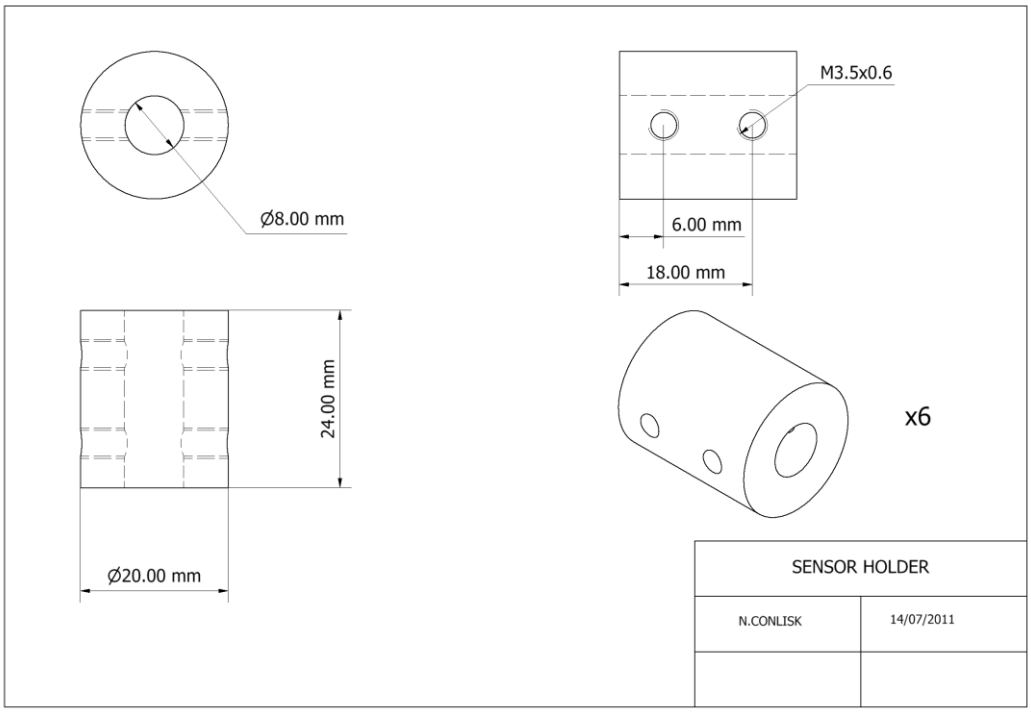
Ø8.00 mm
M3.5x0.6
6.00 mm
18.00 mm
24.00 mm
Ø20.00 mm
x6
SENSOR HOLDER
N.CONLISK
14/07/2011

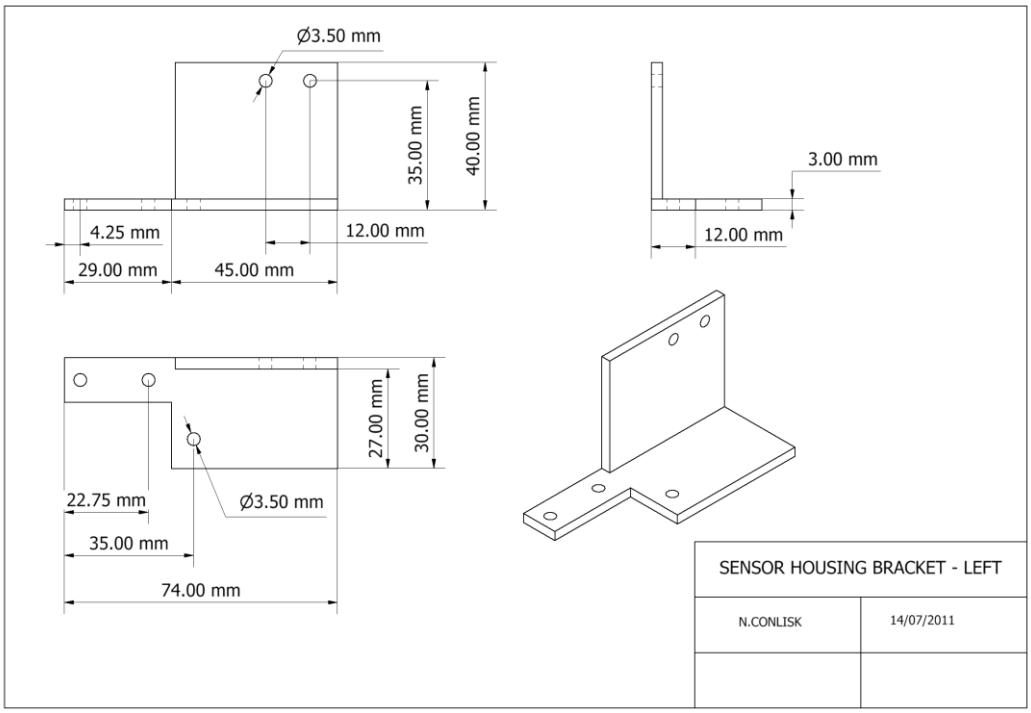
Ø3.50 mm
35.00 mm
40.00 mm
4.25 mm
12.00 mm
29.00 mm
45.00 mm
3.00 mm
12.00 mm
27.00 mm
30.00 mm
22.75 mm
Ø3.50 mm
35.00 mm
74.00 mm
SENSOR HOUSING BRACKET - LEFT
N.CONLISK
14/07/2011

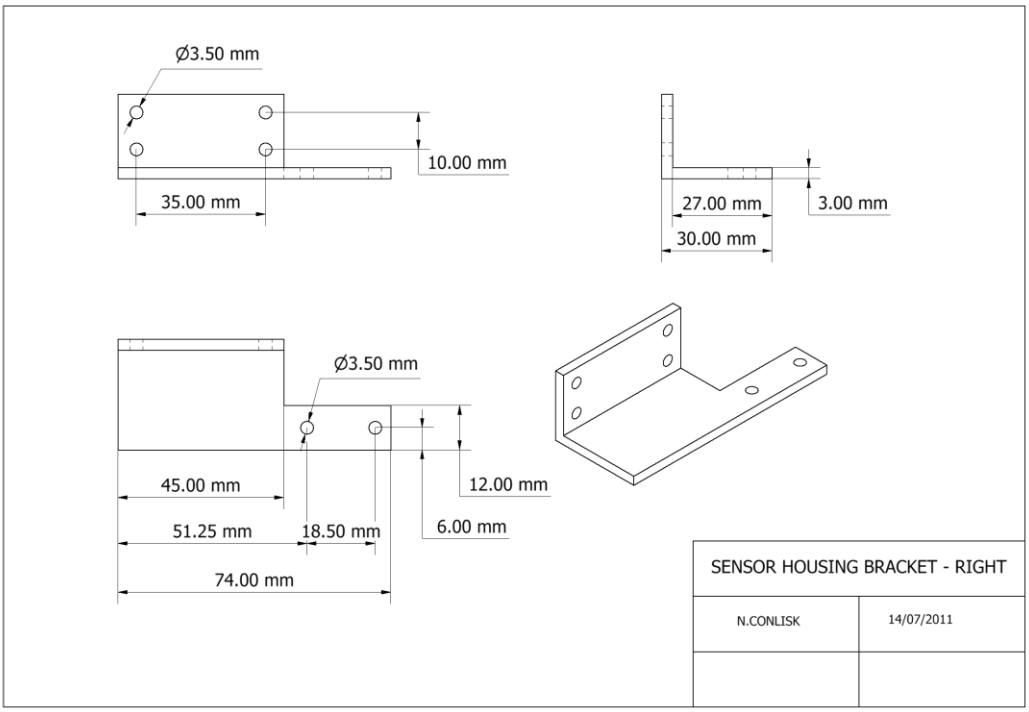
Ø3.50 mm
10.00 mm
35.00 mm
27.00 mm
3.00 mm
30.00 mm
Ø3.50 mm
45.00 mm
12.00 mm
51.25 mm
18.50 mm
6.00 mm
74.00 mm
SENSOR HOUSING BRACKET - RIGHT
N.CONLISK
14/07/2011

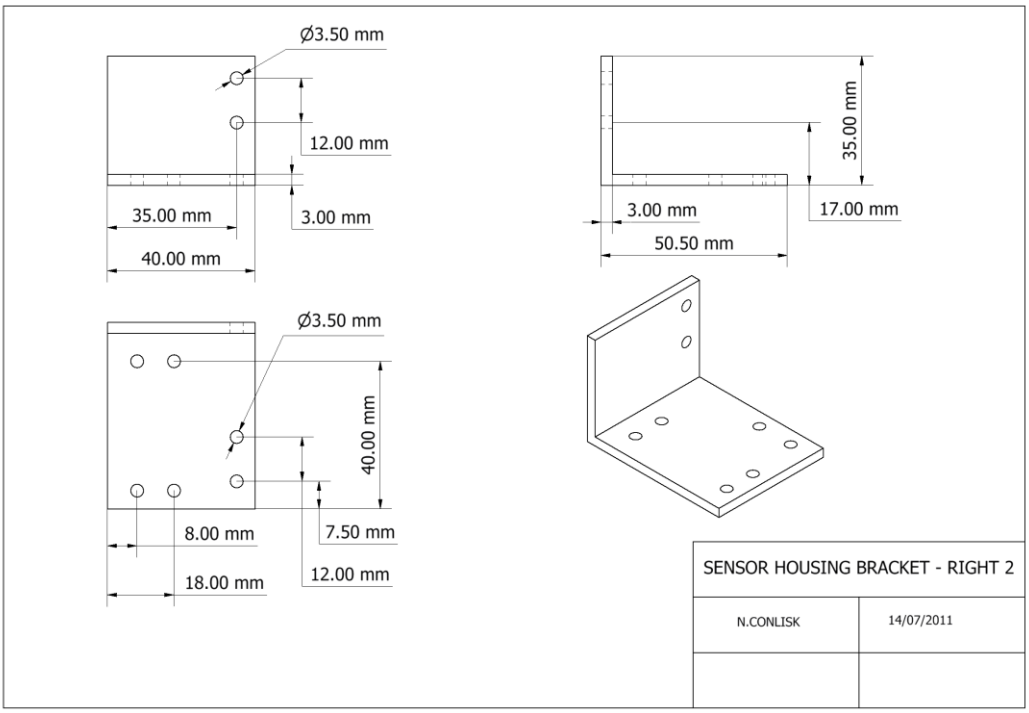
Ø3.50 mm
12.00 mm
35.00 mm
3.00 mm
40.00 mm
35.00 mm
3.00 mm
17.00 mm
50.50 mm
Ø3.50 mm
40.00 mm
8.00 mm
7.50 mm
18.00 mm
12.00 mm
SENSOR HOUSING BRACKET - RIGHT 2
N.CONLISK
14/07/2011

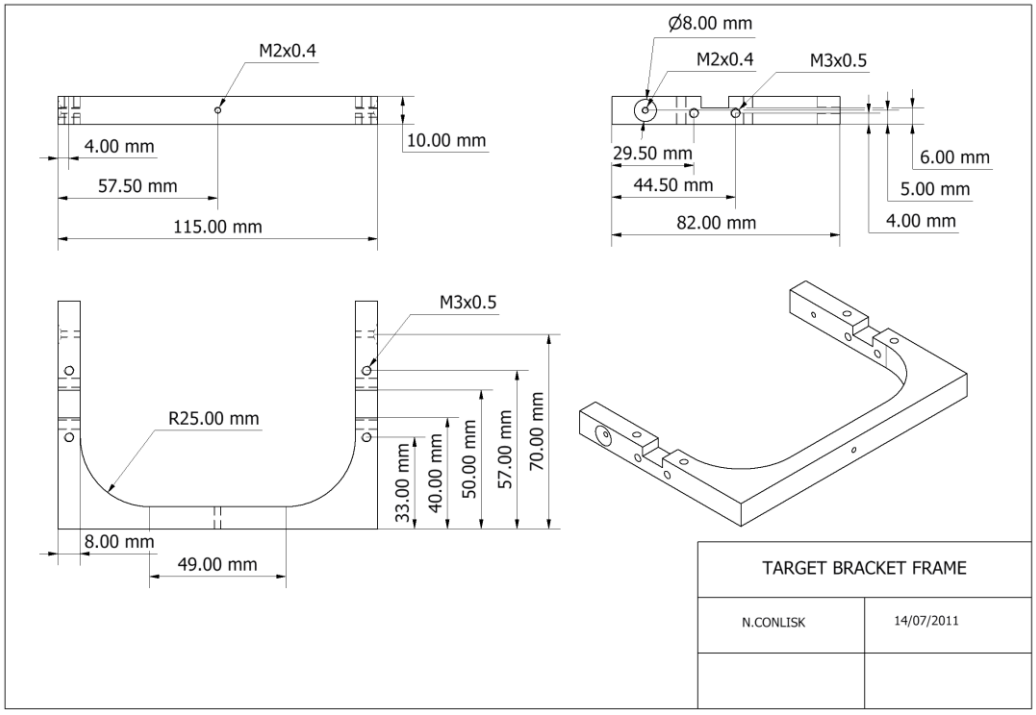
M2x0.4
4.00 mm
57.50 mm
115.00 mm
10.00 mm
Ø8.00 mm
M2x0.4
M3x0.5
29.50 mm
44.50 mm
82.00 mm
6.00 mm
5.00 mm
4.00 mm
M3x0.5
R25.00 mm
33.00 mm
40.00 mm
50.00 mm
57.00 mm
70.00 mm
8.00 mm
49.00 mm
TARGET BRACKET FRAME
N.CONLISK
14/07/2011

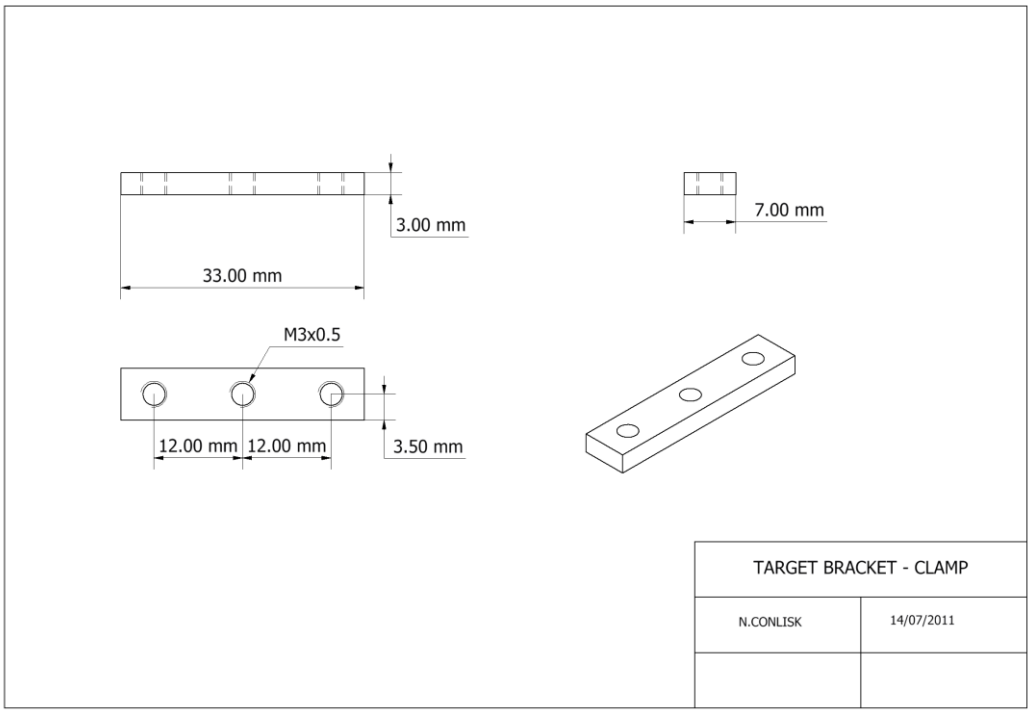
3.00 mm
33.00 mm
7.00 mm
M3x0.5
12.00 mm
12.00 mm
3.50 mm
TARGET BRACKET - CLAMP
N.CONLISK
14/07/2011

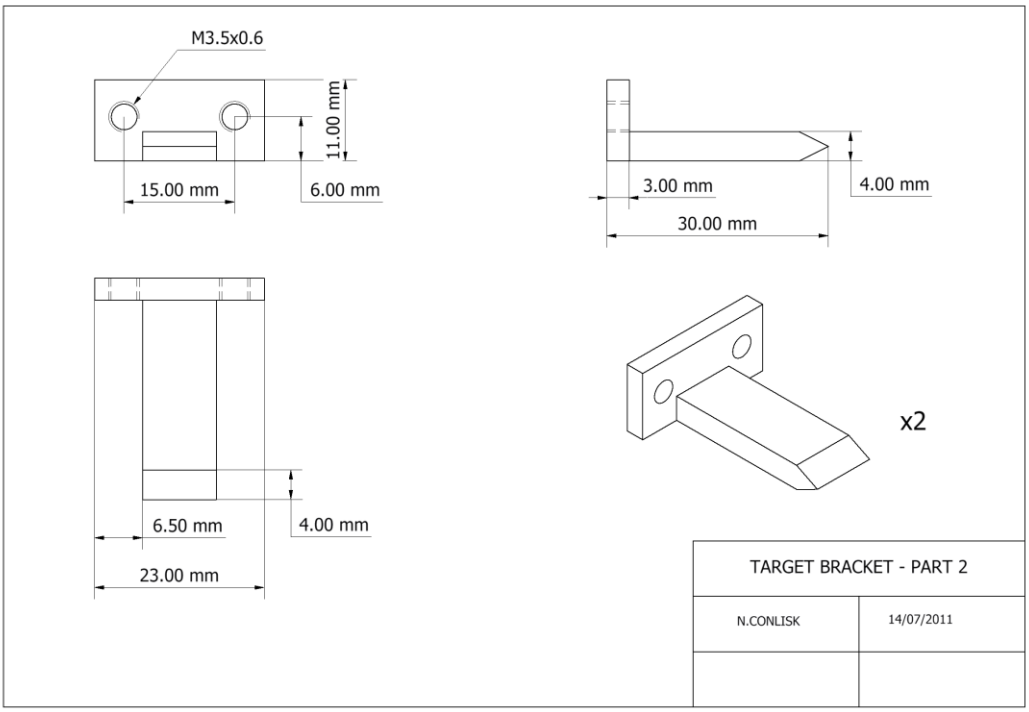
M3.5x0.6
11.00 mm
15.00 mm
6.00 mm
3.00 mm
4.00 mm
30.00 mm
6.50 mm
4.00 mm
23.00 mm
x2
TARGET BRACKET - PART 2
N.CONLISK
14/07/2011

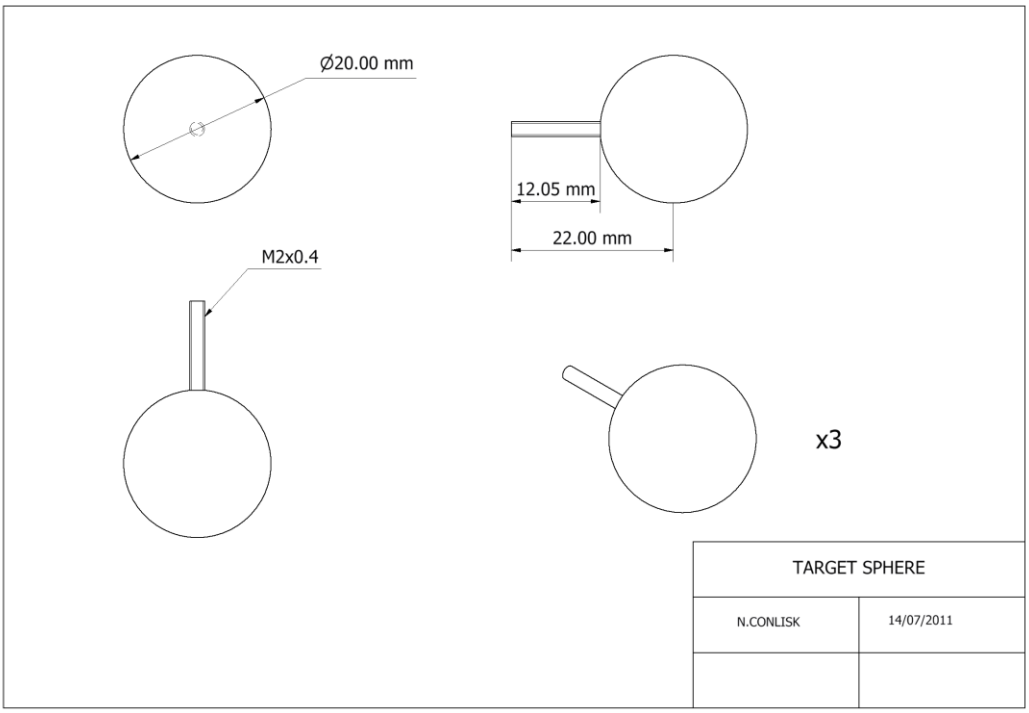
Ø20.00 mm
12.05 mm
22.00 mm
M2x0.4
x3
TARGET SPHERE
N.CONLISK
14/07/2011

## C.5 – Femoral preparation and cementing protocols

# Femoral preparation protocol

## Equipment:

Stryker TS instrument kit.

Stryker System 5 sagittal saw.

Adjustable bench top clamp.

Cordless drill with Jacobs chuck.

## Notes:

Due to the starting point for both primary and revision implantation being an intact sawbones fourth generation composite femur a slightly modified surgical technique had to be adopted.

## Procedure:

- Composite femur was mounted in bench top clamp.
- Pre-existing intramedullary hole was reamed up to accept a size 16 reamer placed to a depth of 150mm.
- Distal femoral resection guide was positioned with the aid of the guide tower and secured using two drill pins.
- Resection depth was set to 9mm to most distal point of lateral condyle using the blade runner.
- Distal femoral cut was made and checked visually using the blade runner in both the AP and ML planes.
- The femoral cutting block was placed over the intramedullary rod and pinned in place with two oblique drill pins. Rotation was set with reference to the transepicondylar access and Whiteside's line. No AP offset was selected,

however, a 4mm lateral offset was selected prior to pinning of the cutting block to accommodate placement of the long offset stem.

- The distal femoral cuts were then made in the following order as recommended to maintain cutting block stability: Anterior flange, posterior condyles, posterior chamfer and anterior chamfer.
- The revision box cutting guide was then attached to the cutting block and pinned in place. The box was then cut and finished with the saw.
- All pins and guides were then removed.
- The offset femoral box guide was inserted and fixed with a single drill pin and the intramedullary canal reamed to 19mm for a length of 225mm for all femurs.
- Appropriateness of cuts was then assessed by testing each femoral component.
- Once satisfied with fit, components placement was carried out as per the relevant surgical technique as recommended by the manufacturer.

# Cementing protocol

## Cementing equipment:

1. Hardinge femoral cement restrictor (DePuy, UK).
2. Surgical Simplex-P methyl methacrylate bone cement with radiopaque barium sulphate (Stryker, UK).
3. Mixevac III bone cement mixer (Stryker, UK).

Three different implant types were employed in this study, cementing techniques employed for each implant are discussed here.

## Procedure for PS implant:

- The cut and prepared composite femur was mounted in bench top clamp.
- The Mixevac was placed in a laboratory fume cupboard during use as the device for establishing vacuum was not available. The fume cupboard while primarily used to extract the generated fumes from the chemical interactions also served as a means of ensuring constant temperature during the mixing process.
- Powdered polymer was placed in the Mixevac. The liquid monomer was added to the powder, the timer was then started and the lid sealed.
- The liquid and powder were mixed for 90 seconds at a constant speed.
- Spatula was used to remove cement from the Mixevac at the beginning of the "dough" phase (approximately 3 – 4 minutes).
- Application and pressurisation of the cement to the distal femoral cut, the anterior chamfer cut and the anterior flange cut (at 5 – 6 minutes) were performed.

- Cement application to posterior condyles of the PS component.
- Component was then mounted by hand to the composite femur.
- Final positioning of the implant was done through the use of a femoral impactor and mallet.
- Continued pressurisation and resistance was applied through impactor until cement judged to be sufficiently set.
- Clean up and removal of excess cement prior to setting.

Procedure for TS implant with short stem:

- Same initial setup as PS implant, however, prior to mixing cement the Hardinge cement restrictor was impacted into the femoral canal to a standardised distance (1cm proximal to stem).
- Mixing of cement conducted as previously discussed.
- Once cement was in "dough" phase, a cylindrical cement mass was formed and introduced to the canal. Cement was then pressurised into the canal wall through digital impaction.
- Application of cement to the component and distal surfaces, followed by impaction, pressurisation and clean-up was then carried out as previously stated.

Procedure for TS implant with long offset stem:

- As "hybrid" cementing was employed for the long stemmed implant the same setup and procedure as outlined for the PS implanted femur was used, where cement was only applied to distal/anterior surfaces of the femur and posterior condyles of implant.